

The University of Nottingham

UNITED KINGDOM · CHINA · MALAYSIA

Synthetic and Biophysical Studies on the Tridachiahydropyrone Family of Natural Products

Kimberley Jade Powell, MChem.

Thesis submitted to the University of Nottingham

for the degree of Doctor of Philosophy

July 2014

Abstract

This thesis primarily details synthetic and biophysical studies on the tridachiahydropyrone family of natural products. The general aim of this work was to explore an hypothesis regarding the location and function of these metabolites, isolated from sacoglossan molluscs. Specifically, it was hypothesised that tridachiahydropyrone is synthesised photochemically from linear polyene precursors via a selective double bond isomerisation-6π electrocyclisation sequence which occurs within the cell membrane of the producing organism. Furthermore, it was postulated that this reaction sequence, and subsequent photochemical transformations of tridachiahydropyrone into the related products phototridachiahydropyrone and oxytridachiahydropyrone, serve to protect the producing mollusc from the damaging effects of UV radiation.

Firstly, the proposed polyene precursors were synthesised using a convergent strategy dependent upon a late-stage Suzuki coupling. Their photochemical, biomimetic conversion into tridachiahydropyrone, phototridachiahydropyrone and oxytridachiahydropyrone, was then accomplished.

The interactions of tridachiahydropyrone and its biomimetic precursors with model membrane systems were next explored, using a fluorescence spectroscopic technique. This work demonstrated that the molecules bind to phospholipid vesicles (PLVs) of varying compositions. The synthesis of tridachiahydropyrone within the PLVs was also achieved.

The propensity of the compounds to act as sunscreens was lastly investigated, by measuring the degree of protection against photochemically-induced lipid peroxidation they conferred on irradiated PLVs, using the thiobarbituric acid reactive substances assay. At high compound concentrations the compounds were found to act as sunscreens, whilst at lower concentrations pro-oxidant activity was observed.

In addition to this main work, methodology for the palladium-catalysed cyanation of vinyl halides with acetone cyanohydrin was developed. Conditions were optimised using β-bromostyrene, and shown to be applicable to a range of diverse substrates. The protocol proved chemoselective for vinyl bromides in the presence of aryl bromides, which were left unaffected and available for further chemical transformations, adding to the synthetic utility of the reaction.

Acknowledgements

Firstly I would like to thank my supervisor, Dr John Moses, for giving me the opportunity to work in his group, and for his support, ideas and enthusiasm over the past three years. Thanks also go to all members of the Moses group, past and present, for day to day discussions and camaraderie, in particular Johnny Moore, James Burnley and Guillaume Parra.

In addition I would like to acknowledge Professor Paul O'Shea for his helpful guidance during the biophysical studies, and the members of IBIOS, in particular Jo Richens, for creating a friendly, supportive and inclusive atmosphere in which to work.

Many thanks go to the departmental technical and analytical staff for their invaluable, generous and friendly assistance.

Finally I would like to offer my heartfelt gratitude to the friends and family who have provided emotional support and escapism over the course of my studies, and a continual reminder of what is really important in life.

Table of Contents

Abstract 2

Acknowledgements 4

Table of Contents 5

Abbreviations 10

Part One 14

Chapter 1 Introduction 15

1.1 Tridachiahydropyrone and Related Natural Products 15

1.1.1 γ -Pyrone-Containing Polypropionates from Sacoglossan Molluscs 15

1.1.2 Biosynthesis of γ-Pyrone-Containing Polypropionate Natural Products 17

1.1.3 Biomimetic Electrocyclisations in Natural Product Synthesis 21

1.1.4 Tridachiahydropyrone: Biosynthetic Hypothesis 26

1.2 UV Light-Induced Cell Damage 30

1.2.1 Direct Damage to DNA 31

1.2.2 Cell Damage via Reactive Oxygen Species 32

1.2.2.1 Damage to DNA 34

1.2.2.2 Damage to Proteins 35

1.2.2.3 Damage to Cell Membranes: Lipid Peroxidation 35

1.2.3 Prevention of Oxidative Cell Damage: Low Molecular Mass Antioxidants 37

1.3 Tridachiahydropyrone: Previous Work 39

1.4 Aims of this Work 43

Chapter 2 ***Synthesis of the Tridachiahydropyrones and their Biomimetic Precursors*** 45

2.1 Revised Synthetic Route 45

2.2 Synthesis of the Boronic Ester Coupling Fragment 46

2.3 Synthesis of the Vinyl Iodopyrone Fragments 47

2.4 Suzuki Coupling: Synthesis of the Biomimetic Precursors 55

2.5 Biomimetic Synthesis of the Tridachiahydropyrone Family 59

Chapter 3 ***Interactions of the Tridachiahydropyrones with Model Membrane Systems: Biophysical Studies*** 64

3.1 Liposomes as Experimental Membrane Models 64

3.2 Behaviour of the Polyene Pyrones in Solution: Critical Micelle Concentrations 68

3.3 Exploring Molecular Interactions with Membranes: Exploiting the Membrane Dipole Potential 74

3.3.1 Membrane Potentials 74

3.3.2 Measurement of the Membrane Dipole Potential: Di-8-ANEPPS 75

3.3.3 Effect of Molecular Interactions on the Membrane Dipole Potential: Difference Spectra 76

3.3.4 Concentration Dependence of the Membrane Dipole Potential: Ratiometric Fluorescence Measurements 78

3.3.5 Uptake of Di-8-ANEPPS by Micelles: Effects on Fluorescence 81

3.3.6 Fitting the Binding Profiles: Characterising the Interactions 83

3.4 Electrocyclisations Using PLVs as Chiral Reaction Media 92

Chapter 4 ***Investigations into the Photoprotective and Antioxidant Properties of the Tridachiahydropyrones*** 96

4.1 Thiobarbituric Acid Reactive Substances (TBARS) Assay 97

4.2 2,2-Diphenyl-1-picrahydrazyl (DPPH) Assay 104

4.3 Ferric Reducing Antioxidant Power (FRAP) Assay 107

4.4 Antioxidant Properties: Mechanistic Considerations 109

4.5 Synthetic Studies: Peroxidation of Tridachiahydropyrone Precursors 113

Chapter 5 ***Summary and Conclusions*** 118

Chapter 6 ***Experimental*** 122

6.1 Organic Synthesis 122

6.1.1 Experimental Techniques 122

6.1.2 Analysis 122

6.1.3 Experimental Procedures and Characterisation Data 123

6.1.4 Electrocyclisation in Membranes: General Procedure 150

6.1.5 Analysis of the Separated Enantiomers of Tridachiahydropyrone 150

6.2 Biophysical Techniques 151

6.2.1 Materials and Methods 151

6.2.2 90° Light scattering: Critical Micelle Concentration Determination 152

6.2.3 Liposome Preparation 152

6.2.4 Fluorescent Labelling of PLVs with Di-8-ANEPPS 154

6.2.5 Characterisation of Di-8-ANEPPS-Labelled PLVs 155

6.2.6 Fluorescence Difference Spectra 155

6.2.7 Titration of Ligands into Di-8-ANEPPS-Labelled PLVs: Dual-Wavelength Ratiometric Fluorescence Time Course Measurements 156

6.2.8 Analysis of Titration Data: Generation of Binding Profiles 158

6.3 Assay Procedures 159

6.3.1 Materials and Methods 159

6.3.2 Thiobarbituric Acid Reactive Substances (TBARS) Assay 159

6.3.3 2,2-Diphenyl-1-picrahydrazyl (DPPH) Assay 160

6.3.4 Ferric Reducing Antioxidant Power (FRAP) Assay 161

Part Two 162

Chapter 7 Synthesis of Alkenyl Nitriles by the Palladium-Catalysed Cyanation of Vinyl Halides with Acetone Cyanohydrin 163

7.1 Introduction 163

7.1.1 Prevalence and Utility of Alkenyl Nitriles 163

7.1.2 Transition Metal-Catalysed Cyanation of Vinyl Halides: Existing Methodology 165

7.1.3 Use of Acetone Cyanohydrin in Cyanation Methodology 168

7.1.4 Aims of this Work 170

7.2 Results and Discussion 171

7.2.1 Optimisation of the Reaction Conditions 171

7.2.2 Substrate Scope 179

7.3 Summary and Conclusions 183

7.4 Experimental 185

7.4.1 Experimental Techniques 185

7.4.2 Analysis 185

7.4.3 Preparation of Substrates 186

7.4.4 General Cyanation Procedure 194

7.4.5 Characterisation of Cyanation Products 195

References 203

Appendix 1 *Molecular Modelling: Equilibrium Geometries* 217

Appendix 2 *Statistical Parameters* 219

Abbreviations

Å	angstrom
a	antarafacial
Ac	acetyl
ACP	acyl carrier protein
aq.	aqueous
B_{max}	binding capacity
b.p.	boiling point
Bu	butyl
°C	degrees Celsius
C	cytosine
CE	condensing enzyme
Chol	cholesterol
cm	centimetre(s)
CMC	critical micelle concentration
CoA	coenzyme-A
con	conrotatory
conc.	concentrated or concentration
CPD	cyclobutane pyrimidine dimer
cps	counts per second
Cy	cyclohexyl
Δ	reflux or thermal
$\Delta\Psi$	transmembrane potential difference
dba	dibenzylideneacetone
DBU	1,8-diazabicyclo[5.4.0]undec-7-ene
DIBAL-H	diisobutylaluminium hydride
dis	disrotatory
DMAc	N,N-dimethylacetamide
DMF	N,N-dimethylformamide
DMP	Dess-Martin periodinane

DMSO	dimethyl sulfoxide
DNA	deoxyribonucleic acid
DPPE	1,2-bis(diphenylphosphino)ethane
DPPH	2,2-diphenyl-1-picrahydrazyl
DPPP	1,2-bis(diphenylphosphino)propane
E1cB	elimination, unimolecular, conjugate base
EC_{50}	half maximal effective concentration
ee	enantiomeric excess
ESI	electrospray ionisation
Et	ethyl
equiv.	equivalents
FRAP	ferric reducing antioxidant power
FT	fourier transform
g	gram(s)
h	hour(s)
HHE	trans-4-hydroxy-2-hexenal
HMDS	hexamethyldisilazane
HNE	4-hydroxy-2-trans-nonenal
HPLC	high-performance liquid chromatography
HRMS	high resolution mass spectrometry
$h\nu$	irradiation with light or photochemical
Hz	hertz
^{i}	iso
IPA	iso-propyl alcohol
IR	infra red
K_d	dissociation constant
L	ligand
l_d	liquid disordered
lit	literature
l_o	liquid ordered
M	molar or metal
MDA	malondialdehyde

MCoA	malonyl coenzyme-A
Me	methyl
mg	milligram(s)
MHz	megahertz
min	minute(s)
mL	millilitre(s)
μL	microlitre(s)
mm	millimetre(s)
mM	millimolar
μM	micromolar
mMCoA	methylmalonyl coenzyme-A
mmol	millimole(s)
mp	melting point
^{n}	normal
n	Hill coefficient
NADH	nicotinamide adenine dinucleotide-H
NBS	N-bromosuccinimide
NIS	N-iodoosuccinimide
nm	nanometre(s)
NMR	nuclear magnetic resonance
nOe	nuclear Overhauser effect
PC	phosphatidylcholine
Ph	phenyl
PLV	phospholipid vesicle
POPC	1-palmitoyl-2-oleoyl-*sn*-glycero-3-phosphocholine
PP	photoproduct
ppm	parts per million
Ψ_s	membrane surface potential
Ψ_d	membrane dipole potential
PUFA	polyunsaturated fatty acid
R	alkyl group or fluorescence ratio
R_f	retention factor

ROS	reactive oxygen species
rt.	room temperature
sat.	saturated
SM	sphingomyelin
s_o	solid ordered
SOD	superoxide dismutase
^{t}	tertiary
T	thymine
TBAB	tetrabutylammonium bromide
TBARS	thiobarbituric acid reactive substances
temp.	temperature
TFP	tri(2-furyl)phosphine
THF	tetrahydrofuran
TLC	thin layer chromatography
TMEDA	tetramethylethylenediamine
TMS	trimethylsilyl
TOF	time-of-flight
TPTZ	tripyridyltriazine
UV	ultraviolet
vis	visible
v/v	volume per volume
W	watt(s)

Part One

Chapter 1 Introduction

1.1 Tridachiahydropyrone and Related Natural Products

1.1.1 γ -Pyrone-Containing Polypropionates from Sacoglossan Molluscs

In recent years, a number of structurally diverse γ-pyrone-containing polypropionate natural products have been isolated from opisthobranch molluscs of the order Sacoglossa (Figure 1).[1]

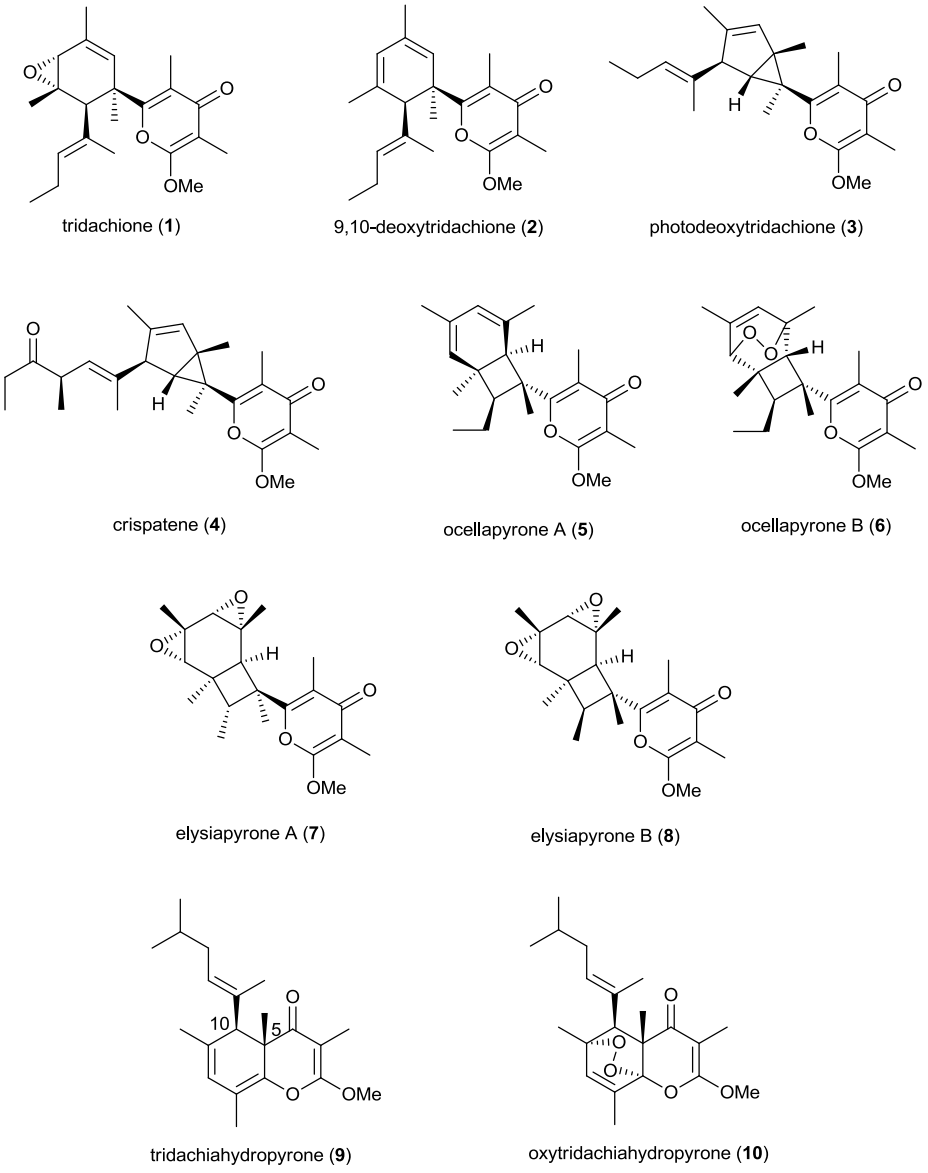


Figure 1. γ-Pyrone-containing polypropionates from sacoglossan molluscs

Many of these possess complex structural frameworks and have been shown to exhibit interesting biological activities.[2] A common structural feature of this family of molecules is a γ-pyrone moiety appended to an unsaturated, polyketide-derived side-chain. Tridachiahydropyrone (**9**)[3] and oxytridachiahydropyrone (**10**)[4] are unusual in possessing a dihydropyrone group, with the γ-dihydropyrone fused to the side-chain, forming a bicyclic core.

Tridachiahydropyrone (**9**) was first isolated by Cimino et al. in 1996 from the Caribbean sacoglossan mollusc *Tridachia crispata.*[3] The relative configuration of the ring substituents at C-5 and C-10 were originally assigned as trans on the basis of nOe studies. However, an unambiguous total synthesis in 2005 of the originally proposed isomer **11** by Perkins and co-workers warranted the structural reassignment of the natural product, as spectroscopic data of the synthesised compound did not match that of the natural sample.[5] It was subsequently speculated that the cis diastereomer **9** might be the true structure of the natural product, and this was confirmed by the completion of its total synthesis in 2008 by Moses et al.[6] Further work by the Moses group also led to the structural reassignment of tridachiahydropyrones B (**12**) and C (**13**) as oxytridachiahydropyrone (**10**) (See Section 1.3).[7]

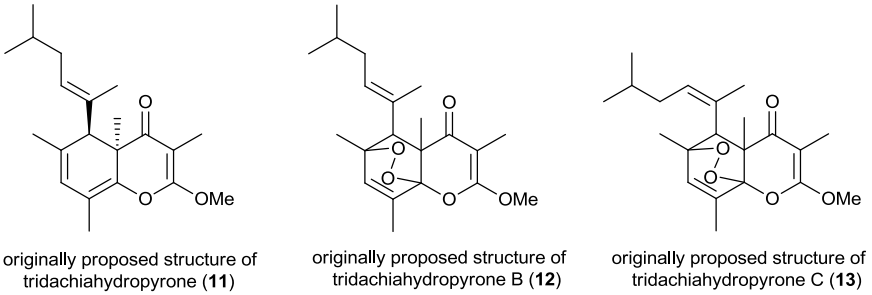
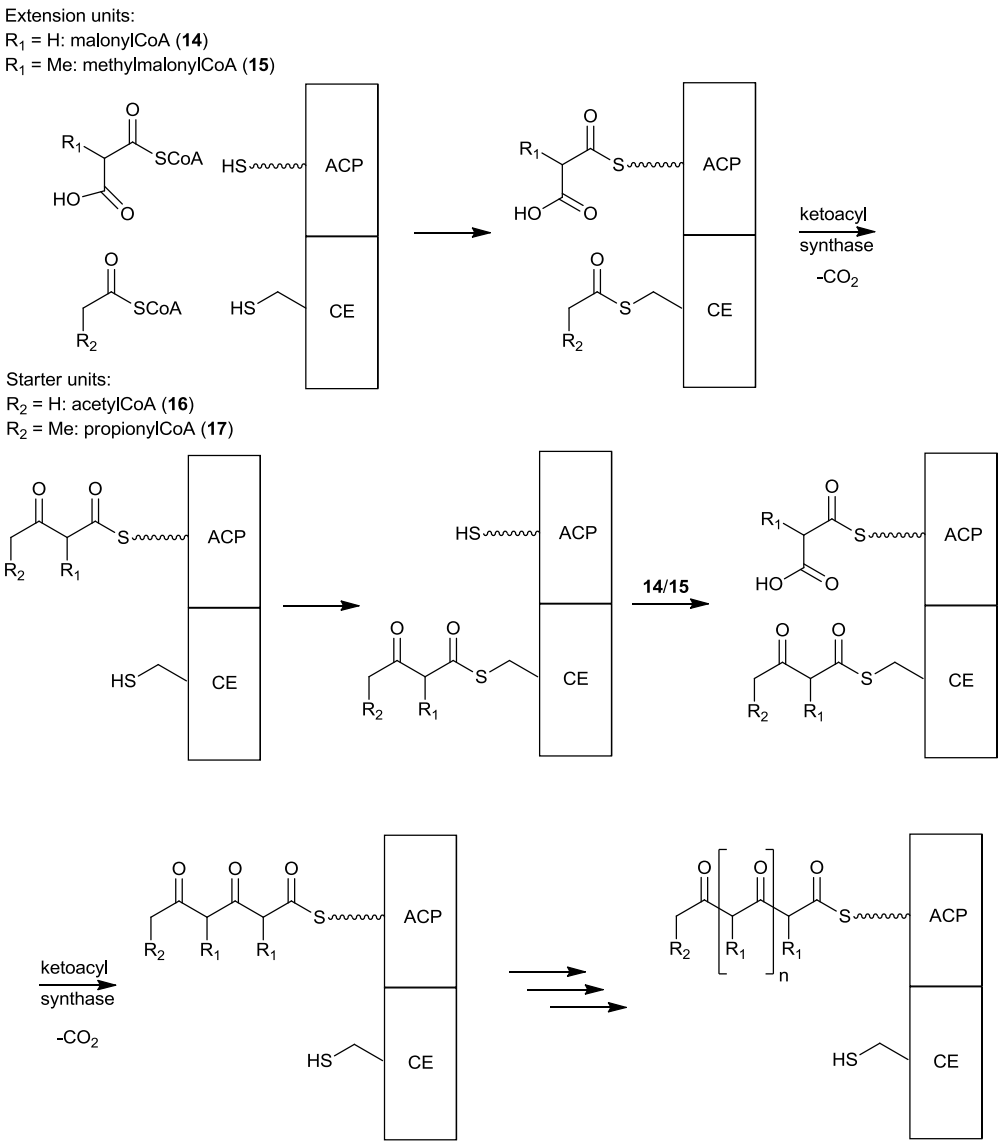


Figure 2. Originally proposed structures of the tridachiahydropyrones

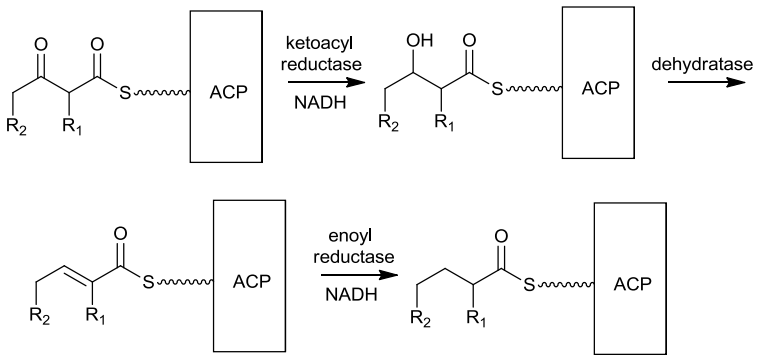
1.1.2 Biosynthesis of γ-Pyrone-Containing Polypropionate Natural Products

γ-Pyrone-containing polypropionate natural products originate from polyketides, which can undergo assorted reductive transformations to give diverse products with varying levels of unsaturation. Polyketide biosynthesis occurs on a multienzyme complex, consisting of a protein dimer of acyl carrier protein (ACP) and condensing enzyme (CE), with the basic sequence involving iterative Claisen condensations of acid derivatives such as malonyl coenzyme-A (MCoA, **14**) and methylmalonyl coenzyme-A (mMCoA, **15**) onto starter units such as acetyl CoA (**16**) and propionyl CoA (**17**) (Scheme 1).[8]



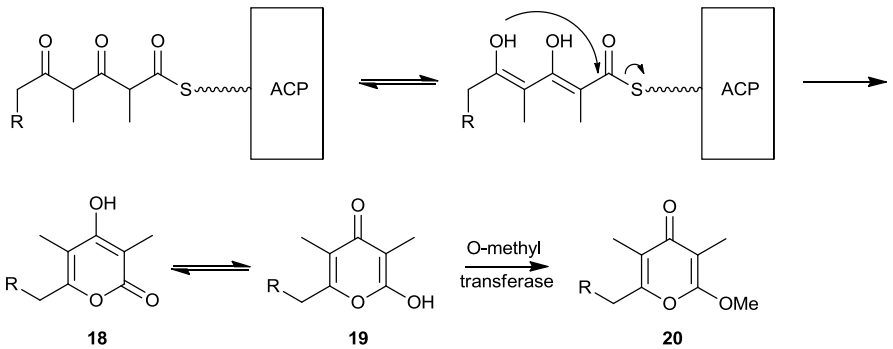
Scheme 1. Polyketide biosynthesis

In addition to chain-extension via the Claisen condensation, further modification of the polyketide backbone can take place by reduction of the carbonyl groups to varying extents. Some carbonyl groups are left untouched, some reduced to hydroxyl groups, some to olefinic motifs, and some reduced completely to alkanes (Scheme 2).



Scheme 2. Reductive modification of the polyketide backbone

The α-methoxy-γ-pyrone unit itself arises from the cyclisation of three ketide units. The final three extension units condensed into the polyketide chain are left unmodified by reductive enzymes, giving a triketide which readily cyclises, with concurrent release from the acyl carrier protein. The immediate product is the γ-hydroxy-α-pyrone **18**. Tautomerisation to the γ-pyrone tautomer **19** followed by an enzyme-mediated regioselective *O*-methylation occurs to give the α-methoxy- γ-pyrone **20** (Scheme 3).[9]

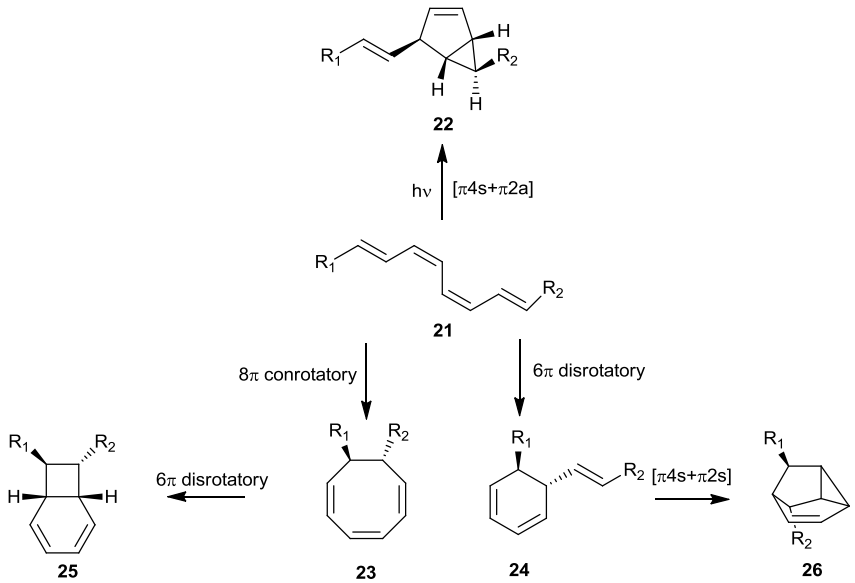


Scheme 3. Biosynthesis of the α-methoxy-γ-pyrone unit

The condensation, reduction, cyclisation and methylation steps shown above result in an α-methoxy- γ-pyrone unit appended to a linear polyketide-derived side-chain of varying degrees of reduction. However, the majority of γ-pyrone-containing natural products isolated from sacoglossan molluscs do not

possess linear side-chains, instead exhibiting complex carbon frameworks commonly characterised by cyclic motifs. For example, 9,10-deoxytridachione (**2**)[10] possesses a 1,3-cyclohexadiene unit, whilst ocellapyrone A (**5**)[1d] is endowed with a bicyclo[4.2.0]octadiene appendage (Figure 1).

It has been proposed that these complex structures arise from various electrocyclisation and cycloaddition reactions of linear polyene side-chains, undergone post-pyrone formation. For example, Trauner pointed out the wide variety of skeletal types that can be theoretically obtained from pericyclic transformations of a relatively simple (*E,Z,Z,E*)-tetraene **21**, further observing that isomerisations of the alkene geometries lead to an even greater number of potential cyclisation products (Scheme 4).[11]



Scheme 4. Structural complexity generated from the tetraene **21**

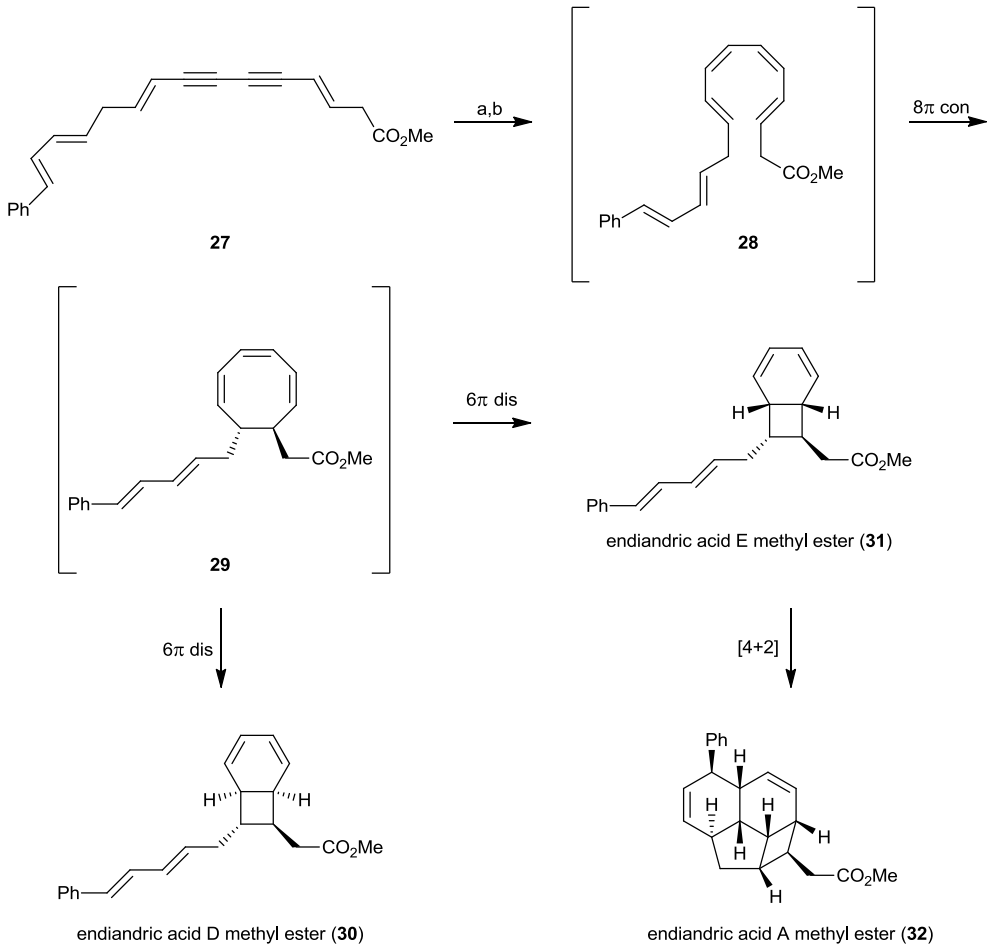
Furthermore, many elegant biomimetic syntheses of natural products have been carried out using electrocyclisation reactions – often as part of cascade

sequences – to generate high structural complexity from relatively simple precursors.

1.1.3 Biomimetic Electrocyclisations in Natural Product Synthesis

The earliest example of a biomimetic electrocyclisation cascade sequence in natural product synthesis is in Nicolaou's syntheses of the endiandric acids, isolated by Black in the early 1980s.[12] To explain the racemic nature of these natural products, Black proposed that they are formed spontaneously from achiral polyene precursors through non-enzymatically assisted electrocyclisation and cycloaddition cascades. In 1982 Nicolaou reported the synthesis of the methyl esters of all endiandric acids A-G in a one-operation cascade approach from linear polyene precursors.[13] The synthesis of endiandric acids A, D and E methyl esters (**32**, **30** and **31** respectively) is outlined below (Scheme 5).

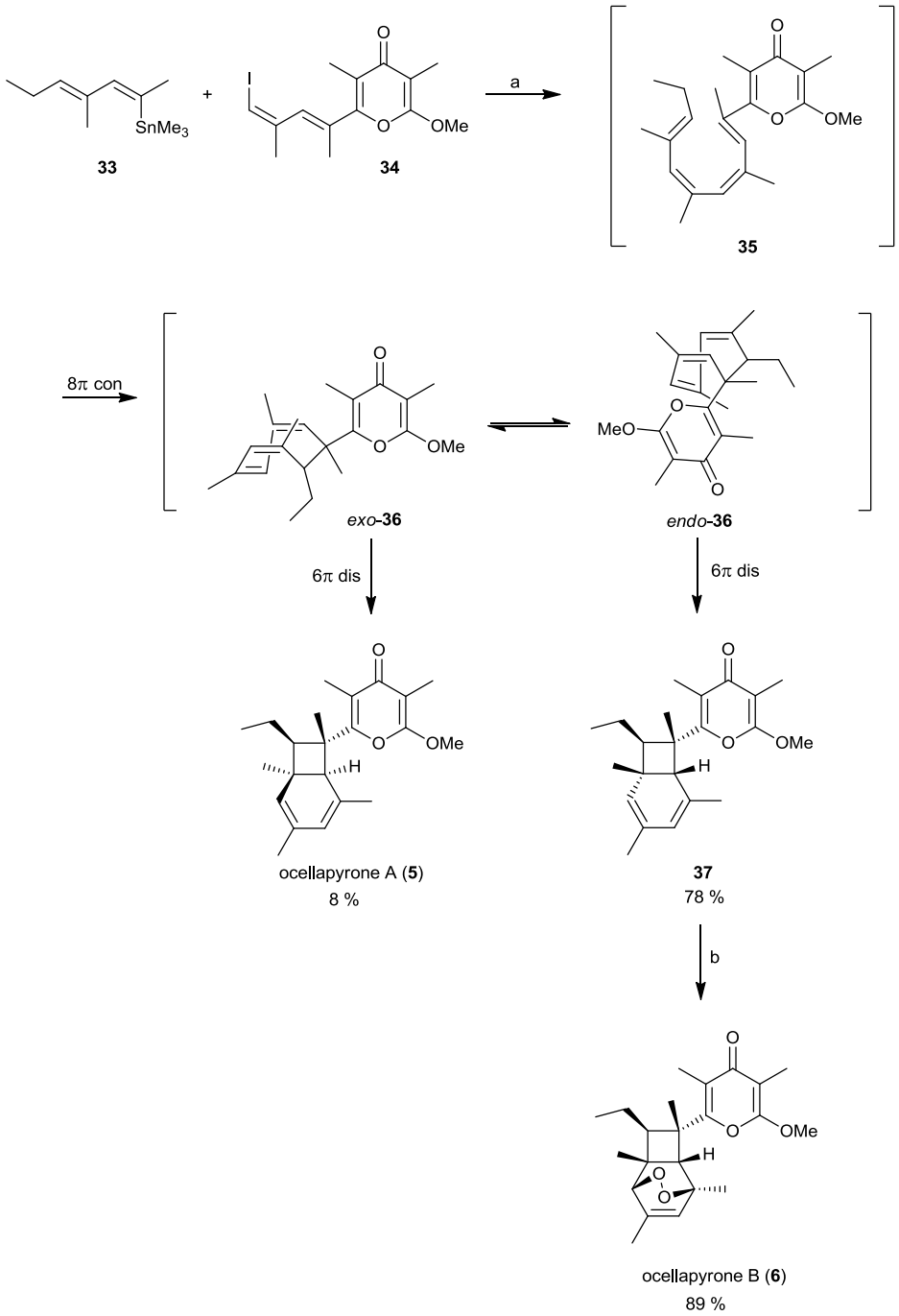
The octatetraene **28** was synthesised by a double Lindlar hydrogenation of dialkyne **27**, and underwent a spontaneous 8π conrotatory electrocyclisation followed by a 6π disrotatory electrocyclisation of the initial cyclisation product **29** (not isolated). This cascade sequence gave rise to endiandric esters D (**30**) and E (**31**). Heating to 100 °C in toluene resulted in an intramolecular Diels-Alder cycloaddition of **31**, affording endiandric ester A (**32**). Endiandric esters B, C, F and G were synthesised analogously from a similar dialkyne precursor.



Scheme 5. Nicolaou's biomimetic synthesis of the endiandric acid methyl esters. Reagents and conditions: (a) H_2, Pd/$BaSO_4$, quinoline; (b) PhMe, 100 °C

Like members of the endiandric acid family, ocellapyrone A (**5**) has a bicyclo[4.2.0]octadiene framework. As such it was hypothesised that **5** is also biosynthesised from a tetraene precursor via an 8π-6π electrocyclisation cascade. To test this hypothesis, Trauner et al. constructed the pyrone-polyene **35** using a Stille coupling of the pyrone fragment **34** with the stannane **33**.[11] The tetraene **35** underwent an 8π-6π electrocyclisation cascade *in situ*. The product of the initial 8π cyclisation, **36**, exists as a mixture of exo and endo conformers, with subsequent 6π cyclisation of these conformers leading to ocellapyrone A (**5**) and isomer **37** respectively. The

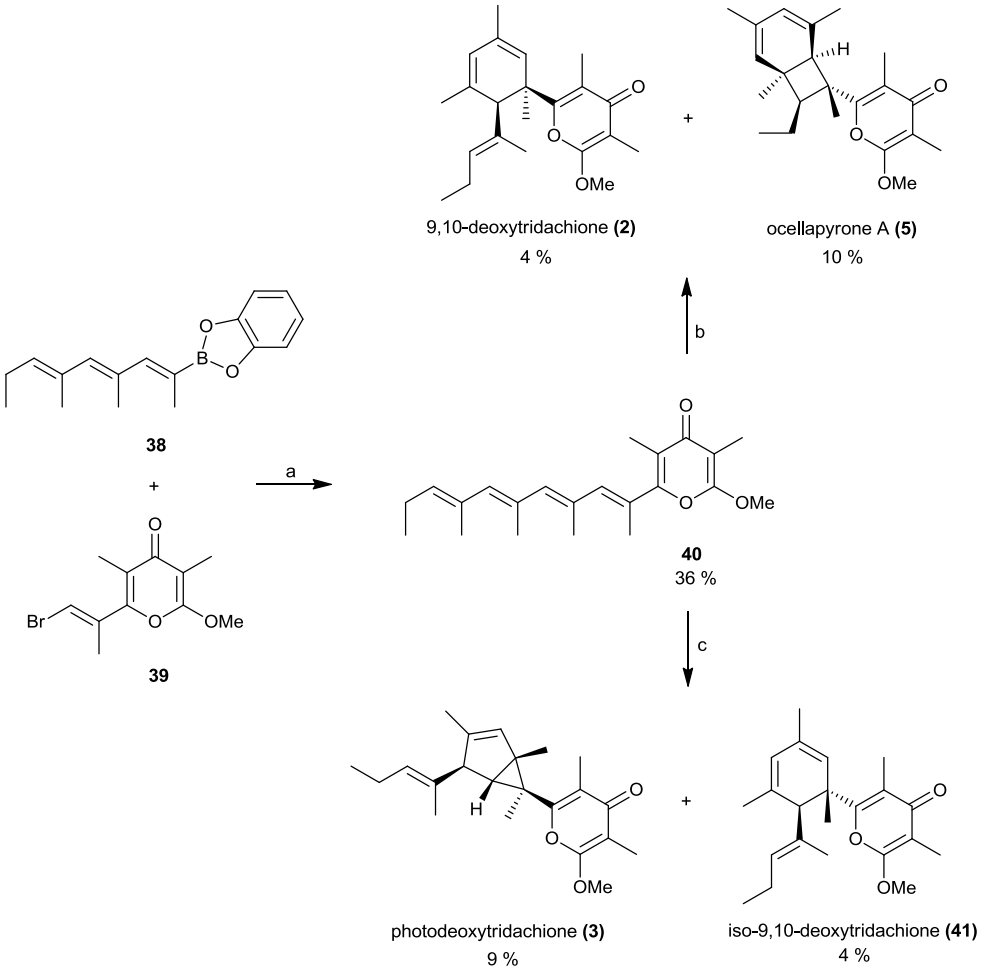
endo product **37** was found to dominate. Ocellapyrone B (**6**) was obtained by exposure of **37** to oxygen (Scheme 6).



Scheme 6. Trauner's synthesis of the ocellapyrones. Reagents and conditions: (a) $Pd(PPh_3)_4$, CsF, CuI, DMF; (b) O_2, methylene blue, $CHCl_3$, hν, reflux

Moses and co-workers took this hypothesis one step further, speculating that the original biosynthetic polyene precursor was not the (*E,Z,Z,E*)-tetraene **35**

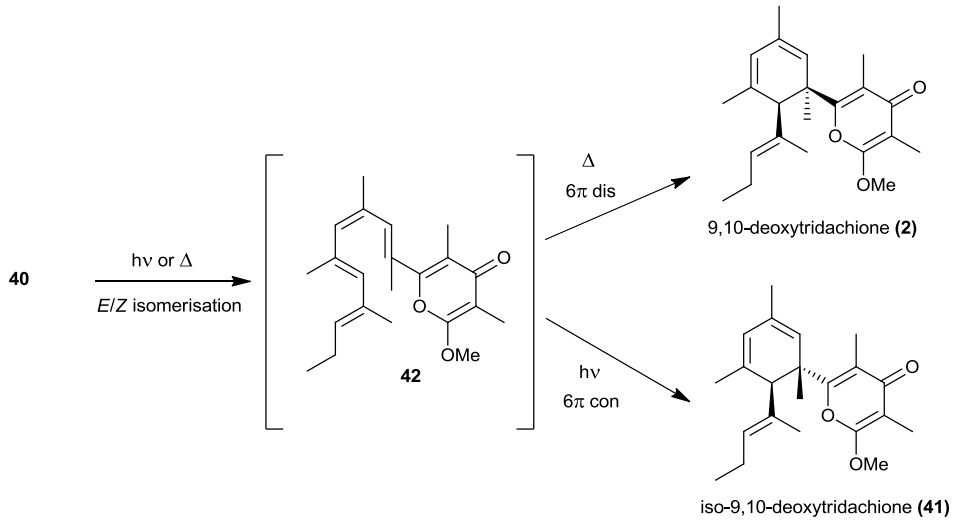
but the all *E* isomer **40**.[14] Furthermore, they postulated that this polyene was the precursor to a number of γ-pyrone polypropionate natural products, diversification occurring via selective double bond isomerisations followed by varying electrocyclisations or cycloadditions. Thus the polyene **40** was synthesised by a Suzuki coupling of the boronic ester **38** with the vinylic bromo-pyrone **39**, and subsequently subjected to thermal and photochemical conditions (Scheme 7).



Scheme 7. Moses' synthesis of γ-pyrone polypropionate natural products from the common precursor **40**. Reagents and conditions: (a) $Pd(PPh_3)_4$, aq. KOH, THF, 80 °C; (b) xylenes, 150 °C, dark; (c) hν, cyclohexane

Thermal conditions afforded 9,10-deoxytridachione (**2**) and ocellapyrone A (**5**), whilst photochemical conditions led to isolation of photodeoxytridachione (**3**) and iso-9,10-deoxytridachione (**41**), all natural products.

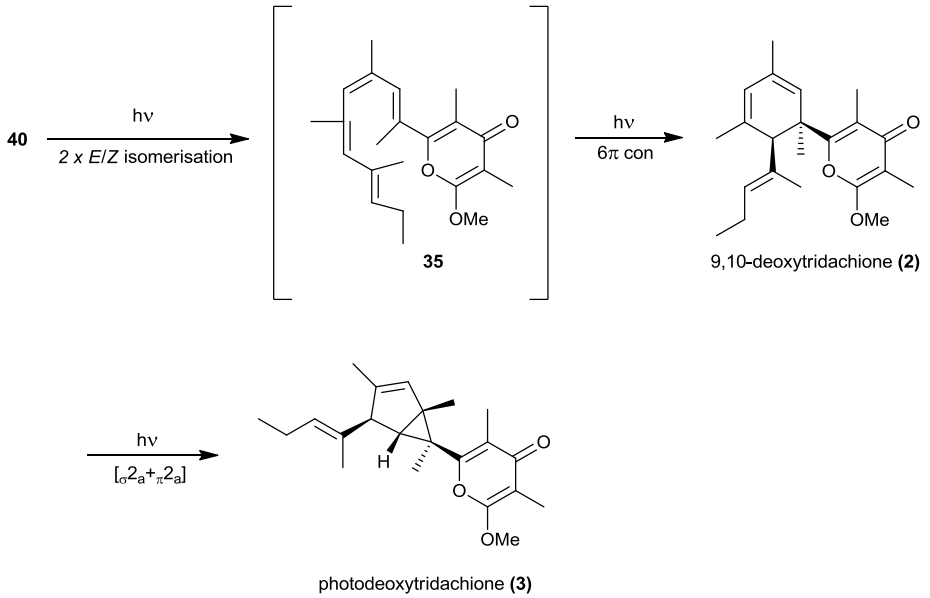
It was proposed that 9,10-deoxytridachione (**2**) and iso-9,10-deoxytridachione (**41**) arise from the all *E* polyene **40** via an initial selective double bond isomerisation followed by 6π electrocyclisation of the (*E,Z,E,E*)-isomer **42** (Scheme 8). Under thermal conditions disrotatory electrocyclisation occurs, leading to 9,10-deoxytridachione (**2**), whilst under photochemical conditions the conrotatory mode is allowed, affording iso-9,10-deoxytridachione (**41**).[14]



Scheme 8. Mechanism for the formation of **2** and **41** from **40**

It is thought that photodeoxytridachione (**3**) arises from **40** via 9,10-deoxytridachione (**2**), which is formed under photochemical conditions following two selective double bond isomerisations of **40** and subsequent 6π conrotatory electrocyclisation of the (*E,Z,Z,E*)-isomer **35**. A photochemical $[_{\sigma}2_a+_{\pi}2_a]$ rearrangement of 9,10-deoxytridachione (**2**) would lead to photodeoxytridachione (**3**) (Scheme 9).[14] An alternative mechanism for the

photochemical conversion of **2** into **3** involving diradical species has also been proposed.[15]



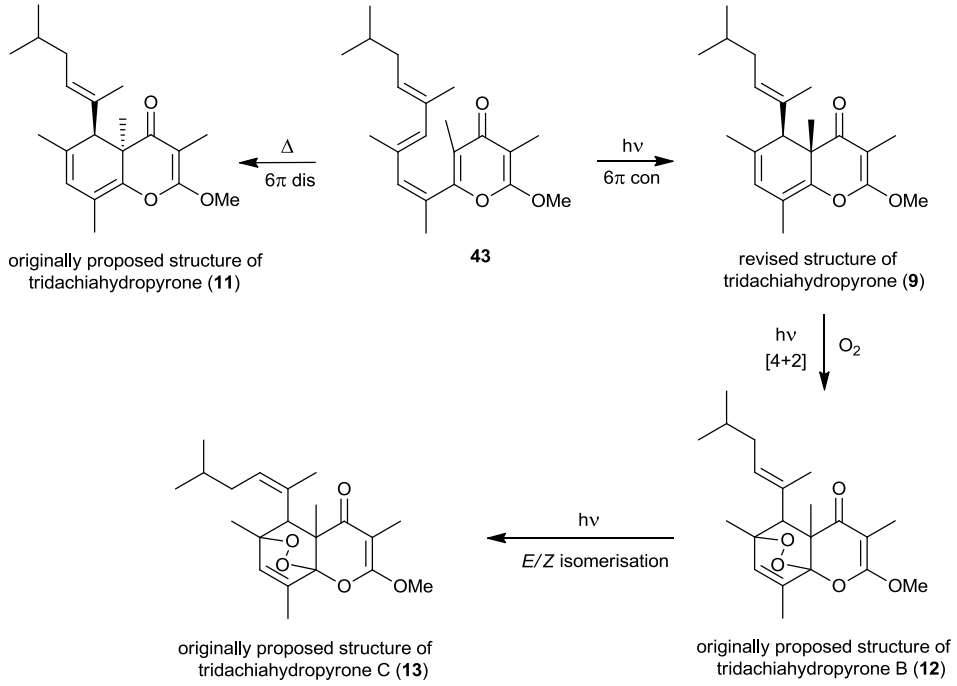
Scheme 9. Possible mechanism for the photochemical formation of photodeoxytridachione (**3**) from **40**

Ocellapyrone A (**5**) also arises from **40** via **35**. Following the two selective double bond isomerisations, this time promoted thermally, an 8π-6π electrocyclisation cascade (Scheme 6) leads to the natural product.[14]

1.1.4 Tridachiahydropyrone: Biosynthetic Hypothesis

Tridachiahydropyrone (**9**) is produced by the marine mollusc *Tridachia crispata.*[3] These molluscs, like many from which a wide range of γ-pyrone polypropionate natural products has been isolated, are shell-less creatures and so are vulnerable to predation. They are known to excrete chemicals as a form of defence,[16] with many of the γ-pyrone polypropionates isolated showing biological activities.[2]

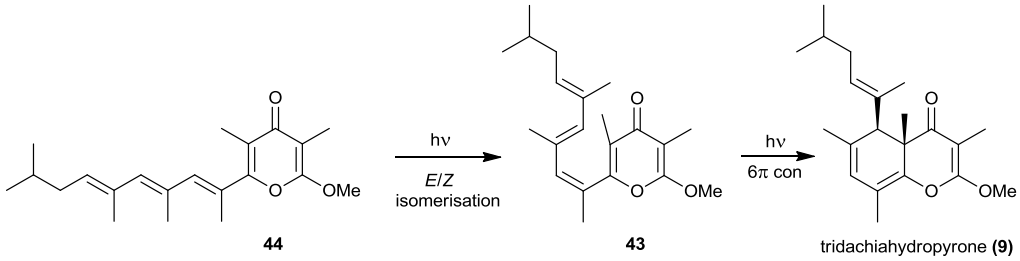
The originally proposed structure of tridachiahydropyrone (**11**) would be formed from the (*Z,E,E*)-polyene **43** upon a thermal 6π disrotatory electrocyclisation. Perkins demonstrated that this structure was not that of the natural product.[5] The revised structure of tridachiahydropyrone (**9**) would be formed from the (*Z,E,E*)-polyene **43** upon a 6π conrotatory electrocyclisation (Scheme 10).



Scheme 10. Possible pathways to the tridachiahydropyrones from polyene **43**

The 6π conrotatory mode of electrocyclisation is promoted under photochemical conditions. Furthermore, a photochemical [4+2] cycloaddition of **9** with singlet oxygen ($^1O_2$) would furnish tridachiahydropyrone B (**12**), with a further *E/Z* isomerisation leading to tridachiahydropyrone C (**13**). These observations, coupled with the fact that the molluscs reside in areas exposed to direct sunlight, underpin the biosynthetic hypothesis proposed by Moses et al.[7]

It is proposed that tridachiahydropyrone (**9**) originates from a photochemical 6π conrotatory electrocyclisation of the (*Z,E,E*)-polyene **43**, itself generated from a selective double bond isomerisation of the all *E* isomer **44** (Scheme 11).



Scheme 11. Proposed origin of tridachiahydropyrone (**9**)

Previous work in the Moses group has resulted in the synthesis of **9** from both **43**[6] and **44**,[7] providing strong experimental support for their hypothesis (see Section 1.3).

Seminal labelling studies carried out by Ireland and Scheuer in 1979 demonstrated the non-enzymatic *in vivo* photochemical transformation of 9,10-deoxytridachione (**2**) into photodeoxytridachione (**3**).[17] This work led them to conclude that γ-pyrone polypropionate metabolites served as sunscreens in the shell-less molluscs which, in addition to being vulnerable to predation, are often found in shallow lagoons exposed to strong sunlight. It was postulated that metabolites such as **2** are biosynthesised and then transported to the tissue of the digestive diverticula, flanking the dorsal surface, with photochemical transformations occurring when the ultraviolet (UV) radiation penetrating this surface exceeds the absorption limits of the γ-pyrone moiety.[17] Thus excess radiation is dispersed by being channelled into

driving photochemical reactions, forming further natural products such as **3,** whilst protecting the mollusc from the damaging effects of UV radiation.

In light of these studies it is proposed that, in the case of tridachiahydropyrone (**9**), the linear polyene **44** is produced by the mollusc as a photoprotective agent, its possession of a conjugated polyene and γ-pyrone unit making it an excellent chromophore. When the level of UV radiation exceeds the absorption limit of **44**, the selective double bond isomerisation-6π conrotatory electrocyclisation sequence outlined in Scheme 11 is triggered.

Given the fact that, in order to act as effective sunscreens, the metabolites need to be near the surface of the mollusc, it is further hypothesised that the polyene **44** is located in the cell membrane. It is reasonable that a linear polyene-pyrone such as **44** would sit comfortably in the phospholipid bilayer of a cell membrane, given its structural resemblance to a phospholipid: both possess a polar head group (γ-pyrone/phosphate moiety) and hydrophobic tail (polyene/fatty acid chain) (Figure 3).

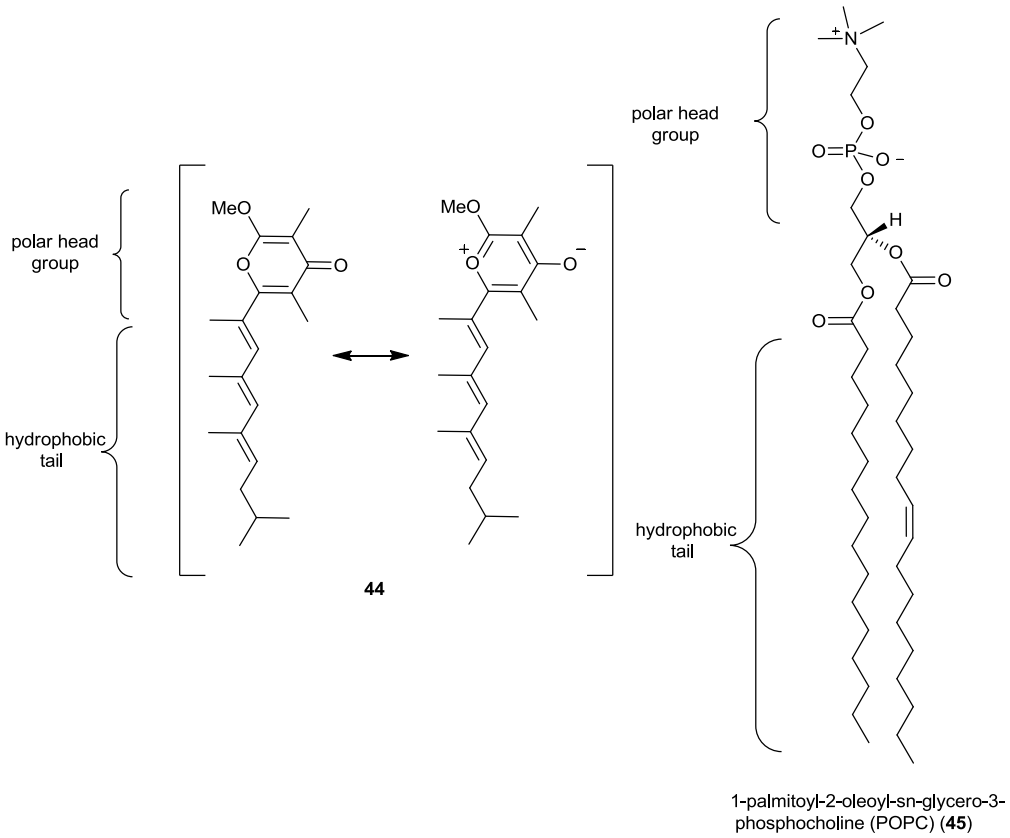


Figure 3. Structural resemblance between polyene-γ-pyrones such as **44** and phospholipids such as POPC (**45**)

Thus it is hypothesised that the polyene **44** becomes embedded in the phospholipid bilayer of the cell membrane near the surface of the mollusc and, upon prolonged exposure to strong sunlight, undergoes the photochemical transformation to tridachiahydropyrone (**9**), which is subsequently released from the bilayer.

1.2 UV Light-Induced Cell Damage

Photochemical damage to biological cells can occur by the direct absorption of UV light by cell components, or via generation of reactive oxygen species (ROS) which attack a wide range of cellular targets, exerting oxidative stress on the cell.

This damage has varying range of effects, leading to DNA mutations, decreased membrane fluidity, and inactivation of vital enzymes. If left unchecked, oxidative injury can induce senescence and even trigger cell death.[18]

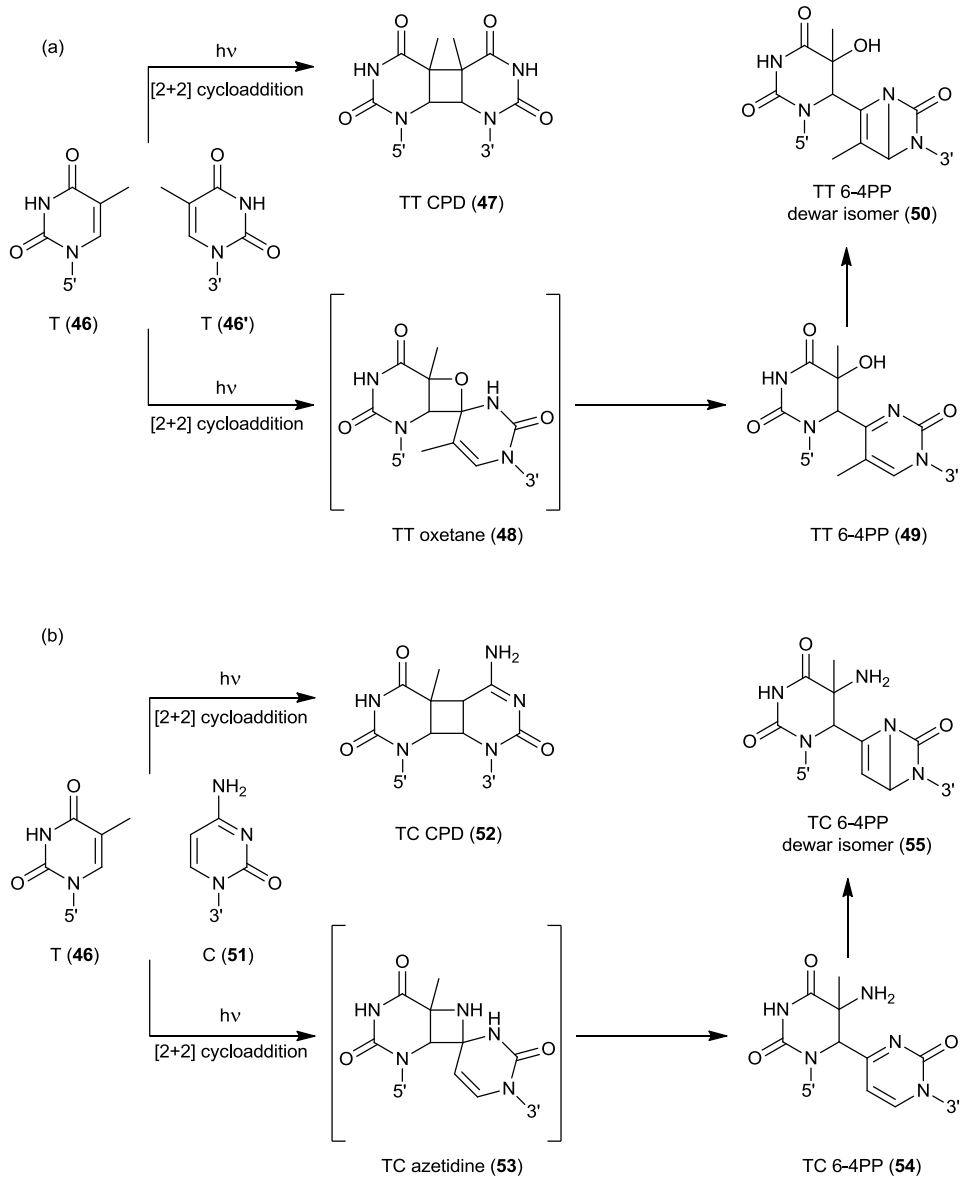
1.2.1 Direct Damage to DNA

Direct absorption of UV-B radiation by cellular DNA results in two major classes of lesion, both affecting the pyrimidine bases thymine (T, **46**) and cytosine (C, **51**) (Scheme 12).[19]

The first is the formation of cyclobutane pyrimidine dimers (CPDs), accounting for ~75% of direct UV-induced damage to DNA. Absorption of UV-B by thymine or cytosine causes a [2+2] cycloaddition between the carbon-carbon double bonds of neighbouring bases, resulting in a four-membered ring structure, **47** or **52**.

The second, accounting for ~25% of lesions, is the formation of 6-4 photoproducts (6-4PPs). These 6-4PPs (**49** and **54**) possess a single covalent bond, between C6 (of the 5' end) and C4 (of the 3' end) of the pyrimidine bases involved. This is formed via collapse of an intermediate unstable oxetane **48** (when the 3' end is thymine) or azetidine **53** (when the 3' end is cytosine), formed photochemically. The 6-4PPs readily undergo photoisomerisation to the dewar isomers **50**/**55** upon exposure to wavelengths longer than 290 nm.

Both types of lesion can cause distortions to the DNA helix, with CPDs and 6-4PPs causing kinks of 7-9 ° and 44 ° respectively.

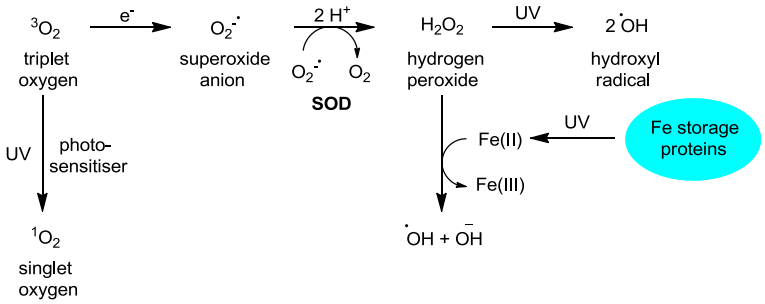


Scheme 12. Pathways of photochemical damage to pyrimidine bases: formation of (a) thymine-thymine adducts; (b) thymine-cytosine adducts

1.2.2 Cell Damage via Reactive Oxygen Species

UV light contributes to the formation of reactive oxygen species (ROS), which can attack various cell components, including DNA and lipids, leading to

oxidative cell damage. The main contribution of UV light to ROS production relates to singlet oxygen and hydroxyl radical formation (Scheme 13).[18]



Scheme 13. Formation of ROS in biological systems: the role of UV light

Singlet oxygen can be generated from the triplet ground state by photosensitisation reactions. This involves absorption of UV radiation by a photosensitiser molecule, raising it in energy to an excited state. This excitation energy can then be transferred to a ground state oxygen molecule, converting it to the excited singlet state, whilst the photosensitiser returns to its ground state. Many biomolecules found in cells are effective photosensitisers, including riboflavin[20] and various porphyrins.[21]

The main mechanism for the formation of hydroxyl radicals in biological systems is from hydrogen peroxide. Hydrogen peroxide is produced in cells by the superoxide dismutase (SOD)-catalysed disproportionation of the superoxide anion.[18] Superoxide is known to form from ground state oxygen through a variety of processes, including auto-oxidation reactions[22] and the mitochondrial electron transport chain.[23] The absorption of UV light by hydrogen peroxide can lead to direct homolysis into hydroxyl radicals. However the more prominent mechanism of hydroxyl formation from hydrogen peroxide is the iron (II)-mediated Fenton reaction. It has been

shown that UV radiation induces release of iron from storage proteins, leading to an increase in free iron (II) available for this Fenton chemistry.[24]

1.2.2.1 Damage to DNA

In addition to direct interaction with pyrimidine bases, UV irradiation leads to the formation of reactive oxygen species (ROS) which can themselves cause damage to DNA. Attack by the hydroxyl radical is the main source of this type of damage.

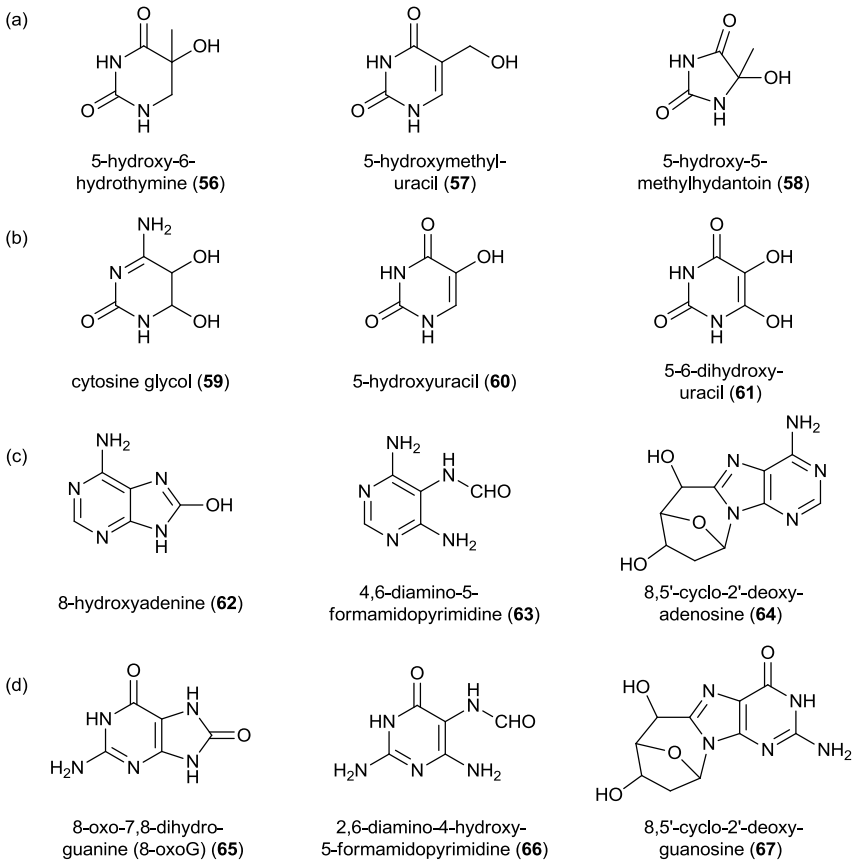


Figure 4. A selection of modified DNA bases formed by attack of ROS on: (a) thymine; (b) cytosine; (c) adenine; (d) guanine

The radical [$^{\bullet}$OH] can add to the purine bases at the 4-, 5- or 8-positions, forming adducts which can further undergo a variety of reduction, oxidation and/or ring opening transformations, affording a wide range of possible end

products. Pyrimidines are also attacked by [˙OH] to give multiple products. A selection of these products is outlined in Figure 4.[18]

Singlet oxygen can also cause DNA lesions, but is far more limited in its attack than the hydroxyl radical, restricted mainly to addition across the 4,8-bond of guanine's imidazole ring, affording unstable endoperoxides which degrade to give various products including 8-oxo-7,8-dihydroguanine (8-oxoG, **65**) (Figure 4).[25]

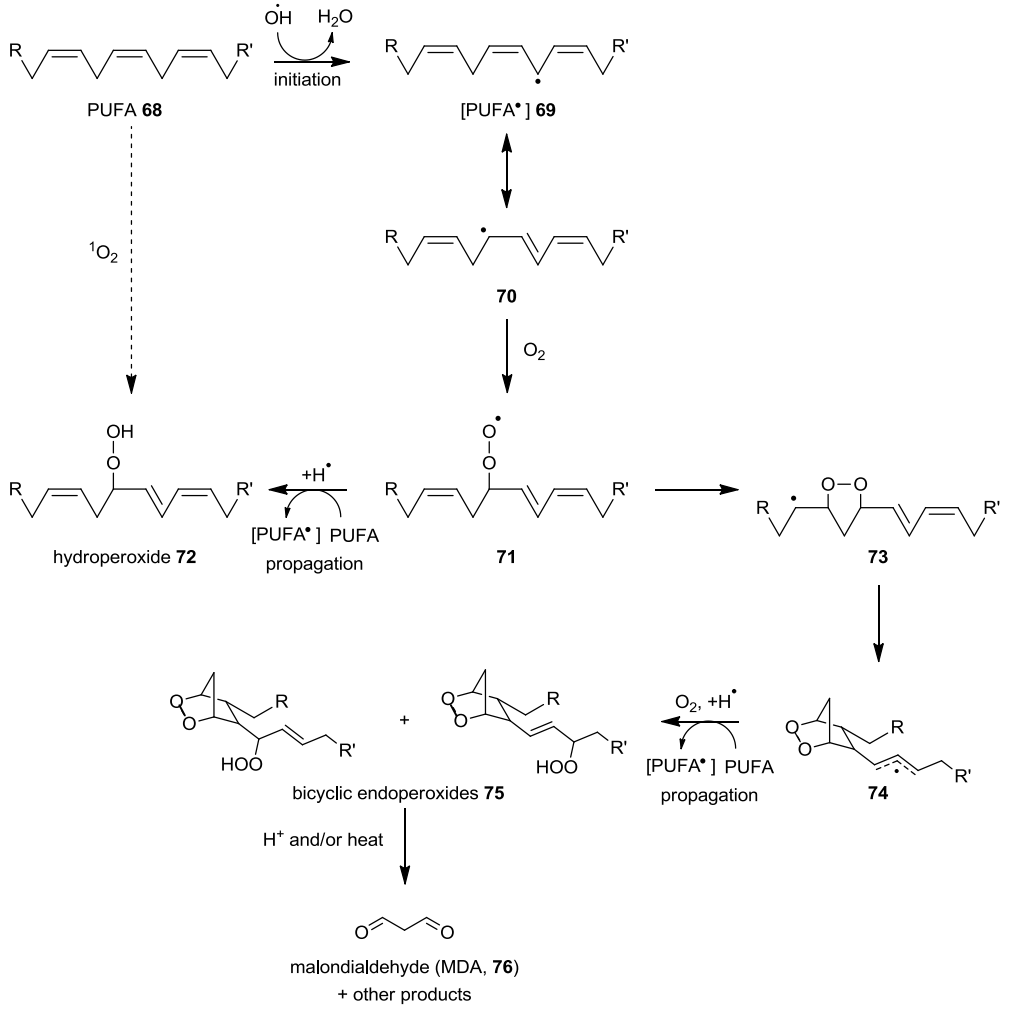
1.2.2.2 Damage to Proteins

The chemistry of oxidative protein damage is even more complex than that of DNA due to the large number of amino acid residues available for modification. Attack by hydroxyl radical or singlet oxygen generates a huge variety of oxidation products, either by addition of the ROS or hydrogen atom abstraction. Initial attack by hydroxyl radical leads to free radicals which can combine with ground state oxygen to form peroxides, or alkoxyl radicals which can fragment by β-scission, releasing carbonyls from the proteins. Furthermore, peroxides can form on the peptide backbone and on amino acid side chains. Oxidative damage to histidine residues in particular can lead to enzyme inactivation. [18]

1.2.2.3 Damage to Cell Membranes: Lipid Peroxidation

The polyunsaturated fatty acid (PUFA) side chains of the phospholipids which comprise the bilayer of cell membranes are a major target of attack for ROS.

The general mechanistic pathway for lipid peroxidation is outlined in Scheme 14.[26]



Scheme 14. General mechanistic pathway of lipid peroxidation

Initiation of peroxidation is usually caused by abstraction of an allylic hydrogen atom from the fatty acid side chain **68** by a radical species – hydroxyl radical readily initiates PUFA peroxidation. Rearrangement of the resultant carbon-centred radical **69** to form a more stable conjugated diene **70** then occurs, followed by combination with ground state oxygen to give a peroxyl radical **71**. This radical can either abstract a hydrogen atom from a neighbouring PUFA to form a hydroperoxide **72**, or cyclise and react with a

further molecule of oxygen before the propagation step of hydrogen abstraction occurs. This latter pathway generates the bicyclic endoperoxides **75**. These can eventually decompose, by heating or in the presence of metal ions, to end products such as malondialdehyde (MDA, **76**) along with a range of unsaturated aldehydes including 4-hydroxy-2-trans-nonenal (HNE), trans-4-hydroxy-2-hexenal (HHE) and acrolein. Epoxides, ketones and hydrocarbons have also been identified as lipid peroxide decomposition products.[18]

Many of these end products of lipid peroxidation are themselves cytotoxic and mutagenic, and can go on to cause further damage to the cell, cross-linking proteins and causing DNA lesions by reaction with amino acid residues and DNA bases.

Hydroperoxides can be generated in a non-radical fashion by an ene reaction of the PUFA with singlet oxygen, although the relevance of this pathway *in vivo* is currently unclear.[27]

1.2.3 Prevention of Oxidative Cell Damage: Low Molecular Mass Antioxidants

Whilst biological systems have developed a number of sophisticated mechanisms to repair the damage caused to cells by oxidative stress,[28] a key element of the defence against such damage lies in prevention. A combination of antioxidant defence enzymes and simple low molecular mass antioxidant molecules are generally used to prevent oxidative damage.[18]

Low molecular mass agents shown to have a protective effect against oxidative cell damage (Figure 5) include tocopherols (eg. α-tocopherol, **77**),[29]

ascorbic acid (**78**),[30] flavonoids (eg. quercetin, **79**)[31] and carotenoids (eg. β-carotene, **80**).[32] The main mechanism of action as antioxidants appears to be the scavenging of ROS. This defence system often involves complex interplay between various antioxidant species; for example ascorbate cooperates with vitamin E, regenerating α-tocopherol (**77**) from α-tocopherol radicals in membranes (see Section 4.4, Scheme 43).[33]

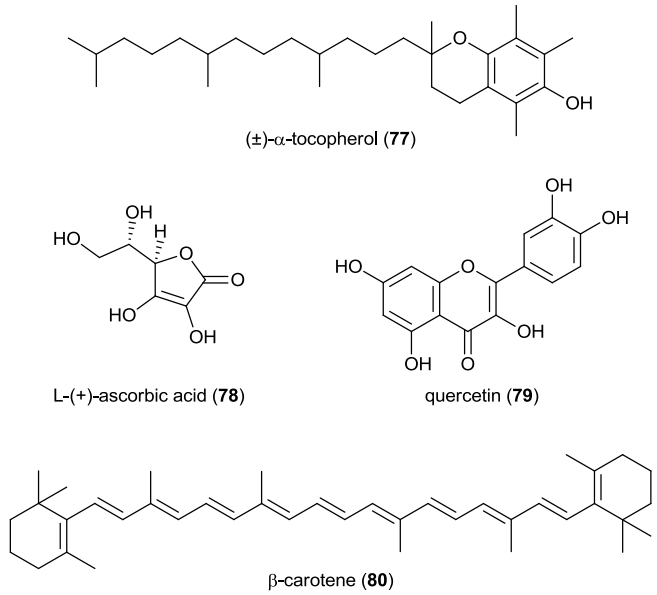
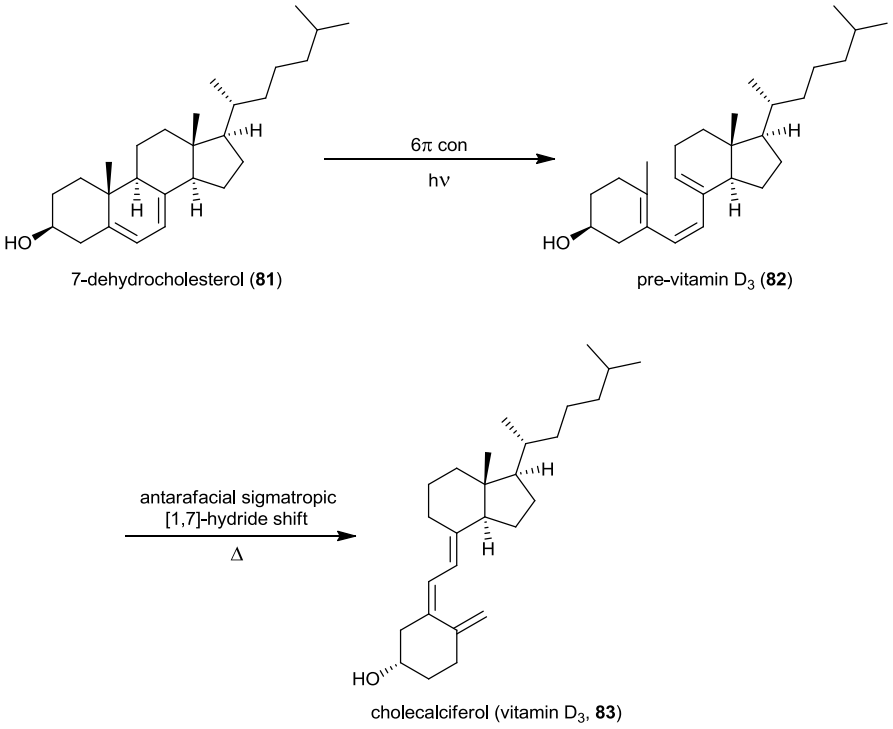


Figure 5. Structures of some well known low molecular mass antioxidants

Many antioxidants are lipophilic in nature and as such tend to reside in the membrane bilayer of cells. A particularly interesting example is that of vitamin D_3 (cholecalciferol, **83**). In addition to its role in the regulation of calcium and phosphate metabolism, cholecalciferol (**83**) has been shown to exert photoprotective effects, in particular as an inhibitor of membrane lipid peroxidation.[34] The biosynthesis of **83** (Scheme 15)[35] bears a striking resemblance to that of the proposed biogenesis of tridachiahydropyrone (**9**), both pathways involving a photochemical 6π electrocyclisation reaction. It has

been suggested that this pathway is partly responsible for the protective action against the damaging effects of UV light.[34]

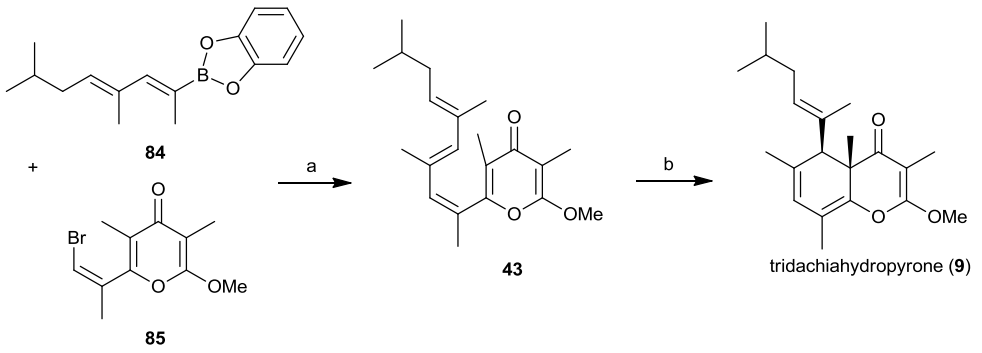


Scheme 15. Biosynthesis of the membrane antioxidant cholecalciferol (**83**)

1.3 Tridachiahydropyrone: Previous Work

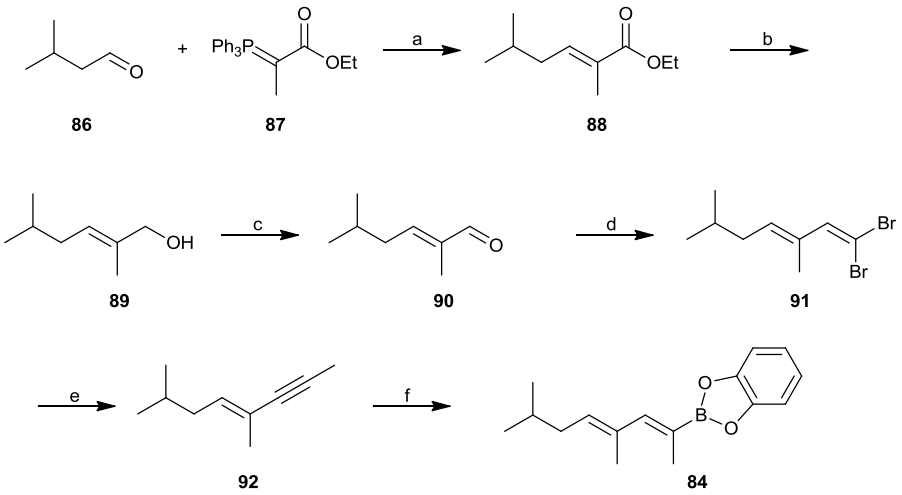
In 2008 Moses and co-workers reported the first total synthesis of tridachiahydropyrone (**9**),[6] prompting the revision of its structure from the originally proposed **11**.[3] The synthesis utilised the (*Z,E,E*)-polyene **43** as a precursor to the natural product, providing support for the biomimetic hypothesis. A Suzuki coupling strategy was employed to construct **43**. Boronic ester **84** was coupled with *Z*-bromopyrone **85**, affording the polyene **43** in 30% yield. The biomimetic step was then attempted, with a solution of **43** in MeOH being placed in natural daylight for three days. This resulted in the

complexity-generating transformation to racemic tridachiahydropyrone (**9**), which was isolated in 29% yield (Scheme 16).



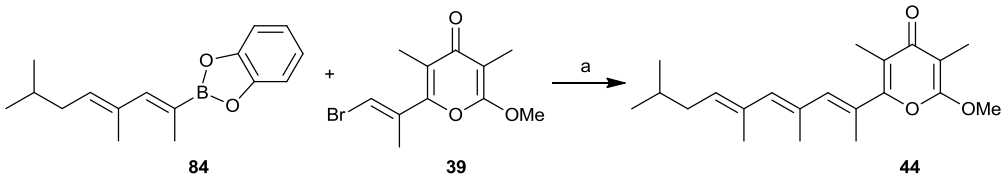
Scheme 16. Moses' biomimetic synthesis of tridachiahydropyrone (**9**) – key steps. Reagents and conditions: (a) $Pd(PPh_3)_4$, aq. KOH, THF, 80 °C, 30%; (b) MeOH, hν, rt., 60 h, 29%

The Suzuki coupling fragment **84** was prepared in six steps from commercially available isovaleraldehyde (**86**), using Wittig and Corey-Fuchs methodology to extend the carbon chain (Scheme 17). The *Z*-bromopyrone **85** was synthesised using a known route.[14]



Scheme 17. Synthesis of boronic ester **84**. Reagents and conditions: (a) CH_2Cl_2, reflux, 12 h, 95%; (b) DIBAL-H, CH_2Cl_2, -78 °C → rt., 12 h, 93%; (c) MnO_2, $CHCl_3$, 50 °C, 71%; (d) PPh_3, CBr_4, CH_2Cl_2, 0 °C → rt., 86%; (e) ^nBuLi, MeI, -78 °C → rt., 70%; (f) catecholborane (neat), 80 °C, >99%

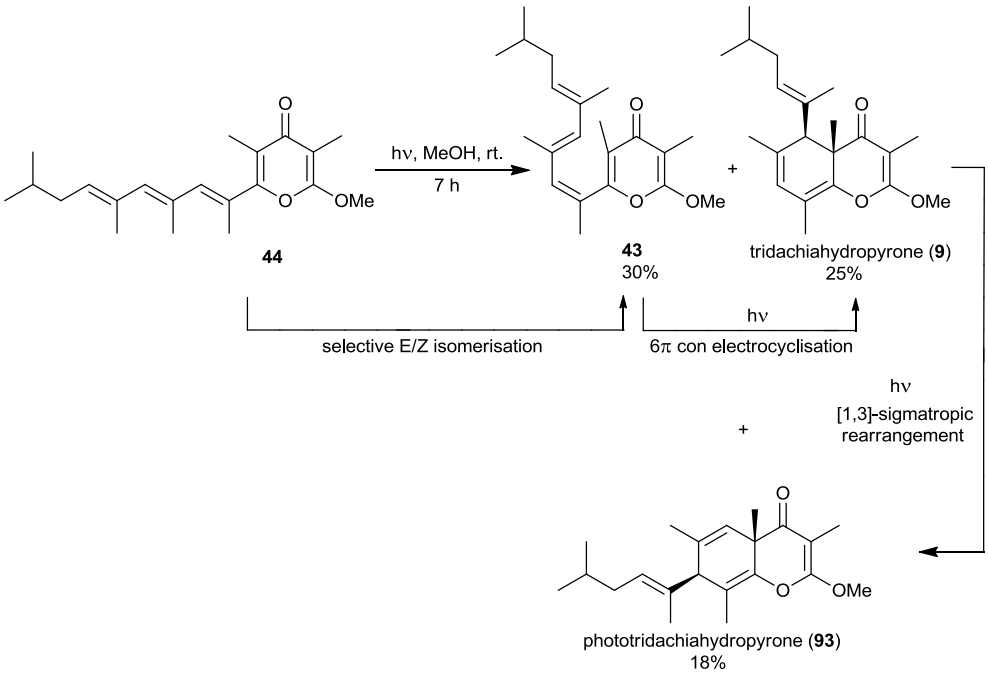
Having proven the feasibility of the 6π conrotatory electrocyclisation, the group then set about constructing the all *E*-polyene **44** in an analogous manner.[7] Boronic ester **84** was coupled to the known *E*-bromopyrone[14] **39** under the same conditions, affording **44** in 55% yield (Scheme 18).



84 **39** **44**

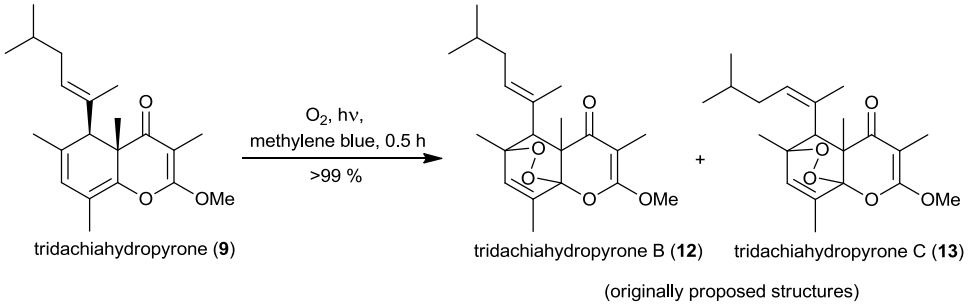
Scheme 18. Construction of (*E,E,E*)-polyene **44**. Reagents and conditions: (a) $Pd(PPh_3)_4$, aq. KOH, THF, 80 °C, 55%

A sample of **44** in deuterated MeOH was irradiated using a UV lamp, and the reaction monitored by ^{1}H NMR spectroscopy (Scheme 19). This revealed formation of the (*Z,E,E*)-polyene **43**, corresponding to a selective *E*/*Z* double bond isomerisation. Further irradiation led to the gradual disappearance of the two polyenes **43** and **44**, accompanied by formation of tridachiahydropyrone (**9**). Prolonged irradiation resulted in the formation of a new, unexpected, product. The structure of the new photoproduct, named phototridachiahydropyrone (**93**), was determined by spectroscopic analysis and X-ray crystallography. The formation of **93** can be explained as arising from a photochemical [1,3]-sigmatropic rearrangement of tridachiahydropyrone (**9**). Whilst phototridachiahydropyrone (**93**) has not been isolated from natural sources, it is reasonable to assume that it is a natural product yet to be discovered.



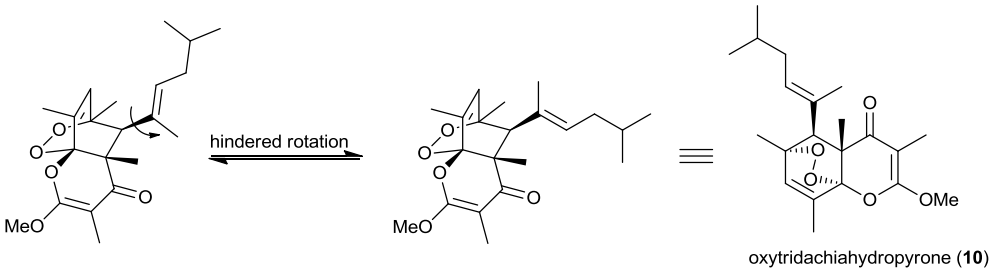
Scheme 19. The biomimetic conversion of **44** into **43**, **9** and **93**

A further biosynthetic hypothesis, namely that tridachiahydropyrones B (**12**) and C (**13**), isolated as an inseparable mixture in 2000 by Schmitz and co-workers,[4] were derived from a photochemical [4+2] cycloaddition of tridachiahydropyrone (**9**) with singlet oxygen, was also explored.[7] Thus a solution of tridachiahydropyrone (**9**) in $CHCl_3$ was irradiated under a continuous flow of molecular oxygen in the presence of methylene blue. This resulted in complete conversion to a new product, the NMR spectroscopic data for which was in agreement with that reported for the inseparable mixture of **12** and **13** (Scheme 20).



Scheme 20. Addition of singlet oxygen to tridachiahydropyrone (**9**)

However, nOe studies indicated that the two proposed inseparable geometric isomers were in fact rotameric forms of a single molecule, which was determined to have the structure **10** and named oxytridachiahydropyrone (Scheme 21). Oxytridachiahydropyrone (**10**) arises from endo addition of singlet oxygen to tridachiahydropyrone (**9**), singlet oxygen approaching its concave face exclusively.



Scheme 21. Rotameric forms of oxytridachiahydropyrone (**10**)

1.4 Aims of this Work

The aim of this work was to further explore the hypothesis regarding the biosynthetic origin of tridachiahydropyrone (**9**) (Section 1.1.4), building on the previous work of the group outlined above (Section 1.3), and focusing on the chemical biology of the molecule and its biomimetic precursors. The research focussed on two main areas.

The first aim of this work was to explore the feasibility of the sunscreen hypothesis, specifically the likelihood that the polyene precursors (**44** and **43**) to tridachiahydropyrone (**9**) are located in the phospholipid bilayer of the cell membrane. This was achieved by studying the interactions of the molecules with a series of model membrane systems, utilising fluorescence-based biophysical techniques.

The second aim was to investigate the photoprotective and antioxidant properties of the pyrone molecules. A number of assay techniques were used in order to establish if the molecules indeed offer protection to cell components from the damaging effects of UV radiation, and furthermore to explore the mechanistic origin of these effects.

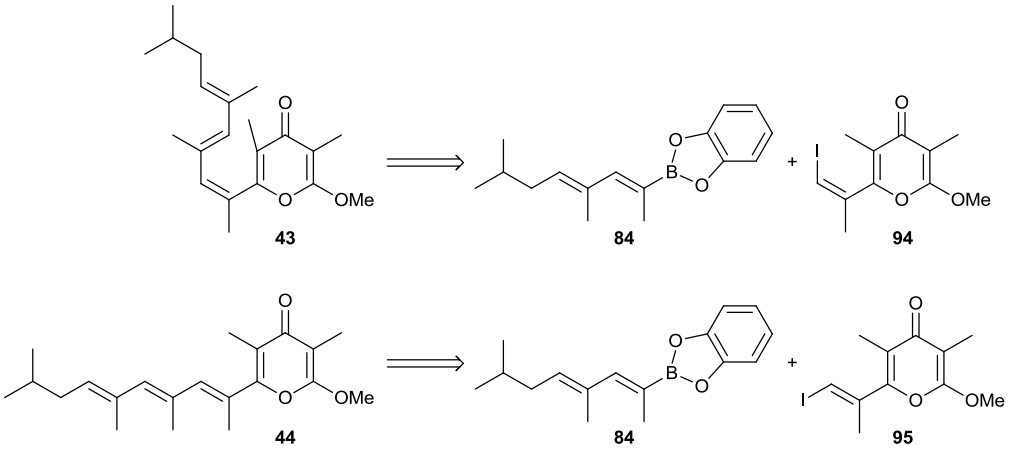
In order to achieve these aims the organic synthesis of tridachiahydropyrone (**9**) and its precursors was initially required.

Chapter 2 Synthesis of the Tridachiahydropyrones and their Biomimetic Precursors

2.1 Revised Synthetic Route

The main problem with the original synthetic route to tridachiahydropyrone (**9**) was the Suzuki coupling step of the boronic ester **84** with the bromo-pyrone fragments **85** and **39** to form the biomimetic precursors **43** and **44** (see Section 1.3, Schemes 16 and 18).[6,7] In addition to being fairly low yielding the yields themselves were found to be inconsistent. As this occurred at such a late stage in the synthesis it was thought preferable to improve upon this reaction if possible.

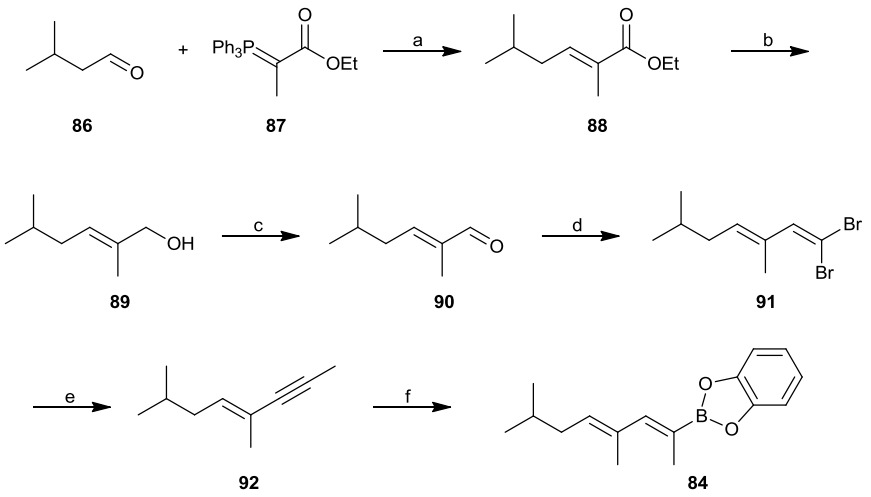
It was postulated that using the iodo-pyrones **94** and **95** in place of their bromo-analogues could improve the efficiency of this step, as iodo compounds are known to be more reactive in cross coupling reactions due to the lower strength of their bonds to carbon in comparison with the other halides.[36] Thus the original retrosynthesis was revised (Scheme 22).



Scheme 22. Revised retrosynthesis of the polyenes **43** and **44**

2.2 Synthesis of the Boronic Ester Coupling Fragment

This synthetic strategy towards the polyenes **43** and **44** had a common intermediate in the boronic ester **84**. This was synthesised from isovaleraldehyde (**86**) in six steps following the known methodology (Scheme 23).[6]

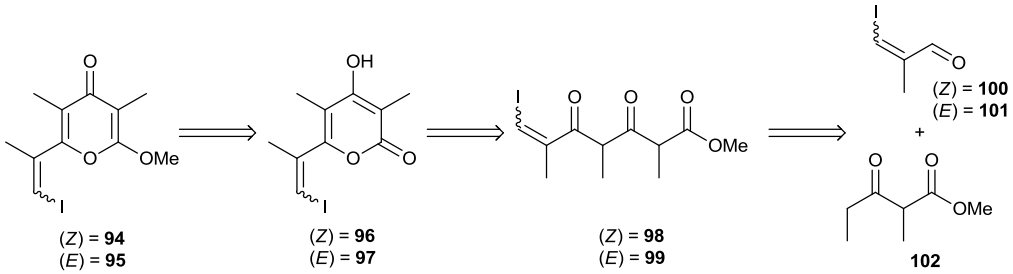


Scheme 23. Synthesis of the coupling fragment **84** from isovaleraldehyde (**86**). Reagents and conditions: (a) CH_2Cl_2, 72 h, Δ, 98%; (b) DIBAL-H, CH_2Cl_2, -78 °C $\rightarrow$ rt., 16 h, 97%; (c) DMP, CH_2Cl_2, 0 °C $\rightarrow$ rt., 30 min, 93%; (d) CBr_4, PPh_3, CH_2Cl_2, 0 °C $\rightarrow$ rt., 1.5 h, 92%; (e) ^{n}BuLi, MeI, THF, -78 °C $\rightarrow$ rt., 18 h, 71%; (f) catecholborane, 80 °C, 2 h, >99%

The synthesis proceeded smoothly, with yields comparable to the literature. One modification was made, with Dess-Martin periodinane (DMP) being used for the oxidation of the allylic alcohol **89** to the aldehyde **90** instead of the original MnO_2-mediated strategy. This improved the yield from 71% to 93%, whilst significantly reducing the reaction time from overnight to just 30 min.

2.3 Synthesis of the Vinyl Iodopyrone Fragments

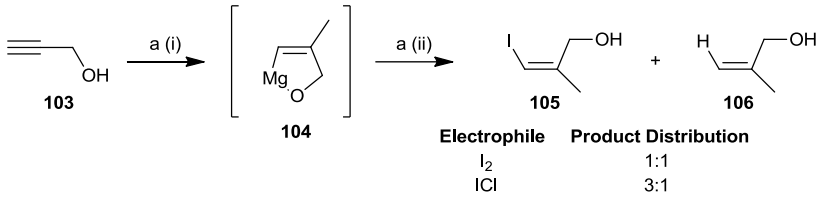
The *Z* and *E* vinyl iodopyrones **94** and **95** had been utilised by Trauner et al. in their syntheses of cyercene A and the placidenes.[37] Their synthetic strategy centred on cyclisation of the triketides **98**/**99**, formed from aldol addition of the dianion of β-ketoester **102** onto the appropriate iodoaldehyde **100**/**101** and subsequent oxidation (Scheme 24).



Scheme 24. Retrosynthesis of the vinyl iodopyrones **94** and **95**

The (*Z*)-iodoaldehyde **100** was synthesised in two steps from commercially available propargyl alcohol (**103**). Addition of Grignard reagent MeMgBr to **103** followed by trapping of the intermediate metallocycle **104** with a source of electrophilic iodine furnished the (*Z*)-iodoalcohol **105**, the required alkene geometry installed stereoselectively by chelation control (Scheme 25). Initial use of I_2 as the electrophile[38] afforded a 1:1 mixture (determined by analysis of the ^{1}H NMR spectrum of the crude reaction mixture) of the desired iodinated and protonated products (**105** and **106** respectively). Whilst these were chromatographically separable, the use of an alternative, more effective electrophile was investigated in order to influence the product ratio in favour of the iodinated product. The use of iodine monochloride[39] proved successful,

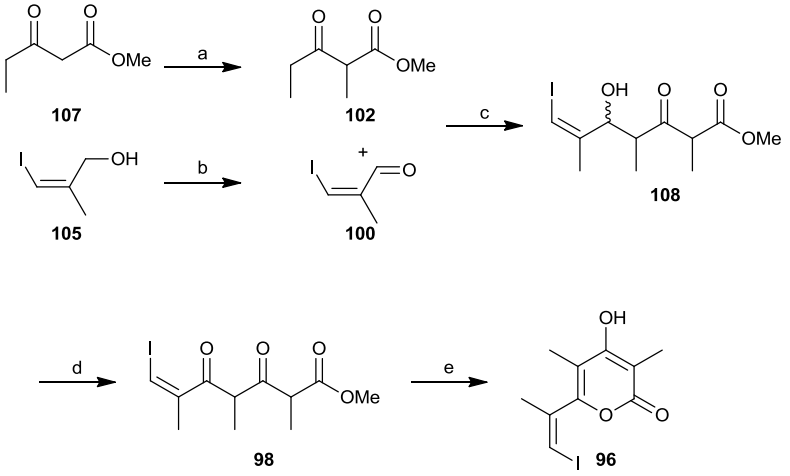
giving an improved product distribution of 3:1 in favour of the desired product.



Scheme 25. Synthesis of the (*Z*)-iodoalcohol **105**. Reagents and conditions: (a) (i) MeMgBr, CuI, Et_2O, -10 °C → rt., 3 h then (ii) ICl, Et_2O, -10 °C → rt., 19 h, 49% (isolated yield of **105**)

Oxidation of **105** with MnO_2 yielded the unstable (*Z*)-iodoaldehyde **100**,[38] which was immediately taken forward to the aldol reaction (Scheme 26). The aldol reaction of **100** with the β-ketoester **102** (itself formed by the facile methylation of methyl propionylacetate (**107**))[40] proceeded smoothly upon a slight modification to Trauner's reported procedure.[37] Formation of the dianion of **102** was reportedly formed by stirring a solution of **102** in THF with NaH for 10 min at 0 °C and then adding ^{n}BuLi and stirring at 0 °C for a further 10 min. A solution of iodoaldehyde **100** in THF was then added to the solution and the mixture stirred at room temperature. However it was found that a stirring time of 10 min at 0 °C was insufficient in this work to promote anion formation, with no product formation observed, and just the β-ketoester **102** recovered upon following this procedure. Stirring the solution at room temperature for 30 min between additions rectified this, with the aldol product **108** formed in good yields as a diastereomeric mixture. Dess-Martin oxidation of **108** and DBU-mediated cyclisation of the resulting triketide **98**

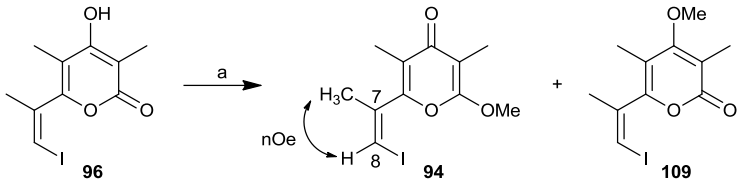
furnished the γ-hydroxy α-pyrone **96** in 73% yield over three steps (from **100** and **102**, Scheme 26).[37]



Scheme 26. Synthesis of the γ-hydroxy α-pyrone **96**. Reagents and conditions: (a) K_2CO_3, THF, Δ, 2.5 h then MeI, 0 °C, 18 h, 97%; (b) MnO_2, CH_2Cl_2, rt., 2 h, 79%; (c) **102**, NaH, THF, 0 °C → rt., 0.5 h then ^{n}BuLi, 0 °C → rt., 0.5 h then **100**, 0 °C → rt., 1.5 h, 80%; (d) DMP, CH_2Cl_2, 0 °C → rt., 3 h, 96%; (e) DBU, toluene, 70 °C, 4 h, 95%

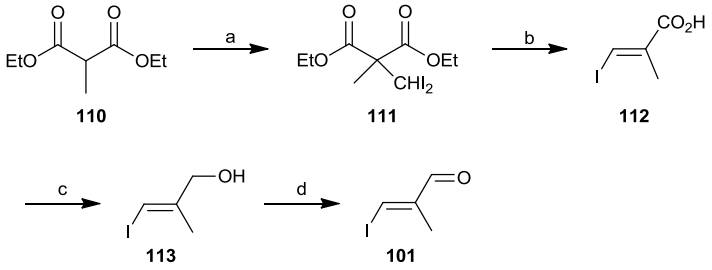
$MeOSO_2F$ is the most effective methylating agent for regioselective α-methylation of γ-hydroxy α-pyrones to form α-methoxy γ-pyrones, and was used by Trauner for the conversion of **96** into the coupling fragment **94**.[37] However, due to its extremely high toxicity alternative methylating agents Me_2SO_4[41] and Me_3OBF_4[42] have also been utilised in γ-pyrone-containing natural product synthesis to achieve analogous transformations.

Treatment of the γ-hydroxy α-pyrone **96** with dimethyl sulfate afforded a mixture of the corresponding γ- and α-pyrones, **94** and **109**, which were easily separable by column chromatography. The desired coupling fragment **94** was thus isolated in 34% yield (Scheme 27). The geometry of the alkene was at this point confirmed as *Z* by nOe studies, a strong through-space correlation observed between the olefinic proton (C8-H) and methyl group (C7-CH_3).



Scheme 27. Formation of the (*Z*)-coupling fragment **94**. Reagents and conditions: (a) Me_2SO_4, Li_2CO_3, acetone, Δ, 96 h, 34% (isolated yield of **94**)

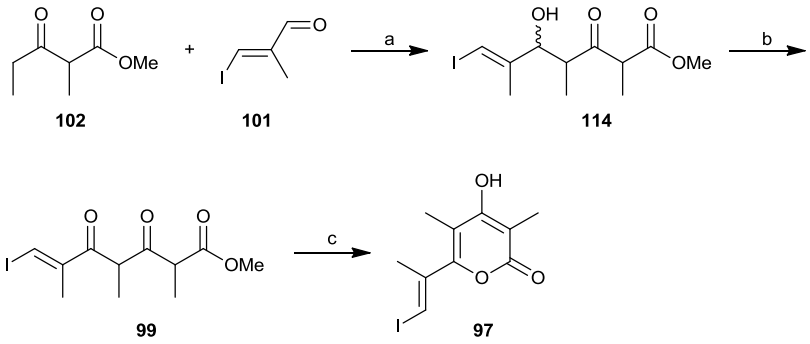
The route to the corresponding *E* isomer **95** was slightly longer, but proved unproblematic, following a published synthesis of the (*E*)-iodoaldehyde **101** in four steps from commercially available diethyl methylmalonate (**110**) (Scheme 28).[43] The key transformation was a base-promoted hydrolysis-decarboxylation-elimination sequence of **111**, itself formed by the nucleophilic substitution reaction between diethyl methylmalonate (**110**) and iodoform. $LiAlH_4$ reduction of the carboxylic acid **112** afforded the corresponding alcohol **113** smoothly, which was oxidised to the desired (*E*)-iodoaldehyde **101** in an analogous manner to its *Z* isomer **100**.



Scheme 28. Synthesis of the (*E*)-iodoaldehyde **101**. Reagents and conditions: (a) NaH, Et_2O, Δ, 2.5 h then CHI_3, Δ, 24 h, 82%; (b) KOH, EtOH-H_2O, Δ, 24 h, 90%; (c) $LiAlH_4$, THF, 0 °C $\rightarrow$ rt., 20 h, 84%; (d) MnO_2, CH_2Cl_2, rt., 2 h, 72%

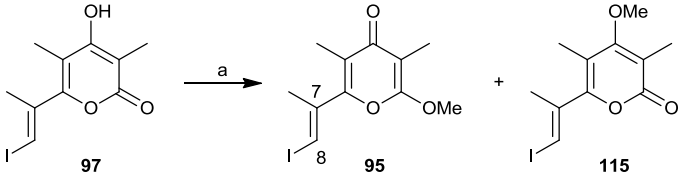
The aldol reaction between (*E*)-iodoaldehyde **101** and β-ketoester **102** proved more sluggish than the analogous reaction with the *Z*-analogue **100**. Whilst addition of **102** to **100** (Scheme 26) was complete (as judged by aldehyde consumption by TLC analysis) within 1.5 h, an extended reaction time of 18 h

was required for the reaction to go to completion in the case of the (*E*)-iodo aldehyde **101**. Shorter reaction times of 2-4 h resulted in incomplete consumption of **101** and disappointing yields of 38-54%. The subsequent oxidation of **114** and DBU-mediated cyclisation of the resultant tricarbonyl **99** afforded the γ-hydroxy α-pyrone **97** in 66% yield over three steps (Scheme 29).



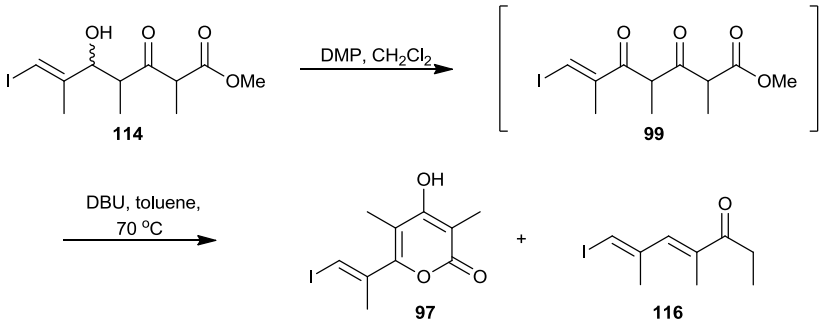
Scheme 29. Synthesis of the γ-hydroxy α-pyrone **97**. Reagents and conditions: (a) **102**, NaH, THF, 0 °C → rt., 0.5 h then ^{n}BuLi, 0 °C → rt., 0.5 h then **101**, 0 °C → rt., 18 h, 71%; (b) DMP, CH_2Cl_2, 0 °C → rt., 1 h, 98%; (c) DBU, toluene, 70 °C, 2 h, 95%

The γ-hydroxy α-pyrone **97** was converted into the coupling fragment **95** under the same conditions used for methylation of the *Z* isomer (Scheme 30). Again an easily separable mixture of isomers was formed, with the desired product **95** isolated in 42% yield. The geometry of the alkene was again confirmed by nOe studies, with no significant nOe observed between the olefinic proton (C8-H) and methyl group (C7-CH_3).



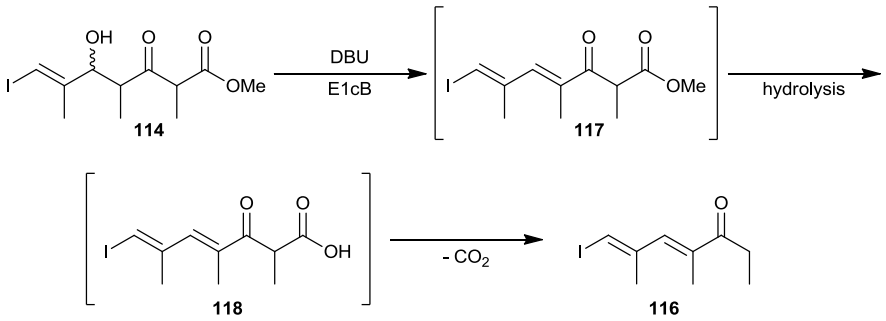
Scheme 30. Formation of the (*E*)-coupling fragment **95**. Reagents and conditions: (a) Me_2SO_4, Li_2CO_3, acetone, Δ, 18 h, 42% (isolated yield of **95**)

During the synthesis of the γ-hydroxy α-pyrone **97** an interesting side reaction was discovered. The conversion of **114** into **97** was attempted in a telescoped manner, without the usual chromatographic purification of the intermediate triketide **99**. At the end of this reaction sequence an unexpected non-polar compound was isolated in addition to the desired pyrone **97**. Spectroscopic analysis revealed this byproduct to be the novel diene **116** (Scheme 31).



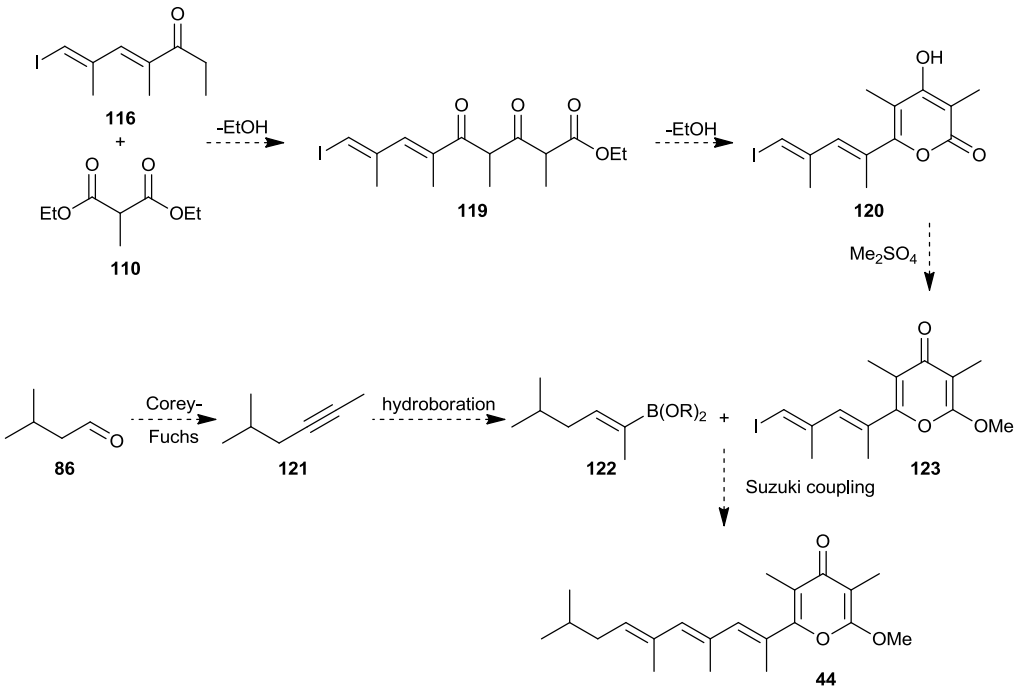
Scheme 31. Unexpected byproduct formation

Analysis of the ^{1}H NMR spectrum of the crude product **99** used in the cyclisation reaction revealed a significant quantity of the unoxidised alcohol **114** to be present. It is thus highly probable that **116** was generated from **114** upon heating in the presence of DBU by an elimination-saponification-decarboxylation sequence, as outlined in Scheme 32.



Scheme 32. Generation of the byproduct **116**: likely mechanism

This side reaction was deemed of interest because the byproduct **116** could potentially be used in an adapted route to the desired polyene pyrone **44**, which would be shorter than the existing route used. This potential new route is outlined in Scheme 33.

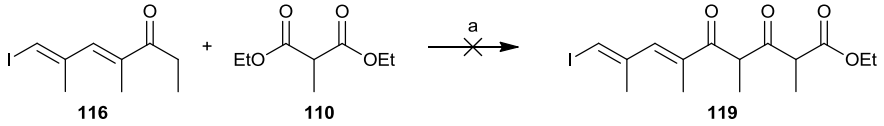


Scheme 33. Proposed new route to the pyrone **44** via **116**

Of this proposed synthetic sequence, the initial condensation step between **116** and diethylmethylmalonate (**110**) to form the extended tricarbonyl **119** was potentially problematic, with several self- and cross-condensation products possible. In addition, literature precedent for this reaction was scarce, the only examples of malonates used as electrophiles in condensation reactions generally involving an activated derivative such as the acyl chloride.[44]

NaHMDS was chosen as a strong bulky base for the initial deprotonation of **116**. This deprotonation was carried out at -78 °C with stirring for 0.5 h, with

the development of a strong yellow colour indicating this step had been successful. This solution was then transferred into a solution of malonate **110** in THF also at -78 °C, and the mixture stirred at -78 °C for 0.5 h. TLC analysis indicated no reaction after this time and so the temperature was increased to -30 °C, to rt., and then further to 50 °C. However still no reaction was observed to have occurred, and upon work up both unreacted starting materials were present in the ^{1}H NMR spectrum of the crude reaction mixture as the only components (Scheme 34).



116 **110** **119**

Scheme 34. Attempted condensation of **116** with diethylmethylmalonate (**110**). Reagents and conditions: (a) NaHMDS, **116**, THF, -78 °C, 0.5 h then **110**, -78 °C → 50 °C, 20 h

There are two possible explanations for the observed outcome in this case. Firstly it is possible that no reaction at all occurred between **110** and the deprotonated **116**, with the anion of **116** remaining stable in solution until the reaction was quenched, whereupon it would have been reprotonated, regenerating the starting material. However, as the temperature was raised to 50 °C during the course of the reaction it seems unlikely that the system would have remained so completely inert. A second plausible explanation then is that, instead of nucleophilic attack of the anion of **116** onto the ester moiety of **110** in a Claisen-type condensation reaction, deprotonation of the acidic malonate proton by the anion of **116** occurred, regenerating **116** in

addition to a relatively stable malonate anion, which remained in solution until being reprotonated upon quenching of the reaction mixture.

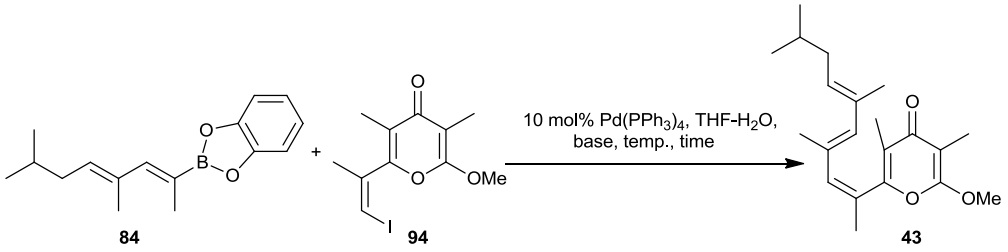
2.4 Suzuki Coupling: Synthesis of the Biomimetic Precursors

With the boronic ester **84**, and the iodopyrones **94** and **95**, in hand, the key Suzuki coupling step was attempted. The (*Z*)-iodopyrone **94** and **84** were first exposed to the coupling conditions used in the original Moses group synthesis with the bromo analogue **85** (see Section 1.3).[6] This used a slight excess of the boronic ester fragment **84**, with KOH as base in an aqueous THF solvent system, and $Pd(PPh_3)_4$ as the catalyst. Heating at 80 °C for 20 h afforded the desired product **43** in a disappointing 19% yield (Table 1, Entry 1). Whilst after this time unreacted starting material was present in the crude reaction mixture (as judged by analysis of TLC and ^{1}H NMR post-work up), increasing the reaction time to 48 h did not increase the yield, or result in full consumption of the limiting substrate **94** (Table 1, Entry 2). This suggested that the catalyst was becoming inactive before the reaction went to completion. It was reasoned that increasing the rate of reaction would likely improve the yield.

Use of TlOEt, in place of more commonly utilised bases such as KOH, K_2CO_3 and NaOMe, has been reported by Roush to greatly accelerate Suzuki coupling reactions and lead to improved yields.[45] Thus the use of TlOEt as base was investigated. The result of the initial experiment (Table 1, Entry 3) was encouraging, with a greatly improved yield of 65% being obtained, at a lower temperature of 50 °C and much reduced reaction time. Whilst the reaction did

indeed go to completion under these conditions, the separation of **43** from the excess unreacted boronic ester **84** proved difficult due to their similar polarities, accounting for the less than perfect 65% yield. A ratio of 3.5:1 boronic ester **84** : iodo **94** had been chosen based on the published representative experimental procedure. Roush et al. had discovered that in many cases a large excess of the boronic acid/ester coupling component was required, due to issues with the solubility of the ate complex formed *in situ*.

A series of reactions was next conducted, systematically lowering the equivalence of the boronic ester **84** used. It was found that lowering the ratio of **84**:**94** increased the isolated yield of **43**, by increasing the ease of chromatographic purification (Table 1, Entries 3-6). 2 equivalents of **84** gave an excellent 95% yield (Table 1, Entry 6).

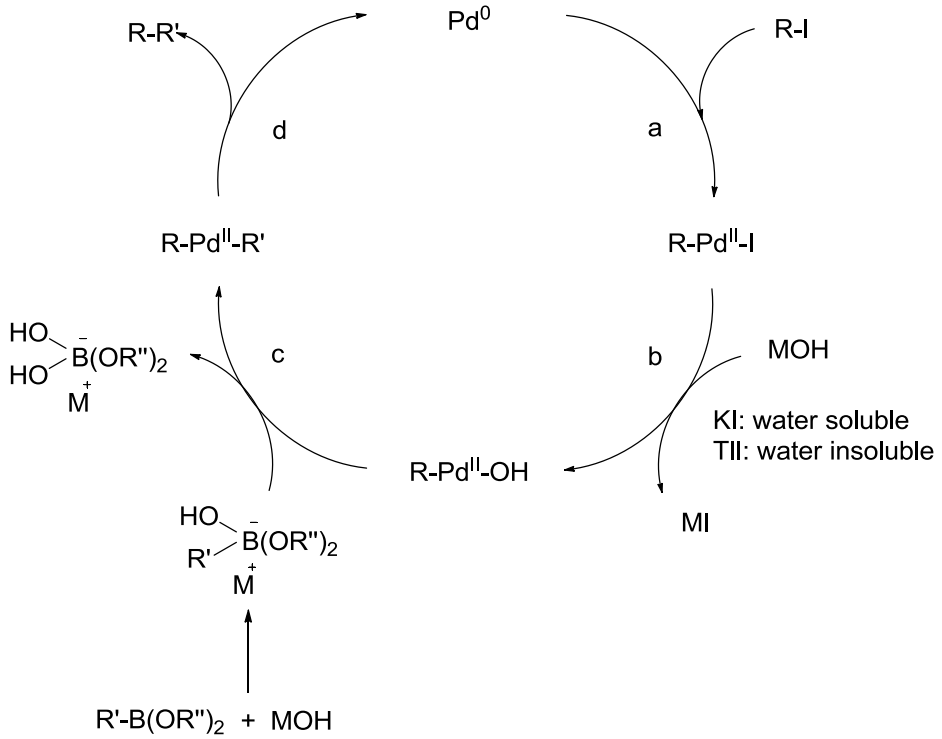


84 94 43

Entry	Ratio 84:94	Base	Temp.	Time	Yield
1	1.3:1	KOH	80 °C	20 h	19%
2	1.3:1	KOH	80 °C	48 h	18%
3	3.5:1	TlOEt	50 °C	3 h	65%
4	3:1	TlOEt	50 °C	3 h	66%
5	2.5:1	TlOEt	50 °C	3 h	77%
6	2:1	TlOEt	50 °C	4 h	95%

Table 1. Key Suzuki coupling to form the (*Z,E,E*)-polyene **43**: conditions screened

The improvement in yield upon switching to TlOEt as base can be rationalised by reference to the catalytic cycle of the Suzuki coupling reaction. A general cycle is depicted in Scheme 35. Kishi et al. suggest step b to be the rate determining step of the cycle for many substrates.[46] When the metal counterion of the base used is potassium or sodium, the metal iodide byproduct is soluble in the reaction medium. However, when the base is TlOH (generated *in situ* from TlOEt and H_2O), the TlI salt formed is insoluble, precipitating out, and thus driving the step forward. Thus the rate of the reaction is increased, allowing the reaction to go to completion before the catalyst becomes deactivated, and resulting in improved yields.

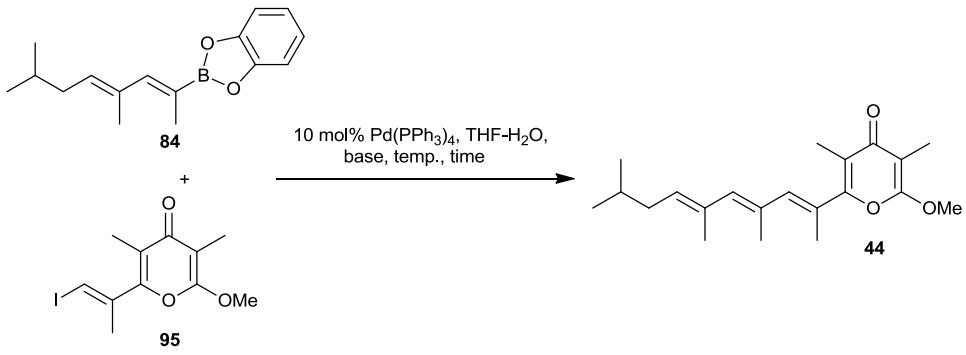


Scheme 35. General catalytic cycle for the Suzuki coupling reaction, depicting (a) oxidative addition, (b) ligand exchange, (c) transmetallation and (d) reductive elimination steps.

This interpretation also accounts for the lack of improvement in reaction outcome observed in switching from the bromopyrone fragment **85** (Section

1.3, Scheme 16: 30%) to its iodo analogue **94** (Table 1, Entry 1: 19%), under the same coupling conditions. The higher reactivity of iodides over bromides in coupling reactions lies in the relative strengths of their bonds to carbon. A carbon-iodine bond is weaker and thus undergoes oxidative addition (step a) more readily. However, if the oxidative addition step is not rate limiting then the reaction outcome is unlikely to be affected by this factor.

A similar trend in yields was observed for the synthesis of the (*E,E,E,)*-polyene pyrone **44** (Table 2).



Entry	Ratio 84:94	Base	Temp.	Time	Yield
1	1.1:1	KOH	80 °C	20 h	14%
2	3:1	TlOEt	50 °C	3 h	58%
3	2.5:1	TlOEt	50 °C	4.5 h	74%
4	2:1	TlOEt	50 °C	4 h	92%
5	1.3:1	TlOEt	50 °C	20 h	23%

Table 2. Key Suzuki coupling to form the (*E,E,E*)-polyene **44**: conditions screened

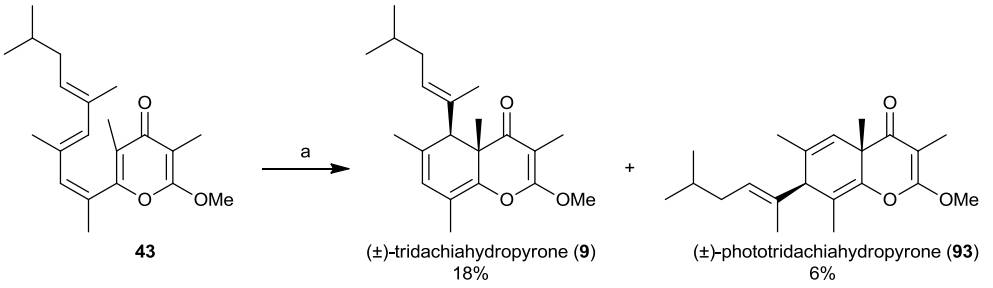
Again, substituting KOH for TlOEt resulted in higher yields, and lowering the equivalence of the boronic ester **84** improved the yields due to increasing the ease of purification. Lowering the equivalence of **84** below 2 however had a

detrimental effect, with the yield dropping from an excellent 92% for 2 equivalents (Table 2, Entry 4) to just 23% when 1.3 equivalents was used instead (Table 2, Entry 5). At such a low concentration, solubility of the ate complex presumably becomes a hindrance.

2.5 Biomimetic Synthesis of the Tridachiahydropyrone Family

The key biomimetic conversion of the (*Z,E,E*)-polyene **43** into tridachiahydropyrone (**9**) was next investigated. A sample of **43** was dissolved in anhydrous methanol, and the solution thoroughly purged with argon. The solution was then irradiated using a medium pressure mercury lamp (125 W). Previous work had shown that after seven hours, further exposure to UV light promoted the rearrangement of the product tridachiahydropyrone (**9**) into phototridachiahydropyrone (**93**).[7] In order to try to avoid this, and maximise tridachiahydropyrone (**9**) synthesis, after an initial six hours of irradiation the solvent was removed under reduced pressure and the product **9** isolated by preparative TLC. However, an additional band was observed on the TLC plate, attributable to the rearranged product **93**. Both products were isolated, and the remaining starting material **43** re-dissolved in anhydrous methanol, re-purged with argon, and re-exposed to UV light. To try and prevent further isomerisation the reaction was this time stopped after 5 h, and the isolation process repeated. As still some phototridachiahydropyrone (**93**) production was observed, the next two cycles of irradiation were limited to three hours each. After a total 17 h of irradiation (6 h + 5 h + 3 h + 3 h) tridachiahydropyrone (**9**) had been isolated in 18% yield, along with 6% of the

rearranged photoproduct **93**, and 70% recovered starting material, (*Z,E,E*)-polyene **43** (Scheme 36).



Scheme 36. Biomimetic conversion of **43** into **9** and **93**, using multiple purification technique. Reagents and conditions: (a) hν, MeOH, rt., 17 h total irradiation time (with purification carried out after 6 h, 5 h, 3 h, 3 h irradiation periods) (70% starting material **43** also recovered)

This technique, with multiple cycles of irradiation and purification, was labour intensive and time consuming, the 17 h of total irradiation time requiring four days work in order to isolate a relatively small quantity of the desired natural product **9**, and still not preventing formation of the phototridachiahydropyrone (**93**) byproduct. In order to discern whether this technique was really beneficial, an NMR study into the photoconversion of **9** to **93** was conducted. Work previously conducted in the group had found that 24 h irradiation promoted full conversion of **9** to **93**.[7] As that work had also led to the generation of comparable yields of tridachiahydropyrone (**9**) (25% yield of **9** from **44** in 7 h, see Section 1.3, Scheme 19) in shorter times than the current work (Scheme 36), it was deemed worthwhile to reinvestigate the kinetics of the photoconversion.

Thus a solution of tridachiahydropyrone (**9**) was dissolved in $CDCl_3$, degassed by purging with argon, and then irradiated. The photochemical sigmatropic rearrangement to form phototridachiahydropyrone (**93**) was monitored over

time by analysis of the ^{1}H NMR spectrum of the reaction mixture. The relative intensities of the olefinic proton signals of the two compounds were used in order to determine the ratio of **9**:**93** at various intervals. The results are depicted in Figure 6.

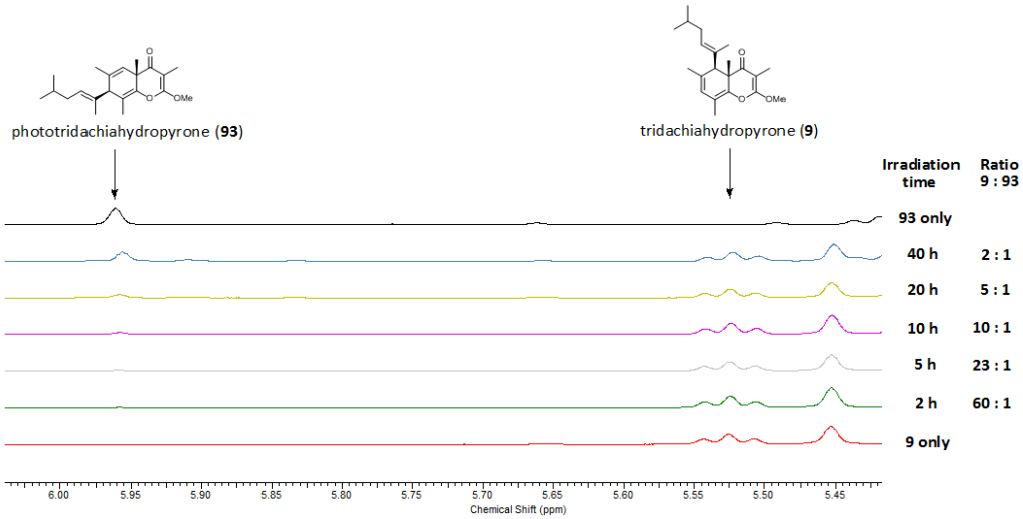
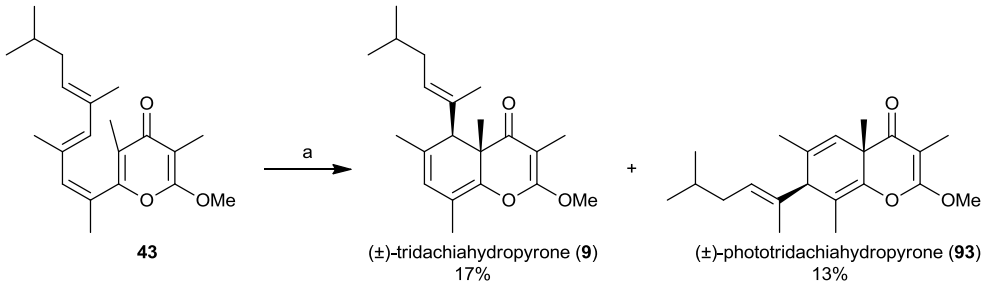


Figure 6. NMR study into the photochemical conversion of **9** into **93**

From this study it can be seen that after even 40 h irradiation time tridachiahydropyrone (**9**) is the major component in the reaction mixture, the ratio of **9**:**93** at this point being 2:1. Whilst the same lamp was used for irradiation in the current and previous work, the differences in reaction rates can perhaps be explained by small experimental differences such as the distance between the reaction vessel and UV light source. From these results it was decided that the time consuming strategy of multiple purification steps after short irradiation times was not necessary in order to prevent significant depletion of the desired tridachiahydropyrone (**9**).

In light of this, the biomimetic photochemical electrocyclisation of the (*Z,E,E*)-polyene pyrone **43** into **9** was repeated, this time exposing the substrate to 37

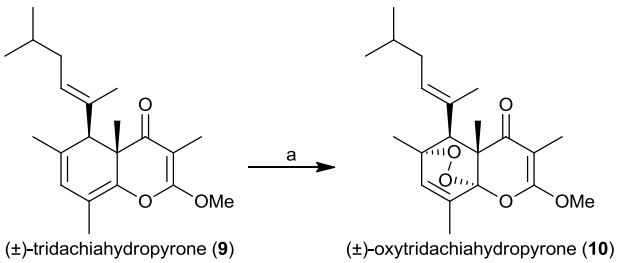
h continuous irradiation (Scheme 37). Whilst this strategy did increase the isolated yield of phototridachiahydropyrone (**93**), the longer overall irradiation time afforded comparable yields of **9** in a shorter space of time, and with just a single purification step required at the end of the irradiation time.



43 (±)-tridachiahydropyrone (**9**) 17% (±)-phototridachiahydropyrone (**93**) 13%

Scheme 37. Biomimetic conversion of **43** into **9** and **93**, by continuous irradiation. Reagents and conditions: (a) hν, MeOH, rt., 37 h (62% starting material **43** also recovered)

Having optimised the synthetic strategy for synthesis of tridachiahydropyrone (**9**), its conversion into the related natural product oxytridachiahydropyrone (**10**) was next conducted. This was achieved by irradiation of a methanolic solution of **9** in the presence of molecular oxygen and the photosensitiser methylene blue. The [4+2] cycloaddition of singlet oxygen to **9** proceeded smoothly, generating the desired product **10** in 97% yield (Scheme 38).



(±)-tridachiahydropyrone (**9**) (±)-oxytridachiahydropyrone (**10**)

Scheme 38. Synthesis of oxytridachiahydropyrone (**10**). Reagents and conditions: (a) MeOH, methylene blue, O_2, hν, 5 h, 97%

As in the previous photochemical reactions studied, a longer irradiation time was again required in comparison with that reported in earlier work (5 h *cf.* 0.5 h, see Section 1.3, Scheme 20).[7]

Having successfully synthesised the compounds of the tridachiahydropyrone family, namely tridachiahydropyrone (**9**), phototridachiahydropyrone (**93**) and oxytridachiahydropyrone (**10**), along with their proposed biomimetic precursors the (*Z,E,E*)-polyene pyrone **43** and the (*E,E,E*)-polyene pyrone **44**, via an optimised synthetic route, attention was next turned to investigating the feasibility of the sunscreen hypothesis, using a range of biophysical techniques.

Chapter 3 Interactions of the Tridachiahydropyrones with Model Membrane Systems: Biophysical Studies

A key facet of the sunscreen hypothesis involves the location of the biomimetic tridachiahydropyrone precursors, **43** and **44**, in the phospholipid bilayer of the cell membrane of the producing mollusc. A range of biophysical studies was thus conducted in order to explore the feasibility of this situation, by assessing the interactions of **43** and **44**, along with tridachiahydropyrone (**9**) itself (Figure 7), with a number of model membrane systems.

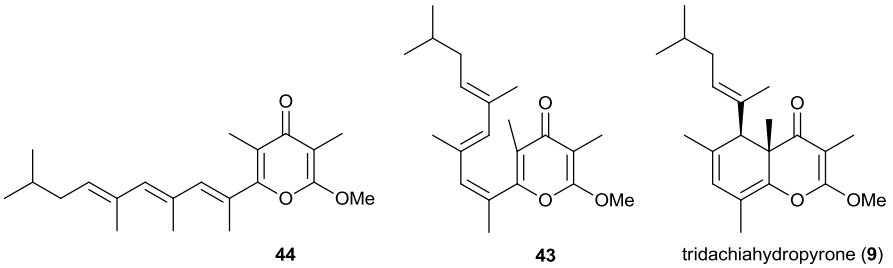


Figure 7. The molecules investigated in the biophysical studies

3.1 Liposomes as Experimental Membrane Models

Liposomes were used as simple experimental models of the lipid bilayer for these studies. The type used were monodisperse, unilamellar phospholipid vesicles (PLVs) of 100 nm diameter, prepared using a pressure extrusion technique (see Section 6.2.3).[47] PLVs of varying compositions were prepared, comprising phosphatidylcholine (PC), cholesterol (Chol) and sphingomyelin (SM) (Figure 8).

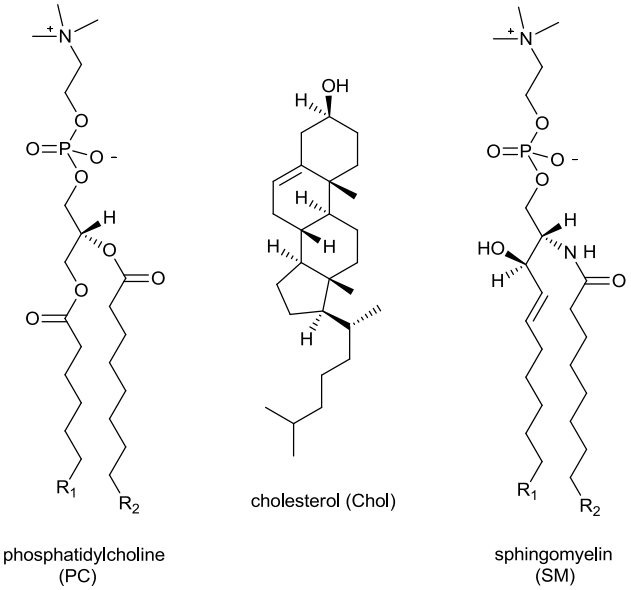


Figure 8. Structures of the membrane components used in this study

These PLVs provided model systems of increasing complexity to represent the membrane bilayer. The plasma membrane is a heterogeneous environment, with specific membrane components, such as cholesterol and sphingomyelin, selectively co-localising into regions of short range order known as microdomains or membrane rafts.[48] There are three main phases found in biological membranes, each of a differing degree of order.[49] These are depicted in Figure 9.

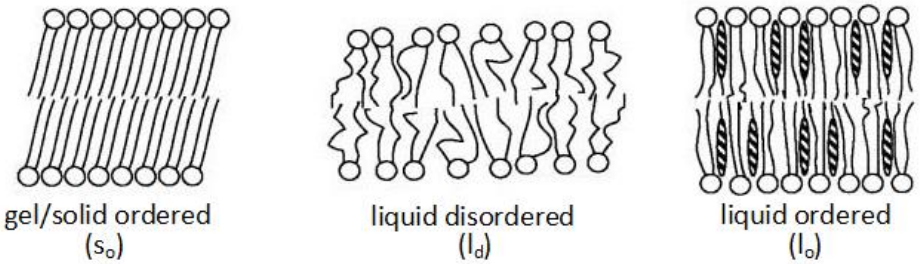


Figure 9. The three phases found within membranes. Adapted from reference 49

Hydrated lipid bilayers undergo phase transitions as a function of temperature. At low temperatures they exist in the solid ordered (s_o), or gel, phase. At higher temperatures they undergo a phase transition to the liquid

disordered (l_d) phase, with the bilayer moving from a quasi-two dimensional crystalline solid to a quasi-two dimensional liquid.[50] There is a drastic reduction in both the translational order in the bilayer plane and also the conformational order of the acyl chains upon this transition. In the s_o phase the hydrocarbon chains are extended and tightly packed together, with the carbon-carbon single bonds predominantly in the trans conformation. Transition to the l_d phase is characterised by an increase in trans-gauche conformational isomerisations in the acyl chains. This increase in disorder of the acyl chains of the lipids has led to this transition being known as the chain-melting transition. The incorporation of cholesterol into phospholipid liposomes induces a third phase, known as the liquid ordered (l_o) phase, which can coexist with the l_d phase.[51] This third phase occurs due to cholesterol's ability to increase the conformational order of the acyl chains of surrounding lipids because of its rigid fused ring structure. In the l_o phase the degree of translational freedom (lateral mobility) of the lipid molecules is similar to that of the l_d phase, whilst the conformational order of the acyl chains is more akin to that of the s_o phase.[49]

In relation to biological cells, at physiological temperatures the plasma membrane is accepted to be liquid, without an s_o phase. The cholesterol-poor bulk phospholipid is considered to be in the l_d phase, with the cholesterol-enriched raft regions constituting the coexisting l_o phase.[50]

Experimental studies on PC/Chol/SM liposomal systems have led to the development of ternary phase diagrams showing the thermotropic phase

behaviour at varying compositions of these three components (Figure 10).[50]

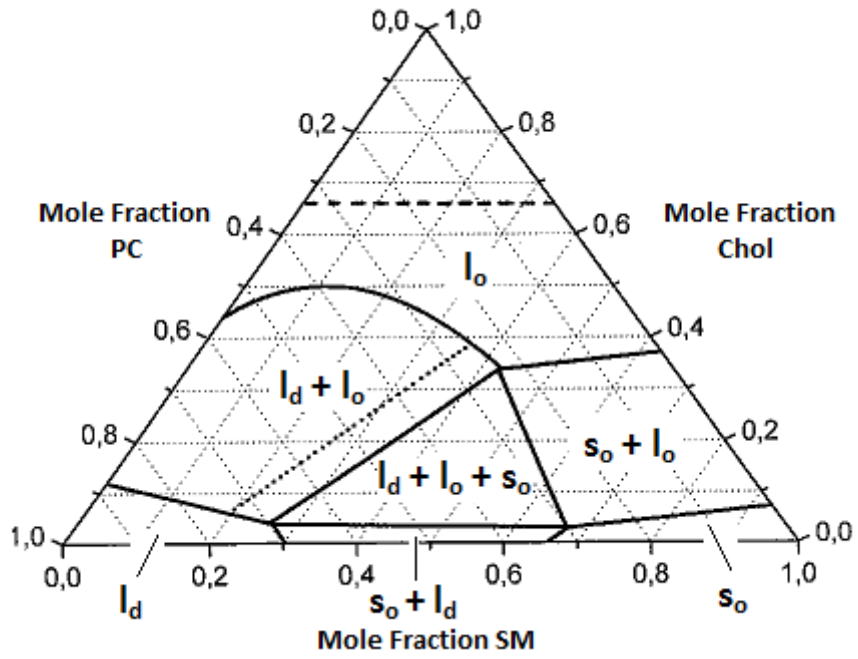


Figure 10. Ternary phase diagram depicting the phase behaviour of PC/Chol/SM liposomes at 25 °C. Adapted from reference 50

The membrane compositions used in this study are as follows, with the subscript value representing the molar percentage of each component in the liposomal mixture. The phases present in the liposomes of each composition, as depicted by Figure 10, are given in brackets:

$PC_{100\%}$ (l_d) $PC_{70\%}Chol_{30\%}$ (l_d+l_o) $PC_{70\%}SM_{30\%}$ (s_o+l_d)

$PC_{60\%}Chol_{20\%}SM_{20\%}$ (l_d+l_o) $PC_{40\%}SM_{60\%}$ (s_o+l_d)

These compositions were chosen as they span the range of phase behaviours at the temperature (25 °C) used in these experiments, enabling the interactions of the tridachiahydropyrones with membrane systems of varying degrees of order to be investigated.

3.2 Behaviour of the Polyene Pyrones in Solution: Critical Micelle Concentrations

Prior to investigating the interactions of the tridachiahydropyrones with the model membranes, the behaviour of the biomimetic precursors **44** and **43** in solution was studied to see whether their amphipathic character caused them to self aggregate to form micelles. This was achieved by determination of the critical micelle concentration (CMC) – that is, the concentration above which molecules form micelles - for each molecule, using a 90° light scattering technique.[52]

This technique is reliant upon the following expression (Equation 1), which, for classical Rayleigh-Debye scattering, relates the intensity of the scattered light (I_s) to the particle concentration (c) and the scattering coefficient (ε_s).

Equation 1: $I_s = \varepsilon_s \cdot c$

The scattering coefficient is proportional to the volume of the scattering particle. Thus micellar aggregates of molecules have a far greater ε_s than the monomeric molecule itself. Since ε_s(micelle)>>ε_s(monomer) a significant increase in I_s is observed upon transition from a monomeric dispersion of molecules to micelles. Measuring the I_s (light scattering of samples at 90°) with increasing compound concentration therefore affords a plot which fits to two straight line equations ($y = mx + c$), one corresponding to pre-CMC

scattering and one to post-CMC scattering, with the intercept of these two lines corresponding to the point of CMC (Figure 11).

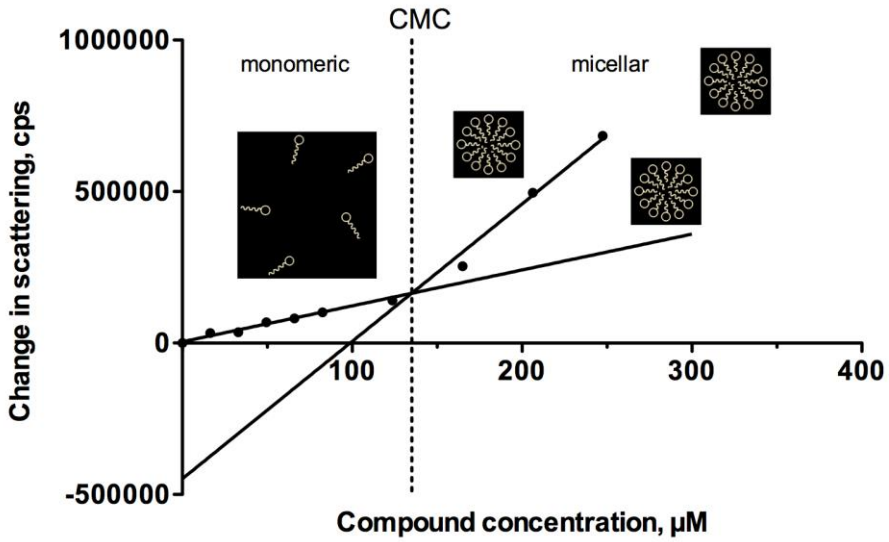


Figure 11. Determination of CMC using 90° light scattering. Exemplified for **44** in $PC_{100\%}$ PLVs

Figure 12A shows that the light scattering observed from a solution of **44** in Tris buffer increased significantly at relatively low concentrations of **44**, confirming the molecule's propensity to self aggregate in solution. This was also the case for **43** (Figure 13A). Analysis of this data showed the CMC of **44** in solution to be 40.1 µM, and that of **43** to be 19.0 µM. These values are comparable to phosphatidylcholine molecules with fatty acid chains of 9-carbon length (CMC of 09:0 PC = 0.029 mM).[53] This behaviour strengthens the argument that **44** and **43** are structurally similar to phospholipids and so would reside comfortably within the lipid bilayer of the plasma membrane.

The CMCs of these two molecules were next determined in the presence of $PC_{100\%}$ and $PC_{70\%}Chol_{30\%}$ phospholipid vesicles (PLVs). This was done in order to ascertain whether the molecules would preferentially interact with the

membrane or preferentially interact with each other. If interaction with membranes was preferred, the presence of PLVs should cause an increase in the CMC. This was indeed observed to be the case for **44** and **43**, with the onset of significantly increased light scattering delayed substantially by the presence of both $PC_{100\%}$ (Figures 12B and 13B) and $PC_{70\%}Chol_{30\%}$ (Figures 12C and 13C) PLVs in the solution.

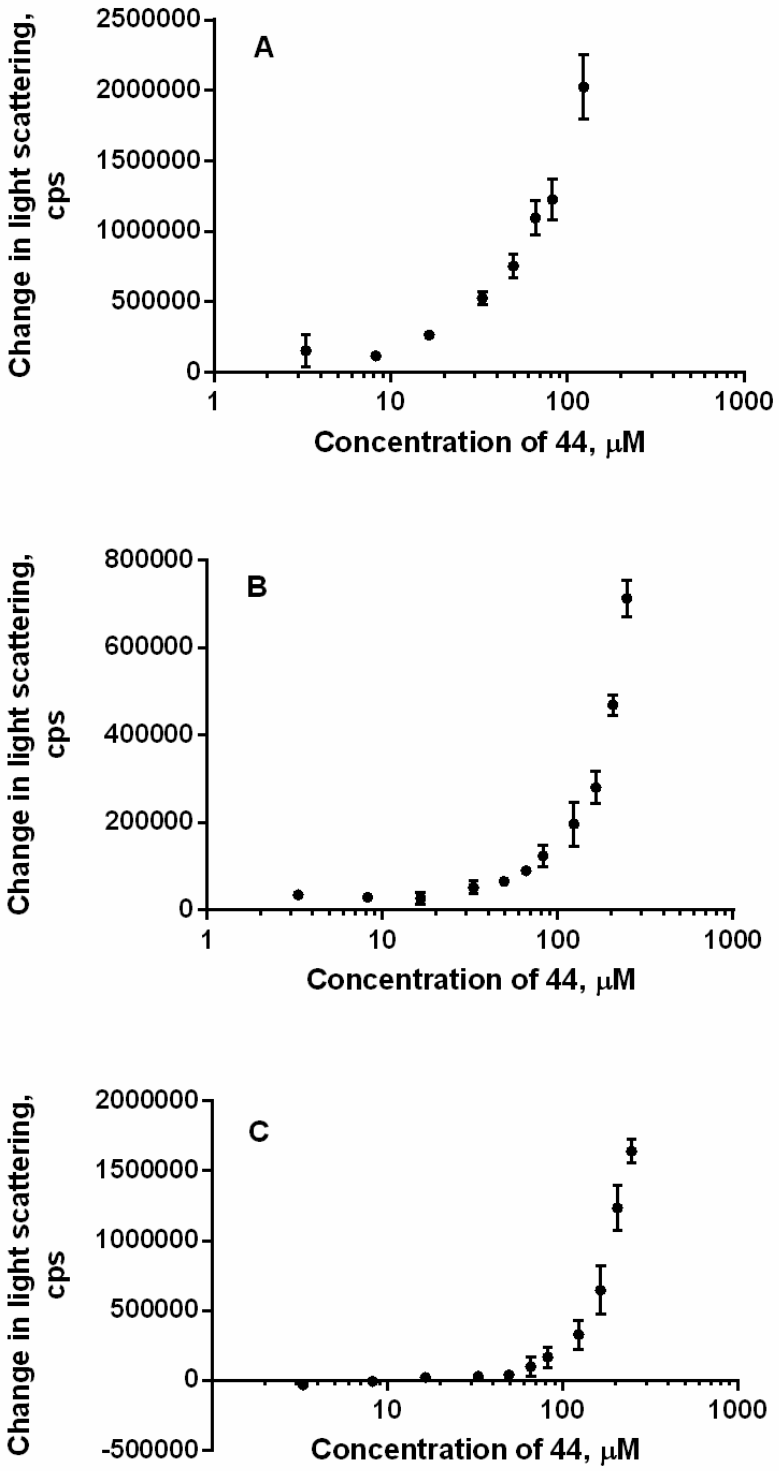


Figure 12. CMC determination for **44** in absence and presence of membrane using 90° Rayleigh-Debye light scattering: Effects of increasing compound concentration on light scattering. **A**: **44** (used as a 33 mM solution in DMSO) in 10 mM pH 7.4 Tris buffer; **B**: **44** (used as a 33 mM solution in DMSO) in 400 μM $PC_{100\%}$ PLVs; **C**: **44** in 400 μM $PC_{70\%}Chol_{30\%}$ PLVs

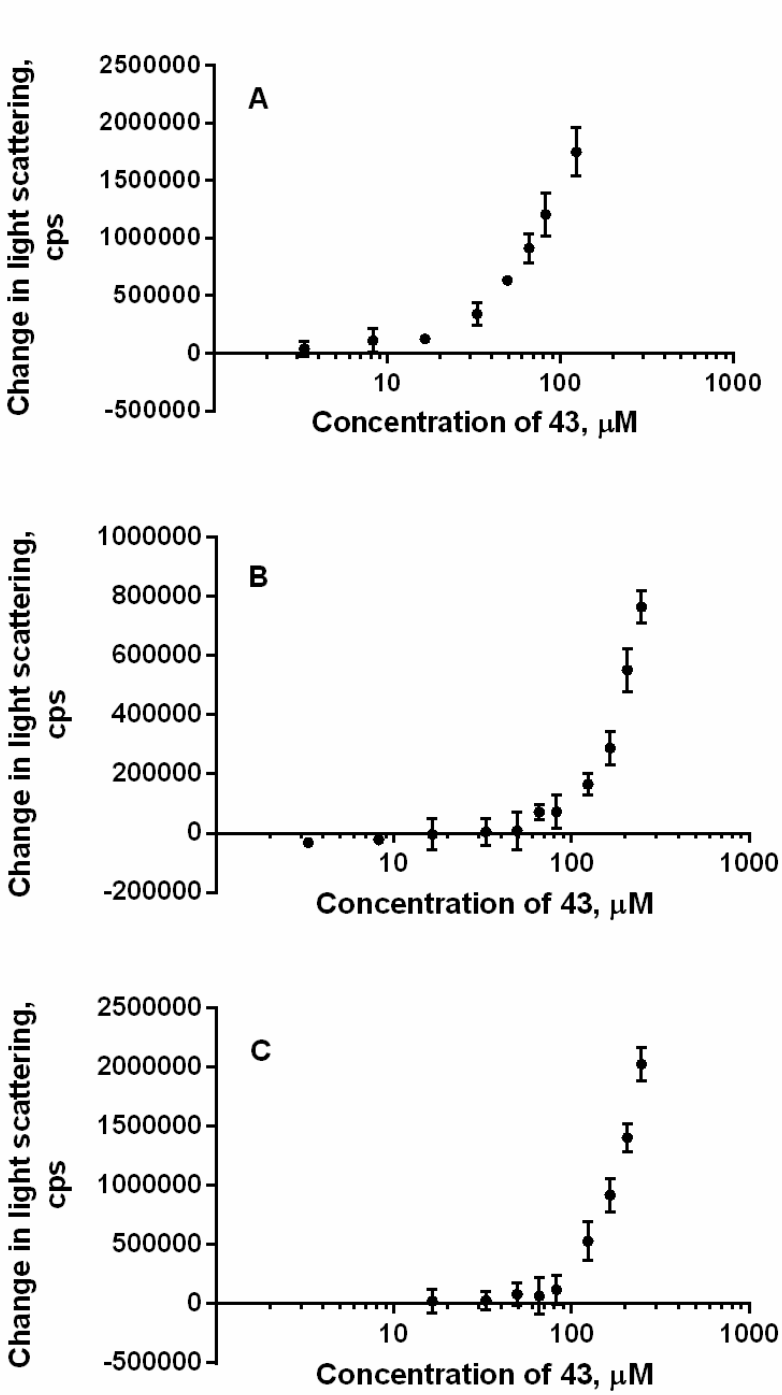


Figure 13. CMC determination for **43** in absence and presence of membrane using 90° Rayleigh-Debye light scattering: Effects of increasing compound concentration on light scattering. **A**: **43** (used as a 33 mM solution in DMSO) in 10 mM pH 7.4 Tris buffer; **B**: **43** (used as a 33 mM solution in DMSO) in 400 μM $PC_{100\%}$ PLVs; **C**: **43** in 400 μM $PC_{70\%}Chol_{30\%}$ PLVs

CMC for **44** was increased to 126.5 µM in the presence of $PC_{100\%}$ and 109.2 µM in the presence of $PC_{70\%}Chol_{30\%}$ liposomes, whilst for **43** very similar values of 117.6 µM ($PC_{100\%}$) and 110.3 µM ($PC_{70\%}Chol_{30\%}$) were observed (Figure 14). A rationalisation of these results is that, below CMC, the monomeric molecules preferentially insert into the PLVs, thereby reducing their effective free concentration in solution. Only when the PLVs approach saturation point does the effective concentration of molecules in solution become great enough for self aggregation into micelles to occur.

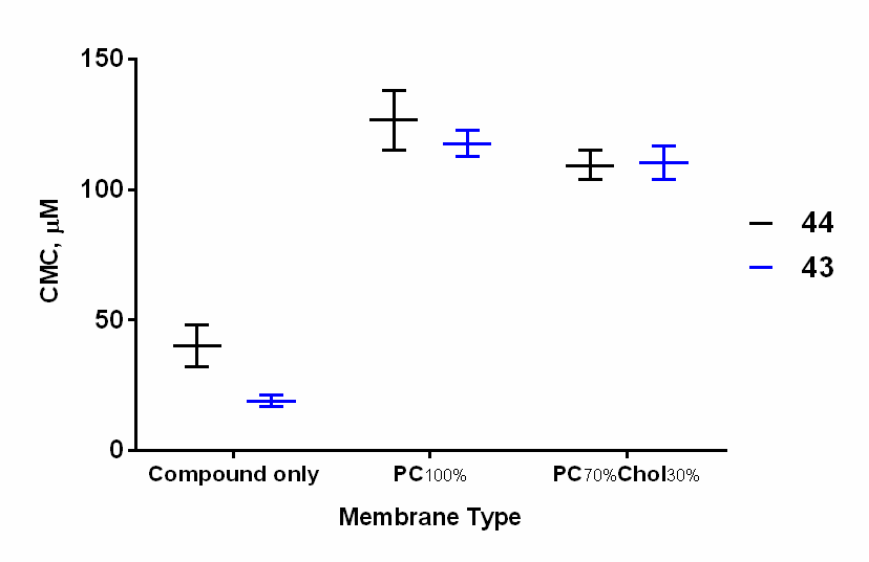


Figure 14. Critical micelle concentrations of **43** and **44** in absence and presence of membrane

The delayed onset of CMC for **43** and **44** caused by the presence of PLVs provides a strong indication that the molecules are inserting into the membrane bilayer. With these initial, encouraging results in hand, a more in depth exploration of the interactions between the tridachiahydropyrones and the model membrane systems was undertaken.

3.3 Exploring Molecular Interactions with Membranes: Exploiting the Membrane Dipole Potential

3.3.1 Membrane Potentials

Membranes, both biological and model, possess three types of electric potential (Figure 15). The first of these is the transmembrane potential difference ($\Delta\Psi$), which is defined as the overall difference in potential between the bulk aqueous phases either side of the membrane.[54] It arises from differences in cation and anion concentrations between the two phases. This charge gradient is maintained by active transport and passive diffusion of ions across the membrane. The second potential is the membrane surface potential (Ψ_s). This is the potential difference between the surface of the membrane and the bulk aqueous phase. It arises from the charged headgroups of the membrane lipids, resulting in an excess of negative electric charge at the membrane surface.[55] The third electric potential associated with membranes is the membrane dipole potential (Ψ_d). This potential exists just within the membrane, between the outer aqueous phase and the hydrophobic interior provided by the acyl lipid chains. It arises from the alignment of the dipoles associated with the polar headgroups of the constituent phospholipids, along with the dipoles of water molecules ordered at the membrane-aqueous interface. The magnitude of Ψ_d varies from 100 to 400 mV (positive in the membrane interior) depending on the composition of lipid, with phosphatidylcholine possessing a membrane dipole potential of 220-280 mV.[56]

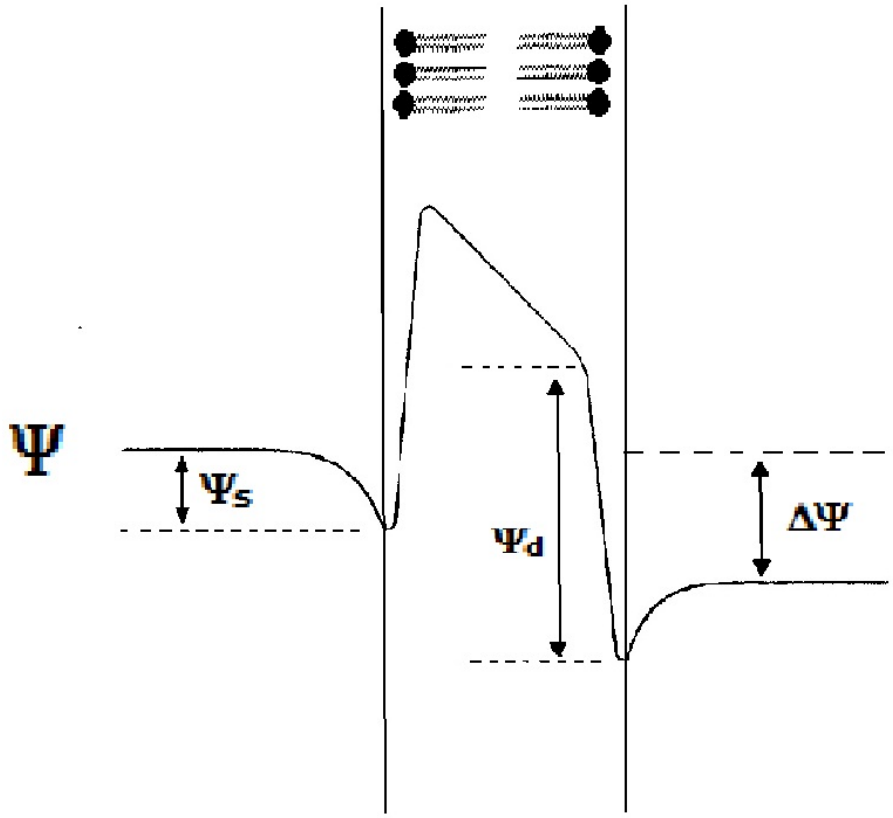


Figure 15. The variation in electrical potential (Ψ) across a phospholipid bilayer. Figure adapted from reference 54

Binding of molecules to a bilayer induces a change in Ψ_d. Thus, measuring the membrane dipole potential enables the interaction between a molecule of interest and a membrane system to be monitored.

3.3.2 Measurement of the Membrane Dipole Potential: Di-8-ANEPPS

The membrane dipole potential (Ψ_d) can be measured using voltage-sensitive fluorescent probes. The use of di-8-ANEPPS for this purpose was first suggested by Loew and co-workers, who noted that the addition of 6-ketocholestanol, known to increase Ψ_d, and phloretin, known to decrease Ψ_d,

to di-8-ANEPPS-bound membranes caused a blue and a red shift, respectively, in the fluorescence excitation spectrum of the dye.[57]

Di-8-ANEPPS has an aminonaphthyl pyridinium-based chromophore, with a pair of long hydrocarbon chains which act as membrane anchors, and a hydrophilic sulfonate headgroup which aligns the molecule perpendicular to the membrane/aqueous interface. A change in voltage across the membrane induces intramolecular charge redistribution (Figure 16), which leads to a shift in the absorbance or fluorescence spectrum of the dye.[58]

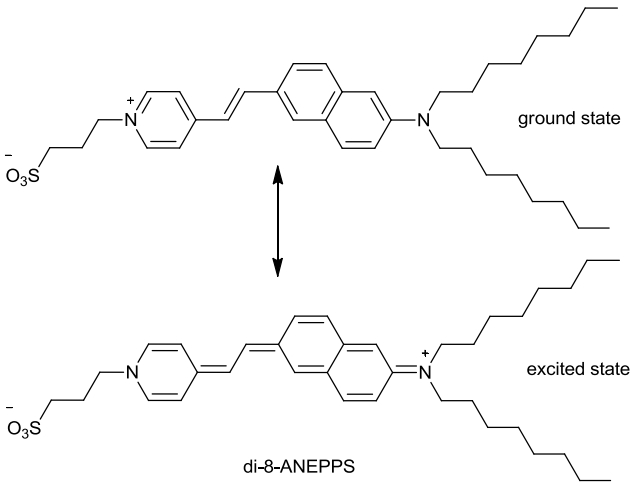


Figure 16. Ground and excited state structures of di-8-ANEPPS

3.3.3 Effect of Molecular Interactions on the Membrane Dipole Potential: Difference Spectra

The effect of addition of **44**, **43**, and **9** to di-8-ANEPPS-stained $PC_{100\%}$ and $PC_{70\%}Chol_{30\%}$ PLVs was investigated using the fluorescence properties of the dye. The fluorescence excitation spectrum of di-8-ANEPPS in membranes is known to undergo a shift upon perturbation of the membrane dipole potential (Ψ_d) caused by binding of molecules to the membrane.[57] Difference

spectra (Figure 17) were obtained by recording the excitation spectrum of di-8-ANEPPS prior to and after addition of compound, and subtracting the former from the latter (see Section 6.2.6 for further details).

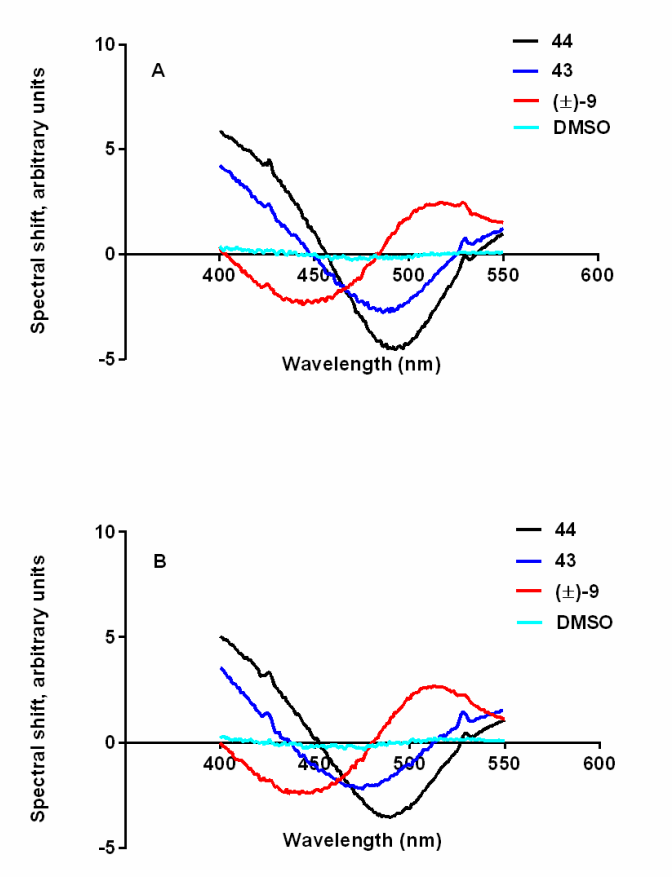


Figure 17. Influence of molecule addition on the fluorescence excitation spectrum (recorded at a fixed emission wavelength of 580 nm) of di-8-ANEPPS: difference spectra. Molecule addition at 288.75 μM in all cases except **43** with $PC_{70\%}Chol_{30\%}$ when the concentration was 247.50 μM. **A**: Difference spectra in presence of 400 μM $PC_{100\%}$ PLVs. **B**: Difference spectra in presence of 400 μM $PC_{70\%}Chol_{30\%}$ PLVs

Figure 17 shows that the (*E,E,E*)-polyene **44** caused a blue shift in the spectrum of di-8-ANEPPS in both membrane types, indicating that it acts to increase Ψ_d. The natural product **9**, conversely, caused a decrease in Ψ_d for both membrane types, manifested in a red shift in the excitation spectrum. Whilst the (*Z,E,E*)-polyene **43** acted in the same manner as **44** in the $PC_{100\%}$ membrane, causing a blue shift (Figure 17A), its influence on the Ψ_d of the

cholesterol-containing membrane was a little more ambiguous (Figure 17B). Whilst it clearly caused a perturbation, both the red and blue ends of the spectrum were positively shifted whilst the central portion was negatively shifted. However, this data provides conclusive experimental evidence that all three molecule types insert into these membranes. In addition, the difference in shift caused by tridachiahydropyrone (**9**) in comparison with its biomimetic precursors suggests that it binds to the membrane with a different geometry. This could be due to its non-planar, puckered ring structure.

3.3.4 Concentration Dependence of the Membrane Dipole Potential: Ratiometric Fluorescence Measurements

Quantification of changes in Ψ_d using di-8-ANEPPS is generally achieved using dual wavelength ratiometric measurements. This technique takes the ratio of fluorescence excited at two wavelengths, one at the blue and one at the red end of the fluorescence spectrum. A shift in the spectrum causes an increase in intensity at one wavelength and a decrease at the other. A variation in fluorescence due to a small change in dye concentration, on the other hand, would affect the intensities at both wavelengths in the same manner (ie. it would either increase or decrease the intensity at both wavelengths). Thus using this ratiometric method normalises away effects arising from changes in dye concentration, allowing the dye's response to its electrical environment to be isolated.[58]

Titrating compound into di-8-ANEPPS-labelled PLVs whilst monitoring the ratio of fluorescence (R) excited at two wavelengths (460 and 520 nm)

enabled information on the dependence of the membrane dipole potential (Ψ_d) upon compound concentration to be collected (see Section 6.2.7 for further details). This was initially investigated for the $PC_{100\%}$ and $PC_{70\%}Chol_{30\%}$ membrane systems. These titration curves are depicted in Figure 18. An increase in R was observed upon titration of **44** into $PC_{100\%}$ (Figure 18A) and $PC_{70\%}Chol_{30\%}$ (Figure 18B) PLVs, confirming its interactions with these membrane systems increases Ψ_d. Also as expected from the difference spectra, tridachiahydropyrone (**9**) caused a concentration-dependent decrease in R, consistent with a decrease in Ψ_d. **43** showed differing effects on Ψ_d between the two membrane types, increasing Ψ_d of the $PC_{100\%}$ membrane (positive ΔR), whilst acting to decrease Ψ_d in the $PC_{70\%}Chol_{30\%}$ case (negative ΔR). This indicates that the presence of cholesterol in the membrane affects the mode of binding of **43**. One explanation for this could be that the ordering presence of the rigid ring structure of cholesterol forces the polyene sidechain of **43** to adopt a different conformation. This would not affect the all *E* polyene **44** as much, as its sidechain is already relatively planar and linear, whilst molecular modelling calculations indicate that the sidechain of **43** adopts a non-planar geometry, partially wrapping around the pyrone headgroup (see Appendix 1).

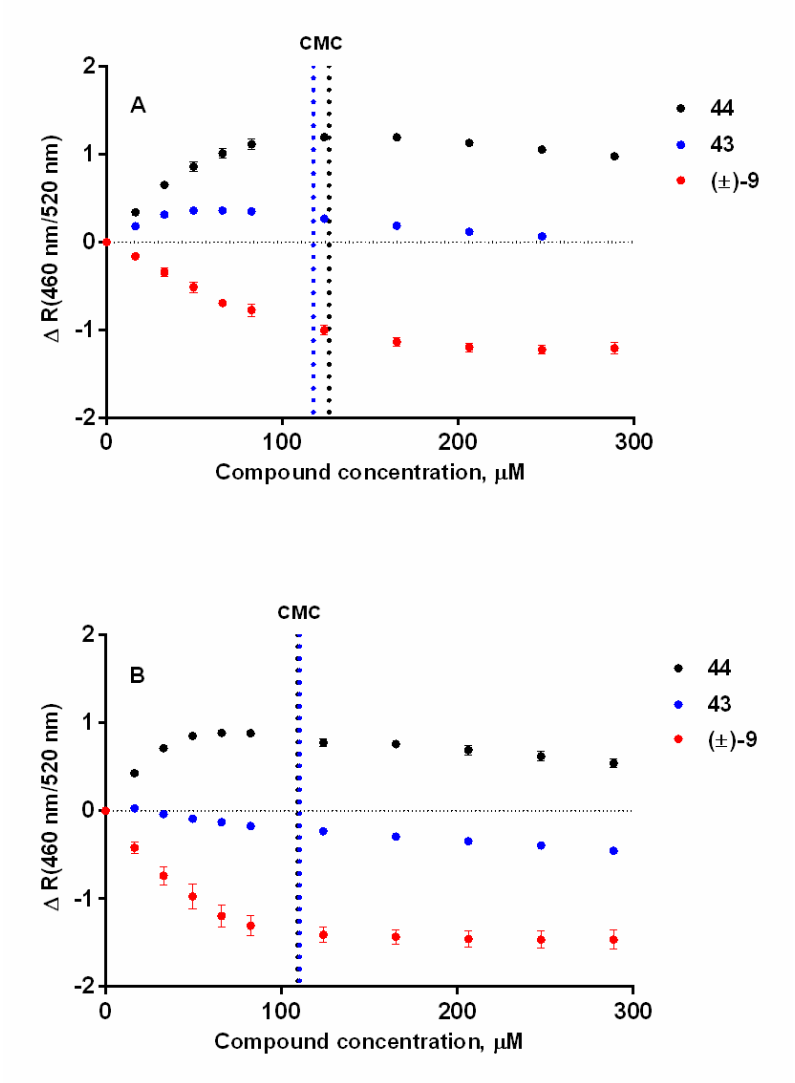


Figure 18. Titration curves showing the change in the fluorescence ratio R with increasing compound concentration (added as a 33 mM solution in DMSO). **A**: Titration of compound into $PC_{100\%}$ PLVs (400 μM); **B**: Titration of compound into $PC_{70\%}Chol_{30\%}$ PLVs (400 μM). Points of CMC for **44** (black dotted line) and **43** (blue dotted line) in the presence of the appropriate PLVs are superimposed as dotted vertical lines

A striking feature of the titration curves is their tendency in the case of **44** and **43** to fall away at high concentrations instead of levelling off, with ΔR decreasing instead of becoming constant. This is not the behaviour that would be expected for simple saturatable binding models. A likely explanation for this becomes obvious when the critical micelle concentrations (CMCs) of these molecules (as determined in Section 3.2), in the presence of the

appropriate PLVs, are superimposed upon the titration profile (Figure 18). In all four cases prior to the CMC the expected saturatable binding behaviour is observed, whilst after this point the curves are disrupted, falling away instead of levelling off. At the point of CMC, the aggregation of molecules in solution appears to be clearly affecting the fluorescence properties of di-8-ANEPPS in a way that disrupts the dataset. This aggregation should not affect the membrane dipole potential of the PLVs. However, it is possible that the micelles themselves take up the di-8-ANEPPS (either from the free solution or out of the PLVs themselves). Depletion of the dye from the PLVs could affect the fluorescence spectrum. It is also likely that the micelles, being possessed of polar headgroup regions in much the same way as the PLVs, would also exhibit a type of dipole potential, which could influence the observed fluorescence properties of the spectroscopic probe.

3.3.5 Uptake of Di-8-ANEPPS by Micelles: Effects on Fluorescence

In order to determine unequivocally if these micellar aggregates were capable of di-8-ANEPPS uptake leading to a change in its fluorescence spectrum, a series of experiments was conducted. **44** was added (as a 33 mM solution in DMSO) to a solution of di-8-ANEPPS at time = 0 min. The fluorescence excitation and emission spectrum was then recorded at 10 minute time intervals. This was done for additions of **44** at both pre- and post-critical micelle concentration (CMC) levels. The results of these experiments are shown in Figure 19.

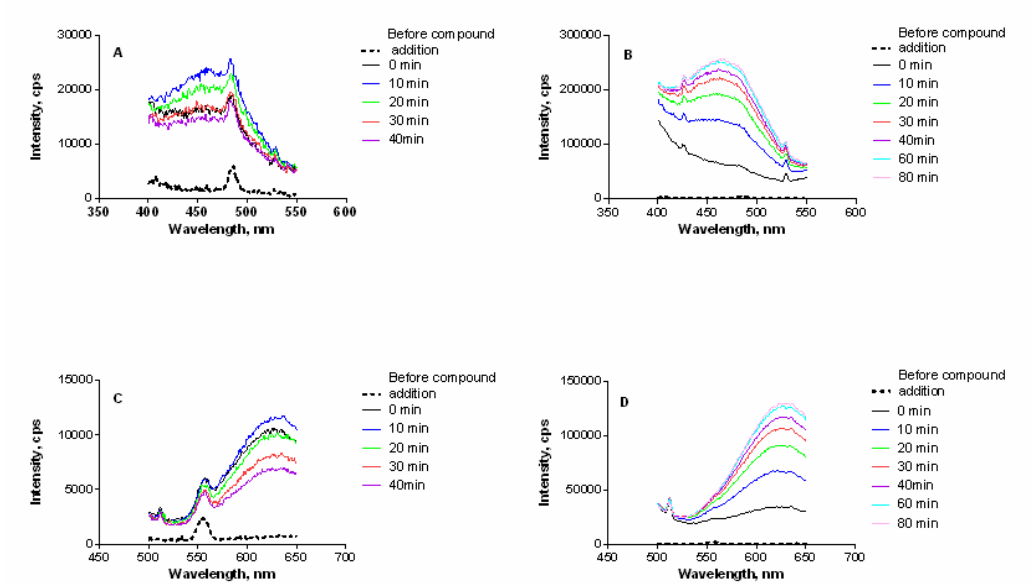


Figure 19. Time-dependent uptake of di-8-ANEPPS by **44** micelles: influence on di-8-ANEPPS excitation and emission spectra. **A**: Excitation spectrum (recorded at a fixed emission wavelength of 580 nm) in presence of pre-CMC concentration of **44** (16.5 µM); **B**: Excitation spectrum in presence of post-CMC concentration of **44** (206.25 µM); **C**: Emission spectrum (recorded at a fixed excitation wavelength of 468 nm) in presence of pre-CMC concentration of **44** (16.5 µM); **D**: Emission spectrum in presence of post-CMC concentration of **44** (206.5 µM)

It can be seen that the presence of post-CMC concentrations of **44** leads to a ten-fold increase in the magnitude of fluorescence intensity in comparison with the pre-CMC case. This is the case for both the excitation (Figure 19B versus Figure 19A) and emission (Figure 19D versus Figure 19C) spectra of di-8-ANEPPS. From this it can be concluded that micelles of **44** do indeed take up the fluorescent probe and cause changes in its spectral properties.

The time-dependent manner in which this occurs is also clear from this data. In the post-CMC cases (Figures 19B and D) the intensity of the signal increases with time, with the increase becoming smaller as time goes on until finally no further increase is observed, at around 60 minutes from compound addition. It can be concluded that this is the time taken for the system to fully

equilibrate, which coincides with the standard incubation period for staining of PLVs with the probe (see Section 6.2.4). In contrast, in the pre-CMC experiments (Figures 19A and C), whilst there are slight variations in the signal intensity, the intensity does not increase steadily with time. Instead these variations in intensity appear to be at random.

3.3.6 Fitting the Binding Profiles: Characterising the Interactions

Having established the ability of the micelles to affect the fluorescence spectrum of di-8-ANEPPS, the post-CMC datapoints in the titration curves for **43** and **44** were discounted, affording data solely reflecting the interaction of the molecules with the liposomal systems. This enabled characterisation of the interactions to be carried out, by fitting of the binding curves to mathematical models in order to obtain best fit values for parameters describing the nature of the interactions (Table 3).

The curves were fitted to one of two likely binding models (Equations 2 and 3). Equation 2 is the simplest model, describing a single site saturation binding situation. Equation 3 describes a single site binding model incorporating a Hill slope, which indicates a degree of cooperativity in the binding of molecules to the membrane. The statistically preferred model for each molecule/membrane system was determined using an extra sum-of-squares F test (see Section 6.2.8 for details, and Appendix 2 for statistical parameters).[59]

Equation 2: $$y = \frac{B_{\max} \cdot x}{K_d + x}$$

Equation 3: $$y = \frac{B_{\max} \cdot x^n}{Kd^n + x^n}$$

Where y is the change in the fluorescence ratio, ΔR(460 nm/520 nm); x denotes ligand concentration; B_{max} is the membrane binding capacity; K_d is the dissociation constant, a measure of a molecule's affinity for the membrane; and n represents the Hill coefficient, a measure of the degree of cooperativity in the binding of ligand molecules to the membrane.

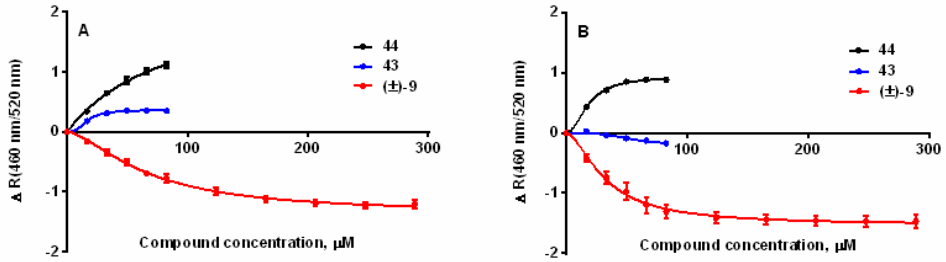
A two-site binding model (Equation 4) was also considered. However this proved to be an unsuitable description for all datasets, producing binding parameters with standard errors many times larger than the parameters themselves, and so was disregarded.

Equation 4: $$y = \left(\frac{B_{\max 1} \cdot x}{Kd1 + x} \right) + \left(\frac{B_{\max 2} \cdot x}{Kd2 + x} \right)$$

The titration curves of molecules **43** and **(±)-9** fit best to Equation 3 for both $PC_{100\%}$ and $PC_{70\%}Chol_{30\%}$ membrane types, indicating a degree of cooperativity in their binding behaviour. **44**, on the other hand, displayed different binding behaviour with the two types of membrane, undergoing a switch from simple hyperbolic (Equation 2) to cooperative (Equation 3) upon moving from the $PC_{100\%}$ membrane to the cholesterol-containing $PC_{70\%}Chol_{30\%}$.

The binding parameters obtained from these fits, together with the respective octanol-water partition coefficient (logP) calculated for each molecule, are presented in Table 3. From this a significant variation in membrane affinities

across the molecules tested, as judged by the dissociation constant (K_d), is apparent. Assessment of their membrane affinity utilising the theoretical LogP parameter, however, is far less discriminating. The calculated logP values show little to no distinction in the predicted lipophilicities. LogP is used under many circumstances as a descriptor of the ability of a molecule to bind to a membrane.[60] The technique reported here thus offers a much better method for determining membrane affinity, as it is sensitive to additional factors such as hydrogen bonding and hydrophobic moment effects which are not accounted for in the logP parameter.



	Compound	44	43	(±)-9
	LogP (±0.47)	3.89	3.54	3.83
Membrane Type	**Parameter**			
$PC_{100\%}$	**B_{max}**	2.31±0.33	0.36±0.01	1.37±0.08
	K_d (μM)	86.5±20.9	16.7±1.05	66.4±6.56
	n	-	2.83±0.78	1.58±0.20
$PC_{70\%}Chol_{30\%}$	**B_{max}**	0.94±0.05	0.21±0.09	1.53±0.07
	K_d (μM)	18.1±1.26	54.1±17.0	32.4±3.43
	n	2.05±0.41	3.51±2.15	1.66±0.32

Table 3. Binding profiles describing interaction of **44**, **43** and **(±)-9** with **A**: $PC_{100\%}$ and **B**: $PC_{70\%}Chol_{30\%}$ PLVs (400 μM), and experimental binding parameters derived from these fits. Values of Hill coefficient n given where Equation 3 gave the best fit, and left blank where Equation 2 was statistically preferred. Theoretical octanol/water partition coefficients (LogP) were determined using CS ChemDraw Ultra v12.0

The binding parameters determined highlight a number of interesting features. Firstly, the (*Z,E,E*)-polyene pyrone **43** displays a far lower binding capacity (B_{max}) than the other molecules tested. This may be due to conformational factors with the polyene tending towards a non-planar geometry. However, it is notable that **43** also displayed the highest degree of cooperativity in its binding, as judged by the magnitude of the Hill coefficient (n). Despite the low binding capacity, **43** displayed the highest affinity for the $PC_{100\%}$ membrane (lowest K_d), suggesting that it is not simply a matter of available space within the membrane that is associated with the binding process.

Focusing on the natural product precursors, polyenes **44** and **43**, it is clear that the presence of cholesterol in the membrane system has a significant effect on the binding interactions. A switch from non-cooperative to cooperative binding is observed in the case of **44**, whilst for **43** an increase in the degree of cooperativity is also apparent. The relatively planar all *E*- isomer **44** displays a greater affinity for the cholesterol-ordered $PC_{70\%}Chol_{30\%}$ membrane, whilst the twisted structure of **43** (see Appendix 1) shows a preference for the more disordered cholesterol-free $PC_{100\%}$ membrane.

As **44** is the parent compound of **43** and **9**, it is reasonable to assume that it is the affinity of this molecule that will dictate the location of all three metabolites in the plasma membrane. As judged by the magnitude of K_d, **44** shows a clear preference for binding to $PC_{70\%}Chol_{30\%}$ PLVs. This suggests that the site of localisation of these molecules within the phospholipid bilayer is

likely to be the cholesterol-rich, liquid ordered (l_o) raft regions, rather than the cholesterol-poor, liquid disordered (l_d) bulk membrane.

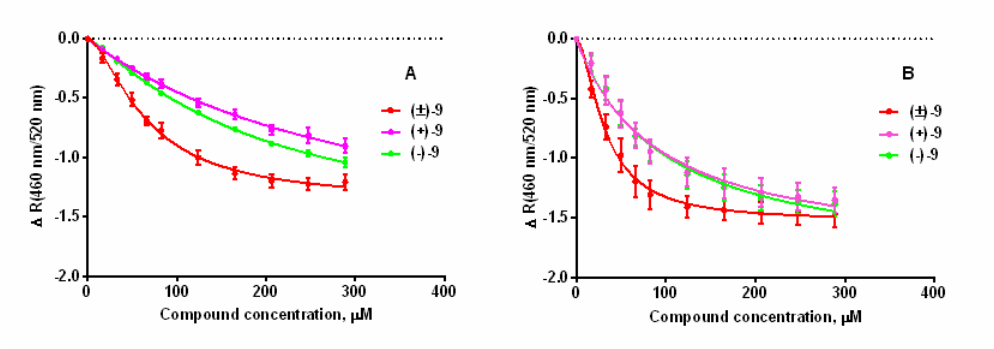
This observation raises an interesting prospect. Whilst the biomimetic synthesis of tridachiahydropyrone (**9**) conducted in the laboratory afforded a racemic mixture of the natural product, the original isolation paper reports an optical rotation ($[\alpha]_D$ -476.1°)[3] associated with the natural sample. This suggests that, in the biological system, tridachiahydropyrone is produced in enantioenriched form. As the biomimetic precursors **44** and **43** are themselves achiral, any enantioselectivity conferred must be associated with the final electrocyclisation step.

Ireland and Scheuer's experiments demonstrated that the *in vivo* photochemical transformation of 9,10-deoxytridachione (**2**) into photodeoxytridachione (**3**) was non-enzymatic,[17] suggesting that the origin of chirality in sacoglossan natural products, derived from achiral polyene precursors, does not lie in enzymatic assistance.

Within the confines of the biosynthetic hypothesis, a possible origin of the enantioselectivity observed in the case of natural tridachiahydropyrone (**9**) could be the chiral components, including phospholipids, sphingolipids and cholesterol, of the membrane bilayer itself, where the electrocyclisation step is proposed to occur. The surrounding chiral environment of the membrane could be a source of chiral induction, favouring the formation of one enantiomer of the natural product **9** over the other, by influencing the relative energies of the alternate transition states. Following this hypothesis, chiral induction would be more likely to occur in regions of higher order, providing a

more rigid surrounding chiral environment for the electrocyclisation. As the parent compound, **44**, showed a higher affinity for the ordered microdomain-containing membrane type ($PC_{70\%}Chol_{30\%}$) over the disordered membrane ($PC_{100\%}$) in the above binding studies, it was deemed of interest to explore this hypothesis further. The increased order of the l_o raft regions could reasonably be considered more able to exert stereocontrol upon the key electrocyclisation reaction than the surrounding l_d phase.

In order to ascertain whether the model membrane systems were capable of enantiodifferentiation between the enantiomers of tridachiahydropyrone (**9**), a sample of racemic synthetic **9** was separated into its constituent optical isomers using preparative chiral HPLC (see section 6.1.4 for details), and the interactions of **(-)-9** and **(+)-9** with $PC_{100\%}$ and $PC_{70\%}Chol_{30\%}$ PLVs characterised using the established ratiometric fluorescent spectroscopic technique. The binding profiles generated, and parameters determined from the fits, are outlined in Table 4, along with those of **(±)-9**, for comparison.



	Compound	(±)-9	(-)-9	(+)-9
Membrane Type	**Parameter**			
$PC_{100\%}$	**B_{max}**	1.37±0.08	1.69±0.16	1.96±0.24
	K_d (μM)	66.4±6.56	194±32.5	337±65.0
	n	1.58±0.20	1.18±0.07	-
$PC_{70\%}Chol_{30\%}$	**B_{max}**	1.53±0.07	1.93±0.15	1.84±0.15
	K_d (μM)	32.4±3.43	96.6±18.1	89.4±19.3
	n	1.66±0.32	-	-

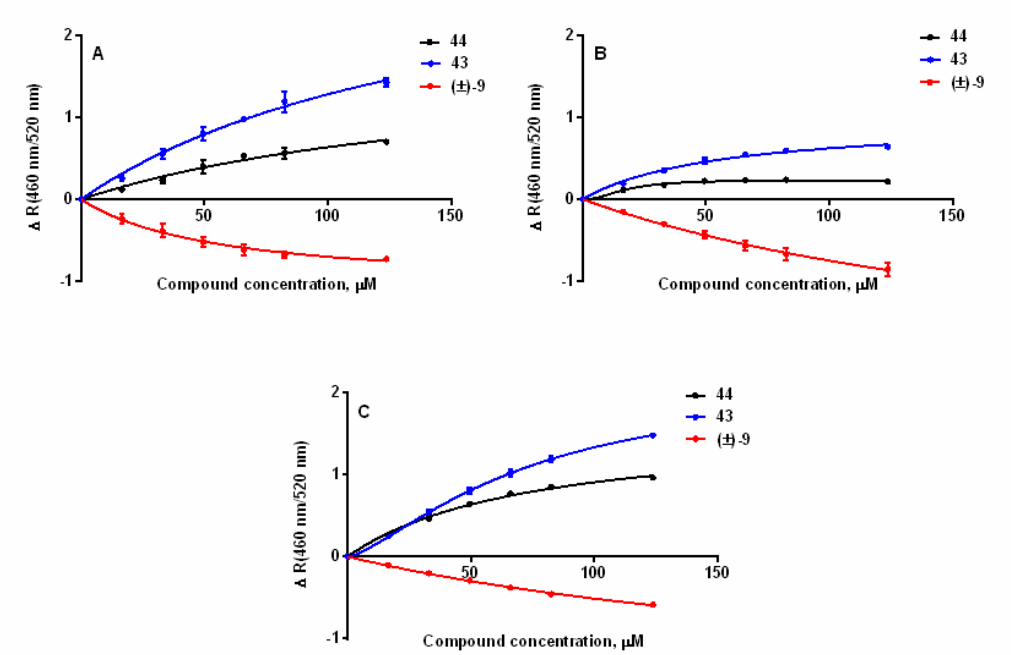
Table 4. Binding profiles describing interaction of **(±)-9**, **(-)-9** and **(+)-9** with **A**: $PC_{100\%}$ and **B**: $PC_{70\%}Chol_{30\%}$ PLVs (400 μM), and experimental binding parameters derived from these fits. Values of Hill coefficient n given where Equation 3 gave the best fit, and left blank where Equation 2 was statistically preferred

Differing behaviour between the interactions of the (+)- and (-)- enantiomers of **9** was indeed observed with both membrane types, as well as differences between the enantiomerically pure and racemic samples. A particular difference between the two enantiomers was observed with the $PC_{100\%}$ membrane, with the behaviour of **(-)-9** best described by the cooperative model (Equation 3) whilst **(+)-9** bound to the membrane in a simple hyperbolic manner (Equation 2). **(-)-9** also showed a higher affinity for this membrane in comparison with its opposite enantiomer.

This data also shows the propensity of the racemic mixture **(±)-9** to bind to membranes with a higher degree of cooperativity than either of its constituent enantiomers alone, as judged by a higher Hill coefficient, n. This may indicate that two opposite enantiomers fit together to insert into the membrane whilst the non-planarity of the structure means that a similar cooperative effect involving two molecules of the same enantiomer is energetically less favourable.

With the ability of the PLVs to distinguish between **(±)-9**, **(-)-9** and **(+)-9** demonstrated, the next logical progression was to attempt to conduct the key tridachiahydropyrone-forming electrocyclisation step using the membrane systems as reaction media, to investigate whether any enantioselectivity would be conferred on this transformation by the surrounding chiral environment of the membrane. It was decided that, along with the fully disordered $PC_{100\%}$, and $PC_{70\%}Chol_{30\%}$ with its coexistence of liquid disordered regions and liquid ordered microdomains, membrane systems with yet a higher degree of order would also be investigated as chiral reaction media. Three more liposomal systems were thus synthesised, this time containing the sphingolipid sphingomyelin (SM): $PC_{70\%}SM_{30\%}$ ($s_o + l_d$); $PC_{60\%}Chol_{20\%}SM_{20\%}$ ($l_d + l_o$); and $PC_{40\%}SM_{60\%}$ ($s_o + l_d$).[50] The phosphatidylcholine/sphingomyelin binary mixtures were chosen for their solid ordered regions, so that the effect of a more rigid chiral environment upon the electrocyclisation reaction could be investigated. The ternary phosphatidylcholine/cholesterol/sphingomyelin system was chosen as a more complex example, thus being a more realistic reflection of the state of affairs found *in vivo*.

Prior to the use of these liposomal systems as reaction media, experimental binding profiles were again generated, in order to ensure that the pyrone molecules did indeed bind to these new systems (Table 5).



	Compound	44	43	(±)-9
$PC_{70\%}SM_{30\%}$	B_{max}	3.33±0.54	1.74±0.52	1.09±0.15
	K_d (μM)	160±39.4	173±77.1	55.7±16.6
	n	-	-	-
$PC_{60\%}Chol_{20\%}SM_{20\%}$	B_{max}	0.97±0.08	0.24±0.01	2.47±0.83
	K_d (μM)	55.8±10.6	17.4±2.05	230±106
	n	-	2.18±0.76	-
$PC_{40\%}SM_{60\%}$	B_{max}	2.19±0.26	1.58±0.09	1.79±0.18
	K_d (μM)	73.0±13.3	74.2±8.60	250±33.0
	n	1.40±0.14	-	-

Table 5. Binding profiles describing interaction of **44**, **43** and **(±)-9** with **A**: $PC_{70\%}SM_{30\%}$, **B**: $PC_{60\%}Chol_{20\%}SM_{20\%}$ and **C**: $PC_{40\%}SM_{60\%}$ PLVs (400 μM), and experimental binding parameters derived from these fits. Values of Hill coefficient n given where Equation 3 gave the best fit, and left blank where Equation 2 was statistically preferred

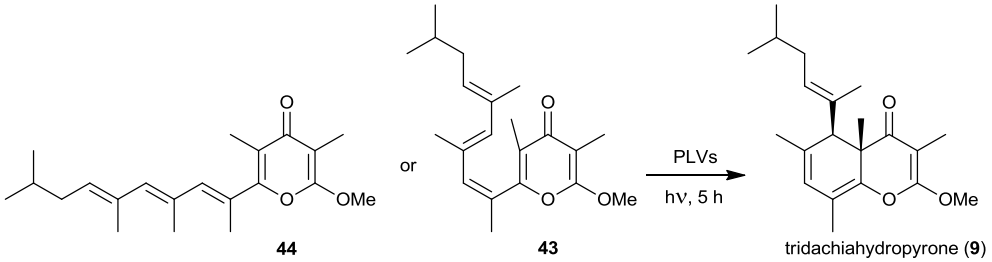
As Table 5 demonstrates, **44**, **43** and **(±)-9** were all found to insert into the three additional membrane types, thus confirming that they were also suitable for use in subsequent investigations into the use of PLVs as chiral reaction media.

3.4 Electrocyclisations Using PLVs as Chiral Reaction Media

Having conclusively established the propensity of the tridachiahydropyrone precursors, **44** and **43** (along with the natural product **9** itself), to insert into the model membrane systems, the key electrocyclisation reaction was attempted utilising the phospholipid vesicles (PLVs) as chiral reaction media. The main aim of these reactions was to ascertain if any asymmetry had been conferred on the reaction by chiral HPLC analysis of the isolated product.

The investigation was accomplished by adding the required precursor (**44** or **43**), as a solution in DMSO, to a preformed suspension of PLVs of the desired composition. The mixture was degassed, and then left to equilibrate for 30 min, in the dark, in order to ensure insertion of the precursor molecules into the membrane bilayers had occurred. After this period the liposomal solutions were irradiated (125 W mercury lamp) for a time period of 5 h, before the product tridachiahydropyrone (**9**) was isolated by extraction with dichloromethane, followed by preparative TLC purification. Due to the low concentrations of compound involved, it was not feasible to establish quantitative yields for these experiments. However, the product was in each case obtained in sufficient quantity and purity for its enantiomeric ratio to be determined unequivocally by analytical chiral HPLC.

Both precursors, the (*E,E,E*)-polyene **44** and the (*Z,E,E*,)-polyene **43**, were tested in each of the five membrane types. The results of the investigation are presented in Table 6.



Entry	Substrate	PLV Composition	Stereochemical Outcome
1	**44**	$PC_{100\%}$	racemic
2	**43**	$PC_{100\%}$	racemic
3	**44**	$PC_{70\%}Chol_{30\%}$	racemic
4	**43**	$PC_{70\%}Chol_{30\%}$	racemic
5	**44**	$PC_{70\%}SM_{30\%}$	racemic
6	**43**	$PC_{70\%}SM_{30\%}$	racemic
7	**44**	$PC_{40\%}Chol_{20\%}SM_{20\%}$	racemic
8	**43**	$PC_{40\%}Chol_{20\%}SM_{20\%}$	racemic
9	**44**	$PC_{40\%}SM_{60\%}$	racemic
10	**43**	$PC_{40\%}SM_{60\%}$	racemic

Table 6. Electrocyclisations utilising PLVs as chiral reaction media – stereochemical outcome

In all cases the desired product **9** was formed, demonstrating the feasibility of this transformation occurring in the cell membrane of the producing mollusc. However, in all cases the isolated product was shown to be racemic upon HPLC analysis.

Several interesting points arise in light of this outcome. The chiral centres of the membrane components used for the formation of liposomes in this study, namely phosphatidylcholine, cholesterol and sphingomyelin, are all located in, or near to, the headgroup region (Figure 8). In contrast, the part of the polyene pyrone molecules **44** and **43** undergoing the electrocyclisation reaction is located primarily in the tail region of the molecules. Assuming the polar pyrone headgroups align with the polar headgroups of the bilayer constituents, the desired source of chiral induction is in actuality remote from the site of reaction at which the chiral induction is required, thus resulting in no enantioselectivity being conferred.

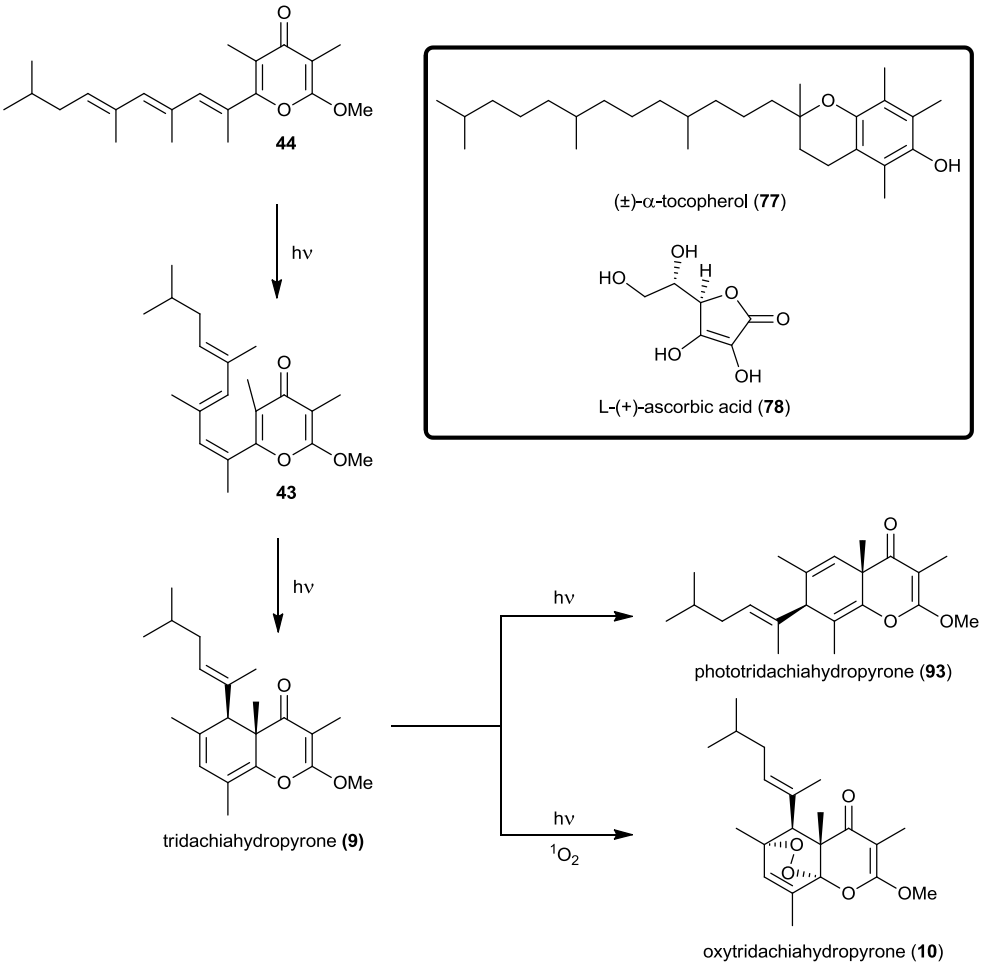
In real biological membranes, there is a plethora of other biomolecules embedded in the membrane bilayer. One significant difference between the membrane models studied in this work and those found in real life systems is the absence/presence of membrane proteins. Of particular relevance are integral transmembrane proteins, which span the whole bilayer.[61] These proteins themselves possess many chiral moieties, which, unlike those in the phospholipids, persist throughout the length of the protein, thus extending into the hydrophobic tailgroup region of the membrane. Thus it is plausible that *in vivo* the source of asymmetric induction is indeed the surrounding chiral environment of the membrane bilayer, but it is the chirality of membrane proteins, not included in the present study, that provides this environment in the relevant region of the bilayer.

A further point of relevance to this discussion is the optical rotation of the natural product reported in the isolation paper.[3] As mentioned previously, a value of $[\alpha]_D$ -476.1° was given. No chiral HPLC data was included, nor was any other form of data relating to the enantioenriched/enantiopure status of the compound reported. In the present work, upon separation of the racemic mixture of tridachiahydropyrone (**9**) into its constituent enantiomers, the optical rotation of both of these separate isomers was measured. The separated enantiomers were also analysed by HPLC in order to assess their enantiopurity (see Section 6.1.5).

The enantiomer which eluted first from the HPLC column was shown, by subsequent analytical HPLC analysis, to be enantiopure (>99% ee). Its optical rotation was measured as $[\alpha]_D^{23}$ = -225.6° (c=0.42 g/100 cm^3, $CHCl_3$). The second-eluted enantiomer was shown to be slightly contaminated with the first-eluted isomer, with the enantiomeric excess determined to be 90% ee (analytical chiral HPLC). The optical rotation of this enantiomer was measured as $[\alpha]_D^{23}$ = +190.4° (c=0.08 g/100 cm^3, $CHCl_3$).

As the first eluted enantiomer was essentially enantiopure, it is surprising that the reported optical rotation for the naturally occurring sample considerably exceeds that of the synthetic sample in magnitude. With no other information regarding the natural sample available, it is difficult to draw any firm conclusions regarding the asymmetric nature of the electrocyclisation as undergone in the biological system.

Chapter 4 Investigations into the Photoprotective and Antioxidant Properties of the Tridachiahydropyrones



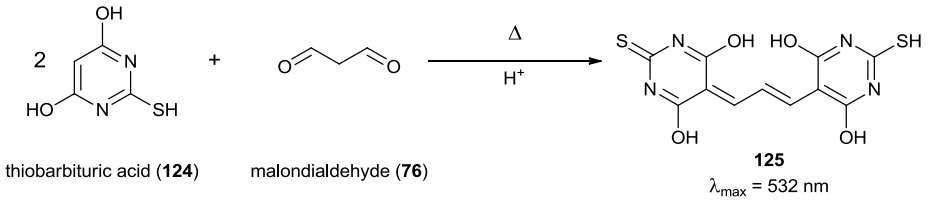
Scheme 39. The photoprotective reaction cascade interrelating members of the tridachiahydropyrone family. Inset: known antioxidant molecules used for comparison in these studies

The propensity of the synthesised pyrone family **44**, **43** and **9** to afford cellular protection against photochemical oxidative damage was assessed using a number of assay techniques. Given the photochemical reaction pathways interrelating the members of the tridachiahydropyrone family (Scheme 39), it was postulated that protection would be conferred by a combination of absorbing UV radiation, which would otherwise contribute to the formation of

damaging reactive oxygen species (ROS) (Section 1.2.2, Scheme 13), and scavenging of the ROS singlet oxygen. In these assays the known biological antioxidants (±)-α-tocopherol (**77**) and L-(+)-ascorbic acid (**78**) were also tested in order to provide a point of comparison.

4.1 Thiobarbituric Acid Reactive Substances (TBARS) Assay

The ability of the pyrone molecules to protect liposomes from photochemically-induced oxidative damage was investigated using the thiobarbituric acid reactive substances (TBARS) assay.[62] This assay is based on the detection of malondialdehyde (**76**), an end product of lipid peroxidation commonly used as a biomarker for cell damage (Section 1.2.2.3, Scheme 14).[63] Malondialdehyde (**76**) reacts with thiobarbituric acid (**124**), when heated under acidic conditions, to form a conjugated adduct, **125**, which absorbs strongly at 532 nm (Scheme 40). Thus treatment of a sample of interest with **124**, followed by comparison of the absorption with that of a standard curve generated from known quantities of **76**, allows the concentration of malondialdehyde (**76**) to be determined colorimetrically (see Section 6.3.2 for further details).



Scheme 40. Colorimetric detection of malondialdehyde (**76**) using the TBARS assay

Irradiation of phosphatidylcholine liposomes (8 mM) using a Wotan Ultravitalux Sunlamp (300 W)[64] induced a time-dependent increase in

oxidative damage, as judged by the generation of malondialdehyde (TBARS), quantified using the assay technique outlined above (Figure 20).

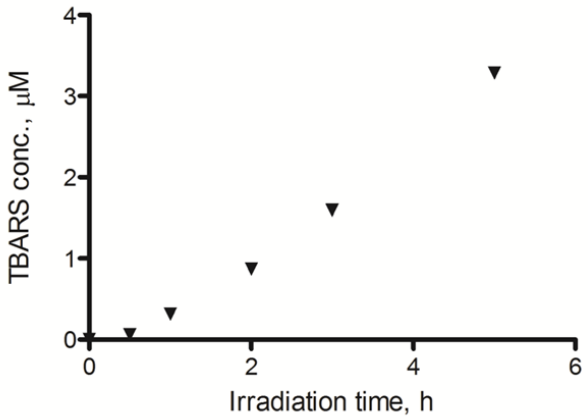


Figure 20. Time-dependent oxidative damage to $PC_{100\%}$ liposomes (8 mM PC), quantified by TBARS assay

The ability of molecules **44**, **43** and **9** to protect the liposomes from this form of damage was investigated by incorporating them into the pre-formed liposomes prior to irradiation, and comparing the TBARS generated in these 'protected' systems to a control system without any sunscreen molecules incorporated. The sunscreen molecules were incorporated at 20 mol%, 10 mol% and 5 mol% (with respect to phosphatidylcholine concentration), in order to discern any concentration dependence. The known lipophilic antioxidant (±)-α-tocopherol (**77**) was also tested.[65] The results are depicted in Figure 21.

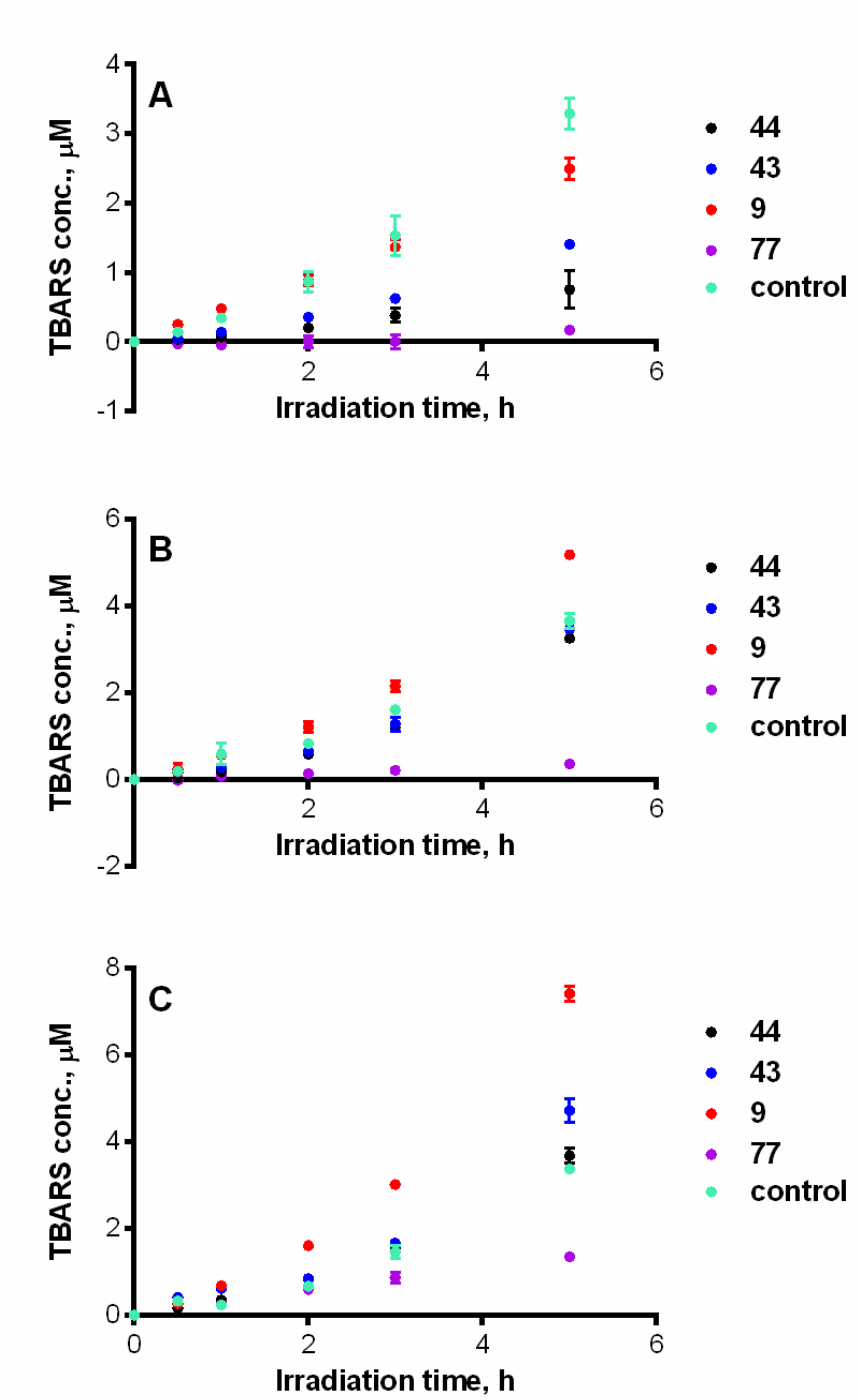


Figure 21. Effect of **44**, **43**, **9** and **77** on the photo-oxidative damage of $PC_{100\%}$ liposomes. Molecules added to liposomal solution (8 mM) as solutions in DMSO (33 mM). Control: addition of corresponding volume of DMSO only. **A**: 20 mol% compound; **B**: 10 mol% compound; **C**: 5 mol% compound

For each compound tested, the level of lipid peroxidation, as judged by TBARS concentration, was lowest for 20 mol% of compound (Figure 21A) and highest

for 5 mol% (Figure 21C). This pattern of increasing oxidative damage with decreasing compound concentration, when taken on its own, would appear to indicate that the pyrone molecules do indeed protect the liposomes from photochemical damage. (±)-α-Tocopherol (**77**) can be seen to be a far superior antioxidant to the pyrone molecules (**44**, **43** and **9**), almost completely suppressing lipid peroxidation at all but the lowest concentration.

When the results for compounds **44**, **43** and **9** are considered in relation to the control sample, the situation appears more complex. Whilst at 20 mol% the compounds act to reduce lipid peroxidation in comparison with the control, at lower concentrations they in fact appear to be exerting a pro-oxidant effect, increasing the level of peroxidation above that of the control sample.

Given the structural similarity between the carbon side-chains of the pyrone molecules and the fatty acid tails of membrane phospholipids, it was considered plausible that peroxidation of the pyrone molecules might occur in a similar fashion to lipid peroxidation (Section 1.2.2.3, Scheme 14), resulting in end products derived from **44**, **43** and **9**, which would themselves form adducts with thiobarbituric acid (**124**), potentially skewing the results of the assay. In order to rule this out a set of negative control experiments were conducted. This involved irradiation of aqueous solutions of the pyrone molecules, at the concentrations used in the liposomal studies, but in the absence of the liposomes themselves. The samples were then tested for

TBARS using the same assay method as above. The results are depicted in Figure 22.

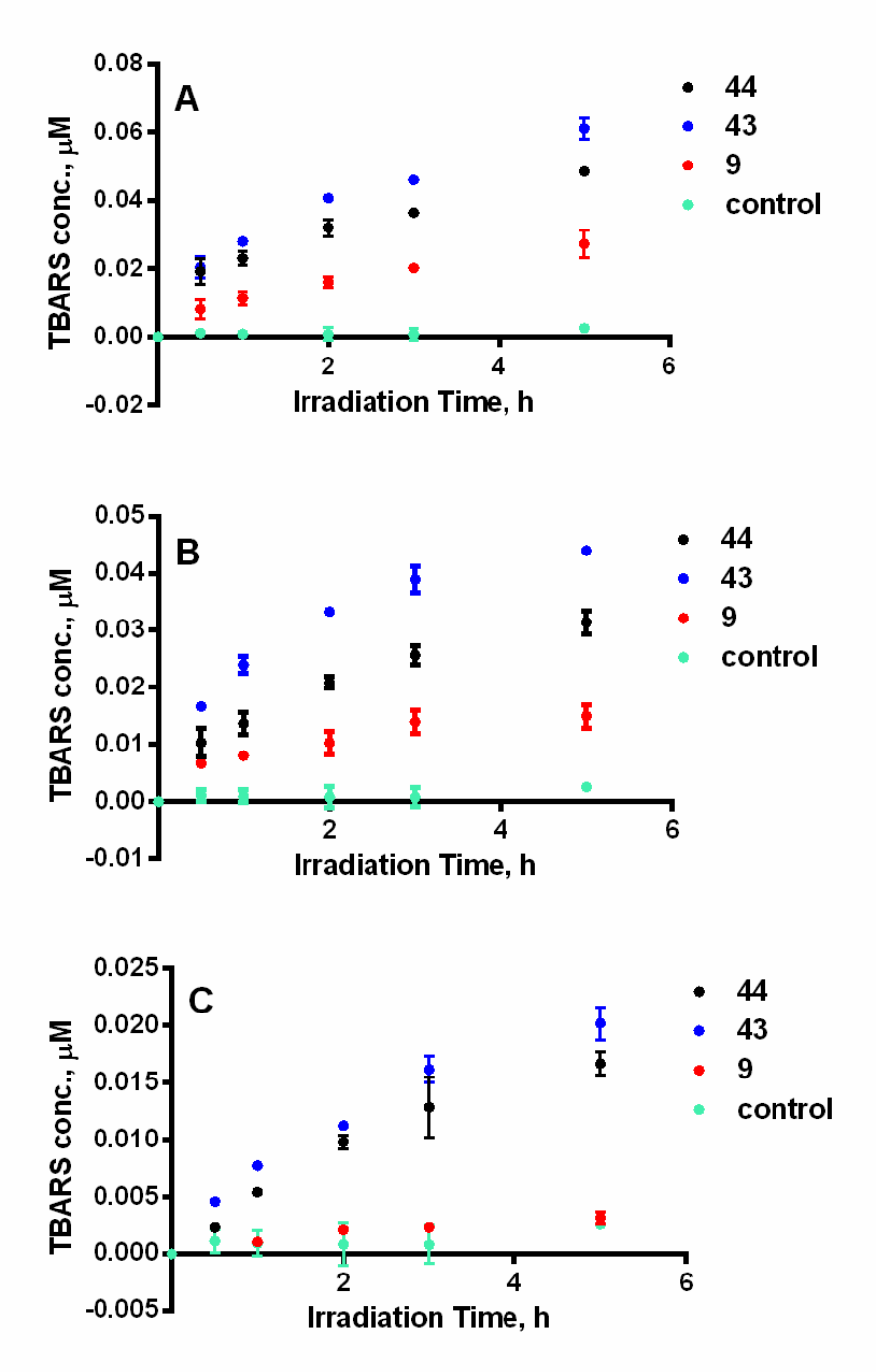


Figure 22. Negative control TBARS experiments: irradiation of protective compounds in the absence of liposomes. **A**: concentration equivalent to 20 mol%; **B**: concentration equivalent to 10 mol%; **C**: concentration equivalent to 5 mol%

Whilst a time-dependent increase in TBARS was observed in the negative control runs, the concentrations generated are only around 1% of those observed in the liposome-containing cases (Figure 21). Thus it can be concluded that TBARS products resulting from the peroxidation of the pyrone molecules themselves are not significantly affecting the experimental results, and that the trends observed relate to the peroxidation of membrane lipids as intended.

Expressing the extent of lipid peroxidation as a percentage of the control TBARS, as outlined in Table 7, enables a closer analysis of the results depicted in Figure 21.

mol%	Compound	% of control TBARS				
		0.5 h	1 h	2 h	3 h	5 h
20	**44**	22%	20%	23%	25%	23%
	43	32%	40%	41%	41%	43%
	9	182%	139%	102%	89%	76%
	77	0%	0%	0%	0%	5%
10	**44**	21%	30%	71%	74%	89%
	43	82%	47%	73%	79%	95%
	9	124%	96%	147%	133%	142%
	77	0%	12%	16%	13%	10%
5	**44**	53%	149%	124%	106%	109%
	43	127%	261%	126%	114%	140%
	9	84%	289%	240%	211%	220%
	77	53%	113%	89%	59%	40%

Table 7. Lipid peroxidation of irradiated $PC_{100\%}$ liposomes in presence of various quantities of compounds **44**, **43**, **9** and **77**, expressed as a percentage of the lipid peroxidation (as judged by TBARS concentration) of the control system (DMSO)

Of the three pyrone molecules, (*E,E,E*)-polyene pyrone **44** suppresses the lipid peroxidation to the greatest extent, with tridachiahydropyrone (**9**) being the least effective. However even **44** begins to show a pro-oxidant effect when

the concentration is lowered to 5 mol%. **9** shows some pro-oxidant activity at all concentrations, whilst the (*Z,E,E*)-polyene pyrone **43** has an intermediate effect.

The observed trend of antioxidant power decreasing in the order **44**>**43**>**9** is consistent with the theory that the origin of the photoprotective properties of the compounds lies in their ability to absorb UV radiation, thus preventing it from causing cell damage. This is most easily explained with reference to Scheme 39. As the parent compound of the tridachiahydropyrone family, **44** has the potential to undergo three discrete sequential photochemical transformations, namely a selective double bond isomerisation to form **43**, followed by a 6π conrotatory electrocyclisation to form **9** and finally a [1,3]-sigmatropic rearrangement to form **93**. **43** has the potential to undergo two sequential photochemical transformations, and **9** just a single photochemical reaction. With each discrete photochemical transformation in the cascade sequence (Scheme 39) requiring the absorption of UV radiation, it follows that if the absorption of UV light is the origin of protective effects, the compound with the highest capacity for photochemical transformation and thus UV absorption, would confer the highest level of photoprotection.

Whilst this rationale accounts for the observed trends between the three pyrone molecules tested, it does not explain the pro-oxidant effects at low compound concentrations. If the molecules were simply pro-oxidants, then an increase in compound concentration would be expected to increase the level of lipid peroxidation. However the reverse is the case. This suggests that there

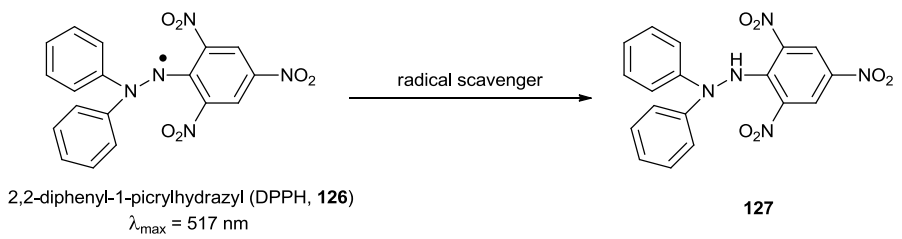
is likely to be a complex interplay of factors affecting the performance of the pyrone molecules as pro/anti-oxidants, and not just simply the factor of UV absorbance.

Further assays were conducted in order to try and ascertain the mechanism of protection by **44**, **43**, and **9**, with the hope of shedding light on the results obtained in the TBARS assay.

4.2 2,2-Diphenyl-1-picrahydrazyl (DPPH) Assay

Many known antioxidants have been shown to operate by acting as a hydrogen atom donor, thus breaking the chain of lipid peroxidation by quenching intermediate lipid peroxyl radicals which would otherwise go on to propagate the peroxidation process.[66] As such, measures of radical scavenging ability are often used as a measure of antioxidant power.

2,2-Diphenyl-1-picrahydrazyl (DPPH, **126**) is a commercially available stable organic nitrogen-centred radical with an absorption maximum at 517 nm. Upon reduction of the DPPH radical to compound **127** (Scheme 41) by hydrogen atom abstraction, the deep purple colour fades, allowing the radical scavenging capacity of a given antioxidant to be determined colorimetrically.[67]



2,2-diphenyl-1-picrylhydrazyl (DPPH, **126**)
λ_{max} = 517 nm

127

Scheme 41. Structure of the stable radical DPPH (**126**), and its conversion into colourless non-radical **127** in the presence of a hydrogen atom donor, forming the basis of the DPPH assay

Briefly, the assay involves incubating methanolic solutions of increasing antioxidant concentrations in the presence of a known concentration (50 μM) of DPPH (**126**) until any observed colour change has finished and the measured absorbance is stable (30 min at rt. in this case). The inhibition of DPPH absorbance is then calculated using Equation 5, and plotted as a function of antioxidant concentration (see Section 6.3.3 for further details).

Equation 5:
$$\%inhibition = \left[1 - \frac{Abs(sample) - Abs(blank)}{Abs(control) - Abs(blank)}\right] \times 100$$

Where the control is methanol (no antioxidant) and DPPH solution; and the blank is methanol only (no antioxidant, no DPPH solution).

The results of the DPPH assay are outlined in Figure 23, depicting the inhibition of DPPH absorption by increasing concentrations of pyrone molecules **44**, **43**, and **9**, and also by the established antioxidant ascorbic acid (**78**).

The curve obtained for ascorbic acid (**78**), and the EC_{50} value of 11.5 μM generated from the data, are consistent with those reported in the literature.[67] The results show that the three pyrone molecules do not act as radical scavengers under these conditions, with no concentration-dependent increase in DPPH inhibition observed.

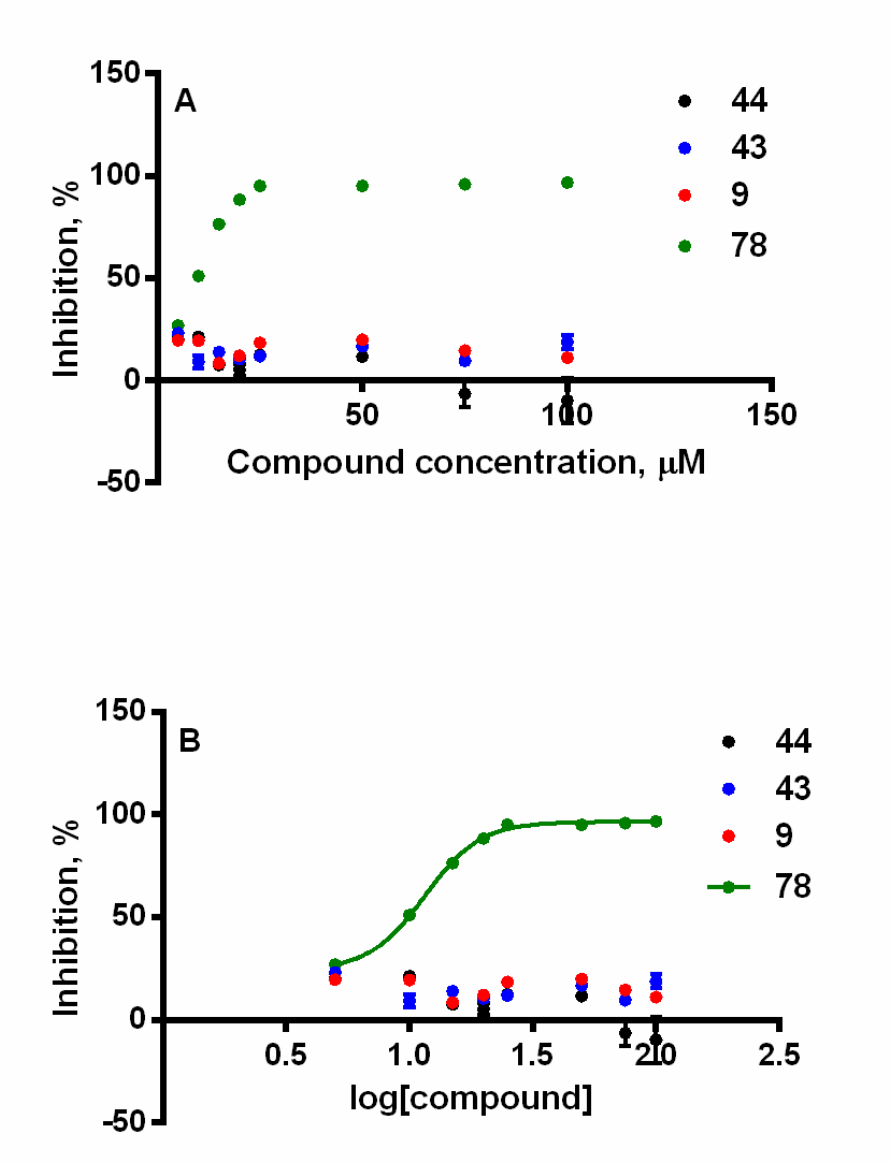
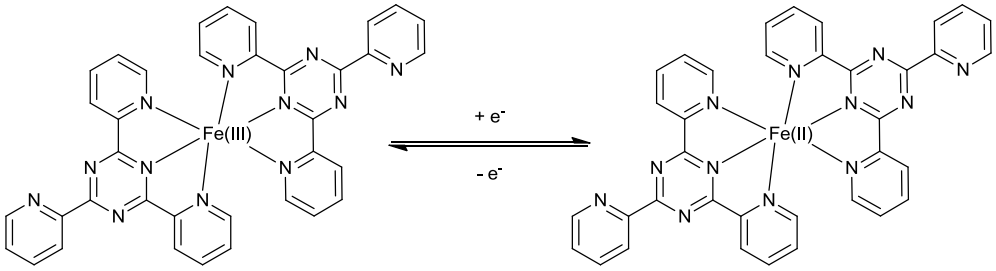


Figure 23. Concentration-dependence of DPPH inhibition by **44**, **43**, **9** and **78**, reflecting radical scavenging ability. **A**: compound concentration expressed on a linear scale; **B**: transformation of data onto a log scale, enabling determination of EC_{50} values

The DPPH assay established the lack of hydrogen atom donating capacity of molecules **44**, **43**, and **9**, showing that any photoprotective ability is not underpinned by this mechanistic pathway.

4.3 Ferric Reducing Antioxidant Power (FRAP) Assay

The Ferric Reducing Antioxidant Power (FRAP) assay uses an electron transfer reaction to assess the reducing ability of a given antioxidant. This colorimetric assay is based on the reduction of an Fe(III)-tripyridyltriazine (TPTZ) complex to its intensely blue coloured Fe(II) analogue (Scheme 42) under acidic conditions.[68]



$[Fe(III)(TPTZ)_2]^{3+}$ (**128**)

$[Fe(II)(TPTZ)_2]^{2+}$ (**129**)
λ_{max} = 593 nm

Scheme 42. Mechanistic basis of the FRAP assay: reduction of the Fe(III)-TPTZ complex **128** to the Fe(II)-TPTZ complex **129** via an electron transfer reaction

This assay works by monitoring the change in absorbance at 593 nm of an acidic solution containing an excess of the Fe(III)-TPTZ complex (**128**) and increasing concentrations of antioxidant. The absorbance change is then related to a standard curve generated by measuring the absorbance of known concentrations of the Fe(II)-TPTZ complex (**129**), allowing the concentration of Fe(II) generated to be determined, and plotted against antioxidant concentration. The results are outlined in Figure 24. (±)-α-Tocopherol (**77**) and ascorbic acid (**78**) were tested alongside the pyrones **44**, **43** and **9**.

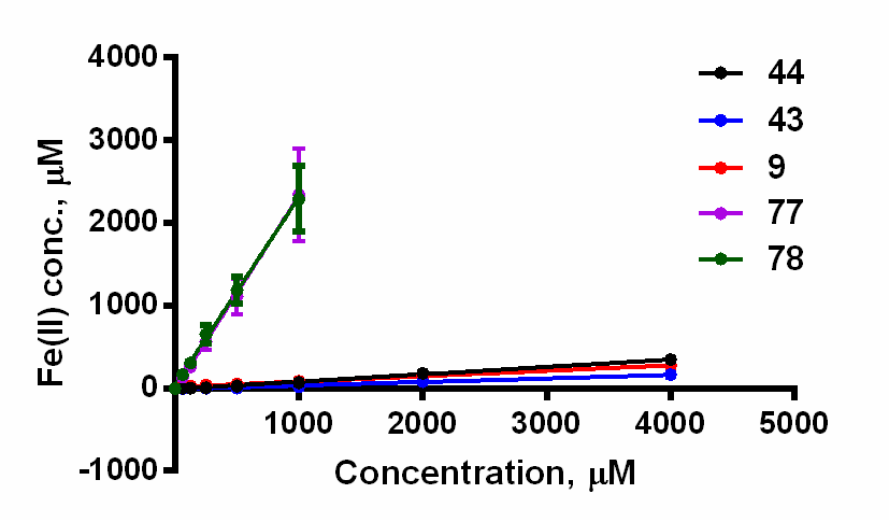


Figure 24. Dose-response lines showing concentration-dependence of Fe(II) generation from Fe(III) in the FRAP assay

It can be seen from Figure 24 that all molecules tested exhibit linear dose-response characteristics, with a concentration-dependent increase in Fe(II) generation observed. It is also apparent that the reducing ability of **77** and **78** is far stronger than that of the pyrones. This can be quantified using FRAP values, defined as the number of moles of Fe(III) that can be reduced to Fe(II) by one mole of a given antioxidant.[69] This value is given by the slope of the dose-response line. The FRAP values for the compounds tested are shown in Table 8.

The FRAP values determined for **77** and **78** match the values of 2 widely reported in the literature.[68] This means that one mole of these antioxidants is able to reduce two moles of Fe(III) to Fe(II), consistent with their known function as two-electron reductants.

Entry	Compound	FRAP value
1	**77**	2.344 ± 0.1487
2	**78**	2.275 ± 0.1208
3	**44**	0.08954 ± 0.002134
4	**43**	0.04253 ± 0.001427
5	**9**	0.06548 ± 0.001467

Table 8. FRAP values for the tested antioxidants, generated by fitting the dose-response curves using linear regression analysis, with the FRAP value equal to the slope of the fitted line

The reducing abilities of **44**, **43** and **9**, on the other hand, are shown to be very low, albeit non-zero. Thus it is unlikely that any antioxidant properties of the pyrones are due to involvement in electron-transfer reactions.

4.4 Antioxidant Properties: Mechanistic Considerations

The results of the TBARS antioxidant study remain perplexing, specifically the apparent switch from antioxidant to pro-oxidant activities displayed by the pyrone molecules upon moving from higher to lower concentrations. Antioxidant activity, particularly in biological systems, is a very complex matter.[70] Indeed, many studies have shown that various compounds have the ability to act both as antioxidants and pro-oxidants, dependent on various conditions including concentration, metal ions, and presence/absence of co-antioxidants. This includes, but is not limited to, flavonoids,[31] carotenoids[71,72] and ascorbate itself.[71,73]

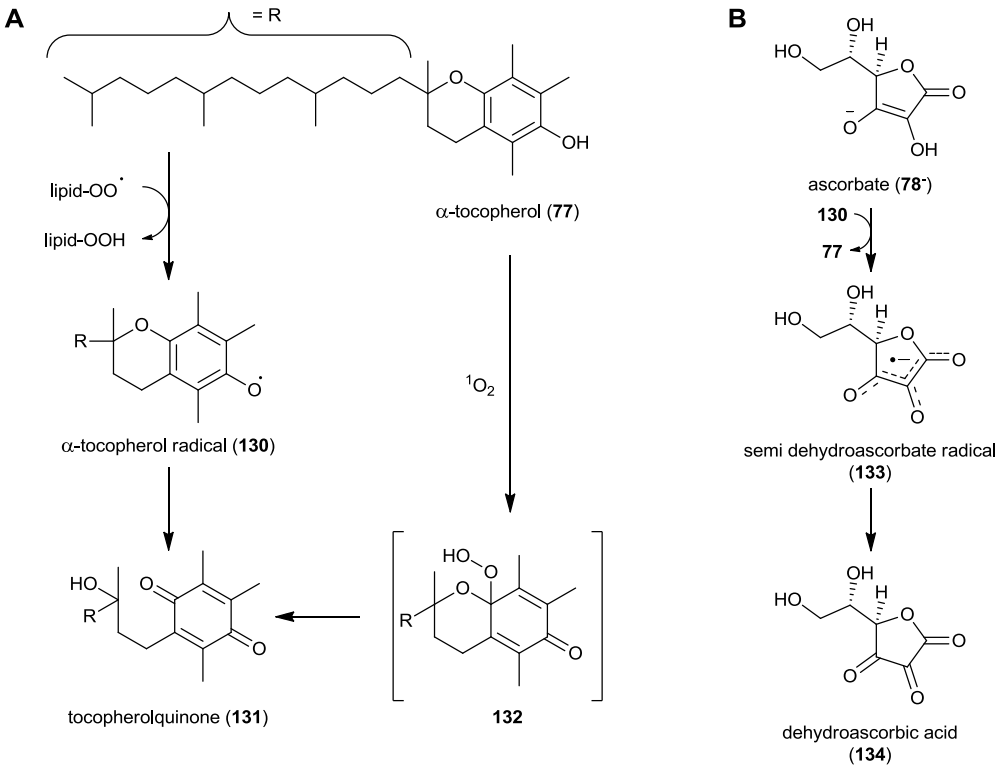
There are a number of possible sources of antioxidant action, with many antioxidants functioning via a combination of different factors.[70]

Photochemical damage to cells occurs mainly through the generation of reactive oxygen species (ROS), and so photoprotection and antioxidant activities are treated as analogous for the purposes of this discussion.

The first way in which a compound can act as an antioxidant is by preventing the generation of damaging ROS in the first place. The absorption of UV light which would otherwise generate ROS falls into this category.

The second broad mechanism of antioxidant activity is the quenching/scavenging of ROS before they get a chance to react with cell components.

The third possibility is for a molecule to act as a chain-breaking antioxidant, quenching intermediates generated by the reaction of ROS with cell components, and thus preventing propagation of the reaction. This is accepted as the main mechanism for α-tocopherol (**77**) activity, neutralising lipid peroxyl radicals and preventing further oxidative damage to the membrane, in combination with ascorbate (**78**$^{-}$), which acts to regenerate α-tocopherol (**77**) from its radical (Scheme 43).[18]



Scheme 43. Mechanistic pathways underpinning the antioxidant activities of **A**: α-tocopherol (**77**) and **B**: ascorbate (**78**$^-$)

The fourth reported method, specific to peroxidative damage to membrane components, is via stabilisation of the membrane bilayer. It has been demonstrated that changes in membrane fluidity and lateral phase separation can markedly affect the rate of lipid oxidation.[34,74]

As has been previously discussed, the pyrone molecules **44**, **43** and **9** all absorb UV radiation as part of the reaction cascade outlined in Scheme 39, and thus could help prevent the generation of ROS in this manner. Conversely, γ-pyrones have also been shown to act as photosensitisers able to promote the generation of singlet oxygen.[75] Thus, whilst reducing ROS production by preferential absorption of UV light, the molecules could also be contributing to their generation via photosensitisation.

The quenching of both first-generated ROS, and peroxidation intermediates, in the main requires an antioxidant to act as an effective reducing agent. The DPPH and FRAP assays have demonstrated that the pyrone molecules are not effective in this manner, and so are unlikely to contribute via these mechanisms. However, tridachiahydropyrone (**9**) has been shown to react with singlet oxygen to generate the related natural product oxytridachiahydropyrone (**10**) (Scheme 39),[7] and so it is possible that they contribute to antioxidant protection by scavenging of this one ROS in particular. Of course, they also might be contributing to its formation via their photosensitisation properties.

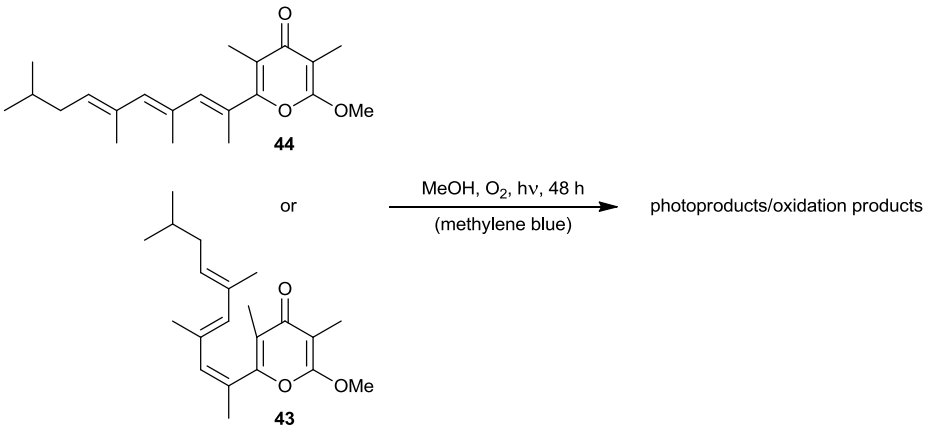
Whilst no specific studies have been conducted to ascertain whether the pyrones affect membrane fluidity, the possibility that they act to stabilise the membrane, and so reduce lipid peroxidation in this way, cannot be ruled out.

Given the higher affinity of the parent compound, (*E,E,E*)-polyene pyrone **44**, for microdomain-containing PLVs (see Section 3.3.6, Table 3), it is possible that, when added to pure phosphatidylcholine liposomes, as in the TBARS study, the pyrone molecules partition into raft regions, clustering together instead of spreading evenly throughout the membrane. This would be more likely to occur at high compound concentrations. When clustered into raft regions, any singlet oxygen generated by the photosensitisation properties of the pyrones would be likely to encounter and react with one of the pyrone molecules itself, thus being quenched before diffusion into the phosphatidylcholine bulk membrane was possible. If at lower compound

concentrations no such partitioning occurred, and the pyrone molecules were spread evenly throughout the bulk membrane, then any singlet oxygen generated via their photosensitisation would be far more likely to encounter and react with the surrounding membrane phospholipids, thus contributing to lipid peroxidation in a pro-oxidant manner. This could explain why, at 5 mol%, the pyrone molecules act as pro-oxidants whilst, at 20 mol%, they act as antioxidants. However, whilst this would explain the observed experimental results, it remains conjecture, as not enough information is available to reach a firm conclusion.

4.5 Synthetic Studies: Peroxidation of Tridachiahydropyrone Precursors

With the ability of tridachiahydropyrone (**9**) to react with singlet oxygen to form oxytridachiahydropyrone (**10**) well established, it was deemed of interest to explore whether the biomimetic precursors **44** and **43** demonstrated similar activity. Whilst the photochemical transformation of both of these molecules into tridachiahydropyrone (**9**) had been achieved in the absence of oxygen, it was not known whether this transformation would be the preferred pathway in the presence of oxygen, or whether the reaction of **44** and **43** with oxygen would take precedence. In order to explore this, a series of experiments was conducted. Methanolic solutions of **44** and **43** were saturated with oxygen, and irradiated for 48 h. The experiments were conducted in both the presence and absence of the photosensitiser methylene blue (Scheme 44).



Scheme 44. Investigation into the $^1O_2$-scavenging ability of **44** and **43**

After the 48 h reaction time, the samples were concentrated and all products generated were isolated by column chromatography. In addition to the previously known compounds **44**, **43**, **9**, **93**, and **10**, two unknown products were also isolated. One of these was formed from both **44** and **43** when irradiated in the presence of methylene blue and oxygen, whilst the minor product was only formed from **44**, again when methylene blue was added. Neither was observed in the experiments with no added photosensitiser.

Mass spectrometric analysis of these new products showed them both to correspond to the chemical formula of the starting molecules plus two oxygen atoms. It was proposed that the products had been formed by addition of singlet oxygen to the substrates via an ene reaction with one of the alkenes of the carbon chain. Additionally, it was reasoned that the two products were geometric isomers, differing only in the configuration of the alkene closest to the pyrone ring. The product isolated from the reaction of both **44** and **43** would have a *Z*-configuration at this position, whilst the product observed only in the reaction of **44** would have an *E*-configuration.

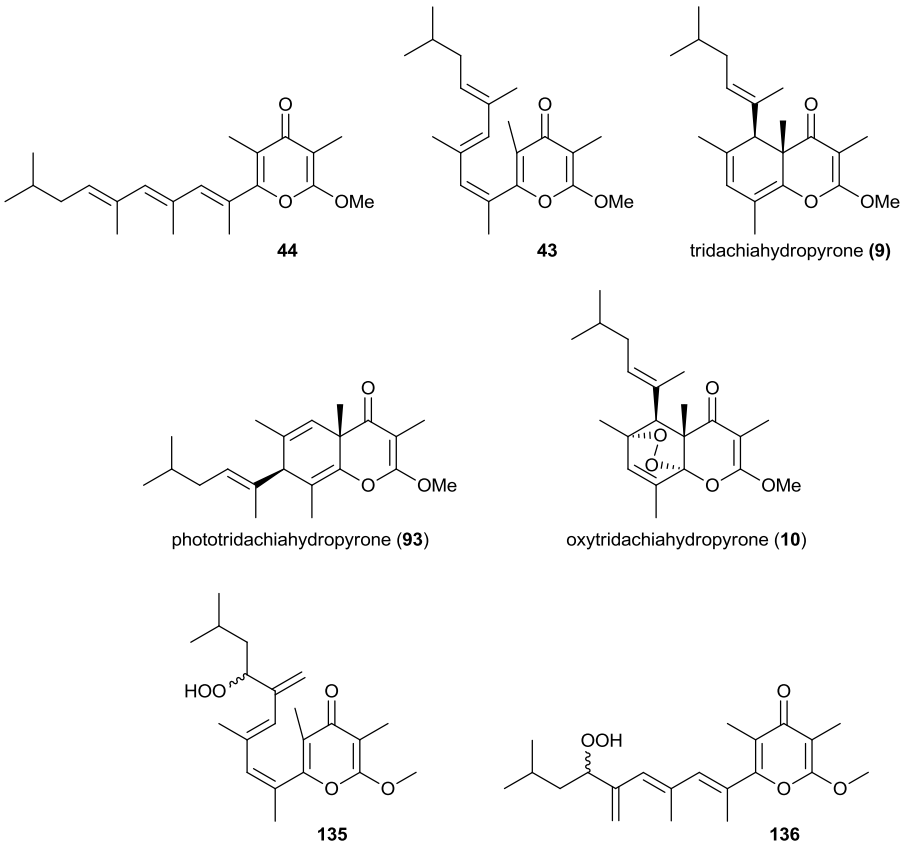


Figure 25. Structures of all the molecules isolated from the oxygenation experiments

Only one of the two new products was isolated in sufficient quantity for full spectroscopic analysis to be conducted – that isolated from both precursors. Analysis of the NMR spectra of this unknown compound revealed that it was the terminal alkene of the polyene sidechain that had undergone the ene reaction with singlet oxygen. The supporting evidence for this conclusion included the splitting of the alkyl CH_2 signal into two separate multiplets, indicating that they had become diastereotopic in nature, and thus must be adjacent to the newly formed stereocentre. Detailed analysis of the 2D NMR spectra confirmed the structure to be **135**. By analogy the structure of the minor product was reasoned to be **136**. Figure 25 shows the structures of these new products, along with the other molecules isolated from the

reaction mixtures. Table 9 shows the product distribution of each of the four experiments conducted.

Entry	Substrate	Methylene Blue	Product Distribution						
			44	**43**	**9**	**93**	**10**	**135**	**136**
1	**44**	20 mol%	15%	29%	3%	-	5%	20%	5%
2	**43**	20 mol%	-	55%	4%	-	3%	13%	-
3	**44**	-	26%	52%	13%	2%	-	-	-
4	**43**	-	-	84%	12%	2%	-	-	-

Table 9. Product distributions obtained from the oxygenation experiments. All isolated yields

No oxygenated products were obtained in the absence of an added photosensitiser (Table 9, Entries 3 and 4). This shows that the photosensitising ability of the pyrone molecules **44** and **43** is not very potent, as not enough singlet oxygen was generated for reaction of the substrates with $^1O_2$ to dominate. Instead in these cases mixtures of the known photochemical products tridachiahydropyrone (**9**) and phototridachiahydropyrone (**93**) were isolated, along with unreacted starting material.

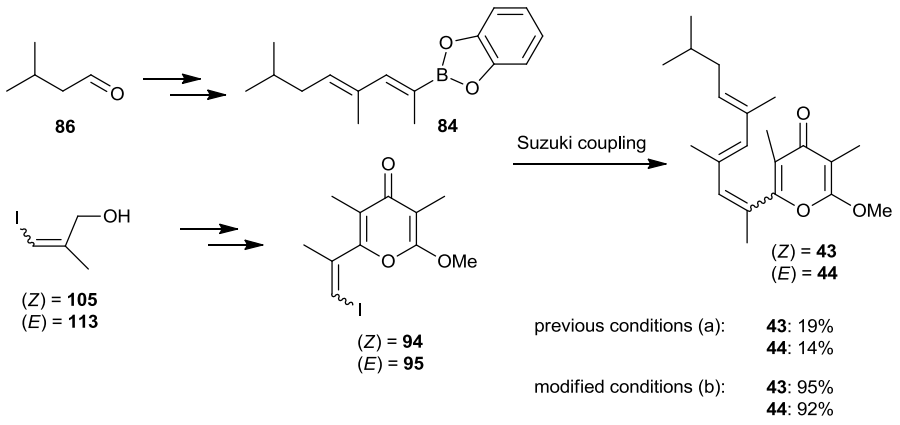
In the experiments with added methylene blue (Table 9, Entries 1 and 2), no phototridachiahydropyrone (**93**) was formed, despite formation of its precursor tridachiahydropyrone (**9**) taking place. Instead formation of oxytridachiahydropyrone (**10**) was observed, showing that, in the presence of singlet oxygen, the cycloaddition reaction of **9** with $^1O_2$ is preferred over the photochemical rearrangement. This is unsurprising, given that no

phototridachiahydropyrone (**93**) was formed during the previous synthesis of **10** from **9** (Section 2.5, Scheme 38). However, whilst oxygenation over photochemical reaction of **9** is clearly preferred under the conditions employed, that is not the case for the reaction of **44** and **43**, otherwise no formation of **9** would have been observed, had the ene reaction with singlet oxygen dominated. Instead a mixture of straightforward photochemical reaction (double bond isomerisation and/or electrocyclisation) and oxygenation products was formed.

The ene reaction of **44** and **43** with singlet oxygen proved highly selective for the terminal alkene of the sidechain. Reaction at this position, as opposed to either of the internal double bonds of the chain, preserves the maximum level of conjugation in the product. The terminal alkene could also be more easily accessible than the others. These results are consistent with those reported for the oxygenation of similar compounds, in particular that of cyercene A, where the analogous ene reaction was also found to occur solely at the terminal alkene site.[75,76]

Chapter 5 Summary and Conclusions

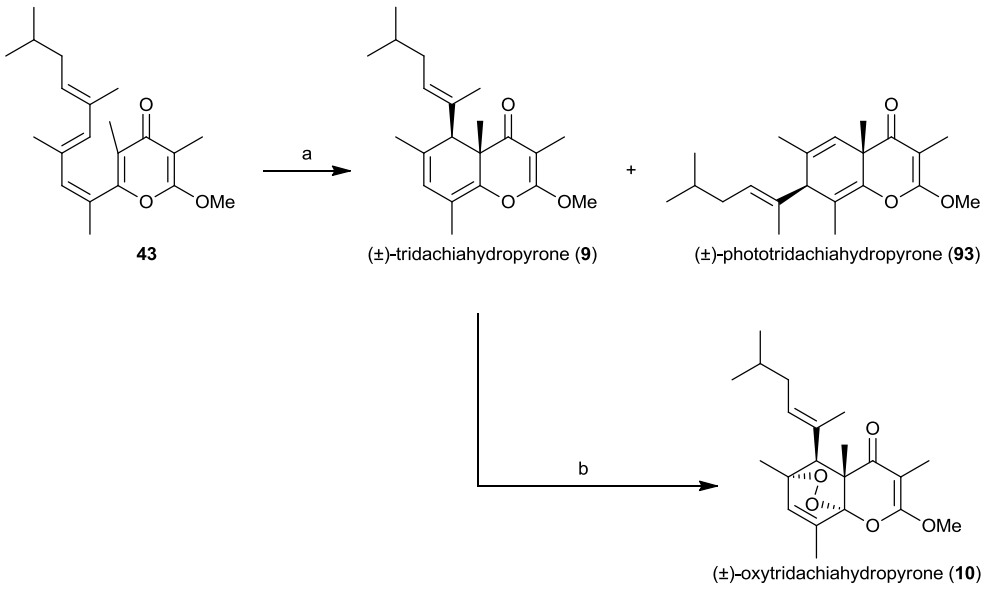
During this work a number of synthetic tasks have been accomplished. The biomimetic polyene precursors, **43** and **44**, of the natural product tridachiahydropyrone (**9**), were synthesised, using an adapted route. Iodo-pyrone coupling fragments **94** and **95** were synthesised instead of the bromo-analogues **39** and **85** used in the original route, in the hope of improving the yield of the key Suzuki coupling reaction. Whilst this approach did not in itself lead to an increased yield, the adoption of a modified coupling protocol, utilising TlOEt as the base, brought about the desired improvement (Scheme 45).



Scheme 45. Improved route to the tridachiahydropyrone precursors **43** and **44**: key step. Reagents and conditions: (a) $Pd(PPh_3)_4$, THF-H_2O, KOH, 80 °C, 20 h; (b) $Pd(PPh_3)_4$, THF-H_2O, TlOEt, 50 °C, 4 h

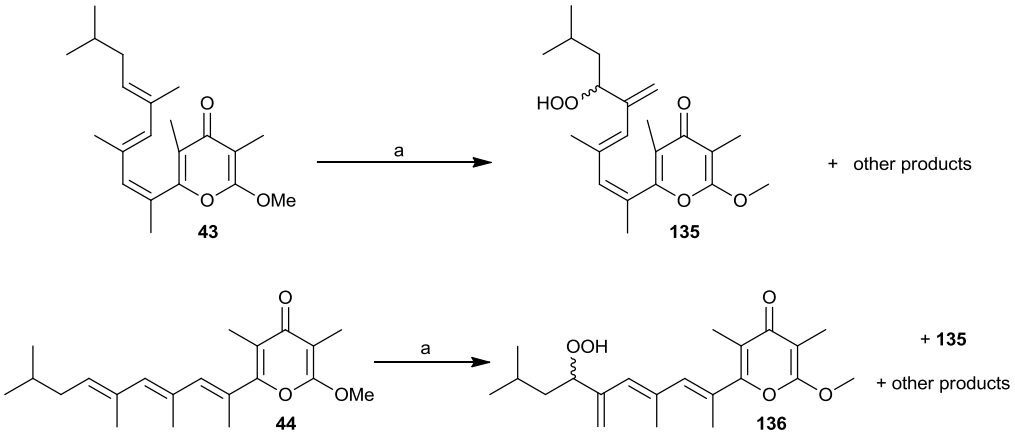
Tridachiahydropyrone (**9**) and phototridachiahydropyrone (**93**) were synthesised by photochemically-induced electrocyclisation and sigmatropic rearrangement reactions of the biomimetic precursors. Oxytridachiahydropyrone (**10**) was also synthesised, by the photochemical

[4+2] cycloaddition of singlet oxygen to tridachiahydropyrone (**9**) (Scheme 46).



Scheme 46. Biomimetic synthesis of **9**, **93** and **10**. Reagents and conditions: (a) MeOH, hν, 37 h, **9**: 17%, **93**: 13%; (b) MeOH, methylene blue, O_2, hν, 5 h, 97%

Two new isomeric hydroperoxides, **135** and **136**, were synthesised by the photochemical oxygenation of **43** and **44**, via ene reactions with singlet oxygen (Scheme 47).



Scheme 47. Synthesis of the novel hydroperoxides **135** and **136**. Reagents and conditions: (a) MeOH, methylene blue, O_2, hν, 48 h, **135**: 13% from **43**, 20% from **44**, **136**: 5% from **44**

Fluorescence spectroscopy-based biophysical studies of the interactions of **9, 43** and **44** with phospholipid vesicles (PLVs) demonstrated their propensity to bind to membranes, supporting the theory that these compounds are located in the cell membrane of the producing mollusc. The photochemical isomerisation and electrocyclisation reactions of the precursors **43** and **44** to form tridachiahydropyrone (**9**) were conducted in the PLVs. The racemic nature of the product isolated from these experiments indicates that if the cell membrane is the biological site of this transformation, then any enantioselectivity conferred in the natural system must be due to the presence of other bilayer components, such as integral membrane proteins, not present in the membrane models here used. This raises a limitation of liposomes as models of biological membranes – they are very simplistic versions of a far more complex system (Figure 26).

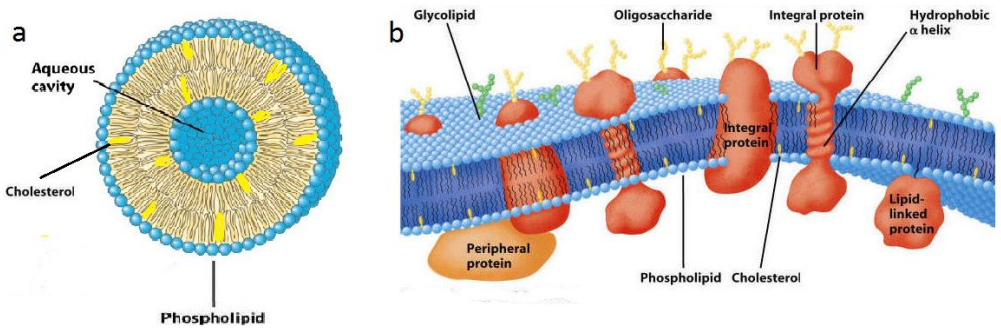


Figure 26. Schematic representation of the simplicity of a PC/cholesterol liposome **(a)** in comparison to a complex biological membrane **(b)**

The feasibility of **9**, **43** and **44** functioning as sunscreens was investigated by measuring their inhibition of photochemical lipid peroxidation in irradiated PLVs. This was achieved using the TBARS assay. The compounds demonstrated photoprotective action at high concentrations, whilst at lower concentrations

pro-oxidant effects were observed. A possible explanation for these contrasting results, involving membrane raft formation at higher concentrations, has been proposed.

The mechanistic basis of these photoprotective effects was investigated using the DPPH and FRAP assays. From these results it was concluded that any antioxidant abilities of **9**, **43** and **44** are not due to radical scavenging and/or reducing actions.

In summary, the theory that the tridachiahydropyrone family of natural products act as a defence system protecting the producing organism, the sacoglossan mollusc *Tridachia crispata*, from the damaging effects of UV radiation and reactive oxygen species has been explored using a combination of synthetic and biophysical studies. The molecules were first synthesised using a modified route, improving on previous yields of key late-stage transformations. The interactions of the molecules with synthetic membrane systems were then explored using fluorescence spectroscopy. Finally, the photoprotective properties of the tridachiahydropyrones were investigated using a number of colorimetric assay techniques.

Chapter 6 Experimental

6.1 Organic Synthesis

6.1.1 Experimental techniques

Reactions were performed in flame-dried glassware under an atmosphere of argon and stirred magnetically unless otherwise stated. For use as a reaction solvent CH_2Cl_2 was freshly distilled from CaH_2; THF was freshly distilled from sodium and benzophenone; Et_2O and toluene were degassed and dried over alumina under nitrogen. All other reagents were obtained commercially and used without further purification. Flash column chromatography was performed using Merck silica gel 60 as the stationary phase. Where not otherwise specified flash column chromatography was performed using petrol-EtOAc mixtures of increasing polarity (as appropriate to the R_f value of the compound to be isolated) as the mobile phase. Petrol refers to petroleum spirit (b.p. 40-60 °C). The lamp used in the photochemical experiments was a 125 W medium-pressure mercury lamp (model 3010; power supply 3110) purchased from Photochemical Reactors Ltd. Photochemical reactions were conducted in standard laboratory round-bottomed flasks, with an approximate distance of 20 cm between sample and light source.

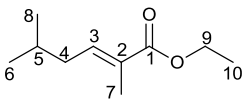
6.1.2 Analysis

Compounds previously described in the literature were characterised to levels consistent with that reported. Thin layer chromatography was carried out on aluminium-backed plates pre-coated with silica (0.2 mm, 60 F_{254}, Merck). The plates were developed using UV light and basic potassium permanganate

solution. Melting points were recorded using a STUART SMP3 apparatus and are uncorrected. Infrared (IR) spectra were recorded using a Bruker Tensor 27 FT-IR spectrophotometer with a neat film on an NaCl disc or as a solution in $CHCl_3$. IR peaks are quoted in as ν_{max} in cm^{-1}. ^1H and ^{13}C NMR spectra were recorded in $CDCl_3$, $(CD_3)_2SO$ or CD_3OD at ambient temperature using Bruker DPX400 (400 MHz), AV400 (400 MHz) and AV(III)400 (400 MHz) spectrometers. Data is expressed as chemical shifts in parts per million (ppm) relative to residual solvent signals of $CDCl_3$ (^1H NMR 7.27; ^{13}C NMR 77.0), $(CD_3)_2SO$ (^1H NMR 2.50; ^{13}C NMR 39.5) or CD_3OD (^1H NMR 3.31; ^{13}C NMR 49.0) as the internal standard on the δ scale. The following abbreviations are used to designate the multiplicity of each signal; s, singlet; d, doublet; dd, doublet of doublets; dt, doublet of triplets; t, triplet; tt, triplet of triplets; tq, triplet of quartets; q, quartet; m, multiplet; br, broad. Coupling constants *J* are given in Hz. High-resolution mass spectra were obtained using a Bruker MicroTOF mass spectrometer operating in electrospray ionisation (ESI) mode.

6.1.3 Experimental Procedures and Characterisation Data

(*E*)-Ethyl 2,5-dimethylhex-2-enoate (88)[6]

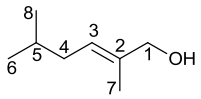


Ethyl 2-(triphenylphosphoranylidene)propanoate (**87**) (42.7 g, 118 mmol) was added in one portion to a stirred solution of isovaleraldehyde (**86**) (8.50 mL, 79.0 mmol) in CH_2Cl_2 (300 mL), and the resultant solution heated at reflux for 72 h. The reaction mixture was cooled to rt. and pentane (80 mL) was added,

causing precipitation of the triphenylphosphine oxide by-product, which was removed by filtration. The filtrate was carefully concentrated under reduced pressure and the residue purified by flash column chromatography (Et_2O), affording (*E*)-ethyl 2,5-dimethylhex-2-enoate (**88**) as a colourless oil (13.2 g, 98%).

$\mathbf{R_f}$ = 0.25 (5% EtOAc in petrol); ν_{max} (cm^{-1}) (thin film): 2958, 2872, 1713, 1650, 1457, 1387, 1368, 1282; δ_H ($CDCl_3$, 400 MHz): 6.79 (tq, *J* = 7.6, 1.4 Hz, 1H, 3-H_1), 4.20 (q, *J* = 7.2 Hz, 2H, 9-H_2), 2.07 (t, *J* = 7.6 Hz, 2H, 4-H_2), 1.83 (br. s, 3H, 7-H_3), 1.71 - 1.82 (m, 1H, 5-H_1), 1.30 (t, *J* = 7.2 Hz, 3H, 10-H_3), 0.94 (d, *J* = 6.7 Hz, 6H, 6-H_3 and 8-H_3); δ_C ($CDCl_3$ 100 MHz): 168.3 (C-1), 141.3 (C-3), 128.3 (C-2), 60.4 (C-9), 37.8 (C-4), 28.3 (C-5), 22.5 (C-6 and C-8), 14.3 (C-10), 12.5 (C-7).

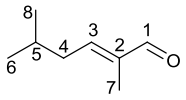
(*E*)-2,5-Dimethylhex-2-en-1-ol (89)[6]



DIBAL-H (1.0 M solution in hexane) (90.5 mL, 90.5 mmol) was added to a stirred solution of (*E*)-ethyl 2,5-dimethylhex-2-enoate (**88**) (7.00 g, 41.1 mmol) in CH_2Cl_2 (70 mL) at -78 °C. The reaction mixture was warmed to rt. and stirred for 16 h, after which time it was cooled to 0 °C and quenched by addition of MeOH (20 mL). Sat. aq. potassium sodium tartrate (50 mL) was added, and the mixture stirred at rt. for 16 h. The organic layer was washed with brine (50 mL), dried over anhydrous $MgSO_4$ and concentrated under reduced pressure. The residue was purified by flash column chromatography (Et_2O), affording (*E*)-2,5-dimethylhex-2-en-1-ol (**89**) as a colourless oil (5.09 g, 97%).

R_f = 0.51 (25% EtOAc in petrol); **ν_{max}** (cm^{-1}) (thin film): 3333, 2956, 2871, 1467, 1385, 1367; **δ_H** ($CDCl_3$, 400 MHz): 5.44 (tq, *J* = 7.3, 1.3 Hz, 1H, 3-H_1), 4.02 (s, 2H, 1-H_2), 1.90 - 1.96 (m, 2H, 4-H_2), 1.67 (br. s, 3H, 7-H_3), 1.59 - 1.66 (m, 1H, 5-H_1), 0.91 (d, *J* = 6.6 Hz, 6H, 6-H_3 and 8-H_3); **δ_C** ($CDCl_3$ 100 MHz): 135.2 (C-2), 125.4 (C-3), 69.1 (C-1), 36.7 (C-4), 28.7 (C-5), 22.4 (C-6 and C-8), 13.8 (C-7).

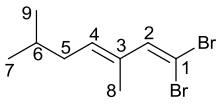
(*E*)-2,5-Dimethylhex-2-enal (90)[6]



Dess Martin periodinane (18.3 g, 43.1 mmol) was added portionwise to a solution of (*E*)-2,5-dimethylhex-2-en-1-ol (**89**) (4.19 g, 32.7 mmol) in CH_2Cl_2 (200 mL) at 0 °C. The resultant reaction mixture was stirred at rt. for 30 min, after which time sat. aq. $NaHCO_3$ (100 mL) was added, and the solution stirred for 20 min. The aqueous layer was extracted with CH_2Cl_2 (3 x 75 mL), and the combined organic extracts were dried over anhydrous $MgSO_4$ and carefully concentrated under reduced pressure. The residue was purified by flash column chromatography (Et_2O) to afford (*E*)-2,5-dimethylhex-2-enal (**90**) as a colourless oil (3.84 g, 93%).

R_f = 0.36 (5% EtOAc in petrol); **ν_{max}** (cm^{-1}) (thin film): 2960, 2873, 1728, 1468, 1370, 1292; **δ_H** ($CDCl_3$, 400 MHz): 9.42 (s, 1H, 1-H_1), 6.53 (tq, *J* = 7.9, 1.5 Hz, 1H, 3-H_1), 2.23 - 2.29 (m, 2H, 4-H_2), 1.80 - 1.88 (m, 1H, 5-H_1), 1.73 - 1.77 (m, 3H, 7-H_3), 0.97 (d, *J* = 6.6 Hz, 6H, 6-H_3 and 8-H_3); **δ_C** ($CDCl_3$ 100 MHz): 195.7 (C-1), 154.2 (C-3), 140.3 (C-2), 38.3 (C-4), 28.6 (C-5), 22.8 (C-6 and C-8), 9.6 (C-7).

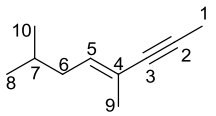
(*E*)-1,1-Dibromo-3,6-dimethylhepta-1,3-diene (91)[6]



Carbon tetrabromide (6.57 g, 19.8 mmol) was added portionwise to a stirred solution of PPh_3 (10.4 g, 39.7 mmol) in CH_2Cl_2 (100 mL) at 0 °C, and the reaction mixture warmed to rt. and stirred for 15 min. The resultant deep red solution was then re-cooled to 0 °C and a solution of (*E*)-2,5-dimethylhex-2-enal (**90**) (1.66 g, 13.2 mmol) in CH_2Cl_2 (30 mL) added. After stirring at rt. for 1.5 h, H_2O (100 mL) was added, and the aqueous layer extracted with CH_2Cl_2 (3 x 50 mL). The combined organic extracts were dried over anhydrous $MgSO_4$ and carefully concentrated under reduced pressure. The residue was purified by flash column chromatography (petrol) to afford (*E*)-1,1-dibromo-3,6-dimethylhepta-1,3-diene (**91**) as a colourless oil (3.41 g, 92%).

$\mathbf{R_f}$ = 0.81 (hexane); ν_{max} (cm^{-1}) (thin film): 2957, 2931, 2869, 1783, 1723, 1603, 1465, 1385, 1368, 1340; δ_H ($CDCl_3$, 400 MHz): 6.95 (s, 1H, 2-H), 5.64 - 5.71 (m, 1H, 4-H), 1.94 - 2.00 (m, 2H, 5-H_2), 1.84 - 1.87 (m, 3H, 8-H_3), 1.65 - 1.74 (m, 1H, 6-H_1), 0.92 (d, *J* = 6.6 Hz, 6H, 7-H_3 and 9-H_3); δ_C ($CDCl_3$ 100 MHz): 141.1 (C-4), 134.8 (C-2), 132.0 (C-3), 85.5 (C-1), 37.2 (C-5), 28.5 (C-6), 22.4 (C-7 and C-9), 15.3 (C-8).

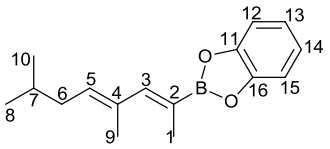
(*E*)-4,7-Dimethyloct-4-en-2-yne (92)[6]



A 1.6 M solution of ^{n}BuLi in hexane (21.3 mL, 34.0 mmol) was added dropwise to a solution of (*E*)-1,1-dibromo-3,6-dimethylhepta-1,3-diene (**91**) (4.80 g, 17.0 mmol) in THF (25 mL) at -78 °C, and the resultant stirred solution warmed to rt. over 2 h. The mixture was then recooled to -78 °C and iodomethane (4.00 mL, 64.0 mmol) added dropwise. The mixture was then warmed to rt. and stirred for a further 18 h. Sat. aq. NH_4Cl (30 mL) was added, the layers separated, and the aqueous layer extracted with Et_2O (3 x 70 mL). The combined organic extracts were dried over anhydrous $MgSO_4$ and concentrated under reduced pressure. The residue was purified by flash column chromatography (petrol) to afford (*E*)-4,7-dimethyloct-4-en-2-yne (**92**) (1.50 g, 71%) as a colourless oil.

$\mathbf{R_f}$ = 0.55 (hexane); ν_{max} (cm^{-1}) (thin film): 2956, 2919, 2870, 1465, 1382, 1257; δ_H ($CDCl_3$, 400 MHz): 5.78 (t, *J* = 7.6 Hz, 1H, 5-H_1), 1.95 - 2.00 (m, 2H, 6-H_2), 1.94 (s, 3H, 1-H_3), 1.75 (br. s, 3H, 9-H_3), 1.61 - 1.69 (m, 1H, 7-H_1), 0.91 (d, *J* = 6.7 Hz, 6H, 8-H_3 and 10-H_3); δ_c ($CDCl_3$, 100 MHz): 135.6 (C-5), 118.4 (C-4), 82.9 (C-3), 81.7 (C-2), 37.5 (C-6), 28.6 (C-7), 22.4 (C-8 and C-10), 17.5 (C-9), 4.1 (C-1).

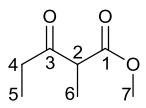
2-((2*Z*,4*E*)-4,7-Dimethylocta-2,4-dien-2-yl)benzo[*d*][1,3,2]dioxaborole (84)[6]



(*E*)-4,7-Dimethyl-oct-4-en-2-yne (**92**) (0.400 g, 2.90 mmol) and catecholborane (0.350 g, 2.90 mmol) were heated at 80 °C with stirring. After 2 h, the mixture was cooled to rt., affording 2-((2*Z*,4*E*)-4,7-dimethylocta-2,4-dien-2-yl)benzo[*d*][1,3,2]dioxaborole (**84**) (0.740 g, >99%) as a colourless oil which was used without purification.

$\mathbf{R_f}$ = 0.38 (25% EtOAc in petrol); ν_{max} (cm^{-1}) (thin film): 3452, 2956, 2869, 1596, 1473, 1411, 1382, 1312, 1238; δ_H ($CDCl_3$, 400 MHz): 7.21 - 7.25 (m, 2H, 12-H_1 and 15-H_1), 7.10 (br. s, 1H, 3-H_1), 7.06 - 7.09 (m, 2H, 13-H_1 and 14-H_1), 5.70 (br. t, *J* = 7.5 Hz, 1H, 5-H_1), 2.12 (d, *J* = 1.6 Hz, 3H, 1-H_3), 2.04 - 2.09 (m, 2H, 6-H_2), 1.90 (d, *J* = 0.9 Hz, 3H, 9-H_3), 1.69 - 1.75 (m, 1H, 7-H_1), 0.95 (d, *J* = 6.6 Hz, 6H, 8-H_3 and 10-H_3); δ_c ($CDCl_3$, 100 MHz): 149.9 (C-3), 148.6 (C-11 and C-16), 134.8 (C-5), 134.1 (C-4), 122.4 (C-13 and C-14), 112.2 (C-12 and C-15), 37.5 (C-6), 28.8 (C-7), 22.5 (C-8 and C-10), 16.6 (C-9), 15.4 (C-1), C-2 not observed.

Methyl 2-methyl-3-oxopentanoate (102)[40]

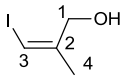


A solution of methyl propionylacetate (**107**) (25.0 mL, 199 mmol) and K_2CO_3 (82.6 g, 598 mmol) in THF (350 mL) was stirred at reflux for 2.5 h. The reaction mixture was then cooled to 0 °C, and iodomethane (15.0 mL, 239 mmol)

added dropwise. After stirring at 0 °C for 18 h, the reaction mixture was filtered through a celite pad and concentrated under reduced pressure, affording methyl 2-methyl-3-oxopentanoate (**102**) (27.8 g, 97%) as a yellow oil.

R_f = 0.15 (5% EtOAc in petrol); **ν_{max}** (cm^{-1}) (thin film): 2984, 2944, 1748, 1717, 1457, 1206; **δ_H** ($CDCl_3$, 400 MHz): 3.73 (s, 3H, 7-H_3), 3.54 (q, *J* = 7.2 Hz, 1H, 2-H_1), 2.41 - 2.70 (m, 2H, 4-H_2), 1.34 (d, *J* = 7.2 Hz, 3H, 6-H_3), 1.07 (t, *J* = 7.3 Hz, 3H, 5-H_3); **δ_C** ($CDCl_3$, 100 MHz): 206.3 (C-3), 171.1 (C-1), 52.4 (C-2), 52.3 (C-7), 34.6 (C-4), 12.9 (C-6), 7.6 (C-5); **HRMS** (ESI) calculated for $C_7H_{12}NaO_3$ $[M+Na]^+$ 167.0679, found 167.0683.

(*Z*)-3-Iodo-2-methylprop-2-en-1-ol (105)[39]

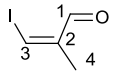


A 3.0 M solution of MeMgBr in Et_2O (50.0 mL, 150 mmol) was added dropwise to a suspension of CuI (10.5 g, 55.0 mmol) in Et_2O (150 mL) at -10 °C. Propargyl alcohol (**103**) (3.20 mL, 55.0 mmol) was then added dropwise to the mixture, and the resultant orange solution stirred at rt. for 3 h. The reaction mixture was cooled to -10 °C, a solution of ICl (12.5 g, 77.0 mmol) in Et_2O (75 mL) added dropwise, and the resultant mixture stirred at rt. for 19 h. The reaction was quenched by addition of 10% aq. NH_4Cl (75 mL) and stirred for 4 h, after which time the mixture was separated and the aqueous layer extracted with Et_2O (3 x 100 mL). The combined organic extracts were dried over anhydrous $MgSO_4$, and concentrated under reduced pressure. The

resultant residue was purified by flash column chromatography to afford (*Z*)-3-iodo-2-methylprop-2-en-1-ol (**105**) (5.34 g, 49%) as a yellow oil.

$\mathbf{R_f}$ = 0.42 (25% EtOAc in petrol); ν_{max} (cm^{-1}) (thin film): 3320, 2914, 2853, 1621, 1445, 1377, 1276; δ_H ($CDCl_3$, 400 MHz): 5.98 (br. s, 1H, 3-H_1), 4.25 (s, 2H, 1-H_2), 1.99 (d, *J* = 1.2 Hz, 3H, 4-H_3); δ_C ($CDCl_3$, 100 MHz): 146.1 (C-2), 74.9 (C-3), 68.1 (C-1), 21.6 (C-4).

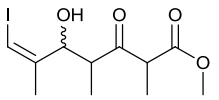
(*Z*)-3-Iodo-2-methylacrylaldehyde (100)[39]



MnO_2 (69.6 g, 800 mmol) was added in one portion to a solution of (*Z*)-3-iodo-2-methylprop-2-en-1-ol (**105**) (7.92 g, 40.0 mmol) in CH_2Cl_2 (450 mL), and the reaction mixture stirred at rt. for 2 h. The mixture was then filtered through celite, and the filtrate concentrated under reduced pressure to afford (*Z*)-3-iodo-2-methylacrylaldehyde (**100**) (6.21 g, 79%) as a yellow oil that was used without further purification.

$\mathbf{R_f}$ = 0.68 (25% EtOAc in petrol); ν_{max} (cm^{-1}) (thin film): 2921, 2851, 1696, 1653, 1458; δ_H ($CDCl_3$, 400 MHz): 9.79 (s, 1H, 1-H_1), 7.46 (q, *J* = 1.4 Hz, 1H, 3-H_1), 1.91 (d, *J* = 1.4 Hz, 3H, 4-H_3); δ_C ($CDCl_3$, 100 MHz): 195.4 (C-1), 141.8 (C-2), 96.6 (C-3), 18.4 (C-4).

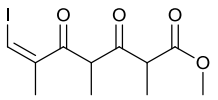
(*Z*)-Methyl 5-hydroxy-7-iodo-2,4-dimethyl-3-oxohept-6-enoate (108)[37]



Methyl 2-methyl-3-oxopentanoate (**102**) (7.21 g, 50.0 mmol) was added dropwise to a suspension of NaH (60% in mineral oil) (2.14 g, 52.5 mmol) in THF (400 mL) at 0 °C and the mixture stirred at rt. for 30 min, after which time the mixture was cooled to 0 °C and ^{n}BuLi (1.6 M in hexanes) (33.4 mL, 53.5 mmol) added dropwise. The resultant mixture was stirred at rt. for a further 30 min before a solution of (*Z*)-3-iodo-2-methylacrylaldehyde (**100**) (6.21 g, 31.7 mmol) in THF (50 mL) was added dropwise at 0 °C. The resultant solution was stirred at rt. for 1.5 h and then quenched by addition of sat. aq. NH_4Cl (250 mL). The mixture was separated and the aqueous layer extracted with Et_2O (2 x 250 mL). The combined organic extracts were dried over anhydrous $MgSO_4$ and concentrated under reduced pressure. The residue was purified by column chromatography to afford (*Z*)-methyl 5-hydroxy-7-iodo-2,4-dimethyl-3-oxohept-6-enoate (**108**) (8.64 g, 80%) as a mixture of diastereomers, which was carried forward without characterisation.

R_f = 0.33 (25% EtOAc in petrol); **HRMS** (ESI) calculated for $C_{11}H_{17}INaO_4$ $[M+Na]^+$ 363.0064, found 363.0060.

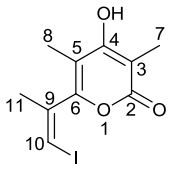
(*Z*)-Methyl 7-iodo-2,4-dimethyl-3,5-dioxohept-6-enoate (98)[37]



Dess-Martin periodinane (11.2 g, 26.4 mmol) was added portionwise to a solution of (*Z*)-methyl 5-hydroxy-7-iodo-2,4-dimethyl-3-oxohept-6-enoate (**108**) (5.31 g, 15.6 mmol) in non-anhydrous CH_2Cl_2 (160 mL) at 0 °C in a flask open to the air and the resultant mixture stirred at rt. for 3 h. Sat. aq. $NaHCO_3$ (100 mL) and sat. aq. Na_2SO_3 (100 mL) were then added, the layers separated, and the aqueous layer extracted with CH_2Cl_2 (2 x 100 mL). The combined organic extracts were dried over anhydrous $MgSO_4$ and concentrated under reduced pressure. The residue was purified by column chromatography to afford (*Z*)-methyl 7-iodo-2,4-dimethyl-3,5-dioxohept-6-enoate (**98**) (5.06 g, 96%) as a mixture of diastereomers that was taken on without characterisation.

R_f = 0.48 (25% EtOAc in petrol); **HRMS** (ESI) calculated for $C_{11}H_{15}INaO_4$ $[M+Na]^+$ 360.9907, found 360.9900.

(*Z*)-4-Hydroxy-6-(1-iodoprop-1-en-2-yl)-3,5-dimethyl-2H-pyran-2-one (96)[37]

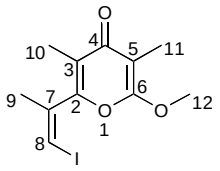


A solution of (*Z*)-methyl 7-iodo-2,4-dimethyl-3,5-dioxohept-6-enoate (**98**) (4.69 g, 13.9 mmol) and DBU (4.10 mL, 27.7 mmol) in toluene (170 mL) was

stirred at 70 °C for 4 h. The reaction mixture was then concentrated under reduced pressure and the residue purified by flash column chromatography (0.1% AcOH, 5% MeOH in CH_2Cl_2) to afford (*Z*)-4-hydroxy-6-(1-iodoprop-1-en-2-yl)-3,5-dimethyl-2H-pyran-2-one (**96**) (4.02 g, 95%) as a white solid.

R_f = 0.11 (5% MeOH in CH_2Cl_2); **mp**: 191-192 °C (lit: 193-194.5 °C)[37]; **ν_{max}** (cm^{-1}) (thin film): 3066 (br), 1673, 1619, 1565; **δ_H** (MeOD-d_4, 400 MHz): 6.73 (q, *J* = 1.5 Hz, 1H, 10-H_1), 2.08 (d, *J* = 1.5 Hz, 3H, 11-H_3), 1.95 (s, 3H, 8-H_3), 1.93 (s, 3H, 7-H_3); **δ_c** (MeOD-d_4, 100 MHz): 168.2 (C-2), 167.6 (C-4), 157.8 (C-6), 142.5 (C-9), 110.1 (C-5), 100.4 (C-3), 83.5 (C-10), 23.4 (C-11), 11.2 (C-8), 9.2 (C-7); **HRMS** (ESI) calculated for $C_{10}H_{11}INaO_3$ $[M+Na]^+$ 328.9645, found 328.9648.

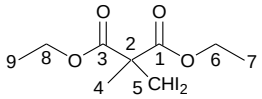
(*Z*)-2-(1-Iodoprop-1-en-2-yl)-6-methoxy-3,5-dimethyl-4*H*-pyran-4-one (94)[37]



A mixture of (*Z*)-4-hydroxy-6-(1-iodoprop-1-en-2-yl)-3,5-dimethyl-2H-pyran-2-one (**96**) (5.80 g, 18.9 mmol), Me_2SO_4 (3.60 mL, 37.9 mmol) and Li_2CO_3 (4.20 g, 56.8 mmol) in acetone (45 mL) was stirred at reflux for 96 h. The reaction mixture was then cooled to rt. and Et_2O (30 mL) added. The solid was filtered off and the filtrate concentrated under reduced pressure. The residue was purified by flash column chromatography to afford (*Z*)-2-(1-iodoprop-1-en-2-yl)-6-methoxy-3,5-dimethyl-4*H*-pyran-4-one (**94**) (2.05 g, 34%) as a yellow oil.

$\mathbf{R_f}$ = 0.14 (25% EtOAc in petrol); ν_{max} (cm^{-1}) (thin film): 1663, 1613, 1586, 1410, 1378; δ_H ($CDCl_3$, 400 MHz): 6.61 (q, *J* = 1.5 Hz, 1H, 8-H_1), 3.97 (s, 3H, 12-H_3), 2.12 (d, *J* = 1.5 Hz, 3H, 9-H_3), 1.92 (s, 3H, 10-H_3), 1.89 (s, 3H, 11-H_3); δ_c ($CDCl_3$, 100 MHz): 180.8 (C-4), 162.5 (C-6), 155.8 (C-2), 140.5 (C-7), 119.0 (C-3), 100.1 (C-5), 83.0 (C-8), 55.6 (C-12), 23.5 (C-9), 10.6 (C-10), 6.9 (C-11); **HRMS** (ESI) calculated for $C_{11}H_{13}INaO_3$ $[M+Na]^+$ 342.9802, found 342.9795.

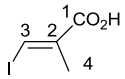
Diethyl 2-(diiodomethyl)-2-methylmalonate (111)[43,77]



Diethyl methylmalonate (**110**) (30.3 g, 174 mmol) was added dropwise to a solution of NaH (60% in mineral oil) (7.08 g, 177 mmol) in Et_2O (250 mL) at 0 °C, and the resultant thick reaction mixture heated at reflux with vigorous stirring for 2.5 h. Iodoform (68.5 g, 174 mmol) was then added in one portion, and the mixture refluxed for a further 24 h, after which time it was cooled to 0 °C. 10% aq. HCl was added (100 mL) and the mixture stirred at 0 °C for 10 min. The layers were separated and the aqueous layer extracted with Et_2O (2 x 70 mL). The combined organic extracts were dried over anhydrous $MgSO_4$ and concentrated under reduced pressure. Petrol (50 mL) was added to the residue, and the precipitated iodoform removed by filtration. The filtrate was concentrated under reduced pressure, and the residue purified by column chromatography to afford diethyl 2-(diiodomethyl)-2-methylmalonate (**111**) (62.6 g, 82%) as a colourless oil.

R_f = 0.21 (5 % EtOAc in petrol); **ν_{max}** (cm^{-1}) (thin film): 1736, 1448, 1381, 1264, 1227; **δ_H** ($CDCl_3$, 400 MHz): 5.78 (br. s, 1H, 5-H_1), 4.20 - 4.26 (m, 4H, 6-H_2 and 8-H_2), 1.80 (br. s, 3H, 4-H_3), 1.30 (t, *J* = 7.1 Hz, 6H, 7-H_3 and 9-H_3); **δ_c** ($CDCl_3$, 100 MHz): 166.1 (C-1 and C-3), 62.7 (C-6 and C-8), 62.1 (C-2), 20.3 (C-4), 14.0 (C-9 and C-7), C-5 not observed; **HRMS** (ESI) calculated for $C_9H_{14}I_2NaO4$ $[M+Na]^+$ 462.8874, found 462.8887.

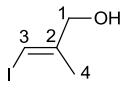
(*E*)-3-Iodo-2-methylacrylic acid (112)[43,77]



KOH (6.12 g, 109 mmol) was added to a solution of diethyl 2-(diiodomethyl)-2-methylmalonate (**111**) (16.0 g, 36.4 mmol) in EtOH-H_2O (3:1, 60 mL). The resultant mixture was heated at reflux for 24 h, after which time it was cooled to rt. and concentrated under reduced pressure. The residue was dissolved in 10% aq. K_2CO_3 (60 mL) and washed with CH_2Cl_2 (2 x 30 mL). The aqueous layer was acidified with conc. HCl, and the resultant white precipitate isolated by filtration to afford (*E*)-3-iodo-2-methylacrylic acid (**112**) (6.95 g, 90%) as a crystalline white solid.

R_f = 0.16 (25% EtOAc in petrol); **mp**: 48-49 °C (lit: 51-53 °C)[43]; **ν_{max}** (cm^{-1}) (thin film): 3100-2500, 1694, 1598, 1417, 1383, 1304, 1234; **δ_H** ($CDCl_3$, 400 MHz): 8.04 (q, *J* = 1.2 Hz, 1H, 3-H_1), 2.07 (d, *J* = 1.2 Hz, 3H, 4-H_3); **δ_c** ($CDCl_3$, 100 MHz): 169.2 (C-1), 139.0 (C-2), 102.0 (C-3), 19.8 (C-4).

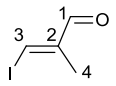
(*E*)-3-Iodo-2-methylprop-2-en-1-ol (113)[43,78]



$LiAlH_4$ (537 mg, 14.2 mmol) was added portionwise over 1 h to a solution of (*E*)-3-iodo-2-methylacrylic acid (**112**) (3.00 g, 14.2 mmol) in THF (25 mL) at 0 °C, and the resultant mixture stirred at rt. for 20 h. The mixture was then cooled to 0 °C and quenched by the cautious dropwise addition of sat. aq. Na_2SO_4. Et_2O (20 mL) was added and the solution poured onto cold H_2SO_4 (2.0 M, 50 mL). The layers were separated, and the aqueous layer extracted with CH_2Cl_2 (2 x 50 mL). The combined organic extracts were concentrated and the residue dissolved in 10% aq. K_2CO_3 (25 mL) and extracted with CH_2Cl_2 (2 x 50 mL). The combined organic extracts were dried over anhydrous $MgSO_4$ and concentrated under reduced pressure. The residue was purified by flash column chromatography to afford (*E*)-3-iodo-2-methylprop-2-en-1-ol (**113**) (2.36 g, 84%) as a colourless oil.

$\mathbf{R_f}$ = 0.41 (25% EtOAc in petrol); ν_{max} (cm^{-1}) (thin film): 3326, 2915, 2870, 1694, 1632, 1447, 1377, 1277, 1254; δ_H ($CDCl_3$, 400 MHz): 6.29 - 6.30 (m, 1H, 3-H_1), 4.14 (br. s, 2H, 1-H_2), 1.85 - 1.87 (m, 3H, 4-H_3); δ_c ($CDCl_3$, 100 MHz): 147.2 (C-2), 77.3 (C-3), 67.2 (C-1), 21.3 (C-4).

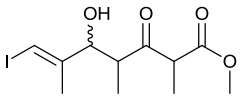
(*E*)-3-Iodo-2-methylacrylaldehyde (101)[43,78]



MnO_2 (19.0 g, 218 mmol) was added in one portion to a solution of (*E)*-3-iodo-2-methyl-prop-2-en-1-ol (**113**) (2.16 g, 10.9 mmol) in CH_2Cl_2 (120 mL) and the resultant mixture stirred at rt. for 2 h. The reaction mixture was then filtered through celite, and the filtrate concentrated under reduced pressure to afford (*E*)-3-iodo-2-methylacrylaldehyde (**101**) (1.54 g, 72%) as a yellow oil that was used without further purification.

R_f = 0.67 (25% EtOAc in petrol); **ν_{max}** (cm^{-1}) (thin film): 3345, 3048, 2822, 2723, 1687, 1593, 1434, 1375, 1293; **δ_H** ($CDCl_3$, 400MHz): 9.53 (s, 1H, 1-H_1), 7.81 (br. s, 1H, 3-H_1), 1.93 (br. s, 3H, 4-H_3); **δ_c** ($CDCl_3$, 100 MHz): 189.4 (C-1), 150.8 (C-2), 109.4 (C-3), 16.4 (C-4).

(*E*)-Methyl 5-hydroxy-7-iodo-2,4-dimethyl-3-oxohept-6-enoate (114)[37]

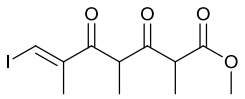


Methyl 2-methyl-3-oxopentanoate (**102**) (1.53 g, 10.6 mmol) was added dropwise to a suspension of NaH (60% in mineral oil) (0.452 g, 11.3 mmol) in THF (65 mL) at 0 °C and the mixture stirred at rt. for 30 min, after which time the mixture was cooled to 0 °C and ^{n}BuLi (1.6 M in hexanes) (7.10 mL, 11.3 mmol) added dropwise. The resultant mixture was stirred at rt. for a further 30 min before a solution of (*E*)-3-iodo-2-methylacrylaldehyde (**101**) (1.03 g,

5.30 mmol) in THF (15 mL) was added dropwise at 0 °C. The mixture was stirred at rt. for 18 h, then cooled to 0 °C and quenched by addition of sat. aq. NH_4Cl (100 mL). The layers were separated, and the aqueous layer extracted with Et_2O (2 x 100 mL). The combined organic extracts were dried over anhydrous $MgSO_4$ and concentrated under reduced pressure. The residue was purified by flash column chromatography to afford (*E*)-methyl 5-hydroxy-7-iodo-2,4-dimethyl-3-oxohept-6-enoate (**114)** (1.28 g, 71%) as a mixture of diastereomers which was carried forward without characterisation.

R_f = 0.51 (25% EtOAc in petrol); **HRMS** (ESI) calculated for $C_{11}H_{17}INaO_4$ $[M+Na]^+$ 363.0064, found 363.0045.

(*E*)-Methyl 7-iodo-2,4-dimethyl-3,5-dioxohept-6-enoate (99)[37]

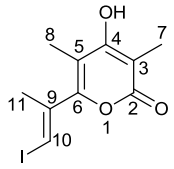


Dess Martin periodinane (3.47 g, 8.20 mmol) was added portionwise to a solution of (*E*)-methyl 5-hydroxy-7-iodo-2,4-dimethyl-3-oxohept-6-enoate (**114**) (2.32 g, 6.80 mmol) in non-anhydrous CH_2Cl_2 (80 mL) at 0 °C in a flask open to the air. The resultant mixture was stirred at rt. for 1 h, after which time sat. aq. $NaHCO_3$ (25 mL) and sat. aq. Na_2SO_3 (25 mL) were added at 0 °C, and the layers separated. The aqueous layer was extracted with CH_2Cl_2 (2 x 60 mL), and the combined organic extracts dried over anhydrous $MgSO_4$ and concentrated under reduced pressure. The residue was purified by flash column chromatography to afford (*E*)-methyl 7-iodo-2,4-dimethyl-3,5-

dioxohept-6-enoate (**99**) (2.25 g, 98%) as a mixture of diastereomers which was carried forward without characterisation.

R_f = 0.60 (25% EtOAc in petrol); **HRMS** (ESI) calculated for $C_{11}H_{15}INaO_4$ $[M+Na]^+$ 360.9907, found 360.9909.

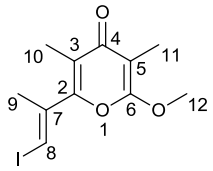
(*E*)-4-Hydroxy-6-(1-iodoprop-1-en-2-yl)-3,5-dimethyl-2H-pyran-2-one (97)[37]



A solution of (*E*)-methyl 7-iodo-2,4-dimethyl-3,5-dioxohept-6-enoate (**99**) (4.22 g, 12.5 mmol) and DBU (3.70 mL, 25.0 mmol) in toluene (150 mL) was stirred at 70 °C for 2 h. The reaction mixture was then concentrated under reduced pressure and the residue purified by flash column chromatography (0.1% AcOH, 5% MeOH in CH_2Cl_2) to afford (*E*)-4-hydroxy-6-(1-iodoprop-1-en-2-yl)-3,5-dimethyl-2H-pyran-2-one (**97**) (3.62 g, 95%) as a white solid.

R_f = 0.18 (0.1% AcOH, 5% MeOH in CH_2Cl_2); **mp**: 157-159 °C (lit: 164-166 °C)[37]; **ν_{max}** (cm^{-1}) (thin film): 3071 (br), 1667, 1558, 1434; **δ_H** ($CDCl_3$, 400 MHz): 6.68 (q, *J* = 1.1 Hz, 1H, 10-H_1), 2.11 (d, *J* = 1.1 Hz, 3H, 11-H_3), 2.02 (s, 3H, 8-H_3), 2.01 (s, 3H, 7-H_3); **δ_c** ($CDCl_3$, 100 MHz): 164.5 (C-2), 164.0 (C-4), 154.9 (C-6), 139.5 (C-9), 107.4 (C-5), 99.8 (C-3), 88.6 (C-10), 23.0 (C-11), 11.4 (C-8), 8.6 (C-7); **HRMS** (ESI) calculated for $C_{10}H_{11}INaO_3$ $[M+Na]^+$ 328.9645, found 328.9657.

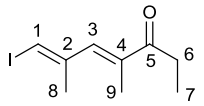
(*E*)-2-(1-Iodoprop-1-en-2-yl)-6-methoxy-3,5-dimethyl-4*H*-pyran-4-one (95)[37]



A mixture of (*E*)-4-hydroxy-6-(1-iodoprop-1-en-2-yl)-3,5-dimethyl-2H-pyran-2-one (**97**) (1.81 g, 5.90 mmol), Me_2SO_4 (1.10 mL, 11.8 mmol) and Li_2CO_3 (1.31 g, 17.7 mmol) in acetone (20 mL) was stirred at reflux for 18 h. The reaction mixture was then cooled to rt. and Et_2O (25 mL) added. The solid was filtered off and the filtrate concentrated under reduced pressure. The residue was purified by flash column chromatography to afford (*E*)-2-(1-iodoprop-1-en-2-yl)-6-methoxy-3,5-dimethyl-4*H*-pyran-4-one (**95**) (0.790 g, 42%) as a yellow oil.

$\mathbf{R_f}$ = 0.33 (40% EtOAc in petrol); $\boldsymbol{\nu_{max}}$ (cm^{-1}) (thin film): 1655, 1611, 1591, 1536, 1463; $\boldsymbol{\delta_H}$ ($CDCl_3$, 400 MHz): 6.75 (q, *J* = 1.2 Hz, 1H, 8-H_1), 3.96 (s, 3H, 12-H_3), 2.14 (d, *J* = 1.2 Hz, 3H, 9-H_3), 1.97 (s, 3H, 10-H_3), 1.86 (s, 3H, 11-H_3); $\boldsymbol{\delta_c}$ ($CDCl_3$, 100 MHz): 180.8 (C-4), 161.7 (C-6), 154.4 (C-2), 139.2 (C-7), 119.1 (C-3), 99.8 (C-5), 89.2 (C-8), 55.4 (C-12), 22.7 (C-9), 11.7 (C-10), 6.9 (C-11); **HRMS** (ESI) calculated for $C_{11}H_{13}INaO_3$ $[M+Na]^+$ 342.9802, found 342.9806.

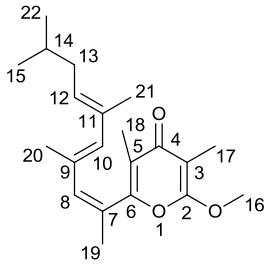
(4*E*,6*E*)-7-Iodo-4,6-dimethylhepta-4,6-dien-3-one (116)



DBU (0.930 mL, 6.26 mmol) was added in one portion to a 1:1 mixture of (*E*)-methyl 7-iodo-2,4-dimethyl-3,5-dioxohept-6-enoate (**99**) and (*E*)-methyl 5-hydroxy-7-iodo-2,4-dimethyl-3-oxohept-6-enoate (**114**) (1.06 g, 3.13 mmol total) in toluene (40 mL). The solution was heated to 70 °C, and stirred at this temperature for 48 h. The mixture was then cooled to rt. and concentrated under reduced pressure. The residue was purified by flash column chromatography to afford (4*E*,6*E*)-7-iodo-4,6-dimethylhepta-4,6-dien-3-one (**116**) (171 mg, 41% based on 1.57 mmol **114** present in starting material) as a yellow oil.

R_f = 0.69 (25% EtOAc in PE); **ν_{max}** (cm^{-1}) (thin film): 2977, 2936, 1671, 1611, 1587; **δ_H** ($CDCl_3$, 400 MHz): 6.88 (br. s, 1H, 3-H_1), 6.44 (q, *J* = 1.1 Hz, 1H, 1-H_1), 2.71 (q, *J* = 7.3 Hz, 2H, 6-H_2), 2.04 (dd, *J* = 1.1, 0.4 Hz, 3H, 8-H_3), 1.91 (d, *J* = 1.4 Hz, 3H, 9-H_3), 1.12 (t, *J* = 7.3 Hz, 3H, 7-H_3); **δ_c** ($CDCl_3$, 100 MHz): 202.6 (C-5), 143.8 (C-2), 137.9 (C-3), 136.6 (C-4), 85.3 (C-1), 30.9 (C-6), 24.7 (C-8), 13.5 (C-9), 8.7 (C-7); **HRMS** (ESI) calculated for $C_9H_{13}IONa$ $[M+Na]^+$ 286.9903, found 286.9900.

2-Methoxy-3,5-dimethyl-6-((2*Z*,4*E*,6*E*)-4,6,9-trimethyldeca-2,4,6-trien-2-yl)-4H-pyran-4-one (43)[6]

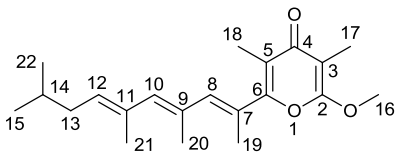


A solution of (*Z*)-2-(1-iodoprop-1-en-2-yl)-6-methoxy-3,5-dimethyl-4H-pyran-4-one (**94**) (0.200 g, 0.620 mmol) and 2-((2*Z*,4*E*)-4,7-dimethylocta-2,4-dien-2-yl)benzo[*d*][1,3,2]dioxaborole (**84**) (0.318 g, 1.24 mmol) in THF (4.5 mL) and H_2O (1.5 mL) was degassed by purging with argon. $Pd(PPh_3)_4$ (69.0 mg, 0.0600 mmol) was then added in one portion and the resultant mixture stirred at rt. for 15 min in the dark. TlOEt (0.130 mL, 1.86 mmol) was then added in one portion, upon which immediate formation of a yellow precipitate was observed. This mixture was heated to 50 °C, in the dark, and stirred for 4 h. The mixture was then cooled to rt. and H_2O (20 mL) added, before being extracted with Et_2O (3 x 20 mL). The combined organic extracts were dried over anhydrous $MgSO_4$ and concentrated under reduced pressure. The residue was purified by flash column chromatography to afford 2-methoxy-3,5-dimethyl-6-((2*Z*,4*E*,6*E*)-4,6,9-trimethyldeca-2,4,6-trien-2-yl)-4H-pyran-4-one (**43**) (0.386 g, 95%) as a colourless oil.

R_f = 0.44 (25% EtOAc in petrol); UV/vis (MeOH, 0.484 mM) **λ_{max}** = 264 nm (ε 20400); **ν_{max}** (cm^{-1}) (thin film): 2956, 2926, 1713, 1659, 1574, 1514, 1380; **δ_H** ($CDCl_3$, 400 MHz): 6.25 (br. s, 1H, 8-H_1), 5.90 (s, 1H, 10-H_1), 5.32 (t, *J* = 7.5 Hz,

1H, 12-H_1), 3.95 (s, 3H, 16-H_3), 2.02 (d, *J* = 1.0 Hz, 3H, 19-H_3), 1.94 - 1.98 (m, 2H, 13-H_2), 1.87 (s, 3H, 17-H_3), 1.85 (s, 3H, 18-H_3), 1.69 (s, 3H, 21-H_3), 1.65 (s, 3H, 20-H_3), 1.57 - 1.63 (m, 1H, 14-H_1), 0.89 (d, *J* = 6.6 Hz, 6H, 15-H_3 and 22-H_3); δ_c ($CDCl_3$, 100 MHz): 180.9 (C-4), 162.3 (C-2), 156.4 (C-6), 138.9 (C-8), 138.0 (C-10), 132.6 (C-11), 131.6 (C-12), 131.1 (C-9), 124.5 (C-7), 119.1 (C-5), 99.7 (C-3), 55.4 (C-16), 37.5 (C-13), 28.8 (C-14), 23.2 (C-19), 22.4 (C-15 and C-22), 16.9 (C-21), 16.2 (C-20), 10.7 (C-18), 6.9 (C-17); **HRMS** (ESI) calculated for $C_{21}H_{30}NaO_3$ $[M+Na]^+$ 353.2087, found 353.2083.

2-Methoxy-3,5-dimethyl-6-((2*E*,4*E*,6*E*)-4,6,9-trimethyldeca-2,4,6-trien-2-yl)-4H-pyran-4-one (44)[7]

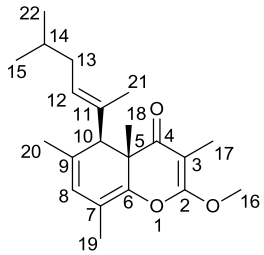


A solution of (*E*)-2-(1-Iodoprop-1-en-2-yl)-6-methoxy-3,5-dimethyl-4*H*-pyran-4-one (**95**) (100 mg, 0.31 mmol) and 2-((2*Z*,4*E*)-4,7-dimethylocta-2,4-dien-2-yl)benzo[*d*][1,3,2]dioxaborole (**84**) (0.200 g, 0.620 mmol) in THF (4.5 mL) and H_2O (1.5 mL) was degassed by purging with argon. $Pd(PPh_3)_4$ (69.0 mg, 0.0600 mmol) was then added in one portion and the resultant mixture stirred at rt. for 15 min in the dark. TlOEt (0.130 mL, 1.86 mmol) was then added in one portion, upon which immediate formation of a yellow precipitate was observed. This mixture was heated to 50 °C, in the dark, and stirred for 4 h. The mixture was then cooled to rt. and H_2O (20 mL) added, before being extracted with Et_2O (3 x 20 mL). The combined organic extracts were dried over anhydrous $MgSO_4$ and concentrated under reduced pressure. The

residue was purified by flash column chromatography to afford 2-methoxy-3,5-dimethyl-6-((2*E*,4*E*,6*E*)-4,6,9-trimethyldeca-2,4,6-trien-2-yl)-4H-pyran-4-one (**44**) (0.188 g, 92%) as a colourless oil.

R_f = 0.33 (25% EtOAc in petrol); UV/vis (MeOH, 0.454 mM) **λ_{max}** = 274 nm (ε 14377); **ν_{max}** (cm^{-1}) (thin film): 2956, 1711, 1656, 1597, 1465, 1377; **δ_H** ($CDCl_3$, 400 MHz): 6.18 (1H, s, 8-H_1), 5.98 (1H, s, 10-H_1), 5.47 (1H, t, *J* = 7.3 Hz, 12-H_1), 3.98 (3H, s, 16-H_3), 2.12 (3H, s, 19-H_3), 2.05 (3H, s, 18-H_3), 2.04 (2H, br. s., 13-H_2), 2.03 (3H, s., 21-H_3), 1.89 (3H, s, 17-H_3), 1.80 (3H, s, 20-H_3), 1.67 - 1.73 (1H, m, 14-H_1), 0.95 (6H, d, *J* = 6.7 Hz, 15-H_3 and 22-H_3); **δ_c** ($CDCl_3$, 100 MHz): 181.6 (C-4), 161.9 (C-2), 159.1 (C-6), 140.4 (C-8), 137.3 (C-10), 132.6 (C-9), 131.4 (C-12), 130.5 (C-11), 125.8 (C-7), 117.7 (C-5), 99.2 (C-3), 55.2 (C-16), 37.5 (C-13), 28.8 (C-14), 22.4 (C-15 and C-22), 18.5 (C-21), 17.0 (C-20), 16.2 (C-19), 11.9 (C-18), 6.8 (C-17); **HRMS** (ESI) calculated for $C_{21}H_{30}O_3$ $[M+Na]^+$ 331.2268, found 331.2274.

(±)-Tridachiahydropyrone (9)[6]

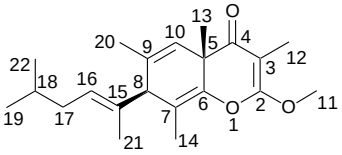


A solution of 2-methoxy-3,5-dimethyl-6-((2*Z*,4*E*,6*E*)-4,6,9-trimethyldeca-2,4,6-trien-2-yl)-4H-pyran-4-one (**43**) (0.0760 g, 0.230 mmol) in anhydrous MeOH (25 mL) was degassed by purging with argon. The solution was then irradiated with a mercury lamp (125 W) for 37 h. The solvent was removed under

reduced pressure and the residue purified by flash column chromatography to afford tridachiahydropyrone (**9**) as a white solid (0.0130 g, 17%).

R_f = 0.55 (10% EtOAc in petrol); **mp**: 79-81 °C (lit: 76-80 °C)[6]; UV/vis (MeOH, 0.303 mM) **λ_{max}** = 271 nm (ε 9026); **ν_{max}** (cm^{-1}) (thin film): 2954, 1657, 1606, 1346, 1292; **δ_H** ($CDCl_3$, 400 MHz): 5.53 (t, *J* = 7.2 Hz, 1H, 12-H_1), 5.45 (s, 1H, 8-H_1), 3.97 (s, 3H, 16-H_3), 3.93 (s, 1H, 10-H_1), 1.91 (t, *J* = 7.2 Hz, 2H, 13-H_2), 1.76 (s, 3H, 19-H_3), 1.67 - 1.70 (m, 1H, 14-H_1), 1.64 (br. s, 6H, 17-H_3 and 20-H_3), 1.54 (s, 3H, 21-H_3), 1.18 (s, 3H, 18-H_3), 0.90 (s, 3H, 22-H_3), 0.89 (s, 3H, 15-H_3); **δ_c** ($CDCl_3$, 100 MHz): 195.9 (C-4), 166.0 (C-2), 145.3 (C-6), 134.4 (C-9), 133.4 (C-11), 130.4 (C-12), 121.3 (C-8), 115.8 (C-7), 87.9 (C-3), 55.1 (C-16), 53.4 (C-10), 46.5 (C-5), 37.2 (C-13), 28.7 (C-14), 22.6 (C-22), 22.5 (C-15), 21.7 (C-20), 21.2 (C-18), 14.6 (C-19), 13.7 (C-21), 7.4 (C-17); **HRMS** (ESI) calculated for $C_{21}H_{30}NaO_3$ $[M+Na]^+$ 353.2087, found 353.2096.

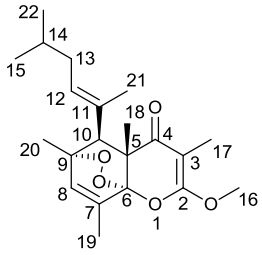
(±)-Phototridachiahydropyrone (93)[7]



A solution of 2-methoxy-3,5-dimethyl-6-((2*Z*,4*E*,6*E*)-4,6,9-trimethyldeca-2,4,6-trien-2-yl)-4H-pyran-4-one (**43**) (0.0760 g, 0.230 mmol) in anhydrous MeOH (25 mL) was degassed by purging with argon. The solution was then irradiated with a mercury lamp (125 W) for 37 h. The solvent was removed under reduced pressure and the residue purified by flash column chromatography to afford phototridachiahydropyrone (**93**) as a white solid (0.0100 g, 13%).

R_f = 0.38 (10% EtOAc in petrol); **mp**: 88-90 °C (lit: 90-92 °C)[7]; **ν_{max}** (cm^{-1}) (thin film): 2926, 1737, 1611, 1462, 1380; **δ_H** ($CDCl_3$, 400 MHz): 5.96 (s, 1H, 10-H_1), 5.42 (t, *J* = 7.0 Hz, 1H, 16-H_1), 4.00 (s, 3H, 11-H_3), 3.09 (s, 1H, 8-H_1), 1.97 (t, *J* = 7.0 Hz, 2H, 17-H_2), 1.68 - 1.70 (m, 1H, 18-H_1), 1.65 (br. s, 6H, 12-H_3 and 20-H_3), 1.61 (s, 3H, 14-H_3), 1.40 (s, 3H, 21-H_3), 1.36 (s, 3H, 13-H_3), 0.93 (s, 3H, 19-H_3), 0.91 (s, 3H, 22-H_3); **δ_c** ($CDCl_3$, 100 MHz): 194.8 (C-4), 165.6 (C-2), 144.9 (C-6), 133.3 (C-9), 131.8 (C-15), 129.2 (C-16), 123.8 (C-10), 117.4 (C-7), 88.0 (C-3), 57.5 (C-8), 55.0 (C-11), 44.6 (C-5), 37.4 (C-17), 28.9 (C-18), 27.6 (C-13), 22.4 (C-19), 22.4 (C-22), 21.0 (C-20), 13.1 (C-14), 11.9 (C-21), 6.7 (C-12); **HRMS** (ESI) calculated for $C_{21}H_{30}NaO_3$ $[M+Na]^+$ 353.2087, found 353.2094.

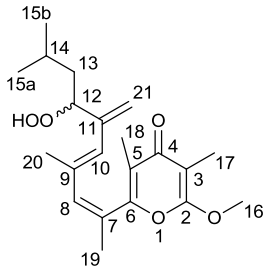
(±)-Oxytridachiahydropyrone (10)[7]



Methylene blue (5.00 mg, 0.0170 mmol) was added to a solution of (±)-tridachiahydropyrone (**9**) (28.0 mg, 0.0850 mmol) in methanol (10 mL). The mixture was purged with oxygen for 30 min via an oxygen balloon and outlet needle, after which time the outlet needle was removed, and the solution irradiated with a mercury lamp (125 W) for 5 h. The mixture was then concentrated under reduced pressure, and the residue purified by preparative TLC (10% EtOAc in petrol) to afford oxytridachiahydropyrone (**10**) (30.0 mg, 97%) as a colourless oil.

R_f = 0.59 (10% EtOAc in petrol); **ν_{max}** (cm^{-1}) (thin film): 2955, 2868, 1621, 1461, 1380, 1350, 1322, 1286; **Rotamer a:** **δ_H** ($CDCl_3$, 400 MHz): 6.18 (s, 1H, 8-H_1), 5.88 (t, *J* = 7.2 Hz, 1H, 12-H_1), 3.92 (s, 3H, 16-H_3), 3.56 (s, 1H, 10-H_1), 2.06 (s, 3H, 19-H_3), 1.88 - 1.98 (m, 2H, 13-H_2), 1.68 (s, 3H, 17-H_3), 1.57 - 1.63 (m, 1H, 14-H_1), 1.47 (s, 3H, 21-H_3), 1.24 (s, 3H, 20-H_3), 1.06 (s, 3H, 18-H_3), 0.89 (d, *J* = 6.7 Hz, 6H, 15-H_3 and 22-H_3); **δ_c** ($CDCl_3$, 100 MHz): 195.9 (C-4), 162.7 (C-2), 137.1 (C-7), 134.9 (C-12), 131.2 (C-8), 129.2 (C-11), 106.8 (C-6), 89.3 (C-3), 80.0 (C-9), 56.2 (C-10), 55.4 (C-16), 50.6 (C-5), 37.3 (C-13), 28.6 (C-14), 22.6 (C-15), 22.4 (C-22), 19.4 (C-20), 18.9 (C-18), 15.3 (C-19), 15.0 (C-21), 6.8 (C-17); **Rotamer b:** **δ_H** ($CDCl_3$, 400 MHz): 6.18 (s, 1H, 8-H_1), 5.02 (t, *J* = 7.2 Hz, 1H, 12-H_1), 3.92 (s, 3H, 16-H_3), 3.26 (s, 1H, 10-H_1), 2.04 (s, 3H, 19-H_3), 1.88 - 1.98 (m, 2H, 13-H_2), 1.85 (s, 3H, 21-H_3), 1.70 (s, 3H, 17-H_3), 1.57 - 1.63 (m, 1H, 14-H_1), 1.35 (s, 3H, 20-H_3), 0.92 (s, 3H, 18-H_3), 0.89 (d, *J* = 6.7 Hz, 6H, 15-H_3 and 22-H_3); **δ_c** ($CDCl_3$, 100 MHz): 195.8 (C-4), 163.0 (C-2), 137.4 (C-7), 132.8 (C-11), 130.4 (C-8), 127.6 (C-12), 106.8 (C-6), 89.9 (C-3), 80.9 (C-9), 55.4 (C-16), 53.8 (C-10), 50.4 (C-5), 37.4 (C-13), 28.9 (C-14), 22.6 (C-15), 22.5 (C-22), 20.2 (C-18), 19.7 (C-20), 19.6 (C-21), 15.3 (C-19), 6.8 (C-17); **HRMS** (ESI) calculated for $C_{21}H_{30}NaO_5$ $[M+Na]^+$ 385.1985, found 385.1983.

2-((2*Z*,4*E*)-7-Hydroperoxy-4,9-dimethyl-6-methylenedeca-2,4-dien-2-yl)-6-methoxy-3,5-dimethyl-4H-pyran-4-one (135)

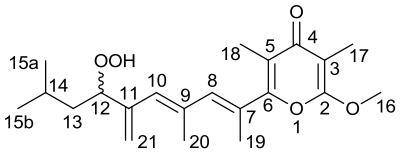


Methylene blue (14.0 mg, 0.0400 mmol) was added to a solution of 2-methoxy-3,5-dimethyl-6-((2*E*,4*E*,6*E*)-4,6,9-trimethyldeca-2,4,6-trien-2-yl)-4H-pyran-4-one (**44**) (70.0 mg, 0.210 mmol) in methanol (70 mL). The mixture was purged with oxygen for 30 min via an oxygen balloon and outlet needle, after which time the outlet needle was removed, and the solution irradiated for 24 h. The mixture was then concentrated under reduced pressure, and the residue purified by flash column chromatography to afford 2-((2*Z*,4*E*)-7-hydroperoxy-4,9-dimethyl-6-methylenedeca-2,4-dien-2-yl)-6-methoxy-3,5-dimethyl-4H-pyran-4-one (**135**) (15.0 mg, 20%) as a colourless oil.

R_f = 0.15 (25% EtOAc in petrol); **ν_{max}** (cm^{-1}) (thin film): 3245, 2957, 2927, 2870, 1656, 1578; **δ_H** ($CDCl_3$, 400 MHz): 8.24 (br. s, 1H, OOH), 6.30 (app. t, *J* = 1.1 Hz, 1H, 8-H_1), 5.90 (br. s, 1H, 10-H_1), 5.35 (d, *J* = 1.0 Hz, 1H, 21-H<u>H</u>'), 5.08 (app. t, *J* = 1.0 Hz, 1H, 21-H<u>H</u>'), 4.39 (t, *J* = 7.0 Hz, 1H, 12-H_1), 3.97 (s, 3H, 16-H_3), 2.05 (d, *J* = 1.4 Hz, 3H, 19-H_3), 1.87 (s, 3H, 17-H_3), 1.85 (s, 3H, 18-H_3), 1.75 (d, *J* = 1.1 Hz, 3H, 20-H_3), 1.60 - 1.65 (m, 1H, 14-H_1), 1.36 - 1.43 (m, 1H, 13-H<u>H</u>'), 1.14 - 1.22 (m, 1H, 14-H<u>H</u>'), 0.89 (d, *J* = 4.3 Hz, 3H, 15a-H_3), 0.87 (d, *J* = 4.3 Hz, 3H, 15b-H_3); **δ_c** ($CDCl_3$, 100 MHz): 181.2 (C-4), 162.5 (C-2), 156.2 (C-6), 143.8 (C-

11), 138.1 (C-8), 136.3 (C-9), 128.5 (C-10), 126.4 (C-7), 119.1 (C-5), 117.5 (C-21), 100.0 (C-3), 87.9 (C-12), 55.4 (C-16), 40.7 (C-13), 24.7 (C-14), 23.0 (C-19), 22.7 (C-15a), 22.6 (C-15b), 16.6 (C-20), 10.7 (C-18), 6.9 (C-17); **HRMS** (ESI) calculated for $C_{21}H_{31}O_5$ $[M+H]^+$ 363.2166, found 363.2165.

2-((2*E*,4*E*)-7-Hydroperoxy-4,9-dimethyl-6-methylenedeca-2,4-dien-2-yl)-6-methoxy-3,5-dimethyl-4H-pyran-4-one (136)



Methylene blue (14.0 mg, 0.0400 mmol) was added to a solution of 2-methoxy-3,5-dimethyl-6-((2*E*,4*E*,6*E*)-4,6,9-trimethyldeca-2,4,6-trien-2-yl)-4H-pyran-4-one (**44**) (70.0 mg, 0.210 mmol) in methanol (70 mL). The mixture was purged with oxygen for 30 min via an oxygen balloon and outlet needle, after which time the outlet needle was removed, and the solution irradiated for 24 h. The mixture was then concentrated under reduced pressure, and the residue purified by flash column chromatography to afford 2-((2*E*,4*E*)-7-hydroperoxy-4,9-dimethyl-6-methylenedeca-2,4-dien-2-yl)-6-methoxy-3,5-dimethyl-4H-pyran-4-one (**136**) (4.0 mg, 5%) as a colourless oil.

R_f = 0.26 (25% EtOAc in petrol); **δ_H** ($CDCl_3$, 400 MHz): 5.84 (br. s, 1H, 10-H_1), 5.81 (d, *J* = 1.0 Hz, 1H, 8-H_1), 5.68 (app. t, *J* = 1.5 Hz, 1H, 21-H<u>H</u>'), 5.27 (app. t, *J* = 1.5 Hz, 1H, 21-H<u>H</u>'), 4.34 (br. s, 1H, 12-H_1), 3.96 (s, 3H, 16-H_3), 2.05 (d, *J* = 1.5 Hz, 3H, 19-H_3), 1.88 (s, 3H, 17-H_3), 1.86 (s, 3H, 18-H_3), 1.74 (br. s, 3H, 20-H_3), 1.52 - 1.58 (m, 1H, 14-H_1), 1.36 - 1.44 (m, 1H, 13-<u>H</u>H'), 1.15 (br. s, 1H, 14-H<u>H</u>'),

0.95 (d, *J* = 3.0 Hz, 3H, 15a-H_3), 0.95 (d, *J* = 3.0 Hz, 3H, 15b-H_3); partial δ_c ($CDCl_3$, 100 MHz): 181.5, 161.9, 158.3, 145.6, 134.3, 134.3, 125.3, 118.0, 99.4, 79.6, 55.3, 39.3, 24.6, 23.8, 23.8, 23.6, 17.5, 11.0, 6.9; **HRMS** (ESI) calculated for $C_{21}H_{31}O_5$ $[M+H]^+$ 363.2166, found 363.2178.

6.1.4 Electrocyclisation in Membranes: General Procedure

A 33.0 mM solution of substrate (**44** or **43**) in DMSO (60.0 µL, 1.98 µmol) was added to an 800 µM solution of PLVs in pH 7.4 Tris buffer (12.0 mL), and the mixture degassed by purging with argon. The mixture was then irradiated (125 W mercury lamp) for 5 h. After irradiation, the mixture was extracted with CH_2Cl_2 (3 x 12 mL). The combined organic extracts were dried over anhydrous $MgSO_4$, and concentrated under reduced pressure. The residue was purified by preparative TLC (5% EtOAc in petrol), and the desired product tridachiahydropyrone (**9**) isolated. This product was then analysed by chiral HPLC, using the conditions outlined in Section 6.1.5.

6.1.5 Analysis of the Separated Enantiomers of Tridachiahydropyrone

HPLC analysis was run using an analytical Chiral Cel OD-H column, with a solvent system of hexane:IPA::99.5:0.5; flow rate = 0.5 mL/min; temperature = 25 °C; injection volume = 10 µL. Retention times: 1st eluted **(-)-9** = 8.41 min; 2nd eluted **(+)-9** = 9.89 min. 1st eluted: $[\alpha]_D^{23}$ = -225.6 (c=0.42 g/100 cm^3, $CHCl_3$) (>99% ee by HPLC), [isolated natural product: $[\alpha]_D$ = -476.1 (c=0.49, $CHCl_3$)][3]; 2nd eluted: $[\alpha]_D^{23}$ = +190.4 (c=0.08 g/100 cm^3, $CHCl_3$) (90% ee by HPLC).

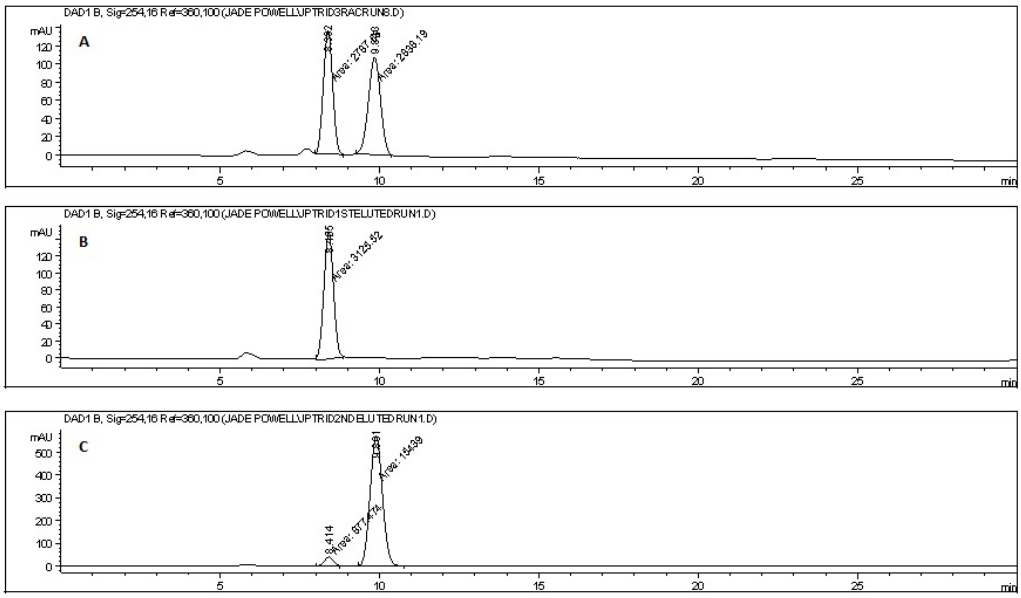


Figure 27. Chiral HPLC analysis of the purity of tridachiahydropyrone (**9**) enantiomers. **A**: racemic mixture **(±)-9**; **B**: first eluted enantiomer **(-)-9**; **C**: second eluted enantiomer **(+)-9**

6.2 Biophysical Techniques

6.2.1 Materials and Methods

Phosphatidylcholine (Grade 1 egg lecithin) was purchased from Lipid Products as a 130 mM solution in $CHCl_3$:MeOH (5:1 v/v). Di-8-ANEPPS was purchased from Invitrogen. Cholesterol (≥99%), sphingomyelin (≥97%) and DMSO (BioReagent for molecular biology, ≥99.9%) were purchased from Sigma Aldrich. Cholesterol was used as a 259 mM solution in $CHCl_3$:MeOH (5:1 v/v). 100 nm pore polycarbonate filters were purchased from Nucleopore Filtration Products. The pressure extruder was purchased from Lipex Biomembranes.

UV-grade cuvettes (3.5 mL) were purchased from Fisher Scientific.

Tris buffer (10 mM, pH 7.4) was filtered before use using Minisart High-Flow single use syringe filters (0.20 µm pore size).

Fluorescence and light scattering experiments were recorded at 25 °C using a HORIBA Jobin Yvon Fluoromax-4 spectrofluorometer. DataMax software was used for monitoring of fluorescence experiments whilst FluorEssence software was used for light scattering experiments.

6.2.2 90° Light scattering: Critical Micelle Concentration Determination

The critical micelle concentrations (CMCs) of **44**, **43** and **9** were determined using analysis of the Rayleigh-Debye light scattering of samples at 90°.[52] Increasing quantities of compound were separately dissolved in 15 μL of DMSO. These solutions were then made up to 2 mL in a cuvette using 1985 μL of either pH 7.4 10 mM Tris buffer or 400 μM PLVs, depending on the experiment. Each cuvette was incubated at 25 °C in the dark for 1 h before analysis, to ensure that equilibrium had been reached. The Rayleigh-Debye light scattering at a 90° angle was then recorded using 600 nm incident radiation with a 2 nm band pass. Plotting the change in light scattering at a fixed angle of 90° against increasing compound concentration enabled determination of the CMC (see Section 3.2).

6.2.3 Liposome Preparation

Unilamellar phospholipid vesicles (PLVs) were prepared using a pressure extrusion technique.[47] Phosphatidylcholine (PC), and cholesterol and/or sphingomyelin (where appropriate), in $CHCl_3$:MeOH (5:1 v/v) were added to a round bottomed flask and the solvent removed under a stream of oxygen-free nitrogen. The resulting thin lipid film was rehydrated to a concentration of 13

mM using Tris buffer (10 mM, pH 7.4), giving a suspension of multilamellar vesicles. This solution was subjected to five freeze-thaw cycles using liquid nitrogen, creating unilamellar vesicles which were then extruded ten times through polycarbonate filters with a 100 nm pore size at 45 °C, giving a monodisperse, unilamellar suspension of PLVs of 100 nm diameter (Figure 28). The PLVs were stored at 4-6 °C and used within one month of preparation.

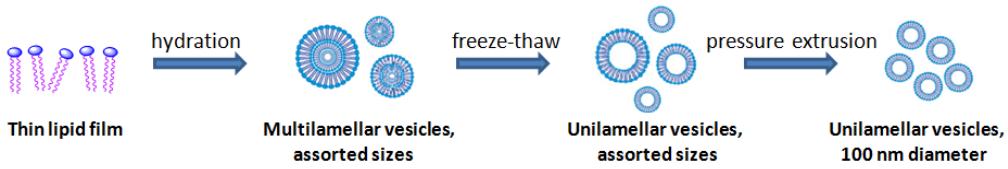


Figure 28. Key steps in the preparation of PLVs

The following lipid compositions, given by molar percent, were used in this study:

$PC_{100\%}$	100% Phosphatidylcholine
$PC_{70\%}Chol_{30\%}$	70% Phosphatidylcholine, 30% Cholesterol
$PC_{70\%}SM_{30\%}$	70% Phosphatidylcholine, 30% Sphingomyelin
$PC_{60\%}Chol_{20\%}SM_{20\%}$	60% Phosphatidylcholine, 20% Cholesterol, 20% Sphingomyelin
$PC_{40\%}SM_{60\%}$	40% Phosphatidylcholine, 60% Sphingomyelin

The PC used in this study was from egg yolk, and contains a variety of different acyl chains appended to the headgroup. An average molecular weight of 770.123 was used in calculating the quantities of PC to use in liposome preparation. This PC mixture was used, as opposed to a single acyl

chain type, as it was thought that it would better reflect the state of affairs found in a biological plasma membrane. Figure 29 outlines the fatty acid distribution of this PC.[79]

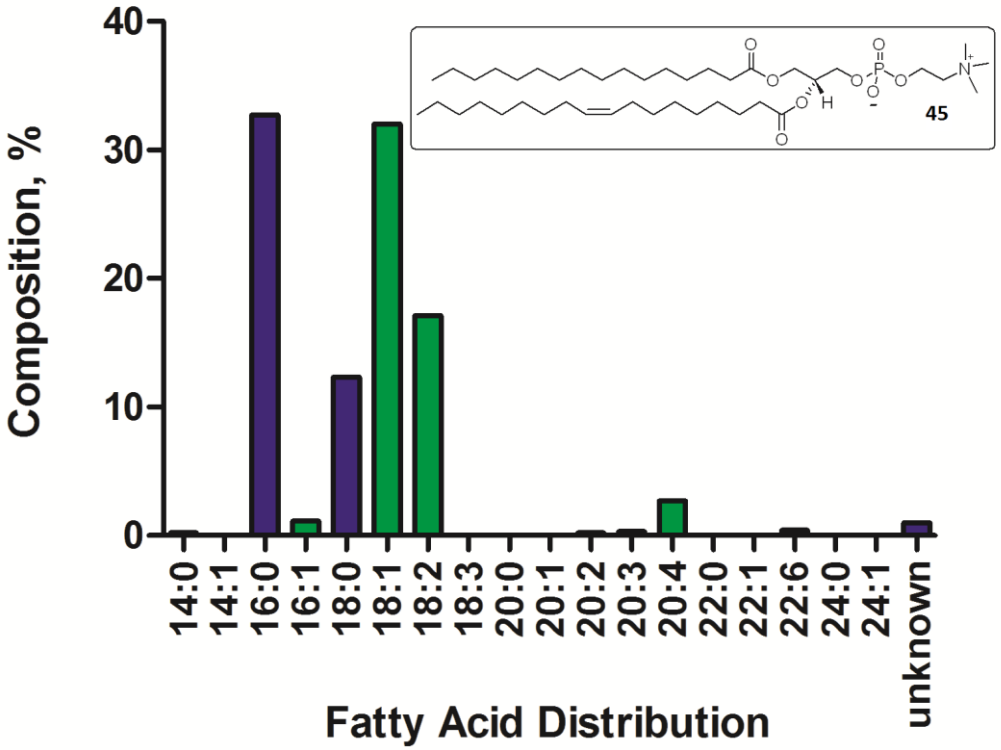


Figure 29. Distribution of acyl chain lengths found in PC from egg yolk. Inset: Structure of the predominant species, 1-palmitoyl-2-oleoyl-sn-glycero-3-phosphocholine (POPC, **45**). Figure adapted from the Avanti Polar Lipid website[79]

6.2.4 Fluorescent Labelling of PLVs with Di-8-ANEPPS

The labelling process was conducted in the dark. Di-8-ANEPPS (1.7 mM in EtOH) was added to a 13 mM solution of PLVs at a concentration of 25 µM, and the mixture incubated at 37 °C (in the dark) for at least 1 h before use. The labelled liposomes were diluted with Tris buffer (10 mM, pH 7.4) to a concentration of 400 µM (di-8-ANEPPS at 0.77 µM) for use in the fluorescence experiments. The stained PLVs were always used within 8 h of labelling.

Unless otherwise stated 2 mL of the labelled PLVs at 400 μM were used in a 3.5 mL UV-grade cuvette for all fluorescence experiments.

6.2.5 Characterisation of Di-8-ANEPPS-Labelled PLVs

To ensure PLVs had been successfully labelled with di-8-ANEPPS excitation and emission spectra were recorded prior to each experiment. These were compared to controls of an equivalent concentration of the probe in buffer alone (no PLVs), and equivalent concentrations of unstained PLVs (no di-8-ANEPPS) (Figure 30). Excitation spectra were recorded from 400 to 550 nm at a fixed emission wavelength of 580 nm; emission spectra were recorded from 500 to 650 nm at a fixed excitation wavelength of 468 nm.

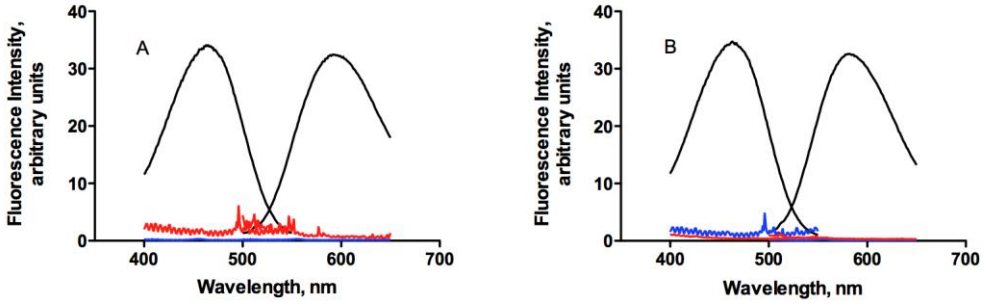


Figure 30. Fluorescence excitation and emission spectra of di-8-ANEPPS in membranes, and controls. Black line: di-8-ANEPPS (0.77 μM) in presence of 400 μM PLVs (in pH 7.4 Tris buffer). Blue line: di-8-ANEPPS (0.77 μM) in pH 7.4 Tris buffer (no PLVs). Red line: 400 μM PLVs (in pH 7.4 Tris buffer) in absence of di-8-ANEPPS. **A**: $PC_{100\%}$ PLVs. **B**: $PC_{70\%}Chol_{30\%}$ PLVs. Spectra normalised to the integral spectral area of di-8-ANEPPS in membranes

6.2.6 Fluorescence Difference Spectra

Fluorescence difference spectra were recorded to determine the effect of binding of molecules **44**, **43** and **9** on the membrane dipole potential (Ψ_d). The excitation spectrum of di-8-ANEPPS-labelled PLVs (recorded from 400 to 550

nm at a fixed emission wavelength of 580 nm) was recorded before and after addition of a known quantity of compound.

These excitation spectra were normalised to their integral area and the difference spectrum then calculated by subtraction of the spectrum in the absence of compound from that in the ligand's presence. This procedure is exemplified by Figure 31, which displays a red shift, corresponding to a decrease in Ψ_d upon addition of ligand **(±)-9**.

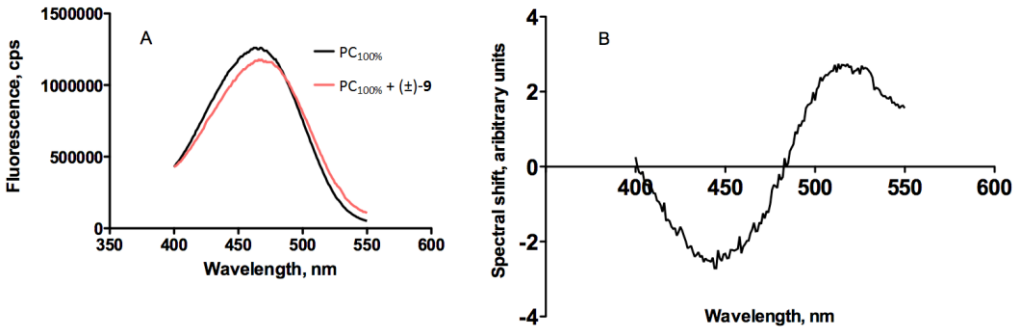


Figure 31. Creation of excitation difference spectra. **A**: Excitation spectra of di-8-ANEPPS (0.77 μM) in presence of 400 μM $PC_{100\%}$ PLVs (in pH 7.4 Tris buffer) before (black line) and after (red line) addition of 288.75 μM **(±)-9. B**: Difference spectrum created by subtraction of the former excitation spectrum from the latter

6.2.7 Titration of Ligands into Di-8-ANEPPS-Labelled PLVs: Dual-Wavelength Ratiometric Fluorescence Time Course Measurements

The ligand concentration dependence of the fluorescence spectrum of di-8-ANEPPS was determined by monitoring the effect on the fluorescence spectrum with time as compound was titrated in.[80] The time-dependent ratio of fluorescence R(460 nm/520 nm) was obtained by exciting the samples at 460 nm and 520 nm, and measuring the intensity ratio at a fixed emission of 590 nm, whilst aliquots of compound (33.0 mM in DMSO) were titrated into

labelled PLVs (400 μM) in a continuously stirred cuvette. The system was allowed to reach equilibrium between each addition, as judged by R remaining constant with time. Control experiments were conducted by titrating equivalent volumes of DMSO over a comparable timeframe (~1 h), and subtracting any signal from that obtained upon compound titration. This allowed correction for any small changes in fluorescence due to dilution effects or photo-bleaching. This ratiometric method was used as it corrects for small variations in dye concentrations, allowing extraction of the response solely to the electrical environment of the surrounding membrane.[33] An example of the ratiometric fluorescence time course obtained is shown in Figure 32. It exemplifies the effect of ligand addition on R, in comparison with the effect of the addition of an equivalent volume of DMSO in the control experiment.

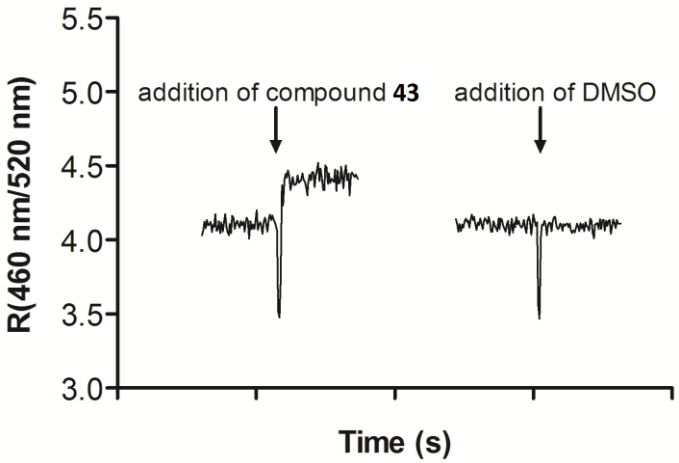


Figure 32. Effect of titration of compound **43** (82.5 μM) into $PC_{100\%}$ PLVs on the fluorescence ratio, R, in comparison to the effect of addition of an equivalent volume of DMSO

6.2.8 Analysis of Titration Data: Generation of Binding Profiles

GraphPad Prism v5.0 software was used to analyse the binding data from the above titrations. Plotting the change in ratio, ΔR(460 nm/520 nm), against ligand concentration (n=3 for all experiments; average taken) gave rise to raw binding profiles. These were then fitted to the binding models described by Equations 2 and 3 (Section 3.3.6).

The best fitting model of Equations 2 and 3 for each binding profile was determined using an extra sum-of-squares F test (Equation 6):

Equation 6: $$F = \frac{(SS1 - SS2)/(DF1 - DF2)}{SS2/DF2}$$

Where *SS*1 = Sum of squares (Equation 2)

*SS*2 = Sum of squares (Equation 3)

*DF*1 = Degrees of freedom (Equation 2)

*DF*2 = Degrees of freedom (Equation 3)

The program uses this F ratio and the two DF values to calculate a P value. On this basis it was determined which of Equations 2 and 3 were the best descriptor for each titration curve. For P≥0.05 the null hypothesis (Equation 2) was accepted. For P<0.05 Equation 3 was deemed the best fitting model.[59]

For the statistical parameters involved in these calculations see Appendix 2.

6.3 Assay Procedures

6.3.1 Materials and Methods

Phosphatidylcholine liposomes were synthesised as outlined in Section 6.2.3. The DMSO used was BioReagent grade for molecular biology (≥99.9%), and was purchased from Sigma Aldrich. All other reagents were obtained commercially and used without further purification.

Flat-bottomed polystyrene 96-well plates (415 μL capacity) were purchased from Fisher Scientific, and read using a Thermo Scientific Multiskan GO microplate spectrophotometer.

Tris buffer (10 mM, pH 7.4) was filtered before use using Minisart High-Flow single use syringe filters (0.20 μm pore size).

Samples were centrifuged using a Fisher Scientific accuSpin Micro 17R microcentrifuge.

6.3.2 Thiobarbituric Acid Reactive Substances (TBARS) Assay

All experiments were conducted in triplicate, and each run assayed in duplicate.

A solution of **44**, **43**, **9**, or **77** (33.0 mM in DMSO, or DMSO only for control experiments) was added to a suspension of phosphatidylcholine liposomes (8.00 mM in pH 7.4 Tris buffer) to give the desired final concentration of sunscreen molecule (20 mol%, 10 mol% or 5 mol%), in a test tube. The test tube was plugged loosely with cotton wool in order to minimise evaporation but allow the free diffusion of air. The mixture was stirred, in the dark, for 30 min in order to allow equilibration, and then irradiated (Wotan Ultravitalux

Sunlamp, 300 W). Aliquots of mixture were removed from the sample at desired time intervals (0 h, 0.5 h, 1 h, 2 h, 3 h, 5 h irradiation). 300 μL of sample was mixed with 300 μL trichloroacetic acid solution (0.6 N aqueous), incubated at rt. for 15 min, and then centrifuged at 12000 g for 10 min. The supernatant was removed and centrifuged once more under the same conditions. 75 μL thiobarbituric acid solution (46.5 mM in H_2O:DMSO::9:1) was added to 150 μL of the supernatant in a 96-well plate, and the absorbance of the sample at 532 nm read.[64] The plate was then incubated for 2 h at 50 °C and the absorbance read again. The pre-incubation optical densities were subtracted from the post-incubation values, and the concentration of TBARS in the sample calculated by interpolation from a standard curve. The standard curve was created by treating 100 μL of 1,1,3,3-tetramethoxypropane solution (500 μM in H_2O:EtOH::49:1) with 200 μL trichloroacetic acid solution (0.6 N aqueous), to give a malondialdehyde stock solution of 167 μM. Serial dilution of this stock gave samples of a range of concentrations (16.7 μM – 0.26 μM), which were treated with thiobarbituric acid solution and assayed in the same manner as the experimental samples.

6.3.3 2,2-Diphenyl-1-picrahydrazyl (DPPH) Assay

All samples were assayed in triplicate.

1 mL of a solution of DPPH (200 μM in methanol) was added to 3 mL of antioxidant solution (**44**, **43**, **9** or **78** in methanol) of varying concentrations, and the resultant mixture incubated at rt., in the dark, for 30 min. The absorbance of the sample was then read at 517 nm. In addition control runs

using 3 mL methanol in place of antioxidant solution, and blank runs using methanol only (no DPPH solution) were read, and the inhibition calculated according to Equation 5 (Section 4.2).[67]

6.3.4 Ferric Reducing Antioxidant Power (FRAP) Assay

FRAP reagent was made up freshly on the day of use by mixing together 25 mL acetate buffer (pH 3.6, 300 mM), 2.5 mL tripyridyltriazine (TPTZ) solution (10 mM in 40 mM aqueous HCl) and 2.5 mL $FeCl_3.6H_2O$ solution (20 mM, aqueous).[68] Solutions of varying concentrations of antioxidants were also made freshly, in ethanol (**44**, **43**, **9** and **77**) or H_2O (**78**), along with standard solutions of $FeSO_4.7H_2O$ (in H_2O). To conduct the assay 150 μL of FRAP reagent was incubated at 37 °C for 15 min, then the absorbance read at 593 nm. 15 μL H_2O and 5 μL sample or standard was added and the mixture incubated for a further 15 min at 37 °C. The absorbance was again read at 593 nm, and the initial absorbance subtracted from the final reading. Interpolation from the standard curve ($FeSO_4$) allowed the concentration of Fe(II) in each sample to be calculated. Samples were assayed in triplicate, and absorbances for each run read in duplicate. The assay was conducted in a 96-well plate, allowing multiple samples to be assayed at the same time.

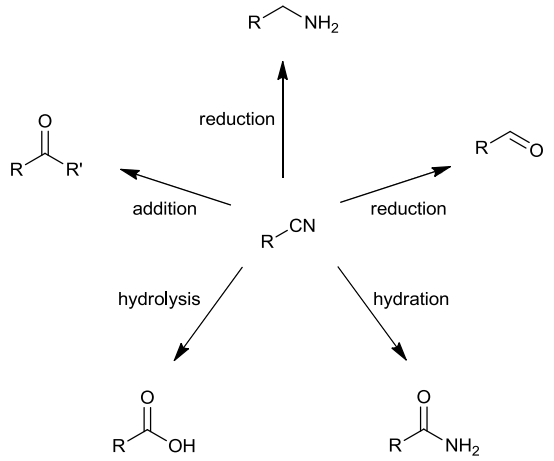
Part Two

Chapter 7 Synthesis of Alkenyl Nitriles by the Palladium-Catalysed Cyanation of Vinyl Halides with Acetone Cyanohydrin

7.1 Introduction

7.1.1 Prevalence and Utility of Alkenyl Nitriles

The nitrile functional group is a valuable intermediate in organic synthesis due to its versatility, being easily transformed into a number of other important functionalities (Scheme 48).



Scheme 48. Synthetic utility of the nitrile functional group

In addition to these simple transformations, nitriles are valuable building blocks for the formation of pharmaceutically important heterocyclic compounds including thiazoles,[81] triazoles[82] and tetrazoles.[83] Alkenyl nitriles in particular have found use as precursors for the synthesis of purines,[84] pyrimidines,[85] pyrazines,[86] porphyrazines[87] and diimines,[88] which find wide ranging applications in pharmaceuticals, dyes and catalysis.

α,β-Unsaturated nitriles are found in a structurally and biologically diverse range of natural products (Figure 33),[89] including the nitrilosides (eg. lanceolin A (**137**));[90] the cyanolipids (eg. **138**);[91] the macrolide antibiotic borrelidin (**139**);[92] and the antitumour calyculin family (eg. calyculin A (**140**)).[93]

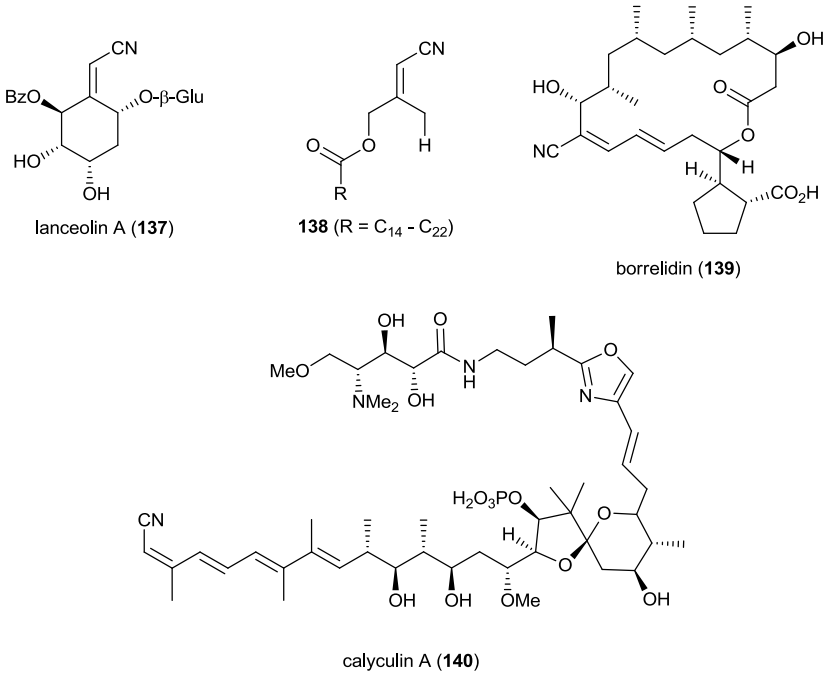


Figure 33. Examples of naturally occurring alkenyl nitriles

As well as being found in nature, alkenyl nitriles comprise an important subsection of the 30-plus nitrile-containing pharmaceuticals currently on the market. These are used to treat a diverse array of medical conditions, with representative examples, **141 – 144**, outlined in Figure 34.[94]

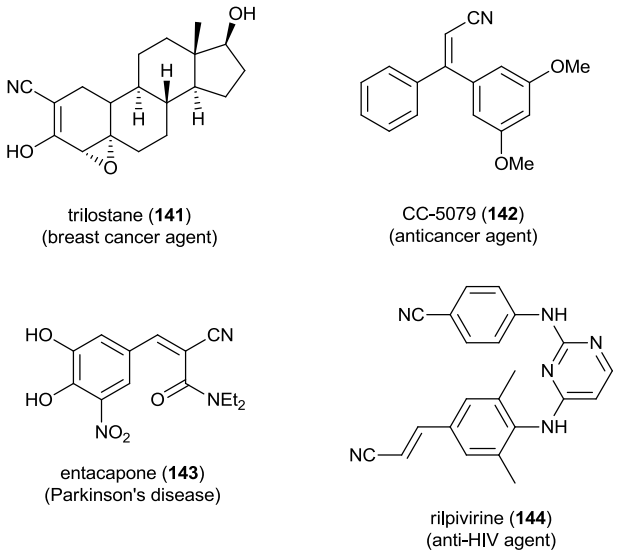


Figure 34. Examples of alkenyl nitrile-containing pharmaceuticals

Due to their synthetic utility and pharmaceutical applications, a number of synthetic routes to α,β-unsaturated nitriles have been developed. Classical methods include dehydration of amides[95] or aldoximes,[96] Wittig-[97] and Peterson-type[98] olefination processes, ammoxidation of alkenes,[99] and carbocyanation of alkynes.[100] These approaches suffer variously from high waste generation, low yields and poor stereoselectivity. As such the transition metal-catalysed cyanation of vinyl halides is an attractive route for the synthesis of alkenyl nitriles. Whilst several instances of such transformations have been reported in the literature, the area remains underdeveloped, particularly in comparison to analagous cyanations of aryl halides.

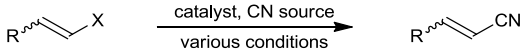
7.1.2 Transition Metal-Catalysed Cyanation of Vinyl Halides: Existing Methodology

Table 10 outlines the existing literature examples of transition metal-catalysed syntheses of alkenyl nitriles from the corresponding halides. The earliest reported method is that of Yamamura, who demonstrated the

transformation of a number of styrenyl bromides to cinnamonitriles using tetrakis(triphenylphosphine)palladium as catalyst and potassium cyanide as the cyanide source (Entry 1).[101] The methodology, involving use of 18-crown-6 as an additive in benzene at high temperature, was also shown to work for butyl bromide and β-chlorostyrene.

In 1982 a further two examples of the cyanation reaction were published, both also utilising potassium cyanide. Funabiki and co-workers employed tetracyanocobaltate(I) as catalyst (Entry 2),[102] whilst Sakakibara et al. pioneered the use of an in situ-generated nickel(0) complex (Entry 3).[103] In both cases alkenyl substituents were restricted to phenyl or simple alkyl groups, and significant erosion of stereochemistry was observed for *Z*-substrates. An attempt by Funabiki to cyanate an ester-bearing substrate resulted in no product formation.

Stuhl (Entry 4), like Funabiki, used a cobalt-based catalyst system to effect the transformation of several basic alkenyl halides into nitriles.[104] However, this method employed an organic cyanide source, $(Et_3MeN)CN$, in acetonitrile. Yields were moderate, stereoselectivity was poor, and an attempt to transform an ether-bearing alkenyl halide failed.



Entry	Catalyst	CN source	Substrate scope	Year	Reference
1	Pd(0)	KCN	R = Ph, alkyl X = Br, Cl	1977	101
2	Co(I)	KCN	R = Ph, Me X = Br, Cl	1982	102
3	Ni(0)	KCN	R = Ph, alkyl X = Br, Cl	1982	103
4	Co[a]	$(Et_3MeN)CN$	R = Ph, Me X = Br, Cl	1985	104
5	Pd(0)	$Zn(CN)_2$	R = Ph X = Br	2000	105
6	Pd(0)	$K_4Fe(CN)_6$	R = aryl X = Br	2006	106
7	Cu(I)	$K_4Fe(CN)_6$	R = aryl X = Br	2012	107

Table 10. Overview of the existing methodology for the transition metal-catalysed cyanation of vinyl halides. [a]Oxidation state of active catalytic species unknown

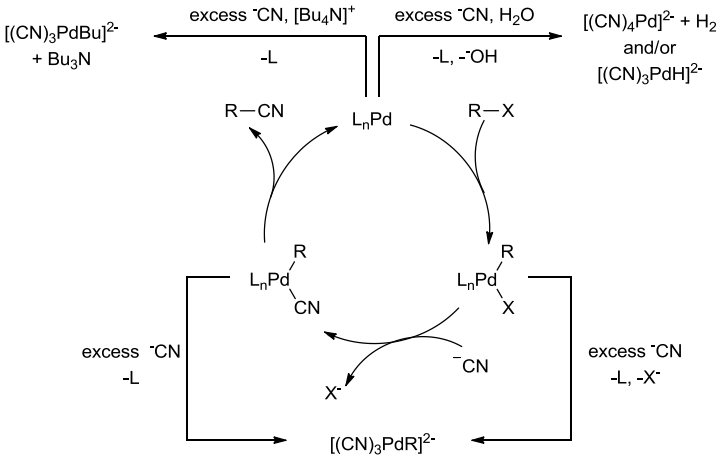
More recently, alternative cyanation sources have been used to effect this transformation. In their paper on the palladium-catalysed, microwave-assisted cyanation of aryl halides, Alterman and Hallberg (Entry 5) employed zinc cyanide, and included a single example of a vinylic substrate, namely trans-β-bromostyrene.[105]

Due to its lack of toxicity, potassium hexacyanoferrate(II) has also been explored as a cyanide source. Li and co-workers (Entry 6) utilised this reagent

in their palladium-catalysed protocol, involving microwave irradiation in ionic liquid.[106] Most recently Saha et al. reported a hydroxyapatite-supported copper(I)-catalysed methodology (Entry 7).[107] Whilst moderate to good yields were obtained, in both of these cases examples were restricted solely to styrenyl bromide substrates.

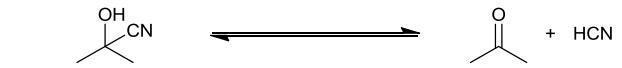
7.1.3 Use of Acetone Cyanohydrin in Cyanation Methodology

The transition metal-catalysed cyanation of aromatic halides is far better developed than that of vinyl halides. Much recent work has focused on palladium as the catalyst,[108] with cyanide sources including KCN,[109] NaCN,[110] TMSCN,[111] $Zn(CN)_2$,[112] and $K_4[Fe(CN)_6]$.[113] A major problem associated with this methodology is the issue of catalyst deactivation by excess cyanation reagent in solution. An increase in the concentration of the strongly binding cyanide anion leads to a breakdown in the catalytic cycle. Mechanistic studies carried out by Grushin and co-workers elucidated the nature of the catalytically inactive palladium complexes formed under various reaction conditions.[114] These are outlined, along with the generally accepted catalytic cycle for the palladium-catalysed cyanation reaction, in Scheme 49.



Scheme 49. Pathways leading to catalyst deactivation during the palladium-catalysed cyanation of halides. Adapted from reference 108b

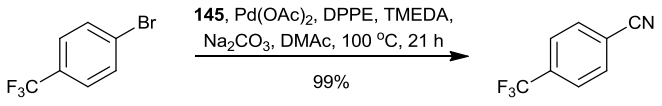
In order to minimise these deactivation pathways and maximise catalytic turnover, it was found that a slow, controlled addition of the cyanating agent was beneficial. The dosage of solid cyanide sources can be difficult to control. To address this issue, Beller et al. pioneered the use of acetone cyanohydrin (**145**) as the cyanide source (Scheme 50) in the palladium-catalysed cyanation of aryl halides.[115]



acetone cyanohydrin (**145**)

Scheme 50. Acetone cyanohydrin as a source of cyanide

As a liquid cyanating agent, the defined dosage of acetone cyanohydrin (**145**) to the reaction mixture was easily achieved using a syringe pump. The reagent system was optimised using 4-bromobenzotrifluoride (**146**) as a substrate (Scheme 51).



146 147

Scheme 51. Optimised conditions for the palladium-catalysed cyanation of 4-bromobenzotrifluoride (**146**) with acetone cyanohydrin (**145**)[115]

Beller demonstrated the applicability of this system to a range of aryl bromides (bearing both electron-donating and electron-withdrawing substituents), heteroaryl bromides, and two electron-deficient aryl chlorides. Whilst the deactivated, electron-rich substrates and the aryl chlorides required higher reaction temperatures, in most cases yields (determined by GC) were good to excellent. The efficacy of the syringe pump delivery technique in preventing catalyst deactivation was also exemplified by lowering of the catalyst loading down as far as 0.05 mol% while maintaining good yields.

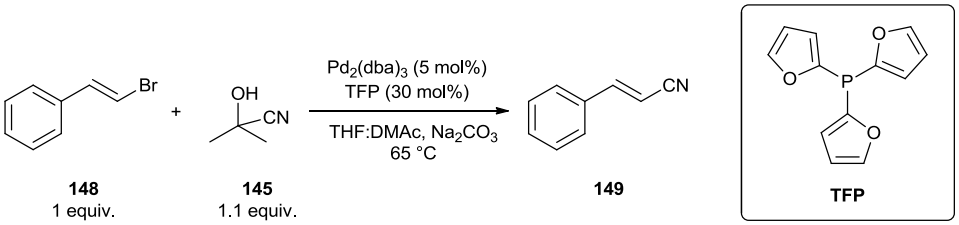
7.1.4 Aims of this Work

The aims of this work were twofold. The first was to build on the work of Beller and co-workers by investigating the applicability of acetone cyanohydrin (**145**) as a cyanating agent to alkenyl halide systems. The second was to develop a straightforward and general method for the palladium-catalysed cyanation of vinyl halides, the scope of which would extend beyond the simple aryl- and alkyl-substituted examples reported thus far in the literature.

7.2 Results and Discussion

7.2.1 Optimisation of the Reaction Conditions

The preliminary investigations into the palladium-catalysed cyanation of vinyl halides using acetone cyanohydrin (**145**) as the cyanating agent were conducted using trans-β-bromostyrene (**148**) as the substrate. The initial conditions tested (Table 11) utilised 5 mol% $Pd_2(dba)_3$ as the palladium source, 30 mol% tri(2-furyl)phosphine (TFP) as the added ligand and Na_2CO_3 (1.1 equivalents) as the base, in a solvent system of THF and dimethylacetamide (DMAc) (2:1 ratio), and with a reaction temperature of 65 °C.



Entry	Duration of 145 addition	Reaction Time[a]	Yield
1	15 min	6 h	23%
2	15 min	15 h	23%
3	15 min	10 min	trace[b]
4	17 h	1 h	trace[b]
5	**one portion**	**6 h**	**24%**

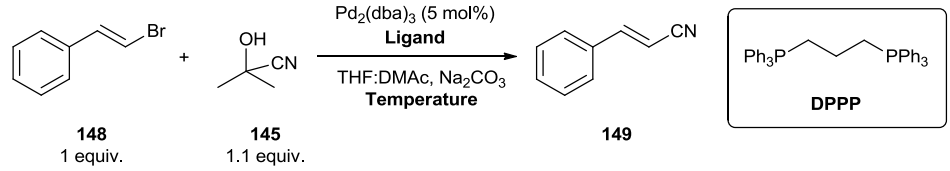
Table 11. Palladium-catalysed cyanation of β-bromostyrene (**148**): effect of duration of acetone cyanohydrin (**145**) addition and reaction time on the isolated yield of cinnamonitrile (**149**). [a]time between completion of addition of **145** and work up of the reaction mixture; [b]trace of product detected in the ^{1}H NMR spectrum of the crude mixture – not isolated

Addition of **145** to the reaction mixture over 15 min followed by a reaction time of 6 h resulted in the desired product cinnamonitrile (**149**) being isolated in 23% yield (Table 11, Entry 1). **149** was generated as a single geometric

isomer, with a lot of unreacted starting material **148** remaining in the crude reaction mixture. Increasing the reaction time to 15 h, however, did not result in an improved yield (Table 11, Entry 2), whilst reduction of the reaction time to 10 min (Table 11, Entry 3) led to just a trace of the product **149** being formed. These results appeared to indicate that the catalyst system was becoming inactive at some point before 6 h reaction time. It was reasoned that the relatively fast addition of acetone cyanohydrin (**145**) was leading to catalyst deactivation due to a high concentration of cyanide ions in solution. To try and solve this, **145** was added via syringe pump over a period of 17 h, as in Beller's work.[115] Surprisingly, however, this method led to just trace formation of **149**, with a vast majority of the starting material **148** remaining unreacted (Table 11, Entry 4). Conversely, addition of the cyanating agent **145** in a single portion resulted in an isolated yield of 24% (Table 11, Entry 5). This indicated that slow addition of **145** was not necessary (and indeed was detrimental) for the cyanation of vinyl halides. Thus in all further experiments **145** was added in a single portion.

It was postulated that by increasing the rate of the initial oxidative addition of **148** to the palladium complex then catalyst deactivation might be suppressed, leading to improved yields. Two ways of accomplishing this were explored, namely an increase in reaction temperature, and the use of a more electron-rich ligand. The results are outlined in Table 12. Increasing the reaction temperature from 65 °C to 100 °C led to an increase in yield to 38% (Table 12, Entry 2), whilst conducting the cyanation at room temperature resulted in trace product formation only (Table 12, Entry 3). Replacing the relatively

electron-withdrawing TFP ligand with the more electron-donating, bidentate, 1,2-bis(diphenylphosphino)propane (DPPP) also had the desired effect of increasing the reaction yield, affording 38% of **149** at 65 °C (Table 12, Entry 4) and 70% at 100 °C (Table 12, Entry 5). The use of the monodentate phosphine ligands PPh_3 and PCy_3 (Table 12, Entries 6 and 7) led to no reaction and trace product formation, respectively. Whilst the reasons for this are unclear, similar detrimental effects on yield have been reported with these ligands in the palladium-catalysed cyanation of aryl chlorides.[116]

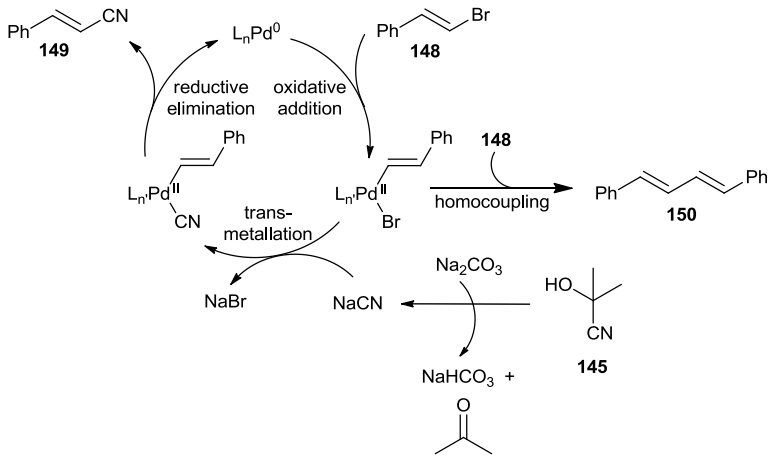


Entry	Ligand[a]	Temperature	Reaction Time[b]	Yield
1	TFP	65 °C	6 h	24%
2	TFP	100 °C	6 h	38%
3	TFP	rt.	6 h	trace[c]
4	DPPP	65 °C	6 h	38%
5	**DPPP**	**100 °C**	**2 h**	**70%**
6	PPh_3	100 °C	6 h	-
7	PCy_3	100 °C	6 h	trace[c]

Table 12. Palladium-catalysed cyanation of β-bromostyrene (**148**): effect of ligand and reaction temperature on the isolated yield of cinnamonitrile (**149**). [a]30 mol% of monodentate ligands TFP, PPh_3 and PCy_3 used, 15 mol% of bidentate ligand DPPP used; [b]reactions were allowed to continue until complete consumption of **148** was observed by TLC, or for 6 h; [c]trace of product detected in the ^{1}H NMR spectrum of the crude mixture – not isolated

During the investigation into temperature and ligand effects, an identifiable minor byproduct was discernible in the ^{1}H NMR spectrum of the crude reaction mixture post work up (in the case of Table 12, Entry 5). Comparison of these peaks with literature data revealed the byproduct to be (1*E*,3*E*)-1,4-diphenylbuta-1,3-diene (**150**).[117] **150** must clearly arise from a homocoupling

reaction of two molecules of β-bromostyrene (**150**), which is in competition with the transmetallation step of the cyanation reaction (Scheme 52).

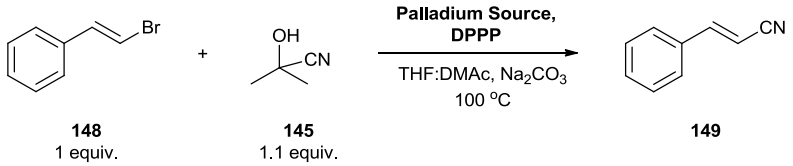


Scheme 52. Suggested catalytic cycle for the cyanation of **148**, and the homocoupling side reaction

The detection of this side reaction raises a possible explanation for the lack of reactivity observed when slow addition of acetone cyanohydrin (**145**) via syringe pump was attempted. If, upon the oxidative insertion taking place, no cyanide ion was readily available for the subsequent transmetallation step of the cyanation reaction, then the homocoupling side reaction would instead occur. Sakakibara and co-workers observed this competing homocoupling reaction in their nickel-based cyanation of vinyl halides, and also found that low cyanide solubilities resulted in inactivation of the catalyst system.[103b] They discovered that the homocoupling reaction resulted in the formation of an inert nickel complex ($NiBr_2L_2$), which prevented further reaction (cyanation or homocoupling) from occurring once a small amount of **150** had been produced. It is feasible that the homocoupling in this case results in an analogous inactive palladium complex, shutting down the catalytic cycle and leading to little or no product formation. The oxidative addition of aryl halides

proceeds at a slower rate than that of vinyl halides, and so inactivation of the catalyst by cyanide ion prior to oxidative addition taking place is a higher risk, resulting in the requirement for a slow dosage of cyanating agent in the former case. In subsequent reactions of β-bromostyrene (**148**) **150** was often present in trace amounts in the ^{1}H NMR spectrum of the crude mixture.

The effect of increasing the ligand concentration on the cyanation reaction was also investigated, in order to find the optimum ligand-to-palladium ratio for stabilisation of an active catalytic species (Table 13).



148 1 equiv. + **145** 1.1 equiv. → **149**

Entry	Palladium Source[a]	P:Pd[b]	Reaction Time	Yield
1	**$Pd_2(dba)_3$**	**3:1**	**2 h**	**70%**
2	$Pd_2(dba)_3$	4:1	3 h	49%
3	$Pd_2(dba)_3$	6:1	3 h	51%
4	$Pd(OAc)_2$	3:1	1.5 h	63%
5	**$Pd(OAc)_2$**	**4:1**	**1.5 h**	**73%**
6	$Pd(OAc)_2$	6:1	1.5 h	37%
7	-	-	6 h	-[c]

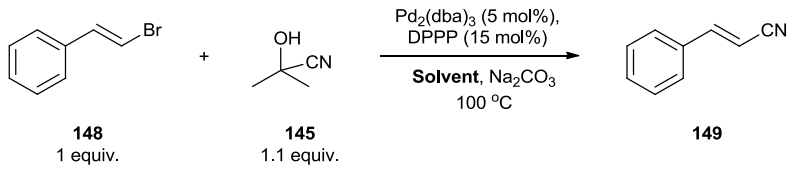
Table 13. Palladium-catalysed cyanation of β-bromostyrene (**148**): effect of palladium source and phosphorous to palladium ratio on the isolated yield of cinnamonitrile (**149**). [a]5 mol% of $Pd_2(dba)_3$ used; 10 mol% of $Pd(OAc)_2$ used; [b]15 mol% DPPP used to achieve P:Pd::3:1, 20 mol% DPPP used to achieve P:Pd::4:1, 30 mol% DPPP used to achieve P:Pd::6:1; [c]Et_2O:DMAc used as the solvent system, 15 mol% DPPP

When $Pd_2(dba)_3$ was used as the palladium source, a phosphorous:palladium ratio of 3:1 proved the most favourable, with increases in this ratio leading to decreased yields (Table 13, Entry 1 versus Entries 2 and 3), and unreacted starting material remaining. It is likely that these higher concentrations of phosphine ligand led to a decrease in catalyst activity by the blocking of free

coordination sites, an effect which has been observed in other cross coupling reactions.[118] When $Pd(OAc)_2$ was used as the palladium source, a higher P:Pd ratio of 4:1 proved optimum (Table 13, Entries 4-6). This is likely because $Pd(OAc)_2$ contains palladium(II), and thus some phosphine ligand is depleted in generating the active palladium(0) species. Whilst the combination of $Pd(OAc)_2$/P:Pd::4:1 (Table 13, Entry 5) produced a yield of 73% in comparison to $Pd_2(dba)_3$ as palladium source with a P:Pd ratio of 3:1 giving a yield of 70% (Table 13, Entry 1), the latter combination was selected to use going forward as it was not thought that the increase in the amount of ligand was offset by the slight improvement in yield.

A survey of solvent systems (Table 14) revealed a combination of Et_2O and DMAc to be the most efficient for the cyanation reaction, affording an isolated yield of 79% (Table 14, Entry 11). This solvent combination, and the use of DMF on its own (Table 14, Entry 7), were the only two solvent systems to completely suppress the formation of **150**, which was present at low levels in the crude mixtures of all the other systems. The results of the solvent screen show the necessity for a polar component such as DMF or DMAc to achieve respectable yields. This is probably due to a combination of their ability to solubilise cyanide ion and their high boiling points preventing the drying out of the reaction mixture at the high temperature utilised. Using the optimised solvent system at 100 °C it is likely that evaporation of at least some of the Et_2O occurs during the course of the reaction. However, its

inclusion in the reaction mixture appears important, resulting in a yield 28% higher than when DMAc was used alone (Table 14, Entry 11 versus 3).



148
1 equiv.

145
1.1 equiv.

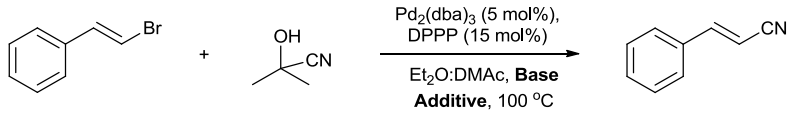
149

Entry	Solvent[a]	Reaction Time	Yield
1	THF:DMAc	2 h	70%
2	THF	3 h	14%
3	DMAc	3 h	51%
4	Toluene	3 h	trace[b]
5	Toluene:DMAc	3 h	trace[b]
6	THF:DMF	3 h	70%
7	DMF	3 h	73%
8	Dioxane	3 h	trace[b]
9	Dioxane:DMAc	3 h	trace[b]
10	Et_2O	4 h	32%
11	**Et_2O:DMAc**	**4 h**	**79%**
12	MeCN	4 h	49%
13	MeCN:DMAc	4 h	59%

Table 14. Palladium-catalysed cyanation of β-bromostyrene (**148**): solvent screen. [a]Where a dual solvent system was used the ratio of solvents was 2:1; [b]trace of product detected in the ^{1}H NMR spectrum of the crude mixture – not isolated

Upon the Et_2O/DMAc combination emerging as the solvent system of choice, the cyanation reaction was also conducted using this solvent system at 50 °C instead of 100 °C. However, at this temperature only a trace of product **149** was generated after 21 h reaction time. These results show that both the inclusion of Et_2O, and the high temperature, are necessary to maintain yields, despite the latter condition almost certainly leading to depletion of the former during the course of the reaction.

The final variables investigated during the optimisation of the cyanation reaction were that of the base used, and the inclusion of additives (Table 15). None of the alternative bases tested proved more effective in promoting the reaction than the originally used Na_2CO_3 (Table 15, Entry 1 versus Entries 3-7).



148 1 equiv. + **145** 1.1 equiv. → **149**

Entry	Base	Additive[a]	Reaction Time	Yield
1	**Na_2CO_3**	**-**	**4 h**	**79%**
2	-	-	6 h	-[b]
3	NaOH	-	3 h	trace[c]
4	NaOAc	-	3 h	66%
5	NaO^tBu	-	3 h	trace[c]
6	Et_3N	-	3 h	59%
7	Ag_2CO_3	-	3 h	trace[c]
8	Na_2CO_3	Zn	1 h	49%
9	Na_2CO_3	TMEDA	3 h	13%
10	Na_2CO_3	CuI	3 h	23%
11	Na_2CO_3	TBAB	2 h	70%

Table 15. Palladium-catalysed cyanation of β-bromostyrene (**148**): base and additive screen. [a]Additives used at 5 mol%; [b]THF:DMAc used as the solvent system; [c]trace of product detected in the ^{1}H NMR spectrum of the crude mixture – not isolated

The inclusion of additives which have been reported to promote cyanation reactions also proved detrimental to the isolated yield of **149** (Table 15, Entries 8-11). Zinc dust was found by Ushkov and Grushin to improve the yields during their mechanistic investigations into the cyanation of aryl bromides by reduction of inert polycyano Pd(II) products of catalyst poisoning back to Pd(0) complexes with weaker binding to cyanide ions.[119] However in

this case, whilst all of the starting material **148** was consumed within 1 h reaction time, the isolated yield was just 49% (Table 15, Entry 8). The consumption of starting material could not be accounted for by the homocoupling side reaction, as **150** was only present in the crude reaction mixture in trace amounts, suggesting that the addition of zinc was promoting other side reactions and/or decomposition. However, no additional byproducts were isolated from the mixture. TMEDA,[109c,116] CuI[110b] and TBAB[118] have all found use as co-catalysts in cyanation reactions. Here the use of TMEDA (Table 15, Entry 9) and CuI (Table 15, Entry 10) severely stilted the reaction, with the reaction not going to completion in either case. TBAB (Table 15, Entry 11) caused a modest reduction in yield as compared to the additive-free case (70% versus 79% yields), but also promoted formation of small amounts of the homocoupled product **150**, whereas **150** was not observed to have formed at all in the additive-free reaction.

7.2.2 Substrate Scope

Having screened many different conditions for the palladium-catalysed cyanation of β-bromostyrene (**148**), the optimised conditions were applied to a number of other vinyl halides in order to explore the scope of the reaction. The results are outlined in Table 16.

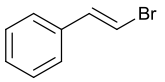
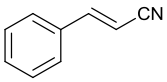
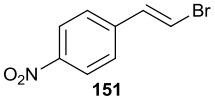
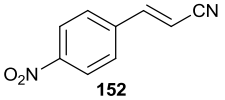
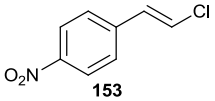
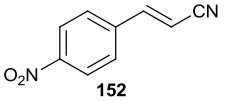
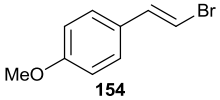
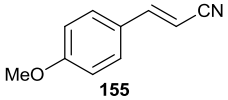
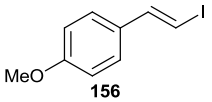
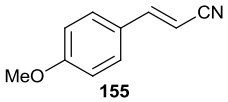
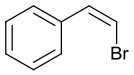
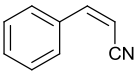
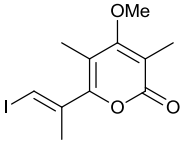
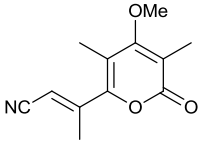
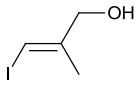
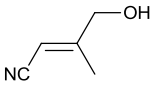
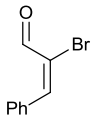
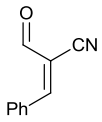
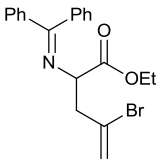
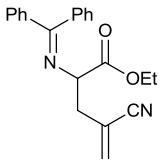
Entry	Substrate	Product	Temperature	Reaction Time	Yield[a]
1	 **148**	 **149**	100 °C	4 h	79%
2	 **151**	 **152**	100 °C	6 h	83%[b]
3	 **153**	 **152**	100 °C	6 h	47%
4	 **154**	 **155**	140 °C	2 h	81%[c]
5	 **156**	 **155**	140 °C	7 h	23%[c]
6	 **157**	 **158**	100 °C	6 h	55%
7	 **115**	 **159**	100 °C	4 h	66%
8	 **113**	 **160**	100 °C	2 h	72%
9	 **161**	 **162**	100 °C	3 h	49%[d]
10	 **163**	 **164**	100 °C	4 h	80%

Table 16. Scope of the palladium-catalysed cyanation of vinyl halides using acetone cyanohydrin (**145**). General conditions: 1 equiv. vinyl halide, 1.1 equiv **145**, 5 mol% $Pd_2(dba)_3$, 15 mol% DPPP, 1.1 equiv. Na_2CO_3, Et_2O:DMAc::2:1. [a]Isolated yield; [b]inseparable 18:1 mixture of *E*:*Z* isomers generated; [c]a reaction temperature of 100 °C gave yields of 69% and 15% from **153** and **155** respectively; [d]generated as an inseparable 3.5:1 mixture with trans-cinnamaldehyde

Substituted cinnamonitriles bearing electron-withdrawing nitro and electron-donating methoxy substituents (**152** and **155**) were both synthesised from

their respective bromo-precursors **151** and **154** in good yields (Table 16, Entries 2 and 4), although the cyanation of **154** did require a higher reaction temperature as the electron-donating group deactivates the substrate towards oxidative addition. The synthesis of **152** from its chloro-precursor **153** was predictably more sluggish than the analogous reaction from bromo **151**, with a 47% yield isolated after 6 h reaction time (Table 16, Entry 3). The higher strength of carbon-chlorine bonds relative to their carbon-bromine counterparts makes them less amenable to oxidative addition and thus less reactive towards transition metal-catalysed couplings. Analysis of the ^{1}H NMR of the crude mixture revealed the ratio of unreacted starting material **153** to product **152** to be 1:1 after this time, and so a longer reaction time would potentially result in greater conversion. In contrast, iodo compounds are generally more reactive to cross coupling reactions than their bromo analogues and so the low yield of **155** generated from **156** (23%, with the remaining material accounted for as unreacted substrate) in comparison to **154** (81%) (Table 16, Entries 5 and 4 respectively) is a surprising result.

Along with these *E*-alkenyl examples, (*Z*)-(2-bromovinyl)benzene (**157**) also underwent cyanation under the reaction conditions, albeit more slowly than its *E* counterpart **148**, with a substantial proportion of the substrate unreacted after the 6 h reaction time (Table 16, Entry 6). A small amount of isomerisation was also observed in this case, with a *Z*:*E* ratio of 12:1 in the crude mixture, as judged by integration of the ^{1}H NMR spectrum, although the two isomers proved chromatographically separable, allowing **158** to be isolated as a single isomer in 55% yield.

In addition to the cinnamonitriles a further four alkenyl nitriles were synthesised using the developed protocol, from vinylic iodo and bromo starting materials, in moderate to good yields (Table 16, Entries 7-10). These examples demonstrate the compatibility of the cyanation procedure with functionalities including hydroxyl (Table 16, Entry 8), aldehyde (Table 16, Entry 9) and imine (Table 16, Entry 10), whilst also showing that trisubstituted alkenes are suitable substrates (Table 16, Entries 7-9). Of these four latter examples, the substrate giving the poorest yield was the aldehyde **161** (Table 16, Entry 9). Despite complete consumption of starting material, nitrile **162** was formed in a modest 49% yield. This is perhaps a reflection of the sensitive nature of the aldehyde functional group, which could reasonably have decomposed under the reaction conditions. This was also the only example in which protodehalogenation was observed, with **162** formed as an inseparable 3.5:1 mixture with trans-cinnamaldehyde, alkene isomerisation also having taken place.

With Beller's work having demonstrated the necessity for a slow dosage of acetone cyanohydrin (**145**) in order to successfully cyanate aryl halides,[115] it was thought that this difference in reactivity could be exploited to chemoselectively transform vinyl halides into nitriles in the presence of aryl halides. Initially, the reaction conditions were applied to bromobenzene (**165**), and pleasingly no reaction was observed to occur (Table 17, Entry 1).

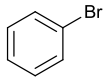
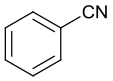
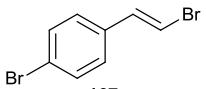
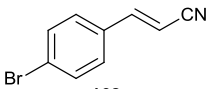
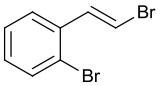
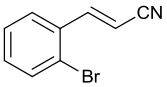
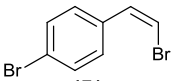
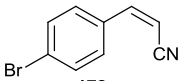
Entry	Substrate	Product	Reaction Time	Yield[a]
1	 **165**	 **166**	6 h	-
2	 **167**	 **168**	4 h	83%
3	 **169**	 **170**	2 h	68%
4	 **171**	 **172**	2 h	67%[b]

Table 17. Chemoselectivity in the palladium-catalysed cyanation reaction. General conditions: 1 equiv. substrate, 1.1 equiv **145**, 5 mol% $Pd_2(dba)_3$, 15 mol% DPPP, 1.1 equiv. Na_2CO_3, Et_2O:DMAc::2:1, 100 °C. [a]Isolated yield; [b]inseparable 11:1 mixture of *Z*:*E* isomers generated

Application of the cyanation protocol to the dibromo compounds **167**, **169** and **171** accordingly led to the chemoselective transformation of the vinyl bromide, leaving the aromatic bromide untouched in the process, to afford **168**, **170** and **172**, respectively (Table 17, Entries 2-4).

7.3 Summary and Conclusions

A protocol for the palladium-catalysed cyanation of vinyl halides has been developed, utilising acetone cyanohydrin (**145**) as the cyanating agent. The conditions for this transformation were optimised extensively using β-bromostyrene (**148**) as the test substrate. During this optimisation process it was found that, in contrast to a previously-reported protocol for the cyanation of aryl halides, fast addition of **145** was required to promote the reaction, with slow dosage via a syringe pump giving no reaction.

Of the ligands investigated the relatively electron-rich, bidentate phosphine ligand DPPP afforded the highest yields, and raising the reaction temperature from the originally-used 65 °C to 100 °C had a beneficial effect. These are both factors known to facilitate the oxidative addition step of the catalytic cycle.

An extensive solvent screen revealed a combination of Et_2O and DMAc to be optimal. Although the high reaction temperature is highly likely to cause some evaporation of the volatile Et_2O during the course of the reaction, the inclusion of this solvent was shown to be essential to maintain a high yield (79% when Et_2O:DMAc was used versus 51% when DMAc was used alone).

Na_2CO_3 proved to be the best base, of those tested, to promote the cyanation, whilst the inclusion of additives had only a detrimental effect on the reaction outcome.

The optimised reaction conditions, namely: one-portion addition of **145** (1.1 equivalents), $Pd_2(dba)_3$ (5 mol%), DPPP (15 mol%), Na_2CO_3 (1.1 equivalents), Et_2O:DMAc::2:1, 100 °C, were then applied to a number of vinyl halides in order to investigate the substrate scope.

A range of substrates were shown to be amenable to the developed protocol, including a number of β-halostyrenes bearing electron-withdrawing and electron-donating substituents, and several alkenyl halides bearing sensitive functionalities including hydroxyl, aldehyde and imine groups. This is significant as previously very few, if any, transition metal-catalysed cyanation reactions of vinyl halides bearing substituents other than simple aryl or alkyl groups have been reported.

In addition, the procedure was shown to be chemoselective for vinyl bromides in the presence of aryl bromides, which are left unaffected and available for further chemical transformations, adding to the synthetic utility of the reaction.

7.4 Experimental

7.4.1 Experimental Techniques

Reactions were performed in flame-dried glassware under an atmosphere of argon and stirred magnetically unless otherwise stated. For use as a reaction solvent CH_2Cl_2 was freshly distilled from CaH_2; Et_2O was freshly distilled from sodium and benzophenone. Triethylamine was stored over KOH pellets. NBS was recrystallised from water. Anhydrous DMAc (99.8%) was purchased from Sigma Aldrich. All other reagents were obtained commercially and used without further purification. Flash column chromatography was performed using Merck silica gel 60 as the stationary phase. Where not otherwise specified flash column chromatography was performed using petrol-EtOAc mixtures of increasing polarity (as appropriate to the R_f value of the compound to be isolated) as the mobile phase. Petrol refers to petroleum spirit (b.p. 40-60 °C).

7.4.2 Analysis

Thin layer chromatography was carried out on aluminium-backed plates pre-coated with silica (0.2 mm, 60 F_{254}, Merck). The plates were developed using UV light and basic potassium permanganate solution. Melting points were

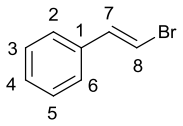
recorded using a STUART SMP3 apparatus and are uncorrected. Infrared (IR) spectra were recorded using a Bruker Tensor 27 FT-IR spectrophotometer with a neat film on an NaCl disc. IR peaks are quoted in as ν_{max} in cm^{-1}. ^{1}H and ^{13}C NMR spectra were recorded in $CDCl_3$ at ambient temperature using Bruker DPX400 (400 MHz), AV400 (400 MHz) and AV(III)400 (400 MHz) spectrometers. Data is expressed as chemical shifts in parts per million (ppm) relative to residual solvent signals of $CDCl_3$ (^{1}H NMR 7.27; ^{13}C NMR 77.0) as the internal standard on the δ scale. The following abbreviations are used to designate the multiplicity of each signal; s, singlet; d, doublet; dd, doublet of doublets; t, triplet; q, quartet; m, multiplet; br., broad. Coupling constants *J* are given in Hz. High-resolution mass spectra were obtained using a Bruker MicroTOF mass spectrometer operating in electrospray ionisation (ESI) mode.

Known substrates were characterised to a level consistent with the reported literature data.

7.4.3 Preparation of Substrates

(*E*)-3-Iodo-2-methylprop-2-en-1-ol (**113**) was synthesised as outlined in Section 6.1.3. (*E*)-1-(2-Bromovinyl)-4-nitrobenzene (**151**),[120] (*E*)-1-(2-chlorovinyl)-4-nitrobenzene (**153**),[120] and ethyl 4-bromo-2-((diphenylmethylene)amino)pent-4-enoate (**163**)[121] were synthesised by other Moses group members, using established literature procedures.

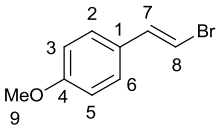
(*E*)-(2-Bromovinyl)benzene (148)[122,123]



Triethylamine (0.360 mL, 2.55 mmol) was added to a solution of trans-cinnamic acid (7.56 g, 51.0 mmol) in CH_2Cl_2 (150 mL), and the mixture stirred at rt. for 30 min. NBS (10.9 g, 61.2 mmol) was then added portionwise over 1 h, and the mixture stirred for a further 70 h at rt. The mixture was concentrated under reduced pressure, and the residue purified by column chromatography (petrol) to afford (*E*)-(2-bromovinyl)benzene (**148**) as a colourless oil (3.62 g, 39%).

$\mathbf{R_f}$ = 0.69 (5% EtOAc in petrol); δ_H ($CDCl_3$, 400 MHz): 7.37 - 7.27 (m, 5H, 5 x Ar CH_1), 7.12 (d, *J* = 14.0 Hz, 1H, 7-H_1), 6.78 (d, *J* = 14.0 Hz, 1H, 8-H_1); δ_c ($CDCl_3$, 100 MHz): 137.1 (C-1), 135.8 (C-8), 128.7 (C-3 and C-5), 128.2 (C-2 and C-6), 126.0 (C-4), 106.4 (C-7).

(*E*)-1-(2-Bromovinyl)-4-methoxybenzene (154)[122,123]

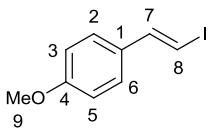


trans-4-Methoxycinnamic acid (890 mg, 5.00 mmol) was added to a solution of triethylamine (0.0400 mL, 0.290 mmol) in CH_2Cl_2 (15.0 mL), and the mixture stirred at rt. for 15 min. NBS (1.07 g, 6.00 mmol) was then added, and the mixture stirred at 40 °C for 40 h. The mixture was cooled to rt. and

concentrated under reduced pressure, and the residue purified by column chromatography (petrol) to afford (*E*)-1-(2-bromovinyl)-4-methoxybenzene (**154**) (887 mg, 83%) as a white solid.

R_f = 0.55 (5% EtOAc in petrol); **ν_{max}** (cm^{-1}) (thin film): 3071, 2953, 2840, 1606, 1505, 1456; **δ_H** ($CDCl_3$, 400 MHz): 7.27 - 7.21 (m, 2H, 2-H_1 and 6-H_1), 7.05 (d, *J* = 13.9 Hz, 1H, 7-H_1), 6.90 - 6.83 (m, 2H, 3-H_1 and 5-H_1), 6.62 (d, *J* = 13.9 Hz, 1H, 8-H_1), 3.82 (s, 3H, 9-H_3); **δ_c** ($CDCl_3$, 100 MHz): 159.6 (C-4), 136.5 (C-8), 128.8 (C-1), 127.3 (C-2 and C-6), 114.2 (C-3 and C-5), 104.0 (C-7), 55.3 (C-9).

(*E*)-1-(2-Iodovinyl)-4-methoxybenzene (156)[122,124]

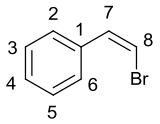


Triethylamine (0.0400 mL, 0.290 mmol) was added to a solution of trans-4-methoxycinnamic acid (890 mg, 5.00 mmol) in CH_2Cl_2 (15.0 mL), and the mixture stirred at rt. for 15 min. NIS (1.35 g, 6.00 mmol) was then added, and the mixture stirred at rt. for 80 h. The mixture was concentrated under reduced pressure, and the residue purified by column chromatography (petrol) to afford (*E*)-1-(2-iodovinyl)-4-methoxybenzene (**156**) (492 mg, 38%) as a white solid.

R_f = 0.55 (5% EtOAc in petrol); **ν_{max}** (cm^{-1}) (thin film): 3056, 2968, 2840, 1603, 1510, 1458; **δ_H** ($CDCl_3$, 400 MHz): 7.37 (d, *J* = 14.8 Hz, 1H, 7-H_1), 7.27 - 7.21 (m, 2H, 2-H_1 and 6-H_1), 6.89 - 6.83 (m, 2H, 3-H_1 and 5-H_1), 6.64 (d, *J* = 14.8 Hz, 1H,

8-H_1), 3.82 (s, 3H, 9-H_3); δ_c ($CDCl_3$, 100 MHz): 159.7 (C-4), 144.2 (C-7), 130.6 (C-1), 127.2 (C-2 and C-6), 114.0 (C-3 and C-5), 73.6 (C-8), 55.3 (C-9).

(*Z*)-(2-Bromovinyl)benzene (157)[125]



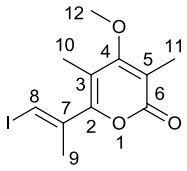
Carbon tetrabromide (26.1 g, 78.6 mmol) was added portionwise to a solution of triphenylphosphine (41.3 g, 158 mmol) in CH_2Cl_2 (300 mL), and the resultant deep red solution stirred at rt. for 15 min. Benzaldehyde (2.00 mL, 19.7 mmol) was then added dropwise at 0 °C, and the mixture stirred at rt. for 2 h. Pentane (200 mL) was added to the mixture, and the precipitated triphenylphosphine oxide removed by filtration through a pad of silica. The filtrate was concentrated under reduced pressure, and the residue purified by column chromatography (petrol) to afford (2,2-dibromovinyl)benzene (2.79 g, 54%) as a pale yellow oil.

$Pd(PPh_3)_4$ (173 mg, 0.150 mmol) and tributyltin hydride (1.00 mL, 3.82 mmol) were added sequentially to a solution of (2,2-dibromovinyl)benzene (1.00 g, 3.82 mmol) in CH_2Cl_2 (15.0 mL), and the resultant mixture stirred at rt., in the dark, for 1.5 h. A solution of potassium fluoride (900 mg) in water (70 mL) was then added, and the mixture stirred for 18 h. The precipitate was removed by filtration through a pad of silica, and the layers of the filtrate separated. The aqueous layer was extracted with CH_2Cl_2 (2 x 100 mL), and the combined organics dried over $MgSO_4$ and concentrated under reduced pressure. The

residue was purified by column chromatography (petrol) to afford (*Z*)-(2-bromovinyl)benzene (**157**) as a colourless oil.

R_f = 0.72 (5% EtOAc in petrol); **δ_H** ($CDCl_3$, 400 MHz): 7.74 - 7.66 (m, 2H, 3-H_1 and 5-H_1), 7.44 - 7.31 (m, 3H, 2-H_1, 4-H_1 and 6-H_1), 7.09 (d, *J* = 8.2 Hz, 1H, 7-H_1), 6.45 (d, *J* = 8.2 Hz, 1H, 8-H_1); **δ_c** ($CDCl_3$, 100 MHz): 134.9 (C-1), 132.3 (C-8), 129.0 (C-3 and C-5), 128.3 (C-4), 128.2 (C-2 and C-6), 106.3 (C-7).

(*E*)-6-(1-Iodoprop-1-en-2-yl)-4-methoxy-3,5-dimethyl-2H-pyran-2-one (115)

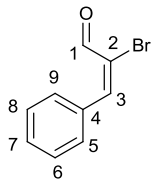


A mixture of (*E*)-4-hydroxy-6-(1-iodoprop-1-en-2-yl)-3,5-dimethyl-2H-pyran-2-one (**97**) (1.79 g, 5.80 mmol), Me_2SO_4 (1.10 mL, 11.6 mmol) and Li_2CO_3 (1.29 g, 17.4 mmol) in acetone (20 mL) was stirred at reflux for 18 h. The reaction mixture was then cooled to room temperature and diluted with EtOAc (20 mL). The solid was removed by filtration, and the filtrate concentrated under reduced pressure. The residue was purified by flash column chromatography to afford (*E*)-6-(1-iodoprop-1-en-2-yl)-4-methoxy-3,5-dimethyl-2H-pyran-2-one (**115**) (741 mg, 40% yield) as a white solid.

R_f = 0.36 (25% EtOAc in petrol); **mp**: 117-119 °C; **ν_{max}** (cm^{-1}) (thin film): 3065, 2946, 1709, 1635, 1564, 1449; **δ_H** ($CDCl_3$, 400 MHz): 6.66 (q, *J* = 1.1 Hz, 1H, 8-H_1), 3.83 (s, 3H, 12-H_3), 2.09 (d, *J* = 1.1 Hz, 3H, 9-H_3), 2.04 (s, 3H, 11-H_3), 1.95 (s, 3H, 10-H_3); **δ_c** ($CDCl_3$, 100 MHz): 167.9 (C-6), 164.7 (C-4), 154.6 (C-7), 139.6

(C-2), 111.0 (C-5), 110.2 (C-3), 88.4 (C-8), 60.3 (12-C), 22.9 (C-9), 11.8 (C-11), 10.4 (C-10); **HRMS** (ESI) calculated for $C_{11}H_{13}INaO_3$ $[M+Na]^+$ 342.9802, found 342.9788.

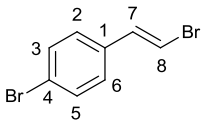
(*E*)-2-Bromo-3-phenylacrylaldehyde (161)[126]



A solution of bromine (0.520 mL, 10.0 mmol) in CH_2Cl_2 (2.00 mL) was added dropwise to a solution of *trans*-cinnamaldehyde (1.30 mL, 10.0 mmol) in CH_2Cl_2 (14.0 mL) at 0 °C, and the mixture stirred at this temperature for 15 min. Triethylamine (2.10 mL, 15.0 mmol) was then added dropwise and the mixture stirred at 0°C for a further 2 h. The mixture was concentrated under reduced pressure, and the residue purified by column chromatography (petrol to 5% EtOAc in petrol) to afford (*E*)-2-bromo-3-phenylacrylaldehyde (**161**) (913 mg, 43%) as a pale yellow oil.

$\mathbf{R_f}$ = 0.30 (5% EtOAc in petrol); ν_{max} (cm^{-1}) (thin film): 3024, 2856, 1678, 1589, 1568; δ_H ($CDCl_3$, 400 MHz): 9.55 (s, 1H, 1-H_1), 8.28 (s, 1H, 3-H_1), 7.53 - 7.33 (m, 5H, 5 x Ar CH); δ_c ($CDCl_3$, 100 MHz): 184.2 (C-1), 150.4 (C-3), 133.3 (C-4), 130.3 (C-7), 129.6 and 128.9 (C-5, C-6, C-8 and C-9), 126.2 (C-2); **HRMS** (ESI) calculated for C_9H_7BrNaO $[M+Na]^+$ 232.9572, found 232.9574.

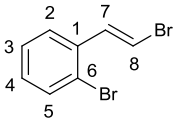
(*E*)-1-Bromo-4-(2-bromovinyl)benzene (167)[127]



A mixture of 4-bromo-*trans*-cinnamic acid (1.59 g, 7.00 mmol), NBS (1.31 g, 7.35 mmol) and $Mn(OAc)_2.4H_2O$ (343 mg, 1.40 mmol) in H_2O (12.0 mL) and MeCN (12.0 mL) were stirred at rt. for 72 h. The mixture was then diluted with H_2O (20 mL) and extracted with EtOAc (3 x 70 mL). The combined organics were dried over $MgSO_4$ and concentrated under reduced pressure. The residue was purified by column chromatography (petrol) to afford (*E*)-1-bromo-4-(2-bromovinyl)benzene (**167**) (561 mg, 31%) as a white solid.

R_f = 0.70 (5% EtOAc in petrol); **mp**: 66-68 °C (lit: 67-68 °C)[128]; **ν_{max}** (cm^{-1}) (thin film): 3071, 1608, 1587, 1486, 1397; **δ_H** ($CDCl_3$, 400 MHz): 7.49 - 7.42 (m, 2H, 2-H_1 and 6-H_1), 7.20 - 7.13 (m, 2H, 3-H_1 and 5-H_1), 7.05 (d, *J* = 14.1 Hz, 1H, 7-H_1), 6.79 (d, *J* = 14.1 Hz, 1H, 8-H_1); **δ_c** ($CDCl_3$, 100 MHz): 136.0 (C-8), 134.8 (C-1), 131.9 (C-3 and C-5), 127.5 (C-2 and C-6), 122.2 (C-4), 107.3 (C-7).

(*E*)-1-Bromo-2-(2-bromovinyl)benzene (169)[127,129]

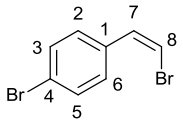


A mixture of 2-bromo-*trans*-cinnamic acid (1.59 g, 7.00 mmol), NBS (1.31 g, 7.35 mmol) and $Mn(OAc)_2.4H_2O$ (343 mg, 1.40 mmol) in H_2O (12.0 mL) and MeCN (12.0 mL) were stirred at rt. for 72 h. The mixture was then diluted with

H_2O (20 mL) and extracted with EtOAc (3 x 70 mL). The combined organics were dried over $MgSO_4$ and concentrated under reduced pressure. The residue was purified by column chromatography (petrol) to afford (*E*)-1-bromo-2-(2-bromovinyl)benzene (**169**) (293 mg, 16%) as a colourless oil.

$\mathbf{R_f}$ = 0.66 (5% EtOAc in petrol); ν_{max} (cm^{-1}) (thin film): 3071, 1604, 1584, 1462, 1436; δ_H ($CDCl_3$, 400 MHz): 7.57 (dd, *J* = 1.2, 8.0 Hz, 1H, 5-H_1), 7.45 (d, *J* = 13.9 Hz, 1H, 7-H_1), 7.40 (dd, *J* = 1.6, 8.0 Hz, 1H, 2-H_1), 7.32 - 7.25 (m, 1H, 4-H_1), 7.19 - 7.13 (m, 1H, 3-H_1), 6.77 (d, *J* = 13.9 Hz, 1H, 8-H_1); δ_c ($CDCl_3$, 100 MHz): 136.2 (C-5), 136.0 (C-1), 133.1 (C-8), 129.6, 127.6 and 127.1 (C-2, C-3 and C-4), 122.7 (C-6), 109.2 (C-7).

(*Z*)-1-Bromo-4-(2-bromovinyl)benzene (171)[130,131]



Bromine (0.270 mL, 5.25 mmol) was added dropwise to a solution of 4-bromo-*trans*-cinnamic acid (1.14 g, 5.00 mmol) in $CHCl_3$ (5.00 mL) at 0 °C, and the mixture stirred at rt. for 18 h. Triethylamine (2.00 mL, 14.0 mmol) was then added dropwise at 0 °C, and the mixture stirred at 50 °C for 4 h. 1 M aqueous HCl (10 mL) was added at 0 °C, and the mixture extracted with EtOAc (3 x 50 mL). The combined organics were dried over $MgSO_4$ and concentrated under reduced pressure. The residue was purified by column chromatography (petrol) to afford (*Z*)-1-bromo-4-(2-bromovinyl)benzene (**171**) (565 mg, 43%) as a colourless oil.

$\mathbf{R_f}$ = 0.69 (5% EtOAc in petrol); ν_{max} (cm^{-1}) (thin film): 3076, 1611, 1587, 1485, 1400; δ_H ($CDCl_3$, 400 MHz): 7.62 - 7.48 (m, 4H, 4 x Ar CH_1), 7.02 (d, *J* = 8.2 Hz, 1H, 7-H_1), 6.48 (d, *J* = 8.2 Hz, 1H, 8-H_1); δ_c ($CDCl_3$, 100 MHz): 133.8 (C-1), 131.4 (C-3 and C-5), 131.3 (C-8), 130.5 (C-2 and C-6), 122.3 (C-4), 107.3 (C-7).

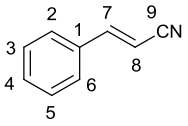
7.4.4 General Cyanation Procedure

A solution of vinyl halide (0.550 mmol), $Pd_2(dba)_3$ (25.0 mg, 0.0300 mmol), and DPPP (34.0 mg, 0.0800 mmol) in Et_2O (1.00 mL) was stirred at rt. for 15 min. Na_2CO_3 (64.0 mg, 0.600 mmol) and DMAc (0.500 mL) were then added, and the mixture heated to 100/140 °C. Upon reaching the required temperature acetone cyanohydrin (55.0 µL, 0.600 mmol) was added in one portion, and the mixture stirred at this temperature for 2-7 h. The mixture was cooled to rt. and H_2O (10 mL) added, then extracted with EtOAc (3 x 10 mL). The combined organic layers were dried over $MgSO_4$ and concentrated under reduced pressure. The residue was purified by silica gel chromatography, eluting with a mixture of petrol/EtOAc, affording the desired alkenyl nitrile.

All reactions were conducted on a 0.55 mmol scale (of vinyl halide) unless otherwise indicated. Where alternative substrate quantities were used, all other reagents and solvents were scaled accordingly.

7.4.5 Characterisation of Cyanation Products

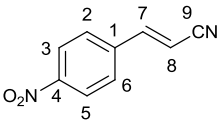
Cinnamonitrile (149)[132]



Reaction mixture heated at 100 °C for 4 h to afford cinnamonitrile (**149**) (56.0 mg, 79%) as a colourless oil.

$\mathbf{R_f}$ = 0.16 (5% EtOAc in petrol); ν_{max} (cm^{-1}) (thin film): 2218, 1619, 1577, 1494, 1449, 967; δ_H ($CDCl_3$, 400 MHz): 7.50 - 7.38 (m, 6H, 5 x Ar CH_1 and 7-H_1), 5.90 (d, *J* = 16.7 Hz, 1H, 8-H_1); δ_c ($CDCl_3$, 100 MHz): 150.6 (C-7), 133.5 (C-1), 131.2 (C-4), 129.1 and 127.3 (C-2, C-3, C-5 and C-6), 118.1 (C-9), 96.3 (C-8); **HRMS** (ESI) calculated for C_9H_7NNa $[M+Na]^+$ 152.0471, found 152.0464.

(*E*)-3-(4-Nitrophenyl)acrylonitrile (152)[133]

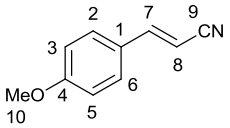


From (*E*)-1-(2-bromovinyl)-4-nitrobenzene (**151**): conducted on 0.460 mmol scale. Reaction mixture heated at 100 °C for 6 h (66.0 mg, 83%, inseparable *E:Z* 18:1 mixture obtained).

From (*E*)-1-(2-chlorovinyl)-4-nitrobenzene (**153**): conducted on 0.220 mmol scale. Reaction mixture heated at 100 °C for 6 h to afford (*E*)-3-(4-nitrophenyl)acrylonitrile (**152**) (18.0 mg, 47%, *E* isomer only) as a yellow solid.

R_f = 0.08 (5% EtOAc in petrol); **mp**: 201-202 °C (lit: 198-200 °C)[133]; **ν_{max}** (cm^{-1}) (thin film): 3065, 2922, 2217, 1594, 1516, 1343; *E*-isomer: **δ_H** ($CDCl_3$, 400 MHz): 8.31 - 8.26 (m, 2H, 3-H_1 and 5-H_1), 7.67 - 7.62 (m, 2H, 2-H_1 and 6-H_1), 7.48 (d, *J* = 16.7 Hz, 1H, 7-H_1), 6.06 (d, *J* = 16.7 Hz, 1H, 8-H_1); **δ_c** ($CDCl_3$, 100 MHz): 149.0 (C-4), 147.7 (C-7), 139.1 (C-2 and C-6), 128.1 (C-3 and C-5), 124.4 (C-1), 116.9 (C-9), 101.0 (C-8); *Z*-isomer[134]: **δ_H** ($CDCl_3$, 400 MHz): 8.31 (d, *J* = 8.6 Hz, 2H, 3-H_1 and 5-H_1), 7.97 (d, *J* = 8.6 Hz, 2H, 2-H_1 and 6-H_1), 7.24 (d, *J* = 12.1 Hz, 1H, 7-H_1), 5.71 (d, *J* = 12.1 Hz, 1H, 8-H_1); **HRMS** (ESI) calculated for $C_9H_7N_2O_2$ $[M+H]^+$ 175.0502, found 175.0505.

(*E*)-3-(4-Methoxyphenyl)acrylonitrile (155)[133]



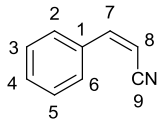
From (*E*)-1-(2-bromovinyl)-4-methoxybenzene (**154**): reaction mixture heated at 140 °C for 2 h (71.0 mg, 81%).

From (*E*)-1-(2-iodovinyl)-4-methoxybenzene (**156**): reaction mixture heated at 140 °C for 7 h to afford (*E*)-3-(4-methoxyphenyl)acrylonitrile (**155**) (20.0 mg, 23%) as a white solid.

R_f = 0.14 (5% EtOAc in petrol); **mp**: 62-64 °C (lit: 63-65 °C)[133]; **ν_{max}** (cm^{-1}) (thin film): 2937, 2218, 1604, 1574, 1512, 1255, 1175; **δ_H** ($CDCl_3$, 400 MHz): 7.43 - 7.38 (m, 2H, 2-H_1 and 6-H_1), 7.34 (d, *J* = 16.6 Hz, 1H, 7-H_1), 6.95 - 6.90 (m, 2H, 3-H_1 and 5-H_1), 5.73 (d, *J* = 16.6 Hz, 1H, 8-H_1), 3.86 (s, 3H, 10-H_3); **δ_c** ($CDCl_3$, 100 MHz): 162.0 (C-4), 150.0 (C-7), 129.1 (C-2 and C-6), 126.4 (C-1), 118.7 (C-

9), 114.5 (C-3 and C-5), 93.4 (C-8), 55.4 (C-10); **HRMS** (ESI) calculated for $C_{10}H_{10}NO$ $[M+H]^+$ 160.0757, found 160.0757.

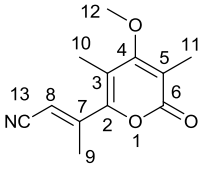
(*Z*)-3-Phenylacrylonitrile (158)[102]



Reaction mixture heated at 100 °C for 6 h to afford (*Z*)-3-phenylacrylonitrile (**158**) (39.0 mg, 55%) as a colourless oil.

$\mathbf{R_f}$ = 0.29 (5% EtOAc in petrol); $\boldsymbol{\nu_{max}}$ (cm^{-1}) (thin film): 2927, 2219, 1602, 1494, 1465; $\boldsymbol{\delta_H}$ ($CDCl_3$, 400 MHz): 7.88 - 7.75 (m, 2H, 2 x Ar CH_1), 7.50 - 7.42 (m, 3H, 3 x Ar CH_1), 7.14 (d, *J* = 12.1 Hz, 1H, 7-H_1), 5.46 (d, *J* = 12.1 Hz, 1H, 8-H_1); $\boldsymbol{\delta_c}$ ($CDCl_3$, 100 MHz): 148.7 (C-7), 133.6 (C-1), 131.0 (C-4), 129.0 and 128.9 (C-2, C-3, C-5 and C-6), 117.3 (C-9), 95.1 (C-8); **HRMS** (ESI) calculated for C_9H_7NNa $[M+Na]^+$ 152.0471, found 152.0465.

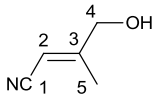
(*E*)-3-(4-Methoxy-3,5-dimethyl-2-oxo-2H-pyran-6-yl)but-2-enenitrile (159)



Reaction mixture heated at 100 °C for 4 h to afford (*E*)-3-(4-methoxy-3,5-dimethyl-2-oxo-2H-pyran-6-yl)but-2-enenitrile (**159**) (80.0 mg, 66%) as a yellow solid.

R_f = 0.12 (25% EtOAc in petrol); **mp**: 127-129 °C; **ν_{max}** (cm^{-1}) (thin film): 3060, 2219, 1704, 1556, 1239, 1136; **δ_H** ($CDCl_3$, 400 MHz): 5.58 (d, *J* = 1.2 Hz, 1H, 8-H_1), 3.86 (s, 3H, 12-H_3), 2.36 (d, *J* = 1.2 Hz, 3H, 9-H_3), 2.09 (s, 3H, 11-H_3), 2.07 (s, 3H, 10-H_3); **δ_c** ($CDCl_3$, 100 MHz): 167.1 (C-6), 163.9 (C4), 152.3 (C-7), 151.4 (C-2), 115.6 (C-13), 112.9 (C-3 and C-5), 102.9 (C-8), 60.5 (C-12), 19.7 (C-9), 11.9 and 10.5 (C-10 and C-11); **HRMS** (ESI) calculated for $C_{12}H_{17}N_2O_3$ $[M+NH_4]^+$ 237.1234, found 237.1236.

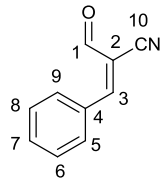
(*E*)-4-Hydroxy-3-methylbut-2-enenitrile (160)[135]



Reaction mixture heated at 100 °C for 2 h to afford (*E*)-4-hydroxy-3-methylbut-2-enenitrile (**160**) (38.0 mg, 72%) as a yellow oil.

R_f = 0.07 (25% EtOAc in petrol); **ν_{max}** (cm^{-1}) (thin film): 3441, 2223, 1734, 1644, 1440, 1377, 1247; **δ_H** ($CDCl_3$, 400 MHz): 5.58 - 5.53 (m, 1H, 2-H_1), 4.20 - 4.15 (m, 2H, 4-H_2), 2.41 (br. s, 1H, OH), 1.99 (d, *J* = 1.0 Hz, 3H, 5-H_3); **δ_c** ($CDCl_3$, 100 MHz): 163.4 (C-3), 117.1 (C-1), 93.4 (C-2), 65.1 (C-4), 17.5 (C-5); **HRMS** (ESI) calculated for C_5H_7NNaO $[M+Na]^+$ 120.0420, found 120.0428.

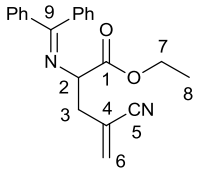
(*Z*)-2-Formyl-3-phenylacrylonitrile (162)



Reaction mixture heated at 100 °C for 6 h to afford (*Z*)-2-formyl-3-phenylacrylonitrile (**162**) (42.0 mg, 49%; formed as an inseparable 3.5:1 mixture with *trans*-cinnamaldehyde) as a pale yellow oil.

R_f = 0.21 (10% EtOAc in petrol); **ν_{max}** (cm^{-1}) (thin film): 3058, 2932, 2190, 1629, 1553, 1414; (*Z*)-2-formyl-3-phenylacrylonitrile (**162**): **δ_H** ($CDCl_3$, 400 MHz): 9.36 (s, 1H, 1-H_1), 8.05 - 7.98 (m, 2H, 5-H_1 and 9-H_1), 7.91 (s, 1H, 3-H_1), 7.52 - 7.47 (m, 3H, 6-H_1, 7-H_1 and 8-H_1); **δ_c** ($CDCl_3$, 100 MHz): 187.0 (C-1), 149.1 (C-3), 131.6 (C-7), 130.9 (C-5 and C-9), 129.1 (C-4), 128.7 (C-6 and C-8), 128.5 (C-2), 124.3 (C-10); trans-cinnamaldehyde[136]: **δ_H** ($CDCl_3$, 400 MHz): 9.72 (d, *J* = 7.7 Hz, 1H), 7.60 - 7.56 (m, 2H), 7.48 - 7.43 (m, 4H), 6.74 (dd, *J* = 7.7, 16.0 Hz, 1H).

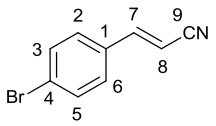
Ethyl 4-cyano-2-((diphenylmethylene)amino)pent-4-enoate (164)



Reaction mixture heated at 100 °C for 4 h to afford ethyl 4-cyano-2-((diphenylmethylene)amino)pent-4-enoate (**164**) (146 mg, 80%) as a yellow oil.

R_f = 0.14 (10% EtOAc in petrol); **ν_{max}** (cm^{-1}) (thin film): 2981, 2223, 1737, 1622, 1598, 1577, 1446; **δ_H** ($CDCl_3$, 400 MHz): 7.71 - 7.64 (m, 2H, 2 x Ar CH), 7.51 - 7.39 (m, 4H, 4 x Ar CH), 7.39 - 7.31 (m, 2H, 2 x Ar CH), 7.26 - 7.19 (m, 2H, 2 x Ar CH), 5.92 (br. s, 1H, 6-HH'), 5.83 (br. s, 1H, 6-HH'), 4.32 (dd, *J* = 5.7, 7.3 Hz, 1H, 2-H_1), 4.26 - 4.15 (m, 2H, 7-H_2), 2.93 - 2.88 (m, 2H, 3-HH'), 1.28 (t, *J* = 7.2 Hz, 3H, 8-H_3); **δ_c** ($CDCl_3$, 100 MHz): 172.3 (C-1), 170.4 (C-9), 139.0 and 135.7 (2 x Ar $C_{quaternary}$), 133.6 (C-6), 130.6 (2 x Ar CH), 128.9 (2 x Ar CH), 128.6 (2 x Ar CH), 128.0 (2 x Ar CH), 127.8 (2 x Ar CH), 119.5 (C-4), 118.2 (C-5), 63.3 (C-2), 61.4 (C-7), 38.4 (C-3), 14.1 (C-8); **HRMS** (ESI) calculated for $C_{21}H_{21}N_2O_2$ $[M+H]^+$ 333.1598, found 333.1584.

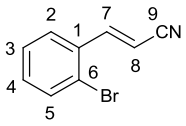
(*E*)-3-(4-Bromophenyl)acrylonitrile (168)[137]



Reaction mixture heated at 100 °C for 4 h to afford (*E*)-3-(4-bromophenyl)acrylonitrile (**168**) (95.0 mg, 83%) as a white solid.

R_f = 0.39 (5% EtOAc in petrol); **mp**: 104-105 °C (lit: 105-105.8 °C)[138]; **ν_{max}** (cm^{-1}) (thin film): 3061, 2222, 1620, 1588, 1487, 1403, 1074; **δ_H** ($CDCl_3$, 400 MHz): 7.59 - 7.53 (m, 2H, 2 x Ar CH_1), 7.35 (d, *J* = 16.7 Hz, 1H, 7-H_1), 7.33 - 7.30 (m, 2H, 2 x Ar CH_1), 5.89 (d, *J* = 16.7 Hz, 1H, 8-H_1); **δ_c** ($CDCl_3$, 100 MHz): 149.2 (C-7), 132.4 (C-1, C-3 and C-5), 128.7 (C-2 and C-6), 125.6 (C-4), 117.8 (C-9), 97.1 (C-8); **HRMS** (ESI) calculated for C_9H_6BrNNa $[M+Na]^+$ 229.9576, found 229.9570.

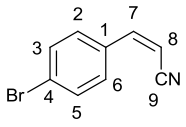
(*E*)-3-(2-Bromophenyl)acrylonitrile (170)[138]



Reaction mixture heated at 100 °C for 2 h to afford (*E*)-3-(2-bromophenyl)acrylonitrile (**170**) (78.0 mg, 68%) as a yellow oil.

R_f = 0.19 (5% EtOAc in petrol); **ν_{max}** (cm^{-1}) (thin film): 3064, 2223, 1617, 1588, 1468, 1437, 1281; **δ_H** ($CDCl_3$, 400 MHz): 7.81 (d, *J* = 16.7 Hz, 1H, 7-H_1), 7.64 (dd, *J* = 1.3, 8.0 Hz, 1H, 5-H_1), 7.53 (dd, *J* = 1.6, 8.0 Hz, 1H, 2-H_1), 7.39 - 7.26 (m, 2H, 3-H_1 and 4-H_1), 5.87 (d, *J* = 16.7 Hz, 1H, 8-H_1); **δ_c** ($CDCl_3$, 100 MHz): 149.1 (C-7), 133.6 (C-5), 133.5 (C-1), 132.1, 127.9 and 127.0 (C-2, C-3 and C-4), 124.8 (C-6), 117.6 (C-9), 99.1 (C-8); **HRMS** (ESI) calculated for C_9H_7BrN $[M+H]^+$ 207.9756, found 207.9751.

(*Z*)-3-(4-Bromophenyl)acrylonitrile (172)[138]



Reaction mixture heated at 100 °C for 7 h to afford (*Z*)-3-(4-bromophenyl)acrylonitrile (**172**) as a yellow oil (75.0 mg, 67%; *Z:E* 11:1).

R_f = 0.25 (5% EtOAc in petrol); **ν_{max}** (cm^{-1}) (thin film): 2219, 1615, 1588, 1488, 1075; **δ_H** ($CDCl_3$, 400 MHz): 7.71 - 7.65 (m, 2H, 2-H_1 and 6-H_1), 7.62 - 7.56 (m, 2H, 3-H_1 and 5-H_1), 7.08 (d, *J* = 12.2 Hz, 1H, 7-H_1), 5.50 (d, *J* = 12.2 Hz, 1H, 8-H_1); **δ_c** ($CDCl_3$, 100 MHz): 147.3 (C-7), 132.4 (C-1), 132.2 and 130.4 (C-2, C-3, C-

5 and C-6), 125.4 (C-4), 117.0 (C-9), 95.8 (C-8); **HRMS** (ESI) calculated for C_9H_7BrN $[M+H]^+$ 207.9756, found 207.9745.

References

1. (a) Ireland, C.; Faulkner, D. J.; Solheim, B. A.; Clardy, J. *J. Am. Chem. Soc.* **1978**, *100*, 1002.

   (b) Ireland, C.; Faulkner, D. J.; Finer, J. S.; Clardy, J. *J. Am. Chem. Soc.* **1979**, *101*, 1275.

   (c) Cueto, M; D'Croz, L.; Maté, J. L.; San-Martín, A.; Darias, J. *Org. Lett.* **2005**, *7*, 415.

   (d) Manzo, E.; Ciavatta, M. L.; Gavagnin, M.; Mollo, E.; Wahidulla, S.; Cimino, G. *Tetrahedron Lett.* **2005**, *46*, 465.

2. Davies-Colman, M. T.; Garson, M. J. *Nat. Prod. Rep.* **1998**, *15*, 477.

3. Gavagnin, M.; Mollo, E.; Cimino, G.; Ortea, J. *Tetrahedron Lett.* **1996**, *37*, 4259.

4. Fu, X.; Hong, E. P.; Schmitz, F. J. *Tetrahedron* **2000**, *56*, 8989.

5. Jeffery, D. W.; Perkins, M. V.; White, J. M. *Org. Lett.* **2005**, *7*, 1581.

6. Sharma, P.; Griffiths, N.; Moses, J. E. *Org. Lett.* **2008**, *10*, 4025.

7. Sharma, P.; Lygo, B.; Lewis, W.; Moses, J. E. *J. Am. Chem. Soc.* **2009**, *131*, 5966.

8. Mann, J. *Secondary Metabolism*, 2nd ed.; Oxford Science Publications, 1987.

9. Müller, M.; He, J.; Hertweck, C. *ChemBioChem.* **2006**, *7*, 37.

10. Ireland, C.; Faulkner, D. J. *Tetrahedron* **1981**, *37* (suppl 1), 233.

11. Miller, A. K.; Trauner, D. *Angew. Chem. Int. Ed.* **2005**, *44*, 4602.

12. Bandaranayake, W. M.; Banfiled, J. E.; Black, D. St. C.; Fallon, G. D.; Gatehouse, B. M. *J. Chem. Soc. Chem. Commun.* **1980**, 162.

13. Nicolaou, K. C.; Petasis, N. A.; Zipkin, R. E.; Uenishi, J. *J. Am. Chem. Soc.* **1982**, *104*, 5555.

14. Eade, S. J.; Walter, M. W.; Byrne, C.; Odell, B.; Rodriguez, R.; Baldwin, J. E.; Adlington, R. M.; Moses, J. E. *J. Org. Chem.* **2008**, *73*, 4830.

15. Zuidema, D. R.; Miller, A. K.; Trauner, D.; Jones, P. B. *Org. Lett.* **2005**, *7*, 4959.

16. Pawlik, J. R. *Chem. Rev.* **1993**, *93*, 1911.

17. Ireland, C.; Scheuer, P. J. *Science* **1979**, *205*, 922.

18. Halliwell, B.; Gutteridge, J. M. C. *Free Radicals in Biology and Medicine*, 4th ed.; Oxford University Press: Oxford, 2007.

19. Rastogi, R. P.; Richa; Kumar, A.; Tyagi, M. B.; Sinha, R. P *J. Nucleic Acids* **2010**, *2010*, doi:10.4061/2010/592980.

20. Remucal, C. K.; McNeill, K. *Environ. Sci. Technol.* **2011**, *45*, 5230.

21. Santos, A.; Rodrigues, A. M.; Sobral, A. J. F. N.; Monsanto, P. V.; Vaz, W. L. C.; Moreno, M. J. *Photochem. Photobiol.* **2009**, *85*, 1409.

22. Saez, G.; Thornalley, P. J.; Hill, H. A. O.; Hems, R.; Bannister, J. V. *Biochim. Biophys. Acta* **1982**, *719*, 24.

23. St-Pierre, J.; Buckingham, J. A.; Roebuck, S. J.; Brand, M. D. *J. Biol. Chem.* **2002**, *277*, 44784.

24. Wolszczak, M.; Gajda, J. *Res. Chem. Intermed.* **2010**, *36*, 549.

25. Duarte, V.; Gasparutto, D.; Jaquinod, M.; Ravanat, J.-L.; Cadet, J. *Chem. Res. Toxicol.* **2001**, *14*, 46.

26. Pryor, W. A.; Stanley, J. P. *J. Org. Chem.* **1975**, *40*, 3615.

27. Girotti, A. W.; Kriska, T. *Antiox. Redox Signal.* **2004**, *6*, 301.

28. Evans, M. D.; Dizdaroglu, M.; Cooke, M. S. *Mutat. Res.* **2004**, *567*, 1.

29. Traber, M. G.; Atkinson, J. *Free Rad. Biol. Med.* **2007**, *43*, 4.

30. Beyer, R. E. *J. Bioenerg. Biomembr.* **1994**, *26*, 349.

31. Procházková, D.; Boušová, I.; Wilhelmová, N. *Fitoterapia* **2011**, *82*, 513.

32. Mortensen, A.; Skibsted, L. H.; Truscott, T. G. *Arch. Biochem. Biophys.* **2001**, *385*, 13.

33. Blokhina, O.; Virolainen, E.; Fagerstedt, K. V. *Ann. Bot.* **2003**, *91*, 179.

34. Wiseman, H. *FEBS Lett.* **1993**, *326*, 285.

35. Holick, M. F.; MacLaughlin, J. A.; Doppelt, S. H. *Science* **1981**, *211*, 590.

36. Suzuki, A. *J. Organomet. Chem.* **1999**, *576*, 147.

37. Liang, G.; Miller, A. K.; Trauner, D. *Org. Lett.* **2005**, *7*, 819.

38. Larock, R. C.; Doty, M. J.; Han, X. *J. Org. Chem.* **1999**, *64*, 8770.

39. Hénaff, N.; Whiting, A. *Tetrahedron* **2000**, *56*, 5193.

40. Kamal, A.; Shaik, A. A.; Azeeza, S.; Malik, M. S.; Sandbhor, M. *Tetrahedron: Asymmetry* **2006**, *17*, 2890.

41. Rodriguez, R.; Adlington, R. M.; Eade, S. J.; Walter, M. W.; Baldwin, J. E.; Moses, J. E. *Tetrahedron* **2007**, *63*, 4500.

42. Garey, D.; Ramirez, M.-l.; Gonzales, S.; Wertsching, A.; Tith, S.; Keefe, K.; Peña, M. R. *J. Org. Chem.* **1996**, *61*, 4853.

43. Baker, R.; Castro, J. L. *J. Chem. Soc. Perkin Trans. 1* **1990**, 47.

44. (a) Miller, A. K.; Trauner, D. *Angew. Chem. Int. Ed.* **2003**, *42*, 549.

(b) Miller, A. K.; Banghart, M. R.; Beaudry, C. M.; Suh, J. M.; Trauner, D. *Tetrahedron* **2003**, *59*, 8919.

(c) Ramirez, M.; Garey, D.; Pena, M. R. *J. Heterocyclic Chem.* **1995**, *32*, 1657.

45. Frank, S. A.; Chen, H.; Kunz, R. K.; Schnaderbeck, M. J.; Roush, W. R. *Org. Lett.* **2000**, *2*, 2691.

46. Uenishi, J.; Beau, J.-M.; Armstrong, R. W.; Kishi, Y. *J. Am. Chem. Soc.* **1987**, *109*, 4756.

47. Asawakarn, T.; Cladera, J.; O'Shea, P. *J. Biol. Chem.* **2001**, *276*, 38457.

48. Simons, K.; Ikonen, E. *Nature* **1997**, *387*, 569.

49. Munro, S. *Cell* **2003**, *115*, 377.

50. Simons, K.; Vaz, W. L. C. *Annu. Rev. Biophys. Biomol. Struct.* **2004**, *33*, 269.

51. Ipsen, J. H.; Mouritsen, O. G.; Zuckermann, M. J. *Biophys. J.* **1989**, *56*, 661.

52. (a) Hobden, C.; Teevan, C.; Jones, L.; O'Shea, P. *Microbiology* **1995**, *141*, 1875.

(b) Davis, B. M.; Richens, J. L.; O'Shea, P. *Biophys. J.* **2011**, *101*, 245.

53. Avanti Polar Lipids: Critical micelle concentrations. http://avantilipids.com/index.php?option=com_content&view=article&id=1703&Itemid=422 (Accessed February 10, 2014).

54. Clarke, R. J. *Biochim. Biophys. Acta* **1997**, *1327*, 269.

55. O'Shea, P. *Biochem. Soc. Trans.* **2003**, *31*, 990.

56. Starke-Peterkovic, T.; Turner, N.; Vitha, M. F.; Waller, M. P.; Hibbs, D. E.; Clarke, R. J. *Biophys. J.* **2006**, *90*, 4060.

57. Gross, E.; Bedlack, Jr., R. S.; Loew, L. M. *Biophys. J.* **1994**, *67*, 208.

58. Loew, L. M. *Pure and Appl. Chem.* **1996**, *68*, 1405.

59. Motulsky, H.; Christopoulos, A. *Fitting Models to Biological Data Using Linear and Nonlinear Regression: A practical guide to curve fitting*; Oxford University Press: Oxford, 2004.

60. Giaginis, C.; Tsantili-Kakoulidou, A. *J. Pharm. Sci.* **2008**, *97*, 2984.

61. Cooper, G. M.; Hausman, R. E. *The Cell: A Molecular Approach*, 4th ed.; Sinauer Associates, Inc.: Sunderland, 2007.

62. Halliwell, B.; Chirico, S. *Am. J. Clin. Nutr.* **1993**, *57 (suppl.)*, 715S.

63. Lykkesfeldt, J. *Clinica Chimica Acta* **2007**, *380*, 50.

64. Record, I. R.; Dreosti, I. E.; McInerney, J. K. *J. Nutr. Biochem.* **1995**, *6*, 481.

65. Fryer, M. J. *Photochem. Photobiol.* **1993**, *58*, 304.

66. Burton, G. W.; Ingold, K. U. *Science* **1984**, *224*, 569.

67. Sharma, O. P.; Bhat, T. K. *Food Chem.* **2009**, *113*, 1202.

68. Benzie, I. F. F.; Strain, J. J. *Anal. Biochem.* **1996**, *239*, 70.

69. Huang, D.; Ou, B.; Prior, R. L. *J. Agric. Food Chem.* **2005**, *53*, 1841.

70. Vertuani, S.; Angusti, A.; Manfredini, S. *Curr. Pharm. Des.* **2004**, *10*, 1677.

71. Zhang, P.; Omaye, S. T. *Toxicol. In Vitro* **2001**, *15*, 13.

72. Obermüller-Jevic, U. C.; Francz, P. I.; Frank, J.; Flaccus, A.; Biesalski, H. K. *FEBS Lett.* **1999**, *460*, 212.

73. (a) Girotti, A. W.; Thomas, J. P.; Jordan, J. E. *Photochem. Photobiol.* **1985**, *41*, 267.

(b) Kanner, J.; Mendel, H. *J. Food Science* **1977**, *42*, 60.

74. (a) Wiseman, H.; Cannon, M.; Arnstein, H. R. V.; Halliwell, B. *FEBS* **1990**, *274*, 107.

(b) Wiseman, H.; Smith, C.; Arnstein, H. R. V.; Halliwell, B.; Cannon, M. *Chem.-Biol. Interactions* **1991**, *79*, 229.

75. Zuidema, D. R.; Jones, P. B. *J. Photochem. Photobiol. B: Biol.* **2006**, *83*, 137.

76. Zuidema, D. R.; Jones, P. B. *J. Nat. Prod.* **2005**, *68*, 481.

77. Trost, B. M.; Waser, J.; Meyer, A. *J. Am. Chem. Soc.* **2008**, *130*, 16424.

78. White, J. D.; Blakemore, P. R.; Green, N. J.; Hauser, E. B.; Holoboski, M. A.; Keown, L. E.; Kolz, C. S. N.; Phillips, B. W. *J. Org. Chem.* **2002**, *67*, 7750.

79. Avanti Polar Lipids: Egg PC. http://www.avantilipids.com/index.php?option=com_content&view=article&id=260&Itemid=212&catnumber=840051 (Accessed February 10, 2014).

80. Davis, B. M.; Jensen, R.; Williams, P.; O'Shea, P. *PLoS ONE* **2010**, *5*, e13522.

81. Elnagdi, M. H.; Khalifa, M. A. E.; Ibraheim, M. K. A.; Elmoghayar, M. R. H. *J. Heterocyclic Chem.* **1981**, *18*, 877.

82. Yeung, K.-S.; Farkas, M. E.; Kadow, J. F.; Meanwell, N. A. *Tetrahedron Lett.* **2005**, *46*, 3429.

83. Aureggi, V.; Sedelmeier, G. *Angew. Chem. Int. Ed.* **2007**, *46*, 8440.

84. Booth, B. L.; Dias, A. M.; Proença, M. F.; Zaki, M. E. A. *J. Org. Chem.* **2001**, *66*, 8436.

85. Ohtsuka, Y. *J. Org. Chem.* **1978**, *43*, 3231.

86. Ohtsuka, Y. *J. Org. Chem.* **1979**, *44*, 827.

87. Beall, L. S.; Mani, N. S.; White, A. J. P.; Williams, D. J.; Barrett, A. G. M.; Hoffman, B. M. *J. Org. Chem.* **1998**, *63*, 5806.

88. Maraval, A.; Igau, A.; Donnadieu, B.; Majoral, J.-P. *Eur. J. Org. Chem.*, **2003**, 385.

89. Fleming, F. F. *Nat. Prod. Rep.* **1999**, *16*, 597.

90. Tih, A. E.; Tih, R. G.; Sondengam, B. L.; Martin, M. T.; Bodo, B. *J. Nat. Prod.* **1994**, *57*, 971.

91. Mikolajczak, K. L. *Prog. Chem. Fats Other Lipids* **1977**, *15*, 97.

92. Olano, C.; Moss, S. J.; Brana, A. F.; Sheridan, R. M.; Math, V.; Weston, A. J.; Méndez, C.; Leadlay, P. F.; Wilkinson, B.; Salas, J. A. *Mol. Microbiol.* **2004**, *52*, 1745.

93. Kato, Y.; Fusetani, N.; Matsunaga, S.; Hashimoto, K.; Koseki, K. *J. Org. Chem.* **1988**, *53*, 3930.

94. Fleming, F. F.; Yao, L.; Ravikumar, P. C.; Funk, L.; Shook, B. C. *J. Med. Chem.* **2010**, *53*, 7902.

95. Maffiolo, S. I.; Marzorati, E.; Marazzi, A. *Org. Lett.* **2005**, *7*, 5237.

96. Singh, M. K.; Lakshman, M. K. *J. Org. Chem.* **2009**, *74*, 3079.

97. Burling, S.; Paine, B. M.; Nama, D.; Brown, V. S.; Mahon, M. F.; Prior, T. J.; Pregosin, P. S.; Whittlesey, M. K.; Williams, J. M. J. *J. Am. Chem. Soc.* **2007**, *129*, 1987.

98. (a) Palomo, C.; Aizpurua, J. M.; Garcia, J. M.; Ganboa, I.; Cossio, F. P.; Lecea, B.; López, C. *J. Org. Chem.* **1990**, *55*, 2498.

(b) Yamakado, Y.; Ishiguro, M.; Ikeda, N.; Yamamoto, H. *J. Am. Chem. Soc.* **1981**, *103*, 5568.

99. Halász, J.; Varga, K.; Fejes, P *J. Mol. Catal.* **1989**, *51*, 303.

100. Nakao, Y.; Yada, A.; Ebata, S.; Hiyama, T. *J. Am. Chem. Soc.* **2007**, *129*, 2428.

101. Yamamura, K.; Murahashi, S.-I. *Tetrahedron Lett.* **1977**, *18*, 4429.

102. Funabiki, T.; Hosomi, H.; Yoshida, S.; Tarama, K. *J. Am. Chem. Soc.* **1982**, *104*, 1560.

103. (a) Sakakibara, Y.; Yadani, N.; Ibuki, I.; Sakai, M.; Uchino, N. *Chem. Lett.* **1982**, 1565.

(b) Sakakibara, Y.; Enami, H.; Ogawa, H.; Fujimoto, S.; Kato, H.; Kunitake, K.; Sasaki, K.; Sakai, M. *Bull. Chem. Soc. Jpn.* **1995**, *68*, 3137.

104. Stuhl, L. S. *J. Org. Chem.* **1985**, *50*, 3934.

105. Alterman, M.; Hallberg, A. *J. Org. Chem.* **2000**, *65*, 7984.

106. Li, L.-H.; Pan, Z.-L.; Duan, X.-H.; Liang, Y.-M. *Synlett* **2006**, 2094.

107. Saha, D.; Adak, L.; Mukherjee, M.; Ranu, B. C. *Org. Biomol. Chem.* **2012**, *10*, 952.

108. (a) Sundermeier, M.; Zapf, A.; Beller, M. *Eur. J. Inorg. Chem.* **2003**, 3513.

(b) Anbarasan, P.; Schareina, T.; Beller, M. *Chem. Soc. Rev.* **2011**, *40*, 5049.

109. (a) Takagi, K.; Okamoto, T.; Sakakibara, Y.; Oka, S. *Chem. Lett.* **1973**, 471.

(b) Sekiya, A.; Ishikawa, N. *Chem. Lett.* **1975**, 277.

(c) Sundermeier, M.; Zapf, A.; Beller, M.; Sans, J. *Tetrahedron Lett.* **2001**, *42*, 6707.

(d) Yang, C.; Williams, J, M, *Org. Lett.* **2004**, *6*, 2837.

110. (a) Dalton, J. R.; Regen, S. L. *J. Org. Chem.* **1979**, *44*, 4443.

(b) Anderson, B. A.; Bell, E. C.; Ginah, F. O.; Harn, N. K.; Pagh, L. M.; Wepsiec, J. P. *J. Org. Chem.* **1998**, *63*, 8224.

111. (a) Chatani, N.; Hanafusa, T. *J. Org. Chem.* **1986**, *51*, 4714.

(b) Sundermeier, M.; Mutyala, S.; Zapf, A.; Spannenberg, A.; Beller, M. *J. Organomet. Chem.* **2003**, *684*, 50.

112. (a) Gundersen, L.-L. *Acta Chem. Scand.* **1996**, *50*, 58.

(b) Jin, F.; Confalone, P. N. *Tetrahedron Lett.* **2000**, *41*, 3271.

(c) Maligres, P. E.; Waters, M. S.; Fleitz, F.; Askin, D. *Tetrahedron Lett.* **1999**, *40*, 8193.

(d) Littke, A.; Soumeillant, M.; Kaltenbach III, R. F.; Cherney, R. J.; Tarby, C. M.; Kiau, S. *Org. Lett.* **2007**, *9*, 1711.

113. (a) Schareina, T.; Zapf, A.; Beller, M. *Chem. Commun.* **2004**, 1388.

(b) Weissman, S. A.; Zewge, D.; Chem, C. *J. Org. Chem.* **2005**, *70*, 1508.

(c) Grossman, O.; Gelman, D. *Org. Lett.* **2006**, *8*, 1189.

(d) Schareina, T.; Zapf, A.; Mägerlein, W.; Müller, N.; Beller, M. *Tetrahedron Lett.* **2007**, *48*, 1087.

114. (a) Dobbs, K. D.; Marshall, W. J.; Grushin, V. V. *J. Am. Chem. Soc.* **2007**, *129*, 30.

(b) Erhardt, S.; Grushin, V. V.; Kilpatrick, A. H.; Macgregor, S. A.; Marshall, W. J.; Roe, D. C. *J. Am. Chem. Soc.* **2008**, *130*, 4828.

115. Sundermeier, M.; Zapf, A.; Beller, M. *Angew. Chem. Int. Ed.* **2003**, *42*, 1661.

116. Sundermeier, M.; Zapf, A.; Mutyala, S.; Baumann, W.; Sans, J.; Weiss, S.; Beller, M. *Chem. Eur. J.* **2003**, *9*, 1828.

117. Cicco, S. R.; Martinelli, C.; Pinto, V.; Naso, F.; Farinola, G. M. *J. Organomet. Chem.* **2013**, *732*, 15.

118. Zapf, A.; Beller, M. *Chem. Eur. J.* **2001**, *7*, 2908.

119. Ushkov, A. V.; Grushin, V. V. *J. Am. Chem. Soc.* **2011**, *133*, 10999.

120. Kuang, C.; Yang, Q.; Senboku, H.; Tokuda, M. *Synthesis* **2005**, 1319.

121. López, A.; Moreno-Mañas, M.; Pleixats, R.; Roglans, A. *Tetrahedron* **1996**, *52*, 8365.

122. Chowdhury, S.; Roy, S. *J. Org. Chem.* **1997**, *62*, 199.

123. Bhorge, Y. R.; Chang, S.-H.; Chang, C.-H.; Yan, T.-H. *Tetrahedron* **2012**, *68*, 4846.

124. Bull, J. A.; Mousseau, J. J.; Charette, A. B. *Org. Lett.* **2008**, *10*, 5485.

125. Uenishi, J.; Kawahama, R.; Yonemitsu, O. *J. Org. Chem.* **1998**, *63*, 8965.

126. Nowak, I.; Robins, M. J. *J. Org. Chem.* **2007**, *72*, 2678.

127. Cheung, C. W.; Buchwald, S. L.; *J. Org. Chem.* **2012**, *77*, 7526.

128. Konz, W. E.; Hechtl, W.; Huisgen, R. *J. Am. Chem. Soc.* **1970**, *92*, 4104.

129. Mousseau, J. J.; Bull, J. A.; Ladd, C. L.; Fortier, A.; Roman, D. S.; Charette, A. B. *J. Org. Chem.* **2011**, *76*, 8243.

130. Kim, S. H.; Wei, H. –X.; Willis, S.; Li, G. *Synthetic Commun.* **1999**, *29*, 4179.

131. Kuang, C.; Yang, Q.; Senboku, H.; Tokuda, M. *Tetrahedron* **2005**, *61*, 4043.

132. Zhou, W.; Xu, J.; Zhang, L.; Jiao, N. *Org. Lett.* **2010**, *12*, 2888.

133. Rokade, B. V.; Malekar, S. K.; Prabhu, K. R. *Chem. Commun.* **2012**, *48*, 5506.

134. Jarowski, P. D.; Wu, Y.-L.; Boudon, C.; Gisselbrecht, J.-P.; Gross, M.; Schweizer, W. B.; Diederich, F. *Org. Biomol. Chem.* **2009**, *7*, 1312.

135. Fleming, F. F.; Wang, Q.; Steward, O. W. *J. Org. Chem.* **2001**, *66*, 2171.

136. Park, C. P.; Kim, D.-P. *J. Am. Chem. Soc.* **2010**, *132*, 10102.

137. Dong, H.; Shen, M.; Redford, J. E.; Stokes, B. J.; Pumphrey, A. L.; Driver, T. G. *Org. Lett.* **2007**, *9*, 5191.

138. Peppe, C.; Mello, P. A.; Chagas, R. P. *J. Organomet. Chem.* **2006**, *691*, 2335.

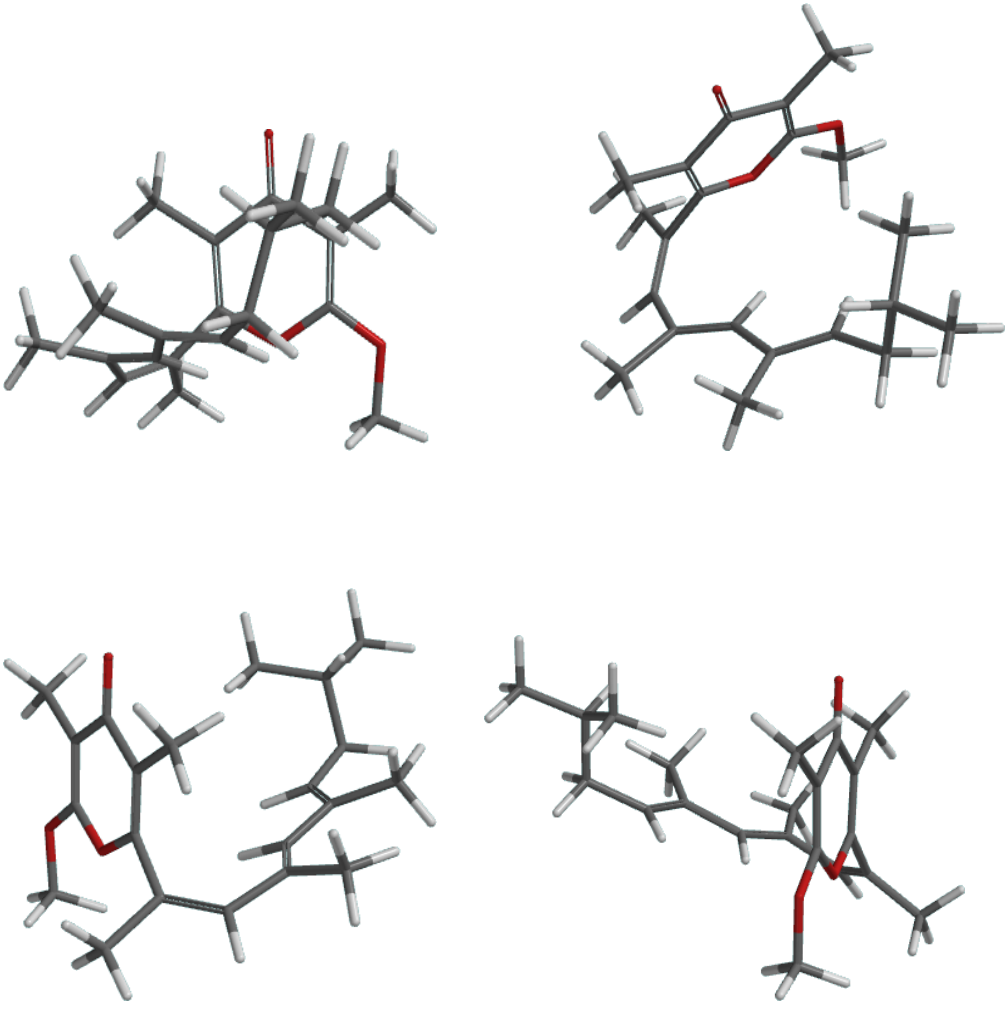
Appendix 1

Molecular Modelling: Equilibrium Geometries

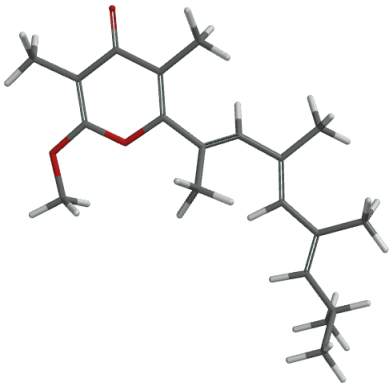
The equilibrium geometries of **43** and **44** were calculated using Spartan '10 Version 1.1.0.

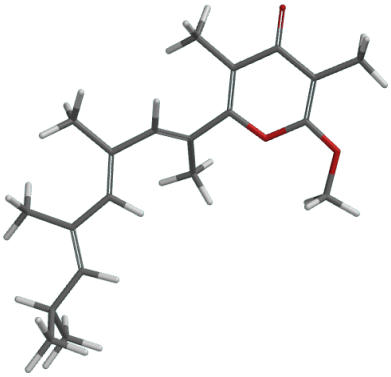
Geometry optimisation was performed using the B3LYP density functional model with a 6-31G* basis set.

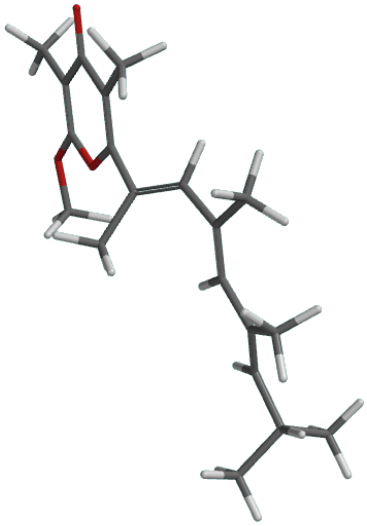
2-Methoxy-3,5-dimethyl-6-((2*Z*,4*E*,6*E*)-4,6,9-trimethyldeca-2,4,6-trien-2-yl)-4H-pyran-4-one (43)

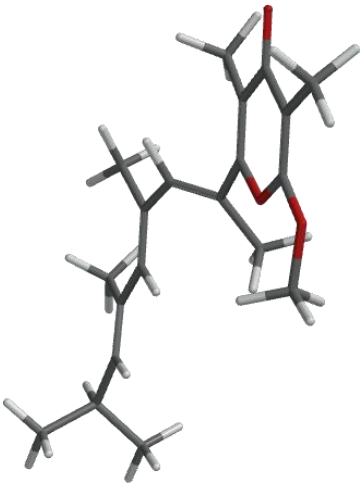


2-Methoxy-3,5-dimethyl-6-((2*E*,4*E*,6*E*)-4,6,9-trimethyldeca-2,4,6-trien-2-yl)-4H-pyran-4-one (44)









Appendix 2

Statistical Parameters

The tables below outline the statistical parameters generated using GraphPad Prism v5.0 when fitting the binding data (see Section 3.3.6) to Equations 2-4, including R Square values, a measure of the goodness of fit, and the F and P values used in the comparison of the goodness of fit of Equations 2 and 3 (using an extra sum-of-squares F test, see Section 6.2.8). Equation 4, even where high R Square values are reported, produced binding parameters with standard errors many times larger than the parameters themselves, and the fits were deemed ambiguous by the software.

DFn = DF1-DF2

DF1 = Degrees of freedom (Equation 2)

DF2 = Degrees of freedom (Equation 3)

			R Square		
Compound	**P Value**	**F (DFn,DF2)**	**Equation 2**	**Equation 3**	**Equation 4**
(±)-9	0.0025	10.94 (1,15)	0.9576	0.9689	0.9864
(-)-9	0.0169	6.403 (1,30)	0.9937	0.9948	1.000
(+)-9	0.6830	0.1700 (1,30)	0.9671	0.9673	1.000
43	0.0049	10.87 (1,15)	0.9451	0.9682	0.9660
44	0.3142	1.084 (1,15)	0.9742	0.9759	1.000

Table 18. Statistical parameters for binding to $PC_{100\%}$ PLVs

			R Square		
Compound	**P Value**	**F (DFn,DF2)**	**Equation 2**	**Equation 3**	**Equation 4**
(±)-9	0.0278	5.348 (1,30)	0.8979	0.9133	0.8979
(-)-9	0.0578	3.893 (1,30)	0.9180	0.9274	0.9180
(+)-9	0.1153	2.631 (1,30)	0.8904	0.8992	0.8904
43	0.0141	7.721 (1,15)	0.7237	0.8176	0.7236
44	0.0097	8.783 (1,15)	0.9711	0.9818	0.9711

Table 19. Statistical parameters for binding to $PC_{70\%}Chol_{30\%}$ PLVs

			R Square		
Compound	**P Value**	**F (DFn,DF2)**	**Equation 2**	**Equation 3**	**Equation 4**
(±)-9	0.4818	0.5158 (1,18)	0.9069	0.9095	0.9069
43	0.1315	2.497 (1,18)	0.9122	0.9229	0.9122
44	0.1792	1.963 (1,17)	0.9687	0.9720	0.9687

Table 20. Statistical parameters for binding to $PC_{70\%}SM_{30\%}$ PLVs

			R Square		
Compound	**P Value**	**F (DFn,DF2)**	**Equation 2**	**Equation 3**	**Equation 4**
(±)-9	0.5872	0.3057 (1,18)	0.9280	0.9292	0.9292
43	0.0463	4.579 (1,18)	0.8972	0.9181	0.9312
44	0.0689	3.742 (1,18)	0.9602	0.9671	0.9602

Table 21. Statistical parameters for binding to $PC_{60\%}Chol_{20\%}SM_{20\%}$ PLVs

			R Square		
Compound	**P Value**	**F (DFn,DF2)**	**Equation 2**	**Equation 3**	**Equation 4**
(±)-9	0.1220	2.633 (1,18)	0.9942	0.9950	0.9950
43	0.0533	4.278 (1,18)	0.9866	0.9892	0.9866
44	0.0100	8.285 (1,18)	0.9861	0.9905	0.9861

Table 22. Statistical parameters for binding to $PC_{40\%}SM_{60\%}$ PLVs